Theses & Dissertations   Graduate Studies

Summer 8-14-2015

Myeloid-derived suppressor cells contribute to the subversion of innate immunity during Staphylococcus aureus biofilm infection

Cortney E. Heim
University of Nebraska Medical Center

Follow this and additional works at: https://digitalcommons.unmc.edu/etd

Part of the Immunity Commons

MYELOID-DERIVED SUPPRESSOR CELLS CONTRIBUTE TO SUBVERSION OF

INNATE IMMUNITY DURING *STAPHYLOCOCCUS AUREUS* BIOFILM INFECTION

By

Cortney Heim

A DISSERTATION

Presented to the Faculty of

The Graduate College of the University of Nebraska Medical Center

In partial fulfillment of the requirements for the degree of

Doctor of Philosophy

Department of Pathology and Microbiology

Under the supervision of Professor Tammy Kielian, Ph.D.

University of Nebraska Medical Center

Omaha, NE

June 2015

Table of contents:

Acknowledgements

I would like to begin by thanking my mentor, Dr. Tammy Kielian, for her continued support and guidance through this process. I had the unique opportunity to work in her laboratory as an undergraduate intern, allowing me to experience science on a whole new level and ultimately led to my decision to enter graduate school. Over the last four years, she has not only imparted scientific knowledge, but has taught me invaluable professional skills while encouraging and challenging me to grow every day.

To my supervisory committee, Dr. Paul Fey, Dr. Jessica Snowden, Dr. Jill Poole and Dr. Jim Talmadge, who have been an instrumental part in the success of my projects and contributed critical and invaluable suggestions.

None of this work would have been possible without the members of Dr. Kielian's laboratory. I've learned many laboratory techniques and skills, including qRT-PCR, flow cytometry, and cell culture with Amy Aldrich, to animal work and models of biofilm infection with Debbie Vidlak and Mark Hanke, all while they have been patient teachers and constant resources. Without their encouragement and willingness to help, many of the studies described in this dissertation would not have been possible. Debbie has been particularly instrumental in much of this work, helping with many animal surgeries, *in vitro* experiments and Milliplex analyses for several studies in the past four years, as well as taking care of ordering needs and assisting with last minute complications. Thank you also to Tyler Scherr who has also worked very closely with me in many of these studies and has also been a resource through many scientific discussions. Additionally, I would like to thank Rachel Fallet, for caring for the breeding colony, answering mouse-related questions, and assisting with breeding protocols for transgenic mice, as well as Megan Bosch, Maria Burkovetskaya, Nikolay Karpuk, Jessica Odvody, Casey Gries, Matt Beaver, Kelsey Yamada, Rama Kakulavarapu, Monica Holley, Teresa Fritz and Amanda Angle for their support. I would like to also acknowledge the flow cytometry core facility, specifically Dr. Phil Hexley, Dr. Charles Kuszynski, Victoria Smith, and Sam Wall for their patience and assistance with many experiments.

Finally, I would like to thank my family for their never ending love and support. To my parents who have lived every success and failure by my side and encouraged me through it all, without whom none of this would have been possible.

Abbreviations:

Ab	Antibody
ACME	arginine catabolic mobile element
Ag	Antigen
Agr	Accessory gene regulator
AIP	Autoinducing peptide
APC	Allophycocyanin
ANOVA	Analysis of variance
Arg-1	Arginase-1
BCA	Bicinchoninic acid
BHI	Brain-heart infusion
BMDMΦ	Bone marrow-derived macrophage
BV	Brilliant violet
C5	Complement component 5
CA-MRSA	Community-associated Methicillin-resistant *Staphylococcus aureus*
CCL	C-C chemokine ligand
CCR	C-C chemokine receptor
CD	Cluster of Differentiation
cDNA	complementary DNA
CFU	Colony forming units
CHIPS	chemotaxis inhibitory protein
CM-H$_2$DCFDA	Cloromethyl derivative of H$_2$DCFDA
COX2	Cyclooxygenase 2
Cre	Carbapenem-resistant Enterobacteriaceae
CSF	Cerebral spinal fluid
CT	Computed tomography
CVC	Central venous catheter
CXCL	C-X-C chemokine ligand

CXCR	C-X-C chemokine receptor
DAPI	4', 6-Diamidino-2-Phenylindole
dH$_2$O	distilled water
(dd)H$_2$O	double distilled water
DMEM	Dulbecco's Modified Eagle's Medium
DNA	Deoxyribonucleic acid
DPEC	Diethylpyrocarbonate
ECM	Extracellular matrix
eDNA	extracellular DNA
ELISA	Enzyme-linked immunosorbent assay
Erm	Erythromycin
EtOH	Ethyl alcohol
FACS	Fluorescence-activated cell sorting
FBS	Fetal bovine serum
Fc	Fragment, crystallizable
FITC	Fluorescein isothiocyanate
Flt-3L	Fms-like tyrosine kinase-3 ligand
GAPDH	Glyceraldehyde-3-phosphate dehydrogenase
G-CSF	Granulocyte colony stimulating factor
GFP	Green fluorescent protein
GM-CSF	Granulocyte-macrophage colony-stimulating factor
G-MDSC	Granulocytic myeloid-derived suppressor cell
HA	Hospital-acquired
HBSS	Hank's balanced salt solution
HEPES	4-(2-hydroxyethyl)-1-piperazineethanesulfonic acid
Hla	α-hemolysin
HLA	Human leukocyte antigen
HPLC	High-performance liquid chromatography

HRP	Horseradish peroixdase
H&E	Hematoxylin and Eosin
H$_2$O$_2$	Hydrogen peroxide
HSC	Hematopoietic stem cell
IACUC	Institutional animal care and use committee
Iba-1	Ionized calcium-binding adaptor molecule-1
IDO	Indoleamine 2,3-dioxygenase
IFN	Interferon
Ig	Immunoglobulin
IL	Interleukin
iNOS	inducible nitric oxide synthase
IP	IFN-γ induced protein
i.p.	Intraperitoneal
IRB	Institutional Review Board
IRES-GFP	Internal ribosome entry site-green fluorescent protein
IVIS	*In vivo* imaging system
KO	Knockout
K-wire	Kirschner wire
LAC	Los Angeles County
L-glut	L-glutamine
loxp	locus of x-over P
LTA	Lipoteichoic acid
MΦ	Macrophage
mAb	Monoclonal antibody
MACS	Magnetic-activated cell sorting
M-CSF	Macrophage colony-stimulating factor
MCP-1	Monocyte chemoattractant protein-1
MDSC	Myeloid-derived suppressor cell

MIP	Macrophage inflammatory protein
M-MDSC	Monocytic myeloid-derived suppressor cell
MRC1	Mannose receptor, C type 1
mROS	Mitochondrial superoxide
MRSA	Methicillin-resistant *Staphylococcus aureus*
MSCRAMM	Microbial surface components recognizing adhesive matrix molecules
MyD88	Myeloid differentiation primary response gene 88
NA	Non-activated
NADPH	Nicotinamide adenine dinucleotide phosphate
ND	Not detected
NOD	nucleotide-binding oligomerization domain-containing protein 2
NOS	Nitric oxide synthase 2
NS	Natural suppressor
OD	Optical density
PAMP	Pathogen-associated molecular pattern
PBP2a	Penicillin-binding protein 2a
PBS	Phosphate-buffered saline
PCR	Polymerase chain reaction
PE	Phycoerythrin
PerCP	Peridinin-chlorophyll-protein complex
PFA	Paraformaldehyde
PGN	Peptidoglycan
PIA	Polysaccharide intercellular adhesin
PJI	Prosthetic joint infection
PMN	Polymorphonuclear cell
PRR	Pattern-recognition receptor
PRTN3	Proteinase 3
PTGS2	Prostaglandin-endoperoxide synthase 2

PVL	Panton-Valentine Leukocidin
Qdot	Quantum dot
qRT-PCR	quantitative real time-polymerase chain reaction
RANTES	Regulated on activation normal T cell expressed and secreted
RNA	Ribonucleic acid
RNS	Reactive nitrogen species
ROS	Reactive oxygen species
RPMI	Roswell Park Memorial Institute
S. aureus	*Staphylococcus aureus*
s.c.	Subcutaneous
SCC	staphylococcal cassette chromosome
SEM	Scanning electron microscopy
S. epidermidis	*Staphylococcus epidermidis*
STAT	Signal transducer and activator of transcription
TBS	Tris-buffered saline
TCR	T cell receptor
TGF	Transforming growth factor
Th	T helper
THA	Total hip arthroplasty
TKA	Total knee arthroplasty
TLR	Toll-like receptor
TNF	Tumor necrosis factor
Treg	Regulatory T cell
TSA	Trypticase soy agar
TSST	Toxic shock syndrome toxin
VISA	Vancomycin intermediate-resistant *Staphylococcus aureus*
VRSA	Vancomycin resistant *Staphylococcus aureus*
WT	Wild-type

List of Figures and Tables

University of Nebraska Medical Center

Omaha, Nebraska

June, 2015

MYELOID-DERIVED SUPPRESSOR CELLS CONTRIBUTE TO SUBVERSION OF INNATE IMMUNITY DURING *STAPHYLOCOCCUS AUREUS* BIOFILM INFECTION

Cortney E. Heim, Ph.D.

University of Nebraska Medical Center, 2015

Advisor: Tammy Kielian, Ph.D.

Abstract

Myeloid-derived suppressor cells (MDSCs) are a heterogeneous population of immature monocytes and granulocytes that are potent inhibitors of T cell activation. A role for MDSCs in bacterial infections has only recently emerged, and our laboratory was the first to demonstrate a functional role for MDSCs during *Staphylococcus aureus* (*S. aureus*) biofilm infection. Biofilm infections often lead to significant morbidity due to their recalcitrance to antibiotics and ability to subvert immune-mediated clearance by skewing the immune response toward an anti-inflammatory, pro-fibrotic phenotype. Therefore, we examined whether MDSCs could play a role in this process. $CD11b^+Gr-1^+$ MDSCs represented the main cellular infiltrate during *S. aureus* orthopedic biofilm infection, and biofilm-associated MDSCs inhibited T cells proliferation and cytokine production, which correlated with a paucity of T cell infiltrates at the infection site. Importantly, tissues obtained from patients undergoing revision surgery for prosthetic joint infections (PJIs) revealed similar patterns of immune cell influx, with increased MDSC-like infiltrates and significantly fewer T cells compared to aseptic revisions. Depletion of MDSCs and improved bacterial clearance by enhancing the intrinsic proinflammatory attributes of infiltrating monocytes and macrophages. However, the mechanisms responsible for MDSC homing to sites of biofilm infection and factors mediating immunosuppression remain unknown. In cancer, proinflammatory signals initially induce MDSC recruitment and activation, while the immunosuppressive functions of MDSCs are mediated through factors like IL-10, Arg-1 and iNOS. IL-12p40 and IL-10 are both significantly elevated during *S. aureus* biofilm infection. These studies demonstrate that IL-12 plays a key role in the recruitment of MDSCs into biofilm infection via a chemoattractant that remains to be identified, while IL-10 is produced by infiltrating MDSCs at the site of biofilm infection, whereupon it plays a critical role in polarizing monocyte/macrophages toward an anti-inflammatory phenotype. Loss of either IL-12 or IL-10 during the early MDSC recruitment or effector phases, respectively, promotes biofilm clearance, implicating key roles for each cytokine at distinct stages of infection. Collectively, these studies demonstrate that MDSCs are key contributors to the chronicity of *S. aureus* biofilm infection, as

their immunosuppressive function prevents monocyte/macrophage proinflammatory activity,

which facilitates biofilm persistence.

Chapter 1: Introduction

1) *S. aureus* **biofilm infection**

a) **Methicillin-resistant *Staphylococcus aureus***

Staphylococcus aureus (*S. aureus*) is a gram-positive bacterium known to colonize the skin and nasal mucosa of approximately one-third of people worldwide [1-4]. Since its discovery in the 1880s, *S. aureus* has been regarded as a serious threat to human health, causing a range of diseases from superficial skin and soft tissue infections to more invasive infections like bacterial pneumonia and sepsis [3]. Prior to the 1960s, these infections were routinely and successfully treated with antibiotics. However, the marked ability of *S. aureus* to adapt to different environments, [5, 6] along with the misuse and overuse of antibiotics, aided bacterial evolution and resulted in the rise of methicillin-resistant *S. aureus* (MRSA) strains [7].

The emergence of MRSA has not only complicated the treatment of *S. aureus* infections, but has led it to become one of the most frequent causes of hospital- and community-associated infection [8, 9] with the ability to cause disease in otherwise healthy individuals [9, 10]. In addition, many MRSA isolates have acquired resistance to other antibiotics, including erythromycin (macrolide), clindamycin (lincosamide), ciprofloxacin (fluoroquinolone) and tetracycline (polyketide) [7]. Due to this widespread resistance to antibiotics and a lack of other alternative therapeutics, the glycopeptide vancomycin has become the standard treatment for MRSA [4]. Although most MRSA strains are known to be susceptible to vancomycin, there are certain *S. aureus* isolates that are vancomycin intermediate-resistant (VISA) and are only susceptible to vancomycin at high concentrations [11]. Full vancomycin resistance is extremely uncommon and has developed much slower than resistance to β-lactam antibiotics. However, the continued increase of vancomyin use in the U.S. has raised concerns that selective pressure will cause vancomycin-resistant *S. aureus* (VRSA) strains to become more prevalent and result in a return to the pre-antibiotic era [3, 4, 6, 12]. Recent U.S. estimates indicate MRSA causes approximately 95,000 invasive infections and 19,000 deaths per year, a mortality rate higher than that for HIV, viral hepatitis, tuberculosis and influenza combined, highlighting a need for more therapeutic options to target this elusive pathogen [6].

The mechanism underlying methicillin resistance is the acquisition and insertion of the staphylococcal cassette chromosome *mec* (SCC*mec*) into the chromosome of susceptible strains, protecting these bacteria from the entire class of available β-lactam antibiotics [2, 11]. Currently there are 11 SCC*mec* types, all of which include the *mecA* gene that encodes for the low-affinity penicillin-binding protein PBP2a [13, 14]. β-lactam antibiotics are unable to inhibit PBP2a, in contrast to other *S. aureus* PBP proteins, which leads to resistance. While the high frequency of antibiotic resistant strains contributes to its ability to cause disease, *S. aureus* also expresses several other virulence factors that contribute to its ability to cause disease. For example, nearly all strains of *S. aureus* secrete α- and γ-hemolysins and some leukocidins, whereas a few secrete superantigen toxic shock syndrome toxin (TSST), and the pore-forming toxin Panton-Valentine leukocidin (PVL) [5, 15]. Not only do these virulence determinants aid the organism in evading the host immune system, but can also directly damage leukocytes and host tissues.

Until recently, MRSA cases were mainly the result of healthcare-associated (HA) infections and affected compromised hosts who were chronically ill or had implanted medical devices [16]. However, the incidence of community-acquired MRSA (CA-MRSA) is increasing and affects healthy persons who do not share the same associated risk factors as patients in the hospital [10, 13, 16]. CA-MRSA strains carry the smaller staphylococcal cassette chromosome IV, and many possess PVL genes [10, 17]. Populations at risk for CA-MRSA infection include intravenous drug users, prison inmates, athletes, military personnel, individuals in close contact with MRSA carriers as well as those with a history of boils or skin infections [18-20]. The most commonly isolated strain of CA-MRSA is pulse-field type USA300 [21], which a recent study estimates accounts for about 67% of all invasive CA-MRSA infections [9]. These CA-MRSA strains have been characterized for their increased virulence compared to HA-MRSA counterparts, allowing for their rapid rise and implication in several outbreaks in the U.S. [22, 23]. This increased virulence may be attributed to two prophages not found in other MRSA strains, namely prophages ΦSa2 and ΦSa3, with prophage ΦSa2 encoding for the PVL genes [24]. In particular, prophage ΦSa2 encodes for staphylokinase, staphylococcal complement inhibitor and

S. aureus chemotaxis inhibitory protein (CHIPS), which are all capable of neutralizing innate immune mechanisms for bacterial elimination [25].

Our laboratory has acquired a USA300 clinical isolate and has used this *S. aureus* strain to strengthen the translational impact of studies in our experimental mouse models of biofilm infection. Specifically, this USA300 LAC 13c strain was isolated from a skin and soft tissue infection in a detainee from the Los Angeles County Jail (LAC) and cured of the p01(cryptic plasmid) and p03 (confers erythromycin resistance) plasmids [9, 26]. The USA300-0114 strains are primarily responsible for CA-MRSA infections in the U.S. and predominantly carry the IVa subtype of SCC*mec*, *spa*type YHGFMBQBLO, *msrA*-mediated macrolide resistance and a number of virulence genes, including *lukS-PV/lukF-PV* and *arcA*, coding for PVL and the arginine catabolic mobile element (ACME), respectively [22, 23].

b)   Biofilms

In addition to antibiotic resistance, staphylococci have alternative mechanisms of survival and virulence, among which is biofilm formation [1, 27-29]. Biofilms are defined as adherent communities of bacteria encased within a complex matrix composed of proteins, polysaccharides and eDNA [27-33] often surrounded by a host fibrotic response, and staphylococci are recognized as the most frequent cause of biofilm-associated infections [34]. Specifically, *S. aureus* is capable of forming biofilms on both natural body surfaces, including the lung and heart, as well as medical devices, such as indwelling catheters and prostheses [27, 32, 33, 35]. Although CA-MRSA strains are able to form biofilms, and show recalcitrance to antibiotics, it is believed that the biofilm offers additional protection against antimicrobial agents, and indeed microorganisms within biofilms have a greater resistance to antimicrobial killing than planktonic cells of the same species [32, 36]. This increased resistance may be related to the reduced growth rate of biofilm microorganisms. Cells encased within the biofilm matrix grow much more slowly than planktonic cells, and as a result, take up antimicrobial agents more slowly. In addition, many antibiotics target cell wall synthesis, which is reduced during biofilm growth, causing them to be less effective [28, 33, 36]. Furthermore, the structure of the biofilm and its secreted products interfere with host innate immune responses and proper recognition of biofilm-associated bacteria [32].

Taken together, the resistance to available therapies and evasion of host immune responses has made biofilm infections a significant human health problem.

Biofilm development is a multi-step process that involves initial attachment of bacterial cells to biotic or abiotic surfaces, followed by accumulation or maturation of the biofilm before single cells or larger cell clusters detach from the biofilm mass [29, 34, 37, 38]. Each of these phases are thought to be physiologically different from one another and require phase-specific gene regulation [34]. During initial attachment, an individual planktonic cell will reversibly associate with a surface, and if the cell does not dissociate, it will bind irreversibly to the surface [30]. *S. aureus* has the ability to attach to nearly any indwelling medical device, and this is thought to occur through direct interaction with the device's polymer surface and host matrix proteins that coat implanted devices [37]. Attachment to the plastic or metal surface of an indwelling medical device is driven mostly by hydrophobic or electrostatic interactions initially [38]. However, almost immediately after implantation these devices are coated in host matrix material which greatly enhances bacterial attachment. Staphylococci express microbial surface components recognizing adhesive matrix molecules (MSCRAMMs), surface-anchored proteins that allow for adherence and colonization of devices and host tissue [29, 38]. In addition to MSCRAMMs, teichoic acids and the surface protein autolysin have also been described as being involved in the attachment phase of staphylococcal biofilm development [38].

Once attachment has occurred, proliferation proceeds through the production of an extracellular matrix (ECM) that contributes to intercellular aggregation [29, 37, 38]. Polysaccharide intercellular adhesion (PIA), which covers most staphylococcal cells, is a major component of the ECM and directly mediates biofilm accumulation [34, 38, 39]. PIA is synthesized, exported, and modified by products of the *ica* locus and its importance in biofilm development has been demonstrated in numerous studies [40-43]. Most *S. aureus* strains have the ability to produce PIA; however, some *S. epidermidis* strains lack the *ica* genes and thus do not produce PIA. These strains are able to form biofilms *in vitro* and *in vivo* [39, 44, 45]. In these cases, it is apparent that other surface-associated proteins such as protein A, fibrinogen-binding proteins (FnBPA and FnBPB), *S. aureus* surface protein (SasG), biofilm-associated protein (Bap),

and clumping factor B (Clf B) are also involved in attachment and accumulation [30]. In addition, Aap, teichoic acids, or DNA released from lysed bacteria (eDNA) facilitate cell-cell adhesion [45-47], further demonstrating the complexity of the biofilm maturation process.

Detachment represents the final stage of biofilm development and is often the cause of bloodstream infection, emboli and metastatic spread of bacteria [27, 34]. In clinical settings, biofilms are often thought of as a reservoir for dissemination of microorganisms to other sites in the host. This phase is facilitated by mechanical forces, cessation of the production of biofilm adhesion molecules, or enzymes that destroy the matrix [34]. In *S. aureus*, the rate of biofilm dissemination is thought to be primarily controlled by the accessory gene regulator (Agr), a quorum-sensing system that controls gene expression in a cell-density dependent manner [38]. Agr upregulates the expression of toxins and proteases while downregulating the expression of surface adhesion proteins upon entry into the stationary phase of growth through sensing of a peptide pheromone, autoinducing peptide (AIP) [38]. Detachment is the result of Agr activation expression in the outer layers of the biofilm, while expression in deeper layers could be required for efficient formation of channels necessary for nutrient access [37, 48].

c) **Prosthetic Joint and Catheter-Associated Infections**

The risk of infection is increased by the presence of foreign materials [4], and infections associated with indwelling medical devices are typically caused by microorganisms that grow in biofilms [36]. It is known that only a small number of organisms are needed to colonize an implant [49]. Thus, bacterial strains that are able to form biofilms have an advantage in this setting, as once they adhere they can proliferate and mature to form a biofilm while avoiding detection by the host innate immune system. Often organisms associated with these devices are skin flora inoculated at the time of implantation [49]. Indeed, staphylococcal species like *S. aureus* are among the most common etiologic agents of device-related infections [38, 50], with the incidence of infection due to resistant strains of staphylococci accounting for up to 50% of prosthetic joint infection (PJI) in one study [16]. In some cases, organisms can seed implants hematogenously or through compromised local tissues, particularly during indwelling catheter implantation [49, 51].

The number of joint replacement surgeries has been continuously increasing, and as with any surgical procedure, complications can arise, including failure due to infection. Currently, the rates of PJI following primary procedures range from 1-9% [52]. The seriousness of this complication is due to the formation of biofilms on prosthetic devices and their inherent recalcitrance to traditional antibiotic therapy. Therefore, these chronic infections often require device resection arthroplasty, and two-stage replacement is the current standard-of-care treatment in North America [16, 49]. The two-stage exchange begins with removal of the infected prosthesis and implantation of an antibiotic-impregnated spacer to control infection during the prosthesis-free interval, during which antibiotic therapy is also administered systemically. Six weeks to three months following the first stage, a new prosthesis is inserted during a second procedure [16, 49]. Despite this lengthy process and continued administration of antimicrobial agents, these devices often fail again due to infection. It is estimated that infection rates reach 40% following revision procedures [52]. This failure can be attributed not only to recurrence of the primary organism, but also to infection by novel organisms [16].

Catheters of all types are used in clinical practice to improve the quality of life of chronically and critically ill patients. However, biofilm formation and bloodstream infections are major risks associated with catheter placement [53], and can result in CSF shunt infections [54-56] or catheter-related bloodstream infections in the case of central venous catheters (CVCs). Since the presence of a biofilm on the implant subjects the host to constant dispersal of biofilm-associated cells through the blood stream coupled with the biofilm's resistance to antibiotic therapy, catheter removal is the conventional management for these infections [53]. Although removing CVCs and reinserting another in a different vascular access site carries its own complications, there are currently a limited number of alternative therapeutic options for physicians [53, 57].

d)   Mouse models of biofilm infection

Currently, the two most commonly employed animal models for the study of *S .aureus* biofilm infection are catheter-associated and orthopedic implant-associated infections. These two models have been employed in many different tissues and cavities to examine host-pathogen

interactions under static or dynamic conditions, including subcutaneous, venous and CNS catheter-associated infections [32, 42, 43, 55, 58] as well as orthopedic implants associated with the femur or tibia [28, 59-62].

In general, the orthopedic implant-associated models explore static biofilm growth and host-pathogen interactions at the site of a chronic infection with direct access to the bone marrow, which could have important immunological implications on the course of infection. Furthermore, this model can be used to examine the incidence of implant-associated osteomyelitis, of which *S. aureus* is a leading cause [61]. Careful attention was paid during the development of this model to use materials that would allow for accurate representation of several facets of human disease seen in the clinical setting. Titanium alloys are the most common metals used in total joint arthroplasties, and thus, nickel-titanium wire was selected for the implant material in the orthopedic model utilized in the Kielian laboratory [63].

The subcutaneous catheter model of *S. aureus* biofilm infection used in our laboratory is a static model, which does not recapitulate the sheer forces that a biofilm would encounter in an indwelling intravascular catheter, but does allow for the investigation of various aspects of host-pathogen interactions. This model can also be highly advantageous due to its easy tissue accessibility to monitor infection, straightforward device placement and relatively high-throughput nature compared to orthopedic implant models that require much more laborious surgery [60]. Collectively, these mouse models of infection have allowed for a better understanding of the mechanisms governing the innate immune response to *S. aureus* biofilm infection [32, 59, 60, 62] as well as ways in which bacteria evade this response through the use of bacterial mutant strains and mice deficient for various immune-related molecules. Continued use of these models could potentially allow for the identification of critical disease determinants as well as therapeutic targets to reduce patient morbidity and mortality associated with bacterial biofilm infection.

2) Innate Immune response to *S. aureus* infection

a)   Innate immune recognition of *S. aureus*

Innate immunity represents the first line of defense against invading pathogens and all cells of the innate immune system rely on a set of germ-line encoded pattern recognition

receptors (PRRs) directed against highly conserved pathogen-associated molecular patterns (PAMPs) to elicit a rapid immune response [64]. Perhaps the most common class of PRRs are Toll-like receptors (TLRs), of which thirteen have been identified in humans, and ten in mice [64, 65]. Despite the differences in ligands for each of the TLRs, most utilize a common signaling pathway through MyD88 and NF-κB/MAPK that leads to the transcriptional activation of proinflammatory cytokines and chemokines [66-69]. In terms of gram-positive bacteria and staphylococcal species, TLR2, expressed on the surface of innate immune cells such as monocytes/macrophages and neutrophils, is involved in the recognition of peptidoglycan (PGN) and lipoproteins [70], while TLR9 is an intracellular receptor that recognizes unmethylated CpG motifs characteristic of bacterial DNA [31].

The involvement of TLRs has been implicated in mediating innate immune recognition and elimination of staphylococcal species during planktonic growth [71-75]. TLR2-deficient mice exhibit increased mortality rates during *S. aureus*-induced sepsis, due to a failure in bacterial recognition and decreased proinflammatory cytokine production [72]. However, patients with mutations inactivating TLR2 have no increased risk of developing post-arthroplasty *S. aureus* infection, which agrees with reports from our laboratory and others that have determined biofilms circumvent TLR2 and TLR9 recognition [32, 62]. Unlike during planktonic *S. aureus* infection, TLR2 and TLR9 KO mice display similar biofilm burdens as WT animals and all display attenuated inflammatory mediator expression. These observations indicate that, in the context of indwelling device-associated biofilm infection, bacteria circumvent traditional PRR recognition strategies of innate immune cells and thus also deter downstream proinflammatory responses to invading pathogens [32, 62]. Although TLR2 is essential for *S. aureus* recognition during planktonic infection, the altered growth state *S. aureus* assumes during biofilm infection could determine whether these sensing mechanisms are effective.

Further hindering TLR engagement is the observation that host leukocytes do not form intimate associations with biofilms, both *in vitro* and *in vivo.* This could be due to the fact that biofilms are encased within a complex structure, with few free bacteria exposed on the outer surface, thereby avoiding detection by PRRs [32, 61]. In addition, the biofilm matrix contains

complex polysaccharide polymers that may interfere with engagement of TLR ligands [76]. *S. aureus* is known to produce staphylococcal superantigen-like (SSL) proteins, of which SSL3 has been shown to block TLR2 activation through direct extracellular interaction with the receptor [77]. However, it is possible that *S. aureus* biofilms may be recognized by alternative PRRs. For example, both AIM2 and DNA-dependent activator of IFN-regulatory factors (DAI) can sense eDNA which is a major component of the *S. aureus* biofilm ECM [78, 79]. Muramyl peptide, the degradation production of staphylococcal PGN, can be sensed by the cytoplasmic PRR nucleotide-binding oligomerization domain-containing protein 2 (NOD2) and elicit proinflammatory mediator release independent of TLR signaling [80, 81].

Although TLR2 and TLR9 do not appear to be involved during staphylococcal biofilm infections, a role for IL-1β has been revealed in controlling early bacterial burdens during PJI [62]. IL-1β KO mice displayed enhanced biofilm formation and decreased neutrophil recruitment, which was most pronounced during early time points. This indicates the proinflammatory properties of IL-1β may have a protective role early before a robust biofilm has gained a foothold on the associated implant. Interestingly, both the IL-1 receptor (IL-1R) and TLRs share a common downstream adaptor, myeloid differentiation factor 88 (MyD88), that when activated leads to NF-κB-mediated transcription. Studies from our laboratory have shown that MyD88 greatly influences the course of biofilm infections, as MyD88 KO mice have significantly higher bacterial burdens and decreased expression of several proinflammatory mediators necessary for mounting a robust immune response against *S. aureus* [31]. Taken together, in the context of what is known about TLR and IL-1β signaling during *S. aureus* biofilm infection, MyD88 appears to play a dual role during biofilm infection. Early MyD88 signals are responsible for biofilm containment and MyD88 loss decreases the proinflammatory capacity of effector cells, such as macrophages, that participate in the clearance of planktonic bacteria that would be encountered during biofilm dispersal and dissemination to distant sites in the host [31, 62].

Altogether the understanding of innate immune signaling to biofilm infection and the timing of these signals is poorly understood. There is likely a very concerted series of events following inoculation of planktonic bacteria, adherence and maturation into a robust biofilm

infection. A better understanding of the innate immune recognition mechanisms that are important during all stages of biofilm development is needed in order to determine alternative ways to target the innate immune system and develop alternative therapeutics to combat these persistent biofilm infections.

b)   Neutrophil response to *S. aureus*

In models of planktonic *S. aureus* infection, it has been shown that association of TLR2, MyD88 and the subsequent production of cytokines and chemokines is involved in the recruitment of neutrophils that mediate innate immune responses at infection sites [82]. Neutrophils are a phagocytic cell of the innate immune system and are often considered the first responder to staphylococcal infection, as they rapidly migrate to sites of inflammation [83, 84]. Mediators such as CXCL1 and CXCL2, among others, are produced in response to damage or invading pathogens and bind specific surface receptors on neutrophils directing their extravasation from the circulation. Specifically, *S. aureus* surface components like LTA, and secreted molecules such as staphylococcal enterotoxins and toxic shock syndrome toxin (TSST)-1, have been shown to elicit chemokine production by monocytes and epithelial cells, thereby recruiting neutrophils to the site of *S. aureus* infection [83, 85, 86]. In addition, the complement component C5a is another potent neutrophil chemotactic molecule and *S. aureus* PGN has been shown to directly activate the complement cascade [87].

Once at the site of planktonic infection, neutrophils have the capability to phagocytose bacteria, including *S. aureus.* As mentioned previously, all cells of the innate immune system express PRRs. In terms of neutrophil responses, engagement of these receptors activates pathways critical to microbicidal activity and prolonged cell survival. Neutrophils are perhaps best known for their production of large amounts of reactive oxygen species (ROS) and degranulation. However, they also secrete proinflammatory cytokines and chemokines, including TNF-α, IL-1β, CXCL2, CXCL11 and CCL3 [31, 88, 89], and have a vast arsenal of anti-microbial peptides such as α-defensins, cathelicidins, cathepsins, and lysozyme that also play a role in neutrophil-mediated immunity [83, 90]. Because these cells possess high cytotoxic capacity and proinflammatory potential, regulation of cell turnover is essential for maintaining homeostasis.

This is accomplished through apoptosis [83]. In the context of infection, where neutrophils are recruited and activated, apoptosis is accelerated and the clearance of apoptotic neutrophils by macrophages is thought to play a key role in the resolution of the inflammatory response [83, 91].

Despite the large arsenal of weapons neutrophils possess to combat invading bacteria, many pathogens have evolved mechanisms to evade neutrophil-mediated host defense strategies. Indeed, *S. aureus* can actively avoid destruction by neutrophils and survive to cause devastating disease. One of the most fundamental features of *S. aureus'* ability to cause infection is the secretion of toxins. α-hemolysin (Hla) is the major cytotoxic exotoxin secreted by *S. aureus,* and functions by binding to a disintegrin and metalloprotease 10 (ADAM10), initiating cytolytic pore formation [92]. In addition, γ-hemolysin and PVL are known to preferentially target and lyse leukocytes [3, 93]. Furthermore, *S. aureus* expresses extracellular adherence proteins (Eap) that bind and inhibit intercellular adhesion molecule-1 (ICAM-1), the endothelial receptor required to initiate leukocyte adhesion and diapedisis from the vasculature [93, 94], and about 60% of *S. aureus* strains are known to secrete the chemotaxis inhibitory protein of staphylococci (CHIPS), which binds to chemokine receptors and inhibits neutrophil recruitment to sites of infection [3, 93]. *S. aureus* blocks complement activation and resists phagocytosis through the production of surface-associated anti-opsonic proteins, like protein A, and a polysaccharide capsule [3, 93]. There is also evidence to suggest that CA-MRSA strains can induce programmed necrosis of neutrophils following phagocytosis, which some consider to be a component of enhanced virulence, since a large proinflammatory response to lysed neutrophils is avoided and the bacteria can go undetected longer within the intracellular compartment [95].

Although *S. aureus* possesses a wide variety of subversion strategies, neutrophils can still exert bactericidal activity under planktonic conditions [70, 96, 97]. However, the direct role of these cells in modulating *S. aureus* biofilm infection is less understood. Some *in vitro* studies, using both static and flow cell biofilms, have suggested that neutrophils are capable of migrating toward and clear the biofilm by phagocytosis [98, 99]. But, the extent of clearance depended on the maturation state of the biofilm, with developing young biofilms being more sensitive to neutrophils than more mature biofilms [99]. It is possible that immature biofilms have more

associated planktonic bacteria, as the structure is still developing, which could account for the effectiveness of a neutrophils. It would be presumed then that a mature biofilm has fewer planktonic cells associated with it and is thereby protected from this response. In addition, many of these studies have only been performed *in vitro*, and our laboratory has shown that several inflammatory signals responsible for recruitment and activation of innate immune cells are attenuated *in vivo* and biofilm-infected tissues have limited numbers of infiltrating neutrophils [32, 59, 60, 100]. This calls into question the *in vivo* relevance of an effective neutrophil response to biofilms. Indeed, studies in our laboratory using adoptive transfer of neutrophils into tissues surrounding catheter-associated biofilms *in vivo* showed these cells were not able to clear biofilm-associated bacteria. Although there have been reports that increasing numbers of neutrophils are present during *S. aureus* post-arthroplasty infection [62], neutrophils were quantified based on H&E staining or EGFP-fluorescent signals from LysM-GFP mice [62]. Furthermore, the use of Ly6G alone is not a good marker for neutrophil populations, due to overlap with immature precursor populations like MDSCs. Therefore, many of these methods have resulted in possible inaccurate quantitation of neutrophil cell numbers present at the site of *S. aureus* infection.

c)   **Macrophage response to *S. aureus***

Along with neutrophils, macrophages are an important innate immune effector cell critical for defense against acute planktonic staphylococcal infection. To date, however, the majority of studies investigating innate immunity to *S. aureus* have focused on neutrophils, and therefore much less is known about macrophage responses during staphylococcal infection. Neutrophils have potent microbicidal activity, but are short-lived and require rapid cell turnover in addition to a limited capacity to produce inflammatory cytokines and chemokines. Macrophages, on the other hand, have important and diverse roles in regulating tissue homeostasis by eliminating apoptotic cells and recycling nutrients by eliminating waste products from tissues [101-103]. Additionally, they are critical for an effective immune responses and produce high levels of proinflammatory mediators that amplify immune cell recruitment/activation cascades [32, 104, 105]. Macrophages are derived from bone marrow precursors of the granulocytic-monocytic lineage that develop into monocytes. Monocytes remain in the bone marrow < 24 h before entering the systemic

circulation. Only after monocytes cross endothelial venules and enter tissue do they transition into macrophages [103]. Unlike neutrophils, nearly all tissues contain resident macrophages and these cells can serve as critical first line defenders against invading microbes [32, 106, 107]. Normally resident macrophages are relatively quiescent, but they can be readily activated by a variety of stimuli during the immune response, in part through their Toll-like and scavenger receptors [103].

Macrophages can exhibit both pro- and anti-inflammatory properties and are generally characterized based on gene expression patterns and cytokine secretion. But these phenotypes are driven largely by the environment in which a macrophage is found and stimuli they encounter, which results in a great deal of plasticity within a macrophage population [101, 103]. Some polarization signals may include apoptotic cells, hormones, immune complexes, cytokines and bacteria-associated PAMPs [103]. It is thought that stimulation by microbial products elicits the production of proinflammatory cytokines like IL-1, IL-6, IL-12, and TNF-α, as well as nitric oxide (NO) and various chemokines, which are generally associated with protective responses and bacterial clearance [101, 108-110]. However, inflammation is a tightly regulated process, and macrophages can become more anti-inflammatory and pro-fibrotic, producing multiple inhibitors and antagonists, like IL-10 and arginase-1 (Arg-1), which suppress activation and proinflammatory mediator production in addition to lowering microbicidal activity [111]. Further compounding this complexity, pathogenic bacteria have developed mechanisms, including biofilm formation, to interfere with or alter macrophage phenotypes in an effort to enhance survival and promote persistence within the host, as described below.

Previous reports have shown that mixed leukocyte and purified neutrophil populations are capable of infiltrating biofilms [98, 112], and our laboratory has demonstrated that macrophages are also able to invade these structures to some extent [32]. However, macrophages displayed a limited ability to phagocytose *S. aureus* biofilm-associated bacteria *in vitro* and *in vivo*. In fact, the majority of macrophages that invaded *S. aureus* biofilms *in vitro* were dead compared to those that remained above the biofilm surface [31, 32]. The reasons for this could be due to several factors. First, biofilms appear to secrete factors that limit the phagocytic potential of

macrophages. Macrophages incubated with conditioned supernatants from *S. aureus* biofilms *in vitro* were unable to phagocytose latex beads or planktonic bacteria, which were readily internalized by untreated macrophages [31]. Second, the sheer size and complex organization of the biofilm structure could inhibit phagocytosis of biofilm-associated bacteria, as it exceeds the size of a macrophage by several orders of magnitude, and macrophages were capable of phagocytosing bacteria from mechanically disrupted biofilms [32]. Even if macrophages do phagocytose some bacteria, *S. aureus* gene products have been associated with the detoxification of ROS and RNS. Thus, *S. aureus* can survive and grow within macrophages [113]. These phenomena could have significant implications during biofilm infections, as macrophages would be impaired in their ability to scavenge dead cell/debris or contribute to tissue remodeling in the vicinity of the biofilm and contribute to biofilm persistence *in vivo* [31].

There is also emerging evidence that suggests staphylococcal biofilms actively skew host immunity toward an anti-inflammatory, pro-fibrotic response that favors bacterial persistence [31, 32, 114]. Studies from our laboratory have shown preferential accumulation of anti-inflammatory macrophages in the *S. aureus* biofilm milieu, both *in vitro* and *in vivo* [31, 32, 61]. These cells have decreased inducible nitric oxide (iNOS) expression, while Arg-1 is increased. Both iNOS and Arg-1 compete for arginine to initiate their respective biosynthetic pathways, and a preferential induction of Arg-1 in biofilm-associated macrophages likely results in skewing the immune response away from bacterial killing [31, 32]. Increased Arg-1 activity has implications beyond innate immune responses as well. For example, Arg-1 leads to L-proline production, which is a precursor in the collagen biosynthetic pathway [115, 116], and studies from our laboratory have shown increased Arg-1 expression associated with pro-fibrotic macrophage responses to *S. aureus* biofilms *in vivo* [32, 117]. Arginine can regulate T cell proliferation and effector functions; therefore, arginine depletion from the environment results in defective TCR signaling through inhibition of CD3ζ expression, cell cycle, and cytokine production. Indeed, our laboratory has found few T cell infiltrates associated with different models of biofilm infection, including human post-arthroplasty implants and cranial bone flap biofilm infection [32, 59, 100, 118]. Currently, there is still a lot to learn regarding the bacteria- and host-derived factors that

play a role in eliciting macrophage dysfunction and its greater impact on the whole immune response to *S. aureus* biofilm infection.

3)   Myeloid-derived suppressor cells

Myeloid-derived suppressor cells (MDSCs) are a heterogeneous population of myeloid progenitor cells, including immature monocytes and granulocytes [119-123]. MDSCs are known for their ability to augment Arg-1 expression, which inhibits T cell effector responses, and also anti-inflammatory cytokine production that polarizes macrophages toward an immunosuppressive phenotype. Our laboratory has shown that *S. aureus* biofilms augment Arg-1 expression *in vivo* and skew macrophages toward an anti-inflammatory state that correlates with a failure to recruit T cells to the site of infection [32]. In addition, T cells are not recruited to sites of PJIs in humans [59]. Therefore, MDSC infiltrates could be responsible for promoting the anti-inflammatory milieu during *S. aureus* biofilm infection.

The role of MDSCs in cancer has been extensively studied; however, accumulation of these cells has also been reported during other pathologic conditions, including bacterial, parasitic and viral infection, acute and chronic inflammation, and traumatic stress [124, 125], and is considered essential to immune regulation [126]. MDSCs can be generated in response to a wide variety of cytokines, which has made deciphering the signals required for their induction very difficult to ascertain and often context-specific. For example, it has been demonstrated in cancer that the precise nature of an MDSC population depends on the tumor itself and host tumor-derived factors [127]. Some studies have shown that the phenotype and suppressive ability of MDSCs is context dependent, and in our studies we have determined that although MDSCs are suppressive when recovered from the site of biofilm infection, MDSCs from the spleen of infected mice do not have the ability to inhibit T cell proliferation [60]. Therefore, understanding of the mechanisms involved in MDSC induction during staphylococcal infection and the role these cells play in the local environment as opposed to systemic sites will be critical to developing novel targets and therapeutics that limit bacterial persistence.

a)   History, nomenclature and definition of phenotypic markers

There has been an emerging interest in the past five decades in understanding the role of suppressor cells as a critical mediator of health and disease, although this has not been without some debate. Natural suppressor (NS) cells were first reported in tumor-bearing mice in the mid-1960s [128, 129], as they actively suppressed anti-tumor responses like T cell proliferation, antibody production and CTL induction to promote immune evasion [129]. Interestingly, NS activity was a characteristic of multiple cell populations from different hematopoietic sites, including the spleen and bone marrow. NS cells were found to be increased by tumor secretions as well as exogenous administration of growth factors like GM-CSF and G-CSF, and were observed in the bone marrow of naïve mice, although they lacked suppressive activity.

Over time, similar observations were made in other tissues and types of cancer, which led NS cells to also be identified by several other monikers, including immune myeloid cells, suppressor macrophages, immature myeloid cells, and most recently MDSCs [130]. This led to controversy over whether they really existed at all [129]. Suppressor cells had started to gain appreciation in extramedullary hematopoiesis and increased neutrophil numbers in tumor-bearing animals, and were later shown to inhibit lymphocyte numbers and cytotoxic activity [131]. But the lack of a defined set of markers surface to positively identify MDSCs caused confusion. After the Gr-1$^+$CD11b$^+$ phenotype was suggested a general agreement was reached that these cells do in fact exist and are distinct from monocytes and granulocytes based on their suppressive activity [32, 132-134]. Finally in 2007, a letter was published by Gabrilovich et al [125] in an effort to end the nomenclature controversy for good, and MDSC was chosen as the term for this immature, immunosuppressive cell population.

Despite the amount of heterogeneity, all MDSCs in mice lack markers of mature myeloid cells, but express both Gr-1 and CD11b [120-123, 126, 130, 131, 135, 136]. Although the Gr-1$^+$CD11b$^+$ population as a whole displays properties characteristic of MDSCs, this surface marker combination makes it difficult to discern the phenotype of the suppressive cell population in a given pathologic condition. This is because the Gr-1 epitope encompasses both Ly6G and Ly6C molecules, and therefore cannot distinguish between monocyte- and granulocyte-like subsets within the whole Gr-1$^+$ population [126].

Based on this differential expression of Ly6G and Ly6C, MDSCs in mice can be divided into two main subsets: granulocytic and monocytic MDSCs (G-MDSCs and M-MDSCs, respectively). In general, G-MDSCs have a CD11b$^+$Ly6G$^+$Ly6C^{low} phenotype, whereas monocytic MDSCs are CD11b$^+$Ly6G$^-$Ly6C^{high}, although there is some variability in the degree to which these markers are expressed [119, 124, 129-131]. In addition to their different surface marker expression, it is thought that these two subsets also have alternate mechanisms of suppressing T cell responses, utilizing NOS2 and Arg-1 differentially to induce immunosuppression [129, 137].

b)   Human MDSCs

MDSCs have also been described in humans, initially in patients with head and neck cancer that were identified by CD24 expression and T cell suppression [138-140]. But ultimately, this classification of MDSCs rendered them indistinguishable from hematopoietic progenitor cells [129]. Unlike mice, humans do not express Gr-1, Ly6G or Ly6C, and therefore, the markers for human MDSCs are different and not as straightforward as in the murine system. For quite some time the human MDSC phenotype was described by negative expression of human leukocyte antigen D-related (HLA-DR) and either or both of the common myeloid markers CD11b or CD33 [139]. Recently, more specific marker subsets have been defined allowing G- and M-MDSCs to be identified in humans. The G-MDSC phenotype in humans is identified as HLA-DR$^-$ CD11b$^+$CD33$^+$CD14$^-$CD15$^+$, whereas M-MDSCs correspond to HLA-DR$^{-/low}$CD11b$^+$CD33$^+$CD14$^+$ [129, 131].

c)   Function of MDSCs in health and disease

MDSCs are the intermediates of normal myeloid development and differentiation stages. The hematopoietic system continually cycles through a small population of pluripotent hematopoietic stem cells (HSCs) to balance self-renewal and differentiation [129] as the numbers of functionally mature myeloid cells must be maintained. [130]. Immature cells expressing the Gr-1$^+$CD11b$^+$ phenotype are maintained at relatively low levels in murine bone marrow (i.e. 20-30%) [130, 131]. In healthy individuals MDSCs do not expand, instead, HSCs and immature myeloid cells are generated primarily in the bone marrow and quickly differentiate into mature granulocytes, macrophages or DCs [129-131, 137]. However, excessive inflammatory mediator

production leads to increased mobilization of mature myeloid cells, which creates niche spaces in the bone marrow reservoir and skews differentiation from mature myeloid cells toward MDSC expansion. Therefore, dysregulated myelopoiesis is considered a prerequisite for MDSC expansion [130].

Disturbances in cytokine homeostasis induced by cancer, infection, or other immune stresses can alter the equilibrium of MDSCs, leading to their accumulation in lymphoid organs and blood [120, 130]. Instead of one factor, GM-CSF for instance, being responsible for both the differentiation and activation of MDSCs, it is now though that two signals are responsible for these processes and are governed by different signal transduction pathways [121, 137]. The first process of MDSC expansion is induced by various cytokines and growth factors produced by tumors, cells responding to infectious agents, or chronic stimulation. These factors can include GM-CSF, M-CSF, G-CSF, IL-6, VEGF, and signals are primarily directed through signal transducer and activator of transcription 3 (STAT3) and STAT5. MDSCs then require a second activating signal that endows their functional characteristics, which manifests as increased Arg-1, NO, and production of immune suppressive cytokines [121]. This type of signaling is provided by proinflammtory molecules like IFN-γ, IL-1β, IL-13, TLR ligands, etc., and utilizes STAT1 and NF-κB transcription factors as well as COX2 [121]. The two-signal model for MDSC expansion and activation explains why steady-state activation of STAT3 and STAT5 in response to growth factors required for normal hematopoiesis does not result in MDSC accumulation in the absence of strong proinflammatory signals, and also explains why acute inflammation, associated with release of proinflammatory factors in the absence of growth factors, also does not augment MDSC recruitment [121].

Activation of MDSCs in pathologic conditions results in their ability to suppress immune responses *in vitro* and *in vivo* [127, 131, 137], including the inhibition of T cell activation and polarization of macrophages toward an anti-inflammatory phenotype . The mechanisms underlying the inhibitory activity of MDSCs range from those requiring cell-cell contact to others that are mediated through the modification of the microenvironment. Indeed, MDSCs have been shown to suppress immune responses through direct and indirect mechanisms [141].

In terms of direct MDSC inhibition, the main proposed mechanisms are NO and ROS production, arginine depletion, secretion of immunosuppressive cytokines such as TGF-β and IL-10 as well as induction of apoptosis meditated by the FAS-FASL pathway [119, 124, 132, 142-145]. In particular, increased iNOS or Arg-1 activity in MDSCs leads to enhanced arginine catabolism, thereby depleting this non-essential amino acid from the environment. A shortage of L-arg inhibits T cell proliferation through several different mechanisms, including decreasing expression of CD3ζ and preventing T cell upregulation of the cell cycle regulators cyclin D3 and cyclin-dependent kinase 4 [137]. Furthermore, the hyperproduction of ROS by MDSCs has been shown to directly disrupt antigen-specific CD8 T cell responses through nitration of tyrosines that interfere with TCR-CD8 complex interaction with MHC [146].

MDSCs are able to suppress indirectly by inducing the development of other cell types with immune suppressor function, including regulatory T cells (Tregs) and anti-inflammatory macrophages [120, 147, 148]. The secretion of immunosuppressive cytokines, like IL-10, by MDSCs can transform the environment in a way that favors the development of these cell types. Tregs and anti-inflammatory macrophages can then go on to produce more anti-inflammatory cytokines, including IL-10, representing a positive feedback loop to propagate immune suppressive activity. MDSC secretion of IL-10 in other models has been shown to downregulate IL-12 production in macrophages [135]. Additionally, cell contact-dependent cross-talk between MDSCs and macrophages has also been reported to occur in tumors [135].

d)   MDSCs and *S. aureus* biofilm infection

As MDSCs are found to be involved in more and more areas of health and disease, the debate over whether they are beneficial or deleterious to host immunity against invading pathogens continues [130]. It is apparent that the immunosuppressive, anti-inflammatory properties of MDSCs could be beneficial under certain circumstances but, to date, no one has identified the tipping point of when these responses become harmful or ways to intervene. During infection it is believed that immature myeloid cells in the bone marrow are recruited to sites of inflammation to replace damaged or exhausted cells, but factors within the local environment,

host- or pathogen-derived, arrest these cells in an immature state and the inflammatory signals present lead to their acquisition of immunosuppressive properties [130].

Our laboratory was the first to demonstrate a role for MDSCs during *S. aureus* infection [60]. MDSCs infiltrating *S. aureus* biofilms were capable of inhibiting T cell proliferation and expressed genes typical of MDSCs described under other pathologic conditions, including Arg-1, iNOS and IL-10. Manipulation of MDSCs with Ab depletion strategies demonstrated that their immunosuppressive function prevents monocytes/macrophages from eliminating biofilm-associated bacteria by attenuating their proinflammatory properties. More recent studies have shown that IL-12 is critical for MDSC recruitment to the site of *S. aureus* PJI and that IL-10 is one mechanism used by MDSCs to exert immunosuppressive functions. Additional details regarding these studies can be found in Chapters 3, 4 and 5 of the dissertation.

During initial stages of infection MDSCs could be protective by limiting tissue damage during potentially overwhelming inflammation [130, 149]. Indeed, a study has shown that depletion of MDSCs during early severe sepsis reduced survival, suggesting they do play an immunoprotective role this this disease setting [150]. However, while early sepsis is proinflammatory, late sepsis is characterized as an anti-inflammatory state and MDSCs contribute greatly to this shift. MDSCs have been observed to secrete copious amounts of IL-10 during late sepsis [123]. Furthermore, it has been reported that T cells play a protective role in a model of systemic *S. aureus* infection. However, they lose their ability to respond to bacterial Ags with the transition from acute infection to persistence and exhibit a dysfunctional state characteristic of suppression by MDSCs [149]. All of these findings demonstrate that MDSCs have a very dynamic role during infection and it is not surprising that bacteria have evolved mechanisms to manipulate immune-regulatory mechanisms to promote their long-term survival [149, 150].

4)   Overview of Dissertation

Initial experiments from our laboratory demonstrated that biofilm infections skew the host innate immune response toward an anti-inflammatory phenotype that allows them to subvert immune clearance mechanisms [32]. Not only do the bacteria circumvent traditional bacterial recognition pathways mediated through TLRs, but also alter the macrophage response leading to

significant Arg-1 production, which has been associated with bacterial persistence. In addition to Arg-1^{+} macrophages being found in close proximity to the catheter surface, other non-macrophage cells were also Arg-1^{+}. This led us to investigate the possibility that biofilms induce the immature, immunosuppressive population of MDSCs to accumulate at the site of infection. In addition, we have also attempted to augment macrophage proinflammatory responses to biofilm infection through therapeutic approaches, including treatment with EP67 and administration of pro-inflammatory macrophages to biofilm-infected tissues.

During the course of my research, I have identified a *bona fide* MDSC infiltrate during *S. aureus* biofilm infection, which could be a result of the biofilm hijacking the immune response to inhibit the formation of mature antimicrobial leukocyte effectors and instead polarize endogenous monocytes and macrophages toward an anti-inflammatory phenotype [59, 60, 129]. There is evidence to suggest that the combination of MDSC recruitment and anti-inflammatory macrophages during *S. aureus* biofilm infection likely contributes to the biofilm persistence. Indeed, we have demonstrated that anywhere from 10^3-10^5 viable organisms can be detected 3 months after infection in both the mouse orthopedic implant- and catheter-associated biofilm infection models, which accurately recapitulates the persistent nature of implant-associated biofilm infections in humans [59, 60]. Our laboratory has demonstrated that our mouse model of orthopedic biofilm infection mimics several aspects of human PJI. For example, very few T cells are associated with PJI, whereas the main cellular infiltrate into aseptic tissues are T cells. Furthermore, a population of MDSC-like cells expressing genes characteristic of MDSC described in other models has been found in human PJI tissues [59]. However, the main objective of this research is to identify the mechanisms used by MDSCs to exert their immunosuppressive functions. My research demonstrates the complexity of MDSC responses and highlights the role of both pro- and anti-inflammatory mediators (IL-12 and IL-10, respectively) during different phases of biofilm development.

<u>Chapter 2: Materials and Methods</u>

1) Mouse strains

A breeding colony of C57BL/6 mice was established in Dr. Kielian's laboratory upon purchasing animals from the National Cancer Institute (Frederick, MD) or Jackson Laboratories (Bar Harbor, ME). These studies were performed in strict accordance with recommendations found in the *Guide for the Care and Use of Laboratory Animals* of the National Institutes of Health (NIH) and were reviewed by the Institutional Animal Care and Use Committee of the University of Nebraska Medical Center.

IL-12p40 KO mice were purchased from The Jackson Laboratory (Bar Harbor, ME, stock number 002693, B6.129S1-Il12b[tm1Jm]/J). A targeting vector containing a PGK-neomycin cassette was used to disrupt part of exon 3 in the *Il12b* gene. Homozygous mice have a severely restricted ability to mount Th1 responses while Th2 responses are enhanced.

IL-12p35 KO mice were purchased from The Jackson Laboratory (Bar Harbor, ME; stock number 002692, B6.129S1-Il12a[tm1Jm]/J) and were generated by replacing exons 1 and 2 of the gene with a neomycin resistance cassette. These KO mice fail to show any delayed-type hypersensitivity (DTH) reaction, and are therefore useful in studying resistance to infection.

IL-23p19 KO mice were provided by Genentech (South San Francisco, CA)

IL-10 KO (stock number 002251, B6.129P2-Il10[tm1Cgn]/J) and IL-10-GFP reporter mice (stock number 008379, B6.129S6-Il10[tm1Flv]/J) were purchased from The Jackson Laboratory (Bar Harbor, ME). The IL-10 gene was disrupted in 129/Ola-derived embryonic stem (ES) cells by replacing codons 5-55 of the first exon by a linker, providing a termination codon and a *neo* gene, and by introducing a termination codon into exon 3. Transfected cells were injected into C57BL/6 blastocysts. Mice homozygous for the *Il10* gene mutation do not produce IL-10 and completely lack IL-10 activity [151], which impacts immunosuppressive mechanisms of the innate and adaptive immune systems. IL-10-GFP mice have an internal ribosome entry site-green

fluorescent protein (IRES-GFP) cassette followed by a *loxP*-flanked neomycin cassette between the stop codon and polyadenylation signal of exon 5 of the gene. This allows for the detection and monitoring of cells committed to IL-10 production.

MyD88 KO mice were originally obtained from Dr. S. Akira (Osaka University, Suita, Osaka, Japan) and were backcrossed with C57BL/6 mice for > 10 generations [152-154]. The *Myd88*-deficient allele encodes a deletion of exon 3 of the myeloid differentiation primary response 88 gene. MyD88 is a cytosolic adaptor protein that plays a central role in the innate and adaptive immune response, and is required to limit bacterial burdens and prolong survival during infection.

CXCR2 KO (stock number 006848, B6.129S2(C)-Cxcr2^{tm1Mwm}/J) mice were purchased from The Jackson Laboratory (Bar Harbor, ME). The CXCR2 gene was knocked out with a neomycin selection cassette that replaced the entire coding sequence of the gene. Homozygous mice have several abnormalities, including neurological defects, impaired wound healing, impaired angiogenesis, altered growth of induced/implanted tumors, splenomegaly and increased susceptibility to various pathogens due to impaired granulocyte recruitment and decreased pathogen clearance during innate immune responses.

2) Bacterial strains and microbiological techniques

Bacterial strains

The USA300 LAC strain of *Staphylococcus aureus* (*S. aureus*) is a community-acquired methicillin-resistant (CA-MRSA) isolate kindly provided by Dr. Frank DeLeo (National Institute of Allergy and Infectious Diseases Rocky Mountain Laboratories, Hamilton, MT). This strain was isolated from the Los Angeles county (LAC) jail inmate with a skin and soft tissue infection and was also responsible for the CA-MRSA outbreak of 2002 [26]. This *S. aureus* strain contains two plasmids, p01 and p03 and the USA300 LAC 13c strain used in the Kielian laboratory has been cured of the erythromycin-resistance plasmid.

For *in vitro* biofilms, USA300 LAC was transformed with the plasmid pCM11 to express GFP driven by the *sarA* P1 promoter (USA300 LAC-GFP), and plasmid expression was maintained with erm selection (10 µg/ml). For *in vivo* studies, USA 300 LAC 13c chromosomally transduced with the bacterial luciferase gene *lux* was used and will be referred to as USA300 LAC::*lux* throughout.

Bacterial storage

Bacterial strains were stored at -80°C in the form of glycerol stocks, prepared by growing bacteria to exponential phase in brain-heart infusion broth (BHI, Fisher Scientific, Pittsburgh, PA) followed by centrifugation at 2,400 rpm for 10 min, 4°C. The pellet was resuspended in 10ml of ice-cold 1X PBS and washed by centrifuging again at 2,400 rpm for 10 min, 4°C. After discarding the supernatant, the pellet was resuspended in 20% glycerol in 1X PBS and this bacterial-glycerol suspension was aliquoted into appropriately labeled cryovials and stored at -80°C.

A new streak plate was made prior to each experiment in an effort to avoid mutation of bacteria by prolonged dormancy at 4°C.

Preparation of bacteria for in vitro experiments

For experimental purposes, overnight cultures were grown by selecting a single bacterial colony from the streak plate using a sterile disposable loop and inoculating BHI in a baffled flask at a 10:1 flask:volume ratio. Inoculations were incubated at 37°C with constant shaking at 250 rpm for 12-16 h. The following day, bacterial titers were determined by plating onto blood agar plates and heat-inactivated bacteria was prepared by incubating a portion of the stock at 55°C for 60 min, with vortexing every 15 min. This heat-inactivated stock was aliquoted and stored at -80°C for future use. In addition, the heat-killed bacterial suspension was plated onto blood agar plates to confirm the absence of growth before being used for experiments.

In vitro S. aureus biofilms

Overnight cultures were grown by selecting a single colony from a streak plate and inoculating 4 ml Complete Biofilm Media (RPMI 1640, 10% FBS, L-glut, Erm10 [for GFP bacteria only], HEPES) with overnight incubation at 37°C with constant shaking (250 rpm). Two-well glass-chamber slides (Nunc, Rochester, NY) were coated with 2 ml per well of 20% human plasma in

sterile carbonate-bicarbonate buffer (Sigma-Aldrich, St. Louis, MO) and incubated overnight at 4°C. The following day, plasma-coating buffer was removed, chambers were inoculated with bacteria (diluted to an OD_{600} of 0.05 in 2 mls) and incubated at 37°C under static aerobic conditions for 6 days. Each day following slide inoculation, 700 µl of spent medium was removed from each well and 1 ml of fresh biofilm medium was added.

Preparation of bacteria for in vivo experiments

A single colony of from a streak plate was grown overnight for 12-16 h at 37°C in a 250 ml baffled flask containing 25 ml of autoclaved BHI broth (10:1 flask:volume ratio) with constant shaking (250rpm). The overnight culture was diluted 1:10 in BHI and the following day the number of planktonic bacteria present was determined by measuring the O.D. (BioMate 3S Spectrophotometer, Thermo Scientific, Waltham, MA) at 620 nm. In addition, 1 ml of the overnight culture was transferred into a 1.5 ml Eppendorf microcentrifuge tube and centrifuged at 14,000 rpm, 4°C for 5 min to pellet the bacteria. The supernatant was removed and the pellet was resuspended in 1 ml PBS and subsequently washed two more times by centrifuging at 14,000 rpm for 5 min, 4°C. To prepare inoculum for injection, the washed culture was diluted in sterile PBS after estimating the CFU/ml of the overnight culture. If the overnight culture was estimated at 3.2×10^9 CFU/ml, two subsequent 1:100 dilutions would follow:

$$1:100 \text{ dilution} = 3.2 \times 10^7 \text{ CFU/ml}$$
$$1:100 \text{ dilution} = 3.2 \times 10^5 \text{ CFU/ml}$$

An equation was then used to determine the amount of diluted culture needed to inject 1×10^3 CFU in 20 µl (5×10^4/ml):

$$(3.2 \times 10^5 \text{ CFU/ml}) * x = 5 \times 10^4 \text{ CFU/ml} * 1\text{ml}$$
$$x = 0.156 \text{ ml in } 0.844\text{ml PBS}$$
$$\text{or}$$
$$x = 156 \text{ µl of diluted } 10^5 \text{ culture} + 844 \text{ µl PBS}$$

The exact concentration of cells/ml in the overnight culture was determined following preparation of bacteria for infection by diluting the washed culture in triplicate as follows:

10^{-2}	20µl of the 1ml washed overnight culture into 180 µl PBS
10^{-3}	20 µl of 10^{-2} dilution into 180 µl PBS
10^{-4}	20 µl of 10^{-3} dilution into 180 µl PBS
10^{-5}	20 µl of 10^{-4} dilution into 180 µl PBS
10^{-6}	20 µl of 10^{-5} dilution into 180 µl PBS
10^{-7}	20 µl of 10^{-6} dilution into 180 µl PBS

$$10^{-8} \qquad 20 \ \mu l \ of \ 10^{-7} \ dilution \ into \ 180 \ \mu l \ PBS$$

100 µl of the 10^{-7} and 10^{-8} dilutions were plated onto blood agar plates and counted the following day. The number of bacteria was enumerated and plate counts were averaged to determine the actual CFU used for infection.

3) Cell culture techniques

Primary mouse bone marrow-derived macrophage (BMDMΦ) culture

Adult C57BL/6 WT and MyD88 KO were euthanized with an overdose of inhaled isoflurane (Isothesia, VetUS, Dublin, OH) using a euthanasia chamber and cervical dislocation was performed as the secondary form of euthanasia. The abdominal surface of the mouse was flooded with 70% EtOH, to prevent fur from contaminating specimens and a subcutaneous incision was made near the midline of the abdomen. Skin was separated from the peritoneum until all hind limbs were exposed and excess muscle was dissected away. Hind limbs were removed at the hip joint and immediately submerged in a petri dish containing 70% EtOH before being kept in 1X PBS on ice. Using Kimwipes, excess connective tissue and muscle was removed from the bone surface and clean bones were placed in fresh 1X PBS. At this point, the entire procedure was carried out under aseptic conditions in a biological safety cabinet with sterile autoclaved instruments. Both ends of the bones were cut with scissors and bone marrow was flushed with sterile DMEM and a 26-gague needle. The bone marrow effluent was collected in a 50 ml conical tube. Once all bones were flushed, cells were pipetted to disrupt cell aggregates, filtered through a 70 µm cell strainer and centrifuged at 1,200 rpm for 5 min, 4°C. The supernatant was aspirated and red blood cells were lysed by adding 500 µl sterile water for 5 sec, followed by immediate addition of 100 µl 10X PBS. Next, cells were washed with medium, centrifuged, and counted using trypan blue (Lonza, Walkersville, Germany) on a hemacytometer. Cells were seeded in 175 mm tissue culture dishes at a density of 1×10^7 cells / plate in 20 mls of media. BMDMΦ media was composed of Dulbecco's modified eagle's medium (DMEM, 4.5 g/L glucose supplemented with 4mM L-glutamine) containing heat-inactivated fetal bovine serum (10% v/v FBS, HyClone, Logan, UT; inactivated at 55°C for 30 min, with swirling at 10 min

intervals), 20% sL929 (ATCC) supernatant as a source of macrophage colony stimulating factor (M-CSF) (Whetton et al Biochim Biophys Acta, 1989), 1% v/v HEPES (1 M stock), 1% v/v Glutamine (200 mM stock, both HyClone, South Logan, UT), 0.1% v/v 50 mM Beta-mercaptoethanol (Fisher Scientific, Pittsburgh, PA) and antibiotic-antimycotic solution (10,000 IU/ml Penicillin, 10,000 μg/ml Streptomycin, 25 μg/ml Amphotericin B, final 1% v/v, Mediatech Inc., Manassas, VA). Medium was replaced on cultures at days 2, 4 and 6 after initial plating and cells were harvested on day 7 for subsequent experimentation.

Primary mouse bone marrow-derived neutrophil culture

Adult C57BL/6 or MyD88 KO mice were euthanized, bone marrow was isolated as previously described and placed on a three-layer Percoll gradient (Amersham Pharmacia Biotech, Uppsala, Sweeden). After filtering, cells were centrifuged at 400g for 10 min, 4°C, resuspended in 3ml of 78% Stock Isotonic Percoll (SIP, 100% SIP [9 parts Percoll to 1 part 10X PBS] in 1X PBS). Next, 3 ml of 69% SIP was layered on top followed by 3 ml of 52% SIP. This three-layer gradient was centrifuged at 1500g for 30 min, 15°C with no brake. Cells from the upper phases were discarded and neutrophils were collected from the 68% / 78% interface and upper part of the 78% layer. Harvested cells were washed with PBS, centrifuged (400g, 10 min, 4°C), resuspended in 1 ml 1X Lysing Buffer (BD Pharm Lyse, BD Biosciences, Franklin Lakes, NJ) and incubated at room temperature for 2 min. HBSS with 10% FBS was added to stop lysing reaction and cells were centrifuged (400g, 10 min, 4°C) before being resuspended in 2 ml buffer for magnetic-activated cell sorting (MACS, PBS without Ca, Mg, + 2% FBS), vortexed and counted with trypan blue on a hemacytometer. Magnetic labeling was done using the Miltenyi anti-Ly6G MicroBead Kit (Miltenyi Biotec, San Diego, CA) according to the manufacturer's instructions. Magnetic separation was performed using an MS column on a MACS Separator. Columns were prepared by rinsing with 500 μl buffer, whereupon the cell suspension was added onto the column. Unlabeled cells were collected by washing the column 3X with 500 μl of buffer, then the column was removed from the separator and placed over a collection tube. Buffer was flushed through the column with a plunger to elute the fraction of labeled cells. Cells were counted and at least 600,000 Ly6G$^+$ cells

were removed to check purity by flow cytometry, while the remaining cells were used for co-cultures with *S. aureus* biofilms.

Primary mouse bone marrow-derived MDSC culture

Adult C57BL/6, IL-10 KO or IL-12p40 KO mice were euthanized and bone marrow was isolated as previously described. After lysing RBCs, cells were washed and resuspended RPMI-1640 medium supplemented with 10% v/v HI FBS, 1% v/v HEPES, 1% v/v L-Glut, 0.1% v/v antibiotic-antimycotic solution, 40 ng/ml G-CSF and 40 ng/ml GM-CSF (both from Peprotech, Rocky Hill, NJ). 10^7 bone marrow cells were plated into 175mm dishes in 20 mls of media and incubated for 4 d at 37°C, 5% CO_2. The $Ly6G^+Ly6C^+$ MDSC population was purified from the mixed cell population by FACS and verified to possess T cell inhibitory activity.

4) Immune cell co-culture with *S. aureus* biofilms *in vitro*

BMDMΦs and neutrophils were labeled with either 5 μM CellTracker Orange or CellTracker Blue (both from Molecular Probes, San Diego, CA) depending on the experimental set up. Labeling was conducted following the manufacturer's instructions. After labelling, some BMDMΦ were activated toward an M1 phenotype by treating with 10 ng/ml IFN-γ or 100 ng/ml TNF-α and 10 μg/ml *S. aureus*-derived peptidoglycan (PGN) for 6 h. Cells were co-cultured with *S. aureus* biofilms by first removing 700 μl of spent medium and then adding 1 ml of fresh biofilm media containing 10^7 neutrophils, nonactivated MΦ or M1-activated MΦ to the biofilms. Co-cultures were incubated at 37°C under static conditions and imaged using a Zeiss 510 META laser scanning microscope (Carl Zeiss, Oberkochen, Germany) at 2 and 24 h following the addition of immune cells. Neutrophil- and MΦ-biofilm co-cultures were harvested 24 h after immune cell addition by mechanical disruption, whereupon bacterial enumeration was performed by serial dilution on tryptic soy agar plates supplemented with 5% sheep blood (Hemostat Laboratories, Dixon, CA).

5) Mouse models of *S. aureus* biofilm infection

Subcutaneous catheter-associated biofilm infection

Age and sex-matched mice (8-10 weeks old) were used to examine the immune response to *S. aureus* catheter-associated biofilm infection. Mice were weighed and anesthetized with Avertin (15 µl/g, 2.5% solution, Sigma-Aldrich, St. Louis, MO) by intraperitoneal (i.p.) injection. Once anesthetized, the left flank was shaved and the skin was cleaned and disinfected with povidone-iodine. Next, a small subcutaneous (s.c.) incision was made in the left flank and a blunt probe was used to create a pocket for the insertion of a sterile, 14-gauge teflon intravenous catheter, 1 cm in length (Exel International, St. Petersburg, FL). The incision was sealed using Vetbond Tissue Adhesive (3M, St. Paul, MN) and 10^3 CFU USA300 LAC::*lux* in 20 µl of sterile PBS was slowly injected through the skin, directly into the catheter lumen using a 27 gauge x ½" needle. Eye ointment (LubriFresh™ P.M., Major Pharmaceuticals, Livonia, MI) was placed on all mice before they were returned to clean cages and kept under heat lamps to maintain core body temperature until fully recovered from anesthesia. Cages were labeled with orange biohazard cards and monitored daily throughout the course of infection.

Orthopedic implant biofilm infection

Age and sex-matched mice (8-10 weeks old) were used to simulate infectious complications in patients following surgical device placement. Animals were weighed and anesthetized with ketamine/xylazine (100 mg/kg and 5 mg/kg, respectively) by i.p. injection before the surgical site was shaved and disinfected with povidone-iodine. A medial parapatellar arthrotomy with lateral displacement of the quandriceps-patella was performed to access the distal femur. Next, the femoral intercondylar notch was located and a burr hole was drilled into the intramedullary canal using a 26-gague needle, whereupon an orthopedic-grade Kirschner wire (0.6 mm diameter, Nitinol [nickel-titanium]; Custom Wire Technologies, Port Washington, WI) precut to 0.8-cm was inserted. Approximately 1 mm of K-wire was left protruding into the joint space and a total of 10^3 CFU of the USA300 LAC::*lux* isolate was inoculated at the implant tip. The quadriceps-patellar complex was reduced to the midline and the fascia was sutured with 6-0 metric absorbable sutures before the skin of the surgical site was closed with 6-0 metric nylon sutures (both from Covidien, Mansfield, MA). In some experiments, control mice received sterile implants using an identical procedure. All animals received Buprenex, (0.1 mg/kg s.c.; Reckitt Benckiser, Hull, U.K.)

for pain relief immediately following the surgical procedure, before being returned to clean cages to under a heat lamp to ensure maintenance of core body temperature until fully recovered from anesthesia. Cages were labeled with orange biohazard cards and monitored daily. A second dose of Buprenex was administered 24 h after surgery and after this interval, all mice exhibited normal ambulation and no discernable pain behaviors.

6) Computed tomography

Bone integrity in the context of aseptic implants, *S. aureus* biofilm infection and Gr-1$^+$ cell depletion was monitored using live computed tomography (CT) scans. Mice were first anesthetized with 1.5% isoflurane in a 70% nitrous oxide/30% oxygen mixture and imaged using a FLEX Triumph x-ray CT/single photon emission CT system and software (TriFoil Imaging, Northridge, CA). One thousand twenty-four CT projections for each image were acquired at 75 kVp and reconstructed using Truimph X-0 4.1. CT images were generated using the three-dimensional image visualization and analysis software VIVID, which is based on Amira 4.1 (TriFoil Imaging).

7) Recovery of implant-associated tissues for *S. aureus* enumeration

Recovery of subcutaneous catheters and surrounding tissues

Animals were sacrificed by overdose of inhaled isoflurane, followed by cervical dislocation. The left flank was sterilized with a povidone-iodine prep pad to prevent potential sample contamination with skin microflora. The section of the flank containing the catheter and associated tissue was removed, whereupon the catheter was separated from the surrounding host tissue and placed in 1 ml PBS on ice. Tissue surrounding the catheter was also collected, weighed and placed in 500 µl homogenization buffer (25 ml of 1X PBS q.s., pH 7.4, 1 Complete™ protease inhibitor cocktail tablet) on ice. In some experiments, the kidney and heart were also collected. These organs were excised, weighed and kept on ice in 500 µl PBS to determine the amount of bacterial dissemination. Once all tissues were removed catheters were sonicated for 5 min on ice while catheter-associated tissue and any organs collected were homogenized using a

Bullet Blender (Next Advance, Averill Park, NY). Serial dilutions of the effluents and homogenates were plated on TSA supplemented with 5% sheep blood to determine bacterial colonization. Bacterial titers were expressed as Log_{10} CFU/ml for catheters or Log_{10} cfu/g wet tissue weight for catheter-associated tissues and other organs.

Recovery of orthopedic implants and surrounding tissues

For collecting inflamed soft tissue surrounding the infected knee joint, animals were euthanized by overdose of inhaled isoflurane, followed by cervical dislocation. The flank and left leg were then flooded with 70% EtOH and an incision was made in the skin so the skin of the left leg could be removed. Next, the subcutaneous tissue dorsal to the patellar tendon was excised, weighed and placed in 500 µl 1X PBS + 2% FBS on ice. Muscle and tendon tissues were excluded from the analysis. This tissue was dissociated with the blunt end of a plunger from a 30-cc syringe and passed through a 35 µm filter (BD Falcon, Bedford, MA). An aliquot of 150 µl was removed at this point for quantitation of bacterial burdens and Milliplex analysis of the supernatant. The remaining filtrated was further processed for flow cytometer as described below. Next, the muscle was cleaned away from the knee joint and femur. The knee joint was separated from the femur allowing for removal of the implant, which was extracted from the femur and sonicated for 5 min in 1 ml 1X PBS on ice to dislodge adherent bacteria. Both the knee joint and femur were weighed and placed in 500 µl homogenization buffer before being homogenized using two sequential procedures. First, tissues were homogenized with a Polytron homogenizer at the highest setting for approximately 30 s. Then tissues were further dissociated using a Bullet Blender. Serial dilutions of effluents from the tissue, joint, femur and implant were plated on TSA supplemented with 5% sheep blood to determine bacterial colonization. For some experiments, the spleen, heart and kidneys were collected to determine the degree of splenomegaly or bacterial dissemination as described above.

Tissues from human prosthetic joint infections (PJIs)

Excess tissues from patients undergoing joint revisions for PJI, or aseptic loosening as controls, were procured by orthopedic surgeons at the University of Nebraska Medical Center. Informed consent was obtained during the presurgical visit and the protocol was approved by the

Institutional Review Board (IRB) of the University of Nebraska Medical Center. Upon excision, tissues were placed in sterile PBS on ice and dissociated using Nitex mesh and a mortar and pestle, before being washed and subsequently stained for FACS analysis as described below.

8) Scanning electron microscopy

Mice were sacrificed and the whole femur harboring the titanium implant was fixed in 0.1 M Sorenson's phosphate buffer containing 2% glutaraldehyde and 2% paraformaldehyde for 1 h at room temperature and held in fixative overnight at 4°C. Fixed specimens were washed three times in TBS followed by three rinses in double distilled (dd)H_2O and decalcification in 14% EDTA for 2d. After rinsing in ddH_2O, specimens were dehydrated using a graded series of ethanol washes and critical point dried in a Pelco CPD2 critical point dryer (Tel Pella, Redding, CA). Dried specimens were mounted on aluminum stubs with carbon tabs and colloidal silver paste before being sputter coated with gold-palladium using a Hummer VI sputter coater (Anatech, Battle Creek, MI). Samples were viewed using a Quanta 200 scanning microscope (FEI, Hillsboro, OR) operated at 25 kV.

9) Immunohistochemistry

Decalcification of femurs for histological evaluation

In order for histological analysis to be performed in the *S. aureus* orthopedic implant model of infection tissues first had to be decalcified. To this end, the whole right leg (femur/knee/tibia) was excised, leaving muscle and soft tissue intact, placed into a tube containing enough 10% formalin to completely cover the tissue and fixed for at least 72 h at room temperature. Formalin was discarded and tissues were washed thoroughly in distilled water. After washing, tubes were filled with enough decalcifier solution (Super Decalcifier I: Delicate, Polysciences, Warrington, PA), to cover the tissue and placed on a rocker at room temperature for 4-6 h to completely decalcify tissue. Following decalcification, tissue was washed 3X with water, before an incision was made in the quadriceps and femur to access and remove the implant. Decalcified tissues were placed in

a histo-cassette and kept in 10% formalin or PBS before being embedded in paraffin and cut into

4 µm sagittal sections.

Deparaffinizing and antigen retrieval

Mice were sacrificed and the section of the flank containing the catheter and associated tissue

was removed as previously described. The catheter and associated tissues were cut in half with a

razor blade, left intact, and transferred to a cassette. Tissues were fixed in 10% formalin and

embedded in paraffin, whereupon 10-µm thick sections were cut by the UNMC Histology Core.

Embedded sections were deparaffinized using the protocol described in Table 9.1.

Table 2.1. Tissue deparaffinization protocol

STATION	REAGENT	TIME
1	Xylene	5 min
2	Xylene	5 min
3	Xylene	5 min
4	100% EtOH	1 min
5	100% EtOH	1 min
6	95% EtOH	1 min
7	70% EtOH	5-10 dips
8	Water	Clear

This process was followed by antigen retrieval, whereupon deparaffinized slides were placed in

sodium citrate solution (10 mM sodium citrate [1.47g sodium citrate in 500 ml dH_2O], 0.05%

Tween 20, pH 6). Slides were completely submerged in the buffer and placed in a plastic bowl

filled 1/3 with water and microwaved for 14 min at power 7. Cooled slides were placed in PBS.

Hematoxylin and Eosin (H&E) staining

Rapid H&E staining was performed on deparaffinized tissue using the protocol described in Table

9.2. Coplin jars with screw caps were used for the procedure.

Alcohol-formalin-acetic acid solution (Fixative) was prepared with 10 ml of 37% formalin, 90 ml of

80% EtOH and 5 ml of glacial acetic acid. Alcoholic eosin stock (Fisher Scientific, Pittsburgh, PA)

was diluted 1:3 with 70% EtOH to prepare the working solution. Harris Modified Hematoxylin

(Fisher Scientific, Pittsburgh, PA) was used undiluted.

For evaluation of pathological conditions during *S. aureus* orthopedic biofilm infection H&E-

stained tissues were evaluated for inflammatory changes by a board certified pathologist (Jessica

A. Kozel, University of Nebraska Medical Center) with the degree of inflammation determined

using a scoring scale (0, no observable pathology; 1, minimal pathology; 2, moderate pathology;

3, severe pathology). Splenic architecture following Ab-mediated cell depletion was also

performed. Spleens were fixed in 10% formalin, paraffin-embedded and sectioned for H&E

staining as described above.

Table 2.2. Rapid Hematoxylin and Eosin staining protocol

STATION	REAGENT	TIME
1	Fixative	30-60 seconds
2	70% EtOH	Rinse briefly
3	Water	Rinse briefly
4	Harris hematoxylin	10-15 seconds
5	Water	Rinse briefly
6	Alcoholic eosin	Counterstain 2 min
7	95% EtOH (fresh)	Dehydrate 5-10 dips
8	95% EtOH (fresh)	Dehydrate 5-10 dips
9	Absolute EtOH	Dehydrate 5-10 dips
10	Absolute EtOH	Dehydrate 5-10 dips
11	Xylene	Clear
12	Xylene	Clear

Gram-staining

Bacteria associated with infected joints were visualized on deparaffinized tissue sections using

the protocol described in Table 9.3.

Table 2.3. Gram-staining protocol

STATION	REAGENT	TIME
1	Crystal Violet	1 min
2	Water	Rinse
3	Gram's Iodine Solution	5 min
4	Water	Rinse
5	100% EtOH	5-6 dips
6	Water	Rinse
7	Safranin	30-60 sec
8	Water	Rinse
9	100% EtOH	Rinse
10	100% EtOH	Rinse
11	Xylene	Clear

Fluorescence staining and confocal microscopy

Tissues surrounding infected catheters were processed for immunofluorescence staining using

primary antibodies specific for the MΦ marker Iba-1 (Biocare Medical, Concord, CA) and

arginase-1 (Arg-1, Santa Cruz Biotechnology, San Diego, CA). First, a pap pen was used to mark around sections and slides were blocked in 10% donkey serum/PBS for 30 min. Blocking serum was drained, primary antibodies were added to sections following dilution in 2% donkey serum (Arg-1, 1:50; Iba-1, 1:100) and slides were incubated overnight, 4°C. The following day, slides were washed three times in PBS for 5 min and donkey anti-rabbit FITC (1:100), donkey anti-rabbit biotin (1:500) (Jackson ImmunoResearch Laboratories, West Grove, PA) with a streptavidin-594 conjugate (Invitrogen, Carlsbad, CA) and Hoescht (1:100) secondary antibodies were added. Slides were incubated for 30 min in the dark, whereupon the fluorescence labeling was shaken off and 0.1% Sudan Black solution was put on top of each section for 15 min in the dark. Subsequently, slides were washed 3X with PBS + 0.3% Tween 20 for 10 min per wash and then coverslipped with Slow Fade® (Life Technologies, Carlsbad, CA). Confocal imaging was performed using a Zeiss 510 META laser scanning microscope (Carl Zeiss). Staining specificity was confirmed by incubating tissues with a primary isotype-matched control antibody and appropriate secondary antibody. Quantitation of Arg-1 or Iba-1 fluorescence was calculated from at least 10 random fields of view using AxioVision software 4.8 (Carl Zeiss).

10) Flow cytometry

Mouse tissues

Fluorescence-activated cell sorting (FACS) was used to characterize leukocyte infiltrates in inflamed soft tissues surrounding subcutaneous catheter or orthopedic implants during *S. aureus* biofilm infection. Animals were sacrificed with an overdose of inhaled isoflurane, tissues were excised as previously described and placed in 500 µl FACS buffer (2% FBS in PBS) on ice. Tissues were dissociated with the blunt end of a plunger from a 30cc syringe, and passed through a 35 µm filter (BD Falcon, Bedford, MA). Following removal of an aliquot for bacterial quantitation and Milliplex analysis, the filtrate was washed with 1X PBS and cells were collected by centrifugation (1200rpm, 5 min, 4°C), whereupon RBCs were lysed using BD Pharm Lyse (BD Biosciences, San Diego, CA) per manufacturer instructions. After lysis, cells were resuspended in 500 µl 1X PBS followed by incubation in Fc Block (2 µl / sample, eBioscience, San Diego, CA) for

20 min at 4°C to minimize nonspecific antibody binding.100 µl of each sample was pooled and subsequently aliquoted into compensation and isotype control tubes to identify gating thresholds and assess the degree of nonspecific staining, respectively. The remaining 400 µl was split into two tubes and q.s. to 500 µl with 1X PBS. Cells were then stained with directly-conjugated antibodies for multi-color flow cytometry analysis, which included two separate panels to identify innate immune populations or T cells. Antibodies in the innate immune cell panel included: CD45-APC, Ly6G-PE, Ly6C-PerCP-Cy5.5, and F4/80 PE-Cy7. Antibodies in the T cell panel included: CD3ε-APC, CD4-Pacific Blue, CD8a-FITC, Ly6C-PerCP-Cy5.5, and TCR γδ-PE. All fluorchrome-conjugated antibodies were purchased from either BD Biosciences or eBioscience. To exclude dead cells from analysis, a Live/Dead Fixable Stain Kit (Life Technologies, Eugene, OR) was also used, following the manufacturer's instructions. Analysis was performed using BD FACSDiva software with cells gated on the life CD45$^+$ leukocyte population.

Human tissues

Immediately post-excision, surgical specimens were placed in isotonic saline on ice and rapidly processed. Tissues were weighed, and placed on a piece of 250 µm Nitex mesh and dissociated with a mortar and pestle in HBSS + 10% FBS. Cells were collected and washed 2X with HBSS + 10% FBS, whereupon they were resuspended in 4 mls HBSS and layered over 3 ml of Ficoll-Paque gradient and centrifuged according to manufacturer's instructions (GE Healthcare, Uppsala, Sweden) Leukocytes were collected from the interface, washed 2X in HBSS + 10% FBS, resuspended in 500 µl HBSS and counted. Cells were then incubated with Human FcR Receptor Binding Inhibitor (eBioscience, San Diego, CA) to minimize non-specific antibody binding for 20 min, 4°C. Next, cells were stained with directly-conjugated antibodies for multi-color flow cytometry analysis for 30 min, 4°C. Antibodies included anti-human CD66b-FITC (BioLegend, San Diego, CA), CD14-PE, CD16-allyphycocyanin, CD33-PECy5, HLA-DR-PE-Cy7, CD45-eFluor450, CD3-APC-Cy7, CD11b-BV510 and CD11c-BV605. All fluorochrome-conjugated antibodies were purchased from either BD or eBioscience unless otherwise noted. To exclude dead cells from analysis, a Live/Dead Fixable Stain Kit (Life Technologies, Eugene, OR) was used according to the manufacturer's instructions. Controls included cells stained with isotype

control antibodies to assess the degree of non-specific staining and compensation beads stained with the same antibodies were used to identify gating thresholds. Analysis was performed using BD FACSDiva software with cells gated on the live CD45$^+$ leukocyte population.

11) Recovery of biofilm-associated MDSCs and *in vitro* assays

Cells were collected from the soft tissue surrounding infected knee joints as described above, and MDSCs were purified by FACS using either Gr-1-PE and CD11b-FITC or Ly6G-PE, Ly6C-PerCP-Cy5.5 and CD11b-eFluor450 depending on the experimental setup. CD11b$^+$Gr-1$^+$ MDSCs were also FACS-purified from the spleens of naïve and *S. aureus*-infected animals for comparisons. The purity of MDSC populations was not examined after sorting owing to limiting cell numbers. However, cytospins and gene expression analysis on sorted populations revealed that sorted MDSCs were highly enriched, as they displayed characteristic markers and nuclear morphologies consistent with those reported for MDSCs in the literature.

In vitro MΦ and MDSC experiments

To assess differences in proinflammatory responses of MΦ and MDSCs, Ly6G$^+$Ly6C$^+$ MDSCs were isolated from *S. aureus* implant-associated tissues or spleens at day 14 by FACS as described above, while BMDMΦ were prepared as previously outlined. MΦ, tissue MDSCs or splenic MDSCs were plated at 5×10^4 cells / well in a round bottom 96-well plate and stimulated with either peptidoglycan (10 μg/ml) or heat-inactivated *S. aureus* (10^7 / well) for 24 h at 37°C, 5%CO_2. After the 24 h incubation period, supernatants were collected and stored at -80°C until Milliplex analysis.

Polyclonal CD4$^+$ proliferation assays

Naïve C57BL/6 WT mice were euthanized with an overdose of inhaled isoflurane, whereupon their flanks were flooded with 70% EtOH and spleens were isolated from the peritoneal cavity and placed into PBS + 10% FBS on ice. Spleens were then pressed through a 250 μm Nitex filter (Genesee, San Diego, CA) to generate a single cell suspension, centrifuged at 1200 rpm for 10 min, 4°C and RBCs were lysed using BD Pharm Lyse (BD Biosciences, San Diego, CA) per the manufacturer's instructions. After lysis, cells were washed, resuspended in 1X PBS + 2% FBS

and incubated in Fc Block (2 µl / 1 x 10^6 cells) for 20 min, 4°C. Splenocytes were subsequently

stained with CD4-Alexa700 (BD Biosciences) and the Live/Dead Fixable Stain Kit, per the

manufacturer's instructions, for 30 min, 4°C. Viable $CD4^+$ T cells were purified by FACS and then

labeled with eFluor 670 cell proliferation dye (eBioscience) according to the manufacturer's

instructions.

For establishing the functional activity of MDSCs associated with *S. aureus* orthopedic biofilm

infections, T cell proliferation assays were performed. eFluor 670-labeled $CD4^+$ T cells were

plated at 1.5 x 10^6 cells/well in a 96-well round bottom plate in RPMI 1640 with 10% FBS,

supplemented with 100 ng/ml recombinant mouse IL-2 (Invitrogen, Frederick, MD). FACS-purified

$CD11b^+Gr-1^+$, $Ly6G^{high}Ly6C^+$, $Ly6G^{low}Ly6C^{low}$, or $Ly6G^-Ly6C^+$ cells were obtained from *S. aureus*-

infected tissues as described above and added at 1:1 or 5:1 ratios to $CD4^+$ T cells. Co-cultures

were subjected to polyclonal stimulation by adding 4 µl / well CD3/CD28 Dynabeads (Life

Technologies, Oslo, Norway). Negative controls of labeled T cells only or labeled T cells

incubated with Dynabeads were also included. Cells were incubated at 37°C for 72 h, whereupon

the extent of T cell proliferation was determined by flow cytometry and supernatants were saved

for cytokine evaluation by Milliplex analysis.

12) Adoptive Transfer Experiments

***Macrophage adoptive transfer into biofilm infections* in vivo**

The subcutaneous catheter model of *S. aureus* biofilm infection was used, as previously

described, to assess the ability of BMDMΦ and neutrophils to attenuate biofilm growth *in vivo.*

WT or MyD88 KO BMDMΦ were isolated as previously described. After 7 d of culture, an aliquot

of WT MΦ was reserved in BMDMΦ media for nonactivated treatment. The remaining WT and

MyD88 KO MΦ were then activated toward an M1 phenotype by incubating with 10 ng/ml IFN-γ

and 10 µg/ml *S. aureus*-derived PGN for 6 h in BMDMΦ media. Meanwhile, neutrophils were

isolated from WT bone marrow as described above. Mice then received injections of 10^6

neutrophils, nonactivated MΦ, or M1-activated WT or MyD88 KO MΦ at four distinct sites (Fig

2.1) surrounding infected catheters beginning at 12 h post-infection, with repeat administration at 24 and 48 h post-infection.
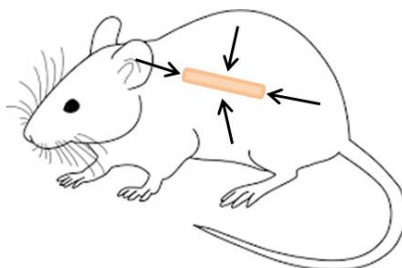
Figure 2.1. Subcutaneous injection sites for treatment of *S. aureus* biofilms *in vivo.*

To determine the longevity of early MΦ treatment on inhibiting biofilm growth, a separate cohort of animals received injections of M1-activated MΦ at only 48 h post-infection. Furthermore, in some experiments, the numbers of injected neutrophils was increased by 1-log (i.e., 10^7) to confirm their inability to impact biofilm clearance.

For treatment of established biofilms, mice received injections of vehicle (PBS), 10^6 nonactivated MΦ, 10^6 M1-activated MΦ or antibiotic (i.p.; rifampicin and daptomycin; 0.125 and 0.25 mg/kg, respectively) on days 7 and 9 post-infection. Animals were sacrificed on day 14 post-infection as described above.

Quantum Dot Labeling of MΦ

To determine the longevity of M1-activated MΦ following transfer into biofilms *in vivo* near-infrared Quantum dots (Qtracker 800; Molecular Probes) were used. BMDMΦ were isolated and activated as described above before being labeled with Qdots according to the manufacturer's instructions. Once labeled, mice were given a single s.c. injection of 10^7 M1-activated MΦ at the ends of the catheter at 24 h or 7 d post-infection for the early and established biofilm paradigms, respectively. Mice were monitored daily using an *in vivo* imaging system (IVIS Spectrum; Caliper Life Sciences, Hopkinton, MA).

MDSC Adoptive Transfer Experiments

MDSCs were generated from the bone marrow of C57BL/6 WT or IL-10 KO mice and the Ly6G$^+$Ly6C$^+$ population was purified by FACS as previously described. Ly6G$^+$Ly6C$^+$ MDSCs

were washed and resuspended in 1X PBS at 2.5 x 10^6 cells / 5 µl. Depending on the

experimental setup, WT MDSCs were injected s.c. into IL-12p40 KO mice at the site of implant-

associated infection one day post-infection, or WT and IL-10 KO MDSCs were injected into IL-10

KO mice at day 7 post-infection. Implant associated tissues from IL-12p40 animals that received

adoptively transferred MDSCs were recovered at day 7 post-infection, while tissues from IL-10

KO animals receiving WT or IL-10 KO MDSCs were collected at day 14 post-infection for analysis

of immune infiltrates by FACS and quantitation of bacterial burdens as described above.

13) EP67 synthesis and treatment

EP67 is a peptide derived from the C-terminal portion of human C5a and is a well-characterized

agonist for the mouse C5aR (CD88). EP67 [YSFKDMP(meL)aR] and its inactive scrambled

sequence [sEP67; (meL)RMYKPa FDS] were generated by a solid-phase Fmoc method of

orthogonal synthesis and purified by analytical and preparative reverse-phase HPLC in the

laboratory of Dr. Sam Sanderson at the University of Nebraska Medical Center. The peptide was

characterized by electrospray mass spectrometry according to previously published methods

(Phillips et al 2009 Bioconjug Chem). Animals were treated with either 200 µg EP67 or the

inactive scrambled derivative (sEP67) directly into the catheter lumen at the time of *S. aureus*

infecteion followed by 800 µg peptide distributed equally at four different sites surrounding the

catheter at 24 and 48 h post-infection (Figure 2.1). To limit animal numbers, sEP67 was not used

in all experiments, because initial studies established that this control peptide did not exert any

biological activity. Animals were sacrificed at days 3 or 14 post-infection for quantitation of

bacterial burdens, as well as Milliplex analysis as described above.

14) *In vivo* depletion studies

MDSCs were depleted *in vivo* during *S. aureus* orthopedic biofilm infection using two approaches.

Either 1A8 (anti-Ly6G), which effectively depletes neutrophils and MDSCs, or RB6-C85 (anti-Gr-

1), which targets both Ly6G and Ly6C epitopes thereby targeting monocytes, neutrophils, MΦ,

plasmycytoid dendritic cells and some T Cell populations, antibodies were used. Antibodies were

administered i.p. (100 µg / each) 1 d prior to *S. aureus* infection and continued every 72 h
thereafter until animals were sacrificed. Control mice received equivalent amounts of isotype-
matched control antibodies (rat IgG2a and IgG2b, respectively) using the same treatment
regimen. All antibodies were purchased in low endotoxin, azide-free form from BioLegend (San
Diego, CA).

Animals were euthanized at 7 or 14 days post-infection to determine the impact of cell depletion
on *S. aureus* persistence and tissue-associated leukocyte infiltrates. Bone marrow and
splenocytes were also collected to determine the efficiency of antibody-mediated depletion.

15) RNA isolation and Quantitative Real-time Polymerase Chain Reaction (qRT-PCR)

RNA isolation from FACS-purified cell populations

MDSCs or monocytes were purified from *S. aureus*-infected tissues by FACS, whereupon total
RNA was immediately isolated using the TaqMan gene expression cell-to-CT kit (Ambion, Austin,
TX). RT and Preamplification reactions were conducted according to the manufacturer's
instructions using a Bio-Rad CFX Connect™ thermocycler.

RNA isolation from whole tissue

RNA isolation was performed on tissue isolated from catheter-associated tissue or orthopedic
implant associated-tissue and knee joints. Tissues were excised from animals following
euthanasia and immediately placed in 0.5 ml TriZol reagent (Life Technologies, Grand Island,
NY), whereupon they were homogenized using a Polytron homogenizer at the highest setting for
approximately 30 s and immediately cooled on ice. Once homogenized, samples were incubated
at room temperature for 10 min to disrupt nuclear complexes. Next, 200 µl of chloroform was
added to each tube, and samples were vortexed for 30 s and incubated at room temperature for 5
min. Samples were then centrifuged at 10,500 rpm for 15 min, 4°C. Three distinct layers were
visible, with the top aqueous phase containing RNA. This layer was carefully transferred to a new
1.5 ml tube and the RNA was precipitated by adding 500 µl of isopropanol to each tube. Samples
were vortexed for 30 s, incubated at room temperature for 10 min, and centrifuged at 10,500 rpm
for 10 min, 4°C, which resulted in a compact, white RNA pellet at the side of each tube. The

supernatant was carefully removed and the RNA pellets were subsequently washed by adding

900 μl cold 75% EtOH to each tube, followed by centrifugation at 6,500 rpm for 5 min, 4°C.

Supernatants were again removed and pellets were air-dried on ice for 5 min before being

resuspended in 30 μl of Diethylpyrocarbonate (DPEC) water or molecular grade RNase-free

water. RNA was heated at 55°C for 10 min on a heating block to dissolve the RNA, whereupon

samples were stored at -80°C. RNA quantification was performed using a NanoDrop Lite

spectrophotometer (Thermo Scientific, Waltham, MA).

Fold-changes in gene expression were evaluated by qRT-PCR. First, 2 μg of total RNA was

treated with DNase (Invitrogen, San Diego, CA). Reaction buffer and RNase-free water was

added and samples were incubated at room temperature for 15 minutes to degrade any

contaminating DNA. DNase was inactivated by adding 1 μl of 25 mM EDTA and heating at 65°C

for 10 min. Reverse transcription (RT) reactions were performed using the iScript™ cDNA

synthesis kit (Bio-Rad, Hercules, CA) per the manufacturer's instructions. A Bio-Rad CFX

Connect™ thermocycler (Bio-Rad, Hercules, CA) was used for cDNA synthesis with the following

parameters: 5 min, 25°C; 30 min, 42°C; 5 min, 85°C; and hold at 4°C until samples were

removed.

qRT-PCR

cDNA samples or preamplified products were diluted 1:2 or 1:4, depending on number of cells

recovered by FACS, in molecular grade water. qRT-PCR was performed on diluted samples

using ABI "Assays on Demand" Taqman primer/probe sets for each specified gene. Universal

PCR cycling conditions optimized for ABI primer/probe sets were utilized (95°C, 10 min; 95°C, 15

s; 60°C, 1 min – 40 cycles of steps 2 and 3). For accurate calculation of expression levels, the

cycle threshold for a particular gene was normalized against the housekeeping gene GAPDH,

and was represented as a fold-induction ($2^{-\Delta\Delta Ct}$) value relative to the control sample for a

particular experiment.

16) MILLIPLEX multi-analyte bead array

Mouse

To evaluate a variety of cytokines/chemokines in the supernatants of catheter-associated tissues, or orthopedic implant-associated tissues, knee joints and femurs, a custom-designed microbead array was utilized according to the manufacturer's instructions (Milliplex; Millipore, Billerica, MA). The particular array used allows for the simultaneous detection of 25 different inflammatory molecules in a single homogenate, and include: G-CSF (Granulocyte colony-stimulating factor), GM-CSF (Granulocyte macrophage colony-stimulating factor), IFN-γ, IL-1α, IL-1β, IL-2, IL-4, IL-5, IL-6, IL-7, IL-9, IL-10, IL-12p70, IL-13, IL-15, IL-17, CCL2 (Monocyte chemoattractant protein 1, MCP-1), CCL3 (Macrophage inflammatory protein 1α, MIP-1α), CCL5 (Regulated upon activated T cell expressed and secreted, RANTES), CXCL1 (Keratinocyte chemoattractant, KC), CXCL2 (MIP-2), CXCL9 (Monokine induced by IFN-γ, MIG), CXCL10 (IFN-induced protein 10, IP-10), TNF-α, and VEGF (Vascular endothelial growth factor). Results were analyzed on the Bio-Plex workstation (Bio-Rad, Hercules, CA) and adjusted based on the total amount of protein extracted from tissue homogenates, determined by a Bicinchoninic acid assay (BCA, Bio-Rad).

Human

For analysis of human PJI tissue specimens, a human 38-plex panel was used to evaluate a variety of cytokines/chemokines in the supernatants of tissue associated with aseptic or infected implants and included: epidermal growth factor, fibroblast growth factor-2, Flt-3L, G-CSF, GM-CSF, IFN-α2, IFN-γ, IL-1α, IL-1β, IL-1ra, IL-2, IL-3, IL-4, IL-5, IL-6, IL-7, IL-8, IL-9, IL-10, IL-12p40, IL-12p70, IL-13, IL-15, IL-17, CX3CL1, CCL2, CCL3, CCL4, CCL7, CCL11, CCL22, CXCL1, CXCL10, soluble CD40L, TGF-α, TGF-β, TNF-α, and vascular endothelial growth factor. Results were analyzed using a Bio-Plex Workstation (Bio-Rad, Hercules, CA) and normalized based on the amount of total protein to account for differences in tissue sampling size. The level of sensitivity for most analytes in the array was 3.2 pg/ml.

17) Enzyme-linked Immunosorbent Assay (ELISA)

In addition to the MILLIPLEX assay, cytokine detection was also performed using ELISAs. For these assays, samples were diluted to fall within the standard curve and the procedure was conducted according to the manufacturers protocol (DuoSet, R&D Systems, Minneapolis, MN;

OPtEIA set, BD Pharmingen, San Diego, CA). In general, 96-well ELISA plates were coated with antibody diluted in a coating solution and incubated overnight at 4°C. The following day, the coating solution was removed and the plate was washed 3X using the appropriate washing buffer specified for each ELISA kit. After a blocking step, wells were washed and samples or standards were added for 2 h at room temperature. The solutions were decanted and the plate was thoroughly washed before incubation with a secondary antibody preparation in combination with streptavidin-horseradish peroxidase (HRP) enzyme solution diluted in assay buffer for 1 h. Following another thorough wash, the enzyme substrate (TMB substrate reagent, BD OPtEIA, San Diego, CA) was added, resulting in color change within 15-20 min. The reaction was stopped by adding 50 μl of 2N H_2SO_4 (Fisher Scientific, Pittsburgh, PA) and the plate was read at specified wavelengths using a spectrophotometer (iMark plate reader, Biorad, Hercules, CA). For PGE_2 ELISAs, a pre-coated plate, washing buffer and other reagents were provided by the manufacturer (Enzo Life Sciences, Inc,. Farmingdale, NY), and the provided protocol was followed. All ELISA values were corrected for total protein content of homogenates.

Chapter 3: Myeloid-derived suppressor cells (MDSCs) contribute to *Staphylococcus*

***aureus* orthopedic biofilm infection**

Published in *Journal of Immunology* 192(8):3778-92, 2014

Copyright 2014. The American Association of Immunologists, Inc.

Abstract

Myeloid-derived suppressor cells (MDSCs) are a heterogeneous population of immature monocytes and granulocytes that are potent inhibitors of T cell activation. A role for MDSCs in bacterial infections has only recently emerged, and nothing is known about MDSC function in the context of *Staphylococcus aureus* (*S. aureus*) infection. Because *S. aureus* biofilms are capable of subverting immune-mediated clearance, we examined whether MDSCs could play a role in this process. $CD11b^+Gr-1^+$ MDSCs represented the main cellular infiltrate during *S. aureus* orthopedic biofilm infection, accounting for >75% of the $CD45^+$ population. Biofilm-associated MDSCs inhibited T cell proliferation and cytokine production, which correlated with a paucity of T cell infiltrates at the infection site. Analysis of FACS-purified MDSCs recovered from *S. aureus* biofilms revealed increased arginase-1, inducible NO synthase and IL-10 expression, key mediators of MDSC suppressive activity. Targeted depletion of MDSCs and neutrophils using the mAb 1A8 (anti-Ly6G) improved bacterial clearance by enhancing the intrinsic proinflammatory attributes of infiltrating monocytes and macrophages. Furthermore, the ability of monocytes/macrophages to promote biofilm clearance in the absence of MDSC action was revealed in significantly increased *S. aureus* burdens both locally and in the periphery, because effector Ly6C monocytes and, by extension, mature macrophages were also depleted. Collectively, these results demonstrate that MDSCs are key contributors to the chronicity of *S. aureus* biofilm infection, as their immunosuppressive function prevents monocyte/macrophage proinflammatory activity, which facilitates biofilm persistence.

Introduction

Myeloid-derived suppressor cells (MDSCs) are a heterogeneous population of immature monocytes and granulocytes that are potent inhibitors of T cell activation [122]. In mice, MDSCs are characterized by their expression of CD11b and Gr-1, but can be further subdivided into monocyte- and granulocyte-like subsets based on their differential expression of Ly6C and Ly6G, which are referred to as M-MDSC and G-MDSCs, respectively [120, 135]. CD11b^{+}Gr-1^{+} cells normally reside in the bone marrow prior to their differentiation into mature granulocytes, macrophages or dendritic cells. However, MDSCs can be recruited into lymphoid and inflamed tissues during pathologic conditions by the actions of growth factors, such as G-CSF, GM-CSF, and VEGF, where disturbances in cytokine homeostasis block their differentiation into mature myeloid effector cells, resulting in MDSC expansion [135, 137].Several factors influence MDSC activation, including proinflammatory cytokines driven by MyD88-dependent signaling (i.e. IL-6), reactive oxygen species (ROS), and cyclooxygenase-2 (COX-2). These proinflamatory molecules induce the expression of arginase-1 (Arg-1) and several anti-inflammatory cytokines that not only contribute to the inhibition of T cell responses, but may also play a role in macrophage polarization towards an alternatively activated M2 phenotype [137]. Although MDSCs are well-recognized for their role in tumor immunosuppression [122, 137, 155], recent evidence suggests that MDSCs can also regulate immune responses during bacterial infections [123, 156-159].

Staphylococcus aureus (*S. aureus*) is a leading cause of community-acquired and nosocomial infections [29, 160]. Infection risk is increased by the presence of foreign materials, and *S. aureus* is a leading cause of biofilm infections on indwelling medical devices and orthopedic implants [28]. Biofilms are heterogeneous bacterial communities encased in a self-produced matrix that represent a serious health care concern based on their chronicity and recalcitrance to antibiotic therapy [33]. Previous work from our laboratory has shown that *S. aureus* biofilms skew macrophages toward an alternatively activated M2 anti-inflammatory phenotype, typified by robust Arg-1 expression that correlates with the failure to recruit T cells to the site of infection[32]. However, Arg-1 expression was also detected in other cell types, leading us to examine the identity of alternative Arg-1^{+} cells associated with *S. aureus* biofilms. In the

current study, we have identified a predominant CD11b$^+$Gr-1$^+$Arg-1$^+$ MDSC infiltrate that contributes to the anti-inflammatory environment typical of *S. aureus* biofilm-associated infections.

Here we sought to examine the functional role of MDSCs in shaping the anti-inflammatory milieu during *S. aureus* orthopedic biofilm infection. Although we identified MDSCs using well-established markers [121, 126, 161], their ability to attenuate T cell proliferation was required to establish their identity as a bona fide MDSC population. Indeed, we found that MDSCs infiltrating S. aureus biofilms were capable of inhibiting T cell proliferation, which represents the first report of MDSCs in any type of staphylococcal infection. Furthermore, qRT-PCR analysis of FACS-purified MDSCs revealed increased expression of typical MDSC molecules, including Arg-1, iNOS, and IL-10. Administration of mAb 1A8 (anti-Ly6G), which specifically depleted the immunosuppressive MDSC population and mature neutrophils, significantly increased monocyte and macrophage proinflammatory activity, which translated into decreased *S. aureus* burdens in the infected joint. Independent evidence to support the importance of monocytes/macrophages in biofilm containment in the absence of MDSCs was demonstrated by the finding that RB6-C85 (anti-Gr-1 or anti-Ly6G/Ly6C) treatment, which depleted effector monocytes and macrophages in addition to MDSCs and granulocytes, significantly increased *S. aureus* burdens and proinflammatory mediator expression as well as bacterial dissemination to peripheral organs. These results indicate that MDSCs establish an anti-inflammatory milieu during *S. aureus* biofilm infection that thwarts monocyte and macrophage proinflammatory activity, leading to persistent colonization. This prominent MDSC infiltrate also explains the paucity of T cells associated with *S. aureus* biofilms. Collectively, these studies demonstrate a role for MDSCs during staphylococcal biofilm infection and preventing their immunosuppressive actions may offer novel treatment strategies to thwart these devastating, chronic infections.

Results

Accumulation of CD11b$^+$Gr-1$^+$ cells during *S. aureus* orthopedic biofilm infection. We

recently reported that *S. aureus* biofilms skew infiltrating macrophages toward an alternatively

activated M2 state typified by Arg-1 expression [31, 32]. However, other Arg-1$^+$ cells distinct from

macrophages were also observed, which led us to investigate their identity. A likely candidate

was MDSCs based on their robust Arg-1 expression and well-described anti-inflammatory

attributes in cancer [120, 137, 155]. In the present study, we used a mouse model of orthopedic

biofilm infection [162] to demonstrate the presence and functional importance of MDSCs in

shaping the anti-inflammatory biofilm milieu in an immunocompetent host. Biofilm formation on

the orthopedic implant was confirmed by scanning electron microscopy, which revealed *S. aureus*

attachment to a dense matrix deposited on the implant surface and bacterial tower formation (Fig.

3.1). A prominent CD11b$^+$Gr-1$^+$ infiltrate was observed, which accounted for ~75% of the total

CD45$^+$ leukocyte population by day 14 post-infection (Fig. 3.2A, 2B). Coexpression of CD11b and

Gr-1 is used to define MDSCs, and cytospin preparations of FACS-purified CD11b$^+$Gr-1$^+$ cells

recovered from the site of *S. aureus* biofilm infection confirmed their heterogeneous composition

of both granulocytic and monocytic morphologies (Fig. 3.2C). In particular, cells with ringed nuclei

suggested the presence of immature granulocytes, and immature monocytes with large rounded

nuclei and little cytoplasm were also observed (Fig. 3.2C). CD11b$^+$Gr-1$^+$ cells were also detected

in mice receiving sterile implants, which was not unexpected, because MDSCs have been

reported in virtually every inflammatory environment and are associated with wound healing

responses under normal conditions [150, 161]; however, their numbers were significantly lower

compared with *S. aureus*-infected animals (Fig. 3.2B). The abundance of CD11b$^+$Gr-1$^+$ cells

during early *S. aureus* orthopedic infection may be one mechanism that contributes to the

establishment of chronic disease.

Figure 3.1
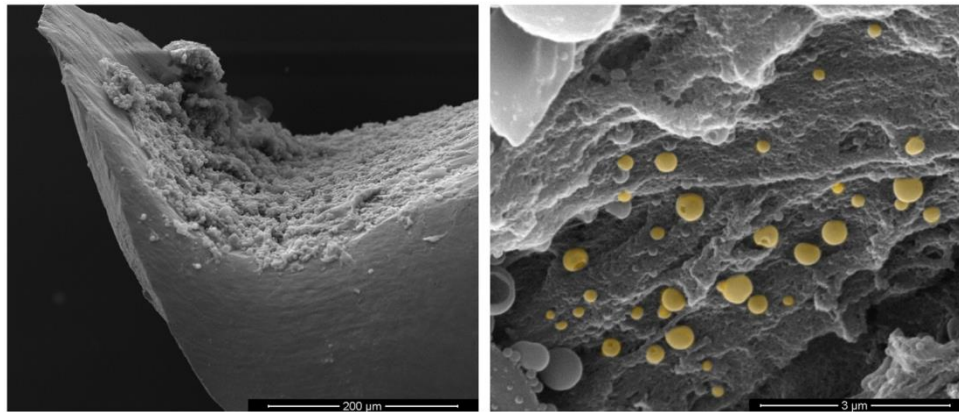
Demonstration of *S. aureus* biofilm formation *in vivo* on orthopedic implants. Titanium orthopedic implants were isolated from C57BL/6 mice at day 45 following *S. aureus* infection and processed for scanning electron microscopy analysis. *Left,* Biofilm formation is visible on the concave surface of the implant (original magnification X300) demonstrating the irregular pattern of the biofilm surface with tower structures visible (arrows). *Right,* Higher magnification of the biofilm surface revealing numerous cocci interspersed with matrix material (original magnification X20,000). The image has been pseudocolored to highlight *S. aureus* (gold).

Figure 3.2
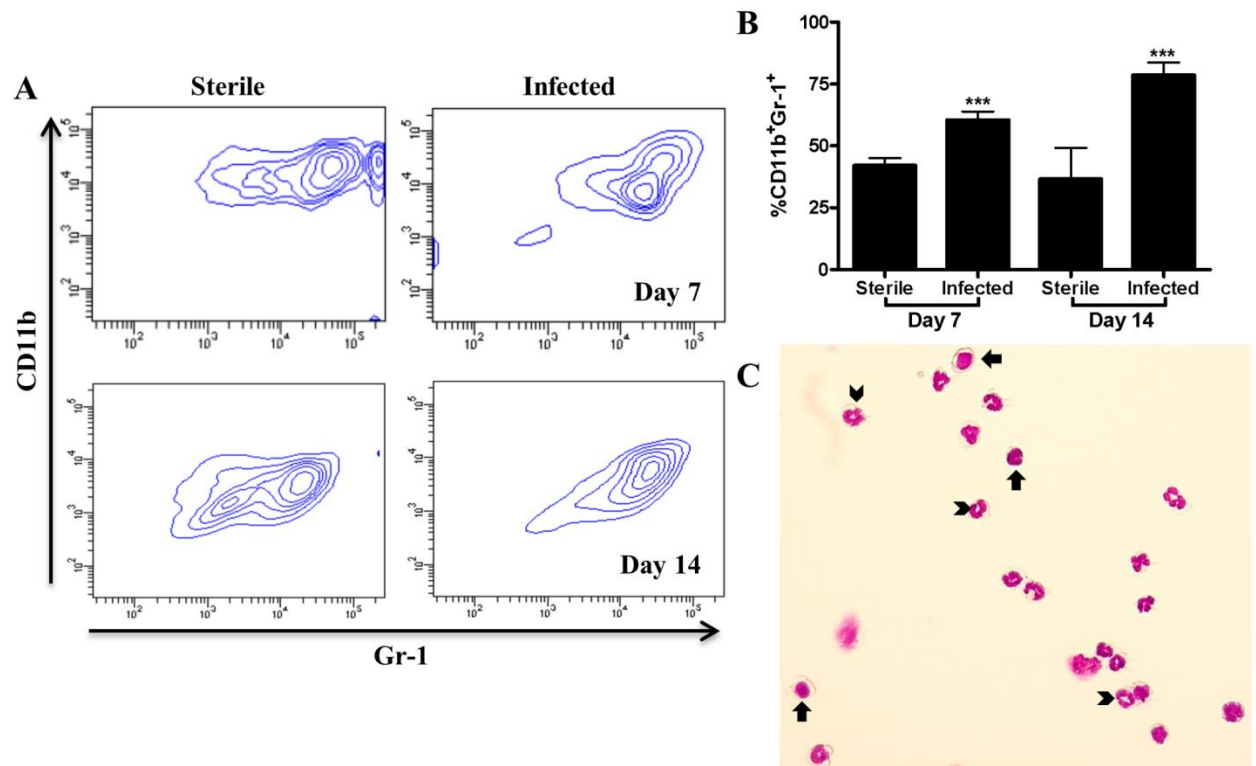
Accumulation of CD11b⁺Gr-1⁺ cells during *S. aureus* orthopedic biofilm infection. Implant-associated tissues were collected from sterile and infected mice and analyzed by flow cytometry for CD11b$^+$Gr-1$^+$ cells at the indicated time points. (**A**) Representative contour plots and (**B**) CD11b$^+$Gr-1$^+$ infiltrates expressed as a percentage of the total CD45$^+$ leukocyte population. (**C**) Cytospin preparations of FACS-purified CD11b$^+$Gr-1$^+$ cells from infected tissues at day 14 were stained with Wright-Giemsa (original magnification X20). Arrowheads and arrows indicate cells suggestive of immature granulocytes and monocytes, respectively. Results are representative of three sterile and five infected mice per group. ***$p < 0.001$, unpaired two-tailed Student *t* test.

CD11b⁺Gr-1⁺ MDSCs recruited to the site of *S. aureus* orthopedic biofilm infection inhibit T cell activation. A hallmark of MDSCs is their ability to inhibit Ag-specific and polyclonal T cell activation [121, 137]. This is a critical attribute based on the promiscuity in surface marker expression between MDSCs and other myeloid lineages [150, 163]. To determine whether *S. aureus* biofilm-associated CD11b⁺Gr-1⁺ infiltrates were bona fide MDSCs, we examined their ability to inhibit polyclonal CD4⁺ T cell activation, because *S. aureus* immunodominant TCR epitopes have not yet been identified. MDSCs were recovered from tissues at day 14, which coincided with maximum cell numbers at the infection site (Fig. 3.2B). CD11b⁺Gr-1⁺ cells from *S. aureus*-infected tissues significantly expressed T cell proliferation (Fig. 3.3A), establishing their identity as MDSCs. The inhibitory activity of biofilm-associated MDSCs was further demonstrated by their ability to significantly impair T cell cytokine secretion, including TNF-α, IFN-γ, IL-17, and IL-4 (Fig. 3B-E).

We next determined whether the immunosuppressive nature of MDSCs was restricted to the biofilm site or whether they were also suppressive in the periphery, which has been reported for MDSCs in tumor-bearing animals [164]. CD11b⁺Gr-1⁺ cells from the spleens of either naïve or infected animals were unable to suppress CD4⁺ T cell proliferation (data not shown). It was not unexpected that MDSCs from naïve animals failed to inhibit T cell activation, as pathologic conditions are known to elicit MDSC expansion and activation [120, 127, 136, 137]. Several groups have reported that MDSCs only acquire suppressive function after exposure to factors in inflammatory environments [150, 164, 165], and our results suggest that these signals are only present in the local biofilm milieu.

Because the Gr-1 Ab RB6-C85 recognizes both Ly6G and Ly6C epitopes [166], we stained for both markers and identified three distinct populations associated with *S. aureus* orthopedic biofilms, namely Ly6G^{high}Ly6C⁺, Ly6G^{low}Ly6C^{low}, and Ly6G⁻Ly6C⁺ (Fig. 4A). Each subset was purified by FACS to determine which was responsible for the observed CD4⁺ T cell proliferation in a ratio-dependent manner, confirming their identity as MDSCs (Fig. 3.4E). Similar to the observations with the bulk CD11b⁺Gr-1⁺ population (Fig. 3), Ly6G^{high}Ly6C⁺ cells decreased TNF-α and IL-17 expression (Fig. 3.4F and 3.4G, respectively). Cytospins of the Ly6G^{high}Ly6C⁺

population revealed an immature granulocytic morphology characterized by numerous ringed nuclei (Fig. 3.4B), which, when taken together with their suppressive action is highly suggestive of these cells as granulocytic MDSCs. The Ly6G$^-$Ly6C$^+$ population was typified by a relatively homogenous monocyte-like morphology that was unable to suppress CD4$^+$ T cell activation (Fig. 3.4D, 3.4E), suggesting that these cells are inflammatory monocytes. Collectively, these results demonstrate the recruitment of a bona fide MDSC population in staphylococcal biofilm infection.

Studies by other groups have reported neutrophil infiltrates in mouse models of *S. aureus* orthopedic infection [167-169]. However, these reports used either immunostaining with Ly6G, Ly6G depletion or LysM-GFP mice to identify neutrophils and, as our results demonstrate, these approaches cannot differentiate between neutrophils and MDSCs [170]. It is possible that the Ly6G^{low}Ly6C^{low} cells observed in our model of *S. aureus* orthopedic biofilm infection are neutrophils based on their cytospin morphology, revealing fewer immature cells compared with the MDSC population (Fig. 3.4C and 3.4B, respectively) and lack of T cell suppressive activity (Fig. 3.4E).

Figure 3.3
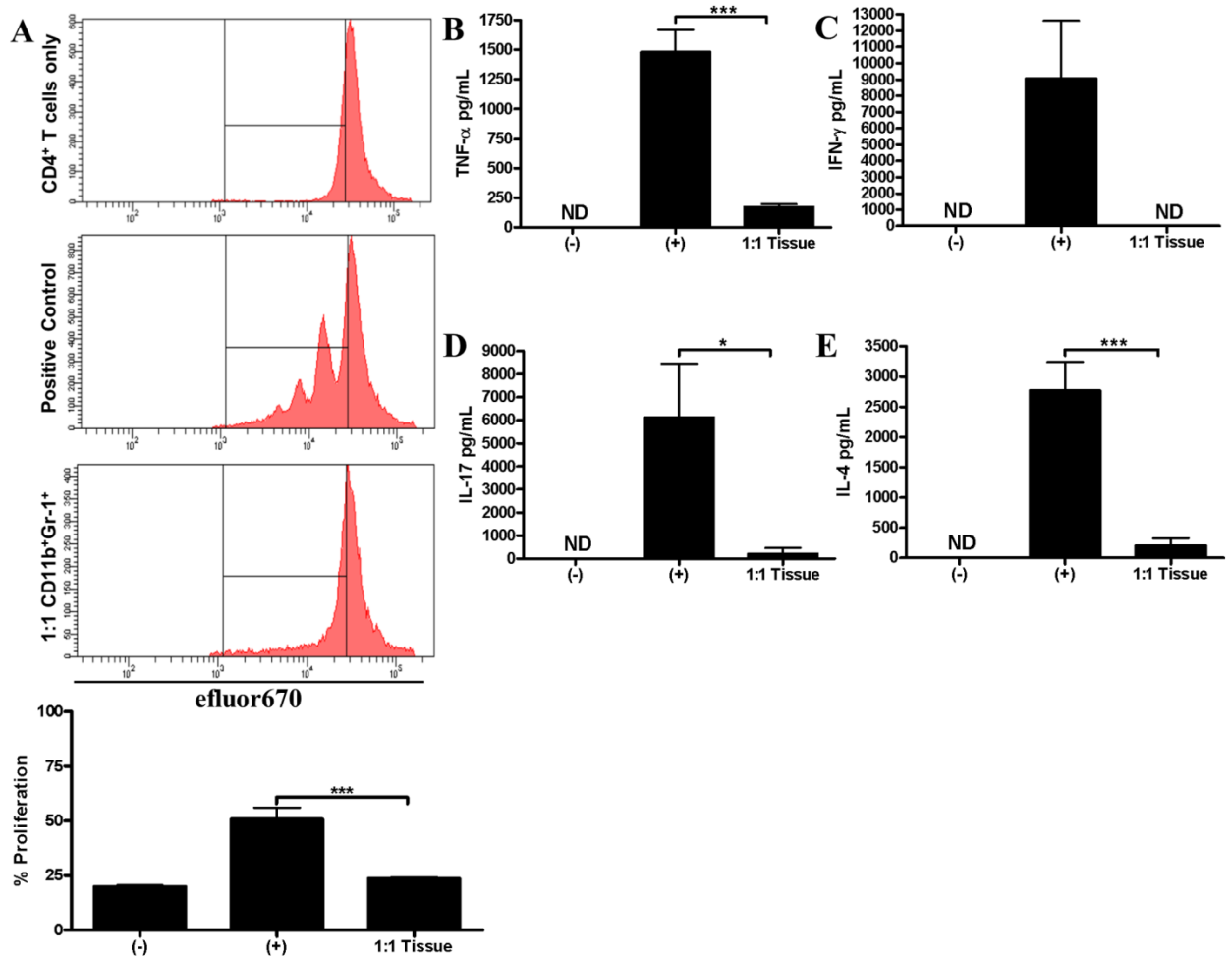
CD11b⁺Gr-1⁺ infiltrates from the site of *S. aureus* biofilm infection inhibit T cell proliferation. FACS-purified CD11b⁺Gr-1⁺ cells recovered from infected joint tissues at day 14 were immediately cultured *ex vivo* with eFluor 670-labled CD4⁺ T cells at a 1:1 ratio for proliferation assays. (**A**) Representative histograms of fluorescence intensity, with percentage proliferation reported. (**B-E**) Supernatants from MDSC/CD4⁺ T cell cocultures were collected at 72 h to quantitate TNF-α (B), IFN-γ (C), IL-17 (D), and IL-4 (E) by Milliplex. Results are representative of three to nine independent experiments *$p < 0.05$, ***$p < 0.001$, unpaired two-tailed Student *t* test. (-), T cells only; (+) T cells incubated with CD3/CD28 Dynabeads; ND, not detected.

Figure 3.4
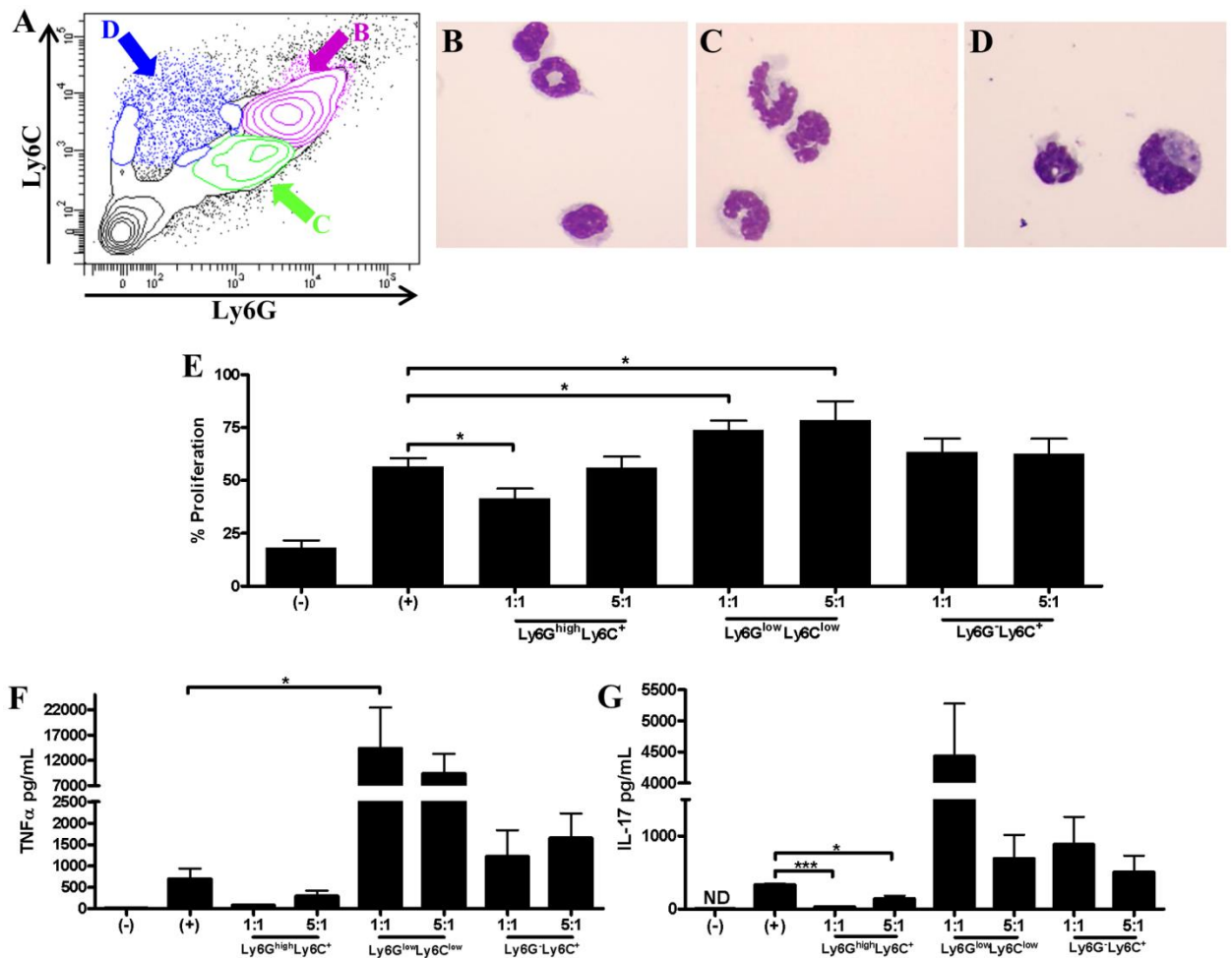
Ly6G^{high}Ly6C⁺ cells infiltrating *S. aureus* biofilms are *bona fide* MDSCs. Leukocyte infiltrates associated with *S. aureus*-infected joints were collected at day 14 and analyzed for Ly6C and Ly6G expression by flow cytometry. Representative conour plot (**A**) and Wright-Giemsa-stained cytospin preparations of FACS-purified Ly6G^{high}Ly6C⁺ (**B**), Ly6G^{low}Ly6C^{low} (**C**), and Ly6G⁻Ly6C⁺ (**D**) cells are shown (original magnification X100). (**E**) Analysis of *ex vivo* polyclonal CD4⁺ T cell proliferation following a 1:1 and 1:5 coculture with Ly6G^{high}Ly6C⁺, Ly6G^{low}Ly6C^{low}, Ly6G⁻Ly6C⁺ cells for 72 h, whereupon conditioned supernatants were assessed for TNF-α (**F**) and IL-17 (**G**) expression by Milliplex. Results are representative of three to nine replicates. $*p < 0.05$, $***p < 0.001$, one-way ANOVA with Bonferroni's multiple comparison post hoc analysis. (-), T cells only; (+), T cells incubated with CD3/CD28 Dynabeads; ND, not detected.

Ly6G^{high}Ly6C⁺ cells recruited to sites of *S. aureus* orthopedic biofilm infection express genes characteristic of MDSCs. Owing to the differential immunosuppressive properties of the Ly6G^{high}Ly6C$^+$ and Ly6G$^-$Ly6C$^+$ subsets associated with *S. aureus* orthopedic biofilm infection, we next examined gene expression profiles of FACS-purified populations immediately *ex vivo* by qRT-PCR as further confirmation of their identity. The Ly6G^{high}Ly6C$^+$ MDSC subset displayed increased iNOS, Arg-1, COX-2, and IL-10 concomitant with reduced IL-12p40 expression compared with the Ly6G$^-$Ly6C$^+$ monocytic fraction (Fig. 3.5), similar to MDSC profiles described in other disease models [122, 171-174].

MDSCs play an important role in regulating inflammatory processes through their production of several pro- and anti-inflammatory cytokines [123, 150]. To assess the inflammatory status of MDSCs, cells were recovered from the site of biofilm infection or the spleen and immediately stimulated *ex vivo* with heat-inactivated *S. aureus* or peptidoglycan. We found that regardless of their origin, Ly6G^{high}Ly6C$^+$ MDSCs were inherently less proinflammatory than macrophages (Supplemental Fig. S3.1). Collectively, these results provide further evidence to support the identity of infiltrating Ly6G^{high}Ly6C$^+$ cells into *S. aureus* orthopedic biofilm infections as MDSCs.

Figure 3.5
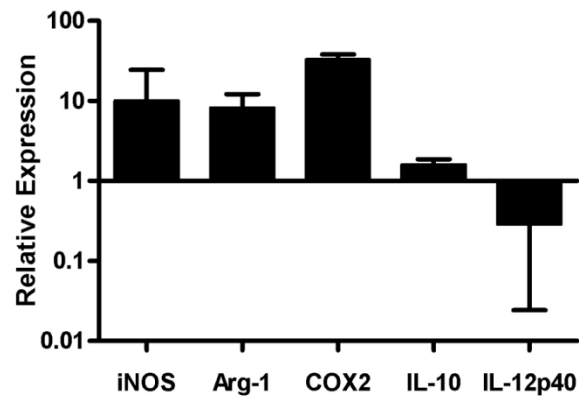
Ly6G^{high}Ly6C⁺ biofilm-associated infiltrates express genes characteristic of MDSCs. FACS-purified Ly6G^{high}Ly6C^{+} MDSCs and Ly6G^{-}Ly6C^{+} inflammatory monocytes were recovered from infected joint tissues at day 14, whereupon RNA was immediately isolated for qRT-PCR analysis. Gene expression levels in Ly6G^{high}Ly6C^{+} MDSCs were calculated after normalizing signals against GAPDH and are presented as the fold change relative to the Ly6G^{-}Ly6C^{+} monocyte population. Results represent the means ± SEM of three independent experiments.

Depletion of Ly6G⁺ MDSCs increases monocyte infiltrates and their intrinsic

proinflammatory activity, resulting in enhanced *S. aureus* biofilm clearance. To assess the

functional role of Ly6G^{high}Ly6C⁺ MDSCs in orchestrating the anti-inflammatory biofilm milieu to

facilitate bacterial persistence, mice were treated with the mAb 1A8 to target Ly6G⁺ cells [171,

175, 176]. This approach would deplete MDSCs, leaving the Ly6C⁺ monocyte and macrophages

populations intact and able to combat *S. aureus* infection, presumably in the absence of

immunosuppression. We confirmed that 1A8 was effective at depleting the Ly6G^{high}Ly6C⁺ MDSC

population, which was more robust at day 7 compared with day 14 (Fig. 3.6A, 6B). Interestingly,

the frequency of Ly6C⁺ monocytes was significantly increased at day 7 (Fig. 3.6C), and we

predicted that the absence of immunosuppressive Ly6G⁺ MDSCs would promote the

proinflammatory attributes of these Ly6C⁺ mononuclear phagocytes. To address this possibility,

we examined the activation state of FACS-purified Ly6G⁻Ly6C⁺ cells from the infection site of

1A8-treated versus isotype control mice by qRT-PCR. In the context of MDSC depletion with 1A8,

expression of iNOS, IL-12p40, and IL-6 was increased in Ly6G⁻Ly6C⁺ cells at day 7 (Fig. 3.7).

Increased Arg-1 and IL-10 expression was also observed in Ly6G⁻Ly6C⁺ cells (Fig. 3.7), and

although both possess anti-inflammatory properties, they may be important in maintaining a

balanced inflammatory environment at the site of infection owing to the absence of normally

immunosuppressive MDSCs.

Because Ly6C⁺ monocyte infiltrates were increased in the context of MDSC depletion

and displayed intrinsic proinflammatory activity, we next examined whether this would translate

into superior anti-biofilm activity. This prediction was confirmed, because Ly6G⁺ cell depletion

with 1A8 significantly reduced *S. aureus* burdens in both the tissue and knee joint at days 7 and

14 compared with isotype control animals (Fig. 3.8B), which correlated with less gross evidence

of exudate formation in MDSC-depleted mice (Fig. 3.8A). Ly6G⁺ cell depletion did not cause *S.

aureus* dissemination from the primary site of infection (Fig. 3.8C), and histopathologic analysis of

H&E-stained tissues showed no dramatic differences in the degree of joint inflammation or

splenic architecture (as a measure of extramedullary hematopoiesis) between 1A8-treated and

istoype control animals (data not shown).

To investigate the impact of Ly6G$^+$ cell depletion on the inflammatory milieu during *S. aureus* orthopedic biofilm infection, soft tissues surrounding the knee, knee joint, and femur were analyzed using Milliplex arrays. Several cytokines (G-CSF, IL-1β, and IL-6) and chemokines (CXCL1, CXCL9, and CCL3) were dramatically reduced in 1A8-treated compared with isotype control mice primarily at day 7 (Fig. 3.9), in agreement with increased bacterial clearance in the former (Fig. 3.8B). Collectively, these results demonstrate that during *S. aureus* orthopedic biofilm infection, Ly6G^{high}Ly6C$^+$ MDSCs elicit a local microenvironment that restricts monocyte/macrophage proinflammatory activity, facilitating the establishment of an anti-inflammatory environment that favors bacterial persistence. We propose that these effects were not significantly influenced by neutrophil loss following 1A8 treatment, because most Ly6G$^+$ leukocytes infiltrating infected joints (i.e., ~75%) were MDSCs.

Figure 3.6
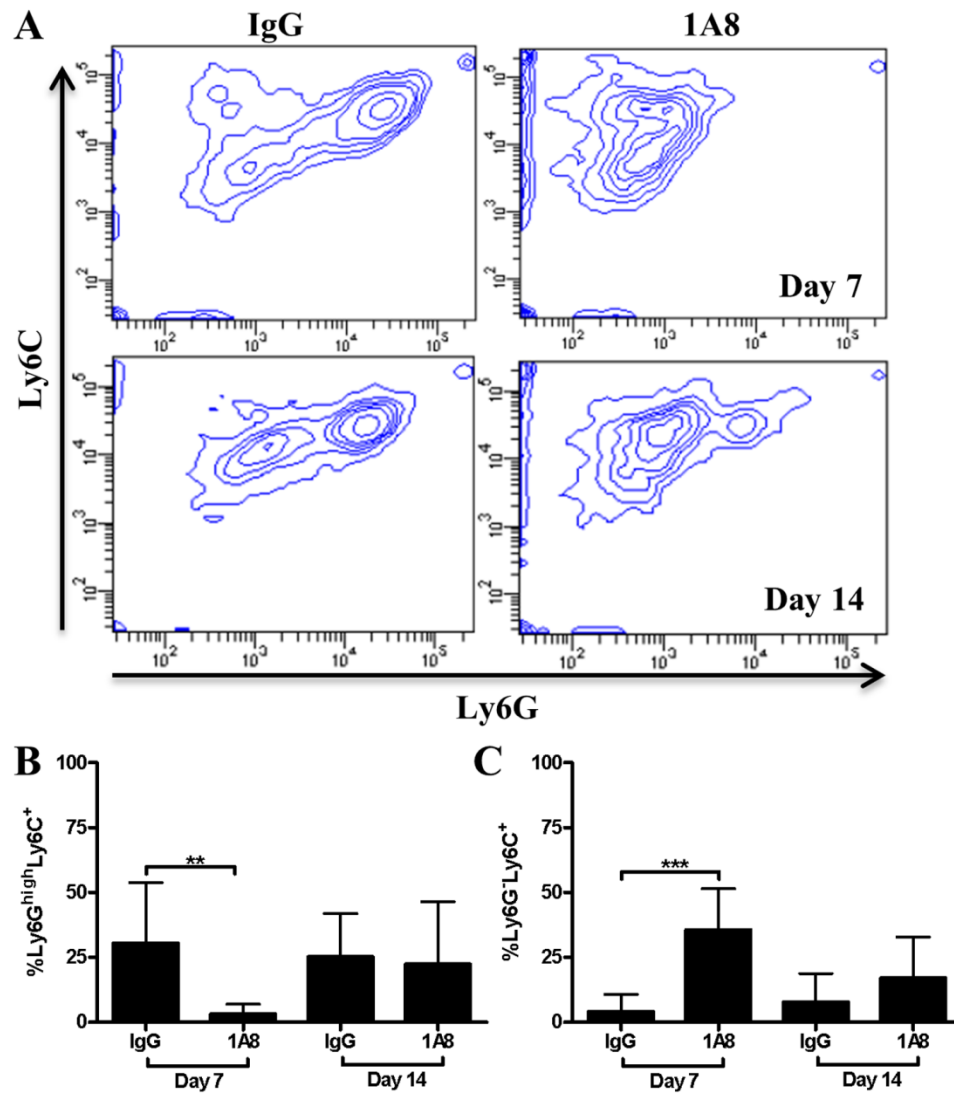
MDSC depletion augments monocyte recruitment during *S. aureus* orthopedic biofilm infection. Implant-associated tissues from 1A8- and isotype control-treated mice were collected at the indicated time points after infection and analyzed by flow cytometry. (**A**) Representative contour plots of Ly6C and Ly6G staining and (**B**) quantitation of Ly6G$^+$Ly6C$^+$ MDSCs and (**C**) Ly6C$^+$ inflammatory monocytes. Results are presented as a percentage of the total leukocyte infiltrate and are representative of two independent experiments (n = 10 mice/group). **$p < 0.01$, ***$p < 0.001$, unpaired two-tailed Student t test.

Figure 3.7
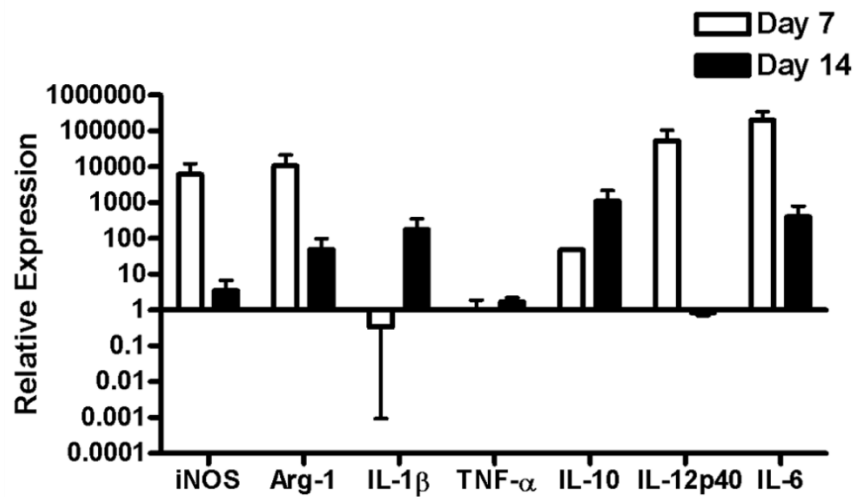
MDSC depletion enhances intrinsic proinflammatory gene expression in Ly6C^{+} monocytes during _S. aureus_ biofilm infection. Ly6G^{-}Ly6C^{+} monocytes were purified from tissues surrounding the infected joints of 1A8- and isotype control-treated mice at days 7 and 14 post-infection by FACS, whereupon RNA was immediately isolated for qRT-PCR analysis. Gene expression levels in Ly6G^{-}Ly6C^{+} monocytes recovered from MDSC-depleted animals were calculated after normalizing signals against GAPDH and are presented as the fold change relative to Ly6G^{-}Ly6C^{+} cells from isotype control mice. Results represent the means ± SEM of two independent experiments.

Figure 3.8
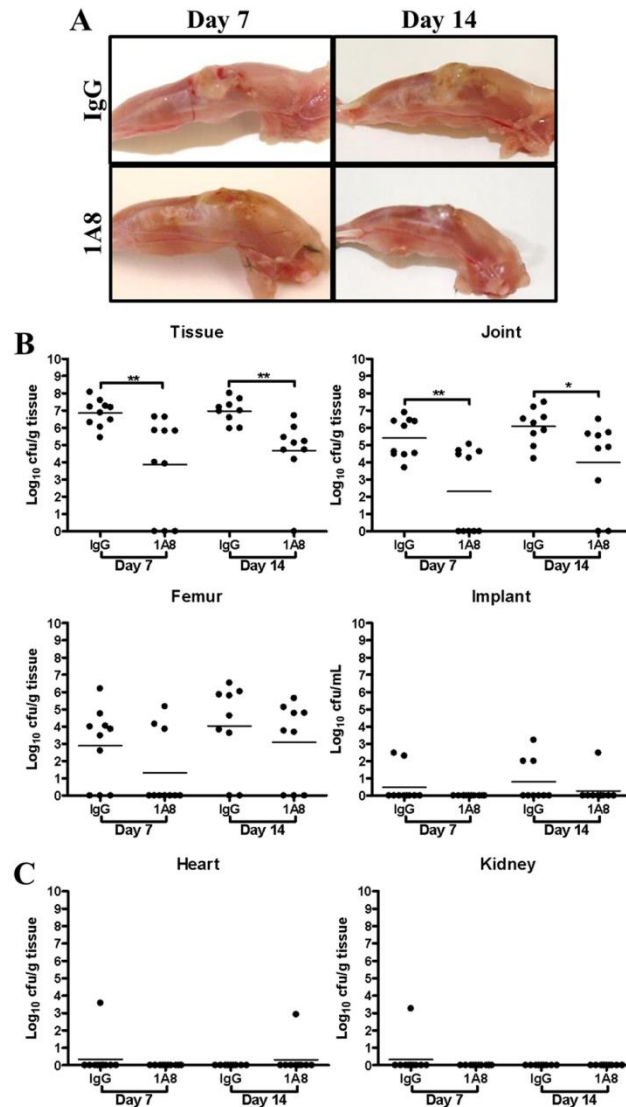
MDSC depletion reduces *S. aureus* burdens during orthopedic biofilm infection. (**A**) Gross appearance of infected tissues from animals receiving 1A8 or an isotype-matched IgG. (**B**) Bacterial burdens associated with the knee joint, surrounding soft tissue, femur, and orthopedic implant and (**C**) heart and kidney of IgG control- or 1A8-treted animals at days 7 and 14 post-infection. Results are expressed as the number of CFU per milliliter for orthopedic implants or CFU per gram tissue to correct for alterations in tissue sampling sizes. Significant differences in bacterial burdens between IgG- and 1A8-treated mice are denoted as *$p < 0.05$ and **$p < 0.01$ (unpaired two-tailed Student *t* test).

Figure 3.9
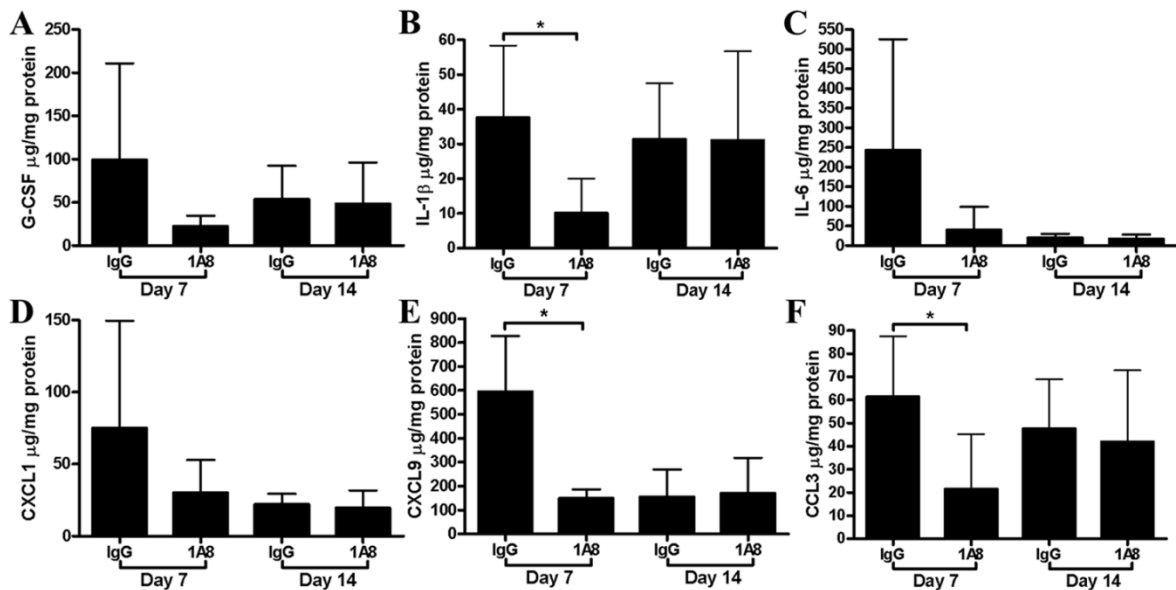
1A8 treatment attenuates proinflammatory mediator production during *S. aureus*

orthopedic biofilm infection. Tissue homogenates surrounding orthopedic implants were

prepared at days 7 and 14 postinfection from 1A8- and isotype-treated mice, whereupon

expression of G-CSF (**A**), IL-1β (**B**), IL-6 (**C**), CXCL1 (**D**), CXCL9 (**E**), and CCL3 (**F**) was

quantitated by Milliplex. Results were normalized to the amount of total protein recovered to

correct for alterations in tissue sampling size. Results are representative of five mice per group.

*$p < 0.05$, unpaired two-tailed Student *t* test.

Gr-1$^+$ cell depletion confirms the inhibitory action of MDSCs on monocyte/macrophages to prevent *S. aureus* biofilm clearance. Our results have established that MDSC depletion with 1A8 facilitated *S. aureus* biofilm clearance, in part due to decreased immunosuppressive effects that promoted the proinflammatory attributes of infiltrating monocytes and macrophages. To further demonstrate that monocyte/macrophages were critical for anti-biofilm activity in the absence of an MDSC infiltrate, we treated mice with the mAb RB6-C85. Similar to 1A8, RB6-C85 depletes Ly6G$^+$ MDSCs and neutrophils, but it also targets monocytes based on its reactivity with Ly6C, which would also impact macrophage numbers by default [136, 171, 175-177]. Therefore, any differences between 1A8 and RB6-C85 depletion would further support a role for monocytes/macrophages in mediating biofilm clearance without the suppressive MDSC population. As previously demonstrated, Ly6G/Ly6C staining detected three cell populations in implant-associated tissues of isotype control animals at days 7 and 14 following infection, namely Ly6G^{high}Ly6C$^+$ MDSCs, a Ly6G^{low}Ly6C^{low} granulocyte-like population, and a Ly6G$^-$Ly6C$^+$ inflammatory monocyte subset (Fig. 3.10A). However, at day 7 RB6-C85-treted animals only displayed one cell population that shifted from Ly6G^{low}Ly6C^{low} to Ly6G^{high}Ly6C$^+$ at day 14 post-infection (Fig. 3.10B). The percentage of Ly6G^{low}Ly6C^{low} cells in RB6-C85-treated animals was significantly higher than isotype-treated controls at day 7; however, no differences were apparent at day 14, because the population had shifted to Ly6G^{high}Ly6C$^+$ (Fig. 3.10B). Although Ly6C$^+$ infiltrates were increased in RB6-C85-treated animals at day 14 post-infection (Fig. 3.10B), they were unable to inhibit T cell proliferation (Supplemental Fig. S3.2), and as such they do not represent a true MDSC phenotype. Therefore, we suggest that the presence of Ly6G^{low}Ly6C^{low} and Ly6G^{high}Ly6C$^+$ populations in the infected joint of RB6-C85-treated mice results from increased demand from the overwhelming infection (Fig. 3.11), which agrees with the results to follow that demonstrate extensive extramedullary hematopoiesis in the spleens of these animals. This is supported by the finding that Ly6G$^+$Ly6C$^+$ cells were significantly lower in RB6-C85-treated mice receiving sterile implants compared with isotype control Ab (data not shown).

We also examined CCR2 and F4/80 expression as markers for inflammatory monocytes and macrophages, respectively [178-180]. Because RB6-C85 also recognizes the Ly6C epitope,

we expected both of these populations to be decreased, as CCR2$^+$ inflammatory monocytes express Ly6C and differentiate into F4/80$^+$ macrophages once they have migrated into tissues [179]. As expected, the percentage of Ly6C$^+$CCR2$^+$ cells was significantly decreased in RB6-C85-treated animals compared with isotype controls at days 7 and 14 postinfection (Fig. 10C). Likewise, there were significantly fewer F4/80$^+$ macrophages in RB6-C85-depleted mice at day 7 post-infection, and only a very small percentage of cells remained at day 14 (Fig. 3.10C).

Figure 3.10
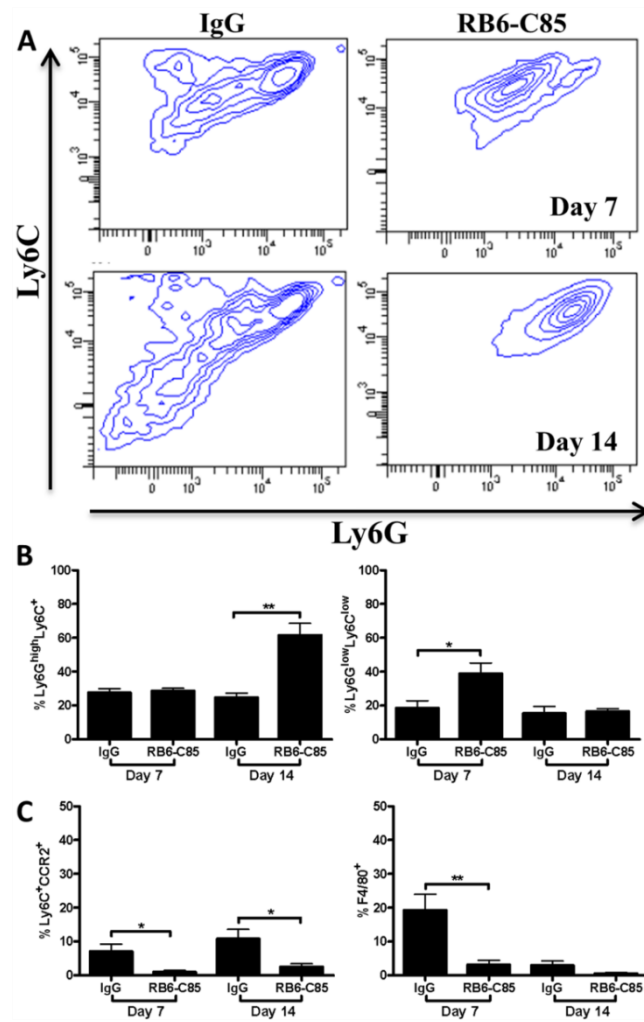
RB6-C85 administration alters leukocyte infiltrates during _S. aureus_ orthopedic biofilm infection. Implant-associated tissues from RB6-C85- and isotype control-treated mice were collected at the indicated time points after infection and analyzed by flow cytometry. (**A**) Representative contour plots of Ly6C and Ly6G staining and quantitation of (**B**) Ly6G^{high}Ly6C^{+} MDSCs and Ly6G^{low}Ly6C^{low} neutrophils and (**C**) inflammatory monocytes (CCR2^{+}) and macrophages (F4/80^{+}) present in infected animals receiving RB6-C85 or isotype control Ab. Results are expressed as a percentage of the total CD45^{+} leukocyte population. Results are representative of 10 mice per group from two independent experiments. *$p < 0.05$, **$p < 0.01$, unpaired two-tailed Student _t_ test.

Gr-1$^+$ cell depletion exacerbates *S. aureus* orthopedic biofilm infection owing to the loss of monocyte/macrophage effectors. Strikingly, *S. aureus*-infected mice treated with RB6-C85 displayed grossly visible caseous exudate (Fig. 3.11A), which was typified by significantly increased bacterial burdens in the knee joint, surrounding soft tissue, and femur at days 7 and 14 postinfection compared with infected animals receiving an isotype-matched control Ab (Fig. 3.11B). Histological analysis of tissues collected from RB6-C85-treated mice revealed increased inflammation in the joint space, surrounding soft tissue, and bone compared with isotype control animals (Table 3.1). Furthermore, the degree of osteolysis was more severe in RB6-C85-treated animals, as evidenced by CT imaging (Fig. 3.12), and femurs were more brittle upon harvest. These results are in stark contrast with those obtained during 1A8 depletion where biofilm burdens were reduced, indicating that monocytes and macrophages are able to promote bacterial clearance in the absence of an immunosuppressive MDSC population, because the only difference between the Ab depletion strategies was the targeting of monocyte/macrophages.

Table 3.1 Degree of inflammation and extramedullary hematopoiesis associated with RB6-C85 mAb treatment during *S. aureus* orthopedic infection.

Spleen	Average Extramedullary Hematopoiesis Score
Naive Spleen	0.5
Day 7 IgG	1
Day 7 RB6-C85	3
Day 14 IgG	1.5
Day 14 RB6-C85	2.5
Tissue	Average Inflammatory Score
Day 7 IgG	2
Day 7 RB6-C85	3

RB6-C85 administration not only increased bacterial burdens and inflammation at the site of *S. aureus* orthopedic biofilm infection, but it also led to significant systemic effects. First, Gr-1$^+$ depletion enhanced *S. aureus* dissemination, as bacterial burdens in the heart, kidney, and spleen of RB6-C85-treated animals were significantly elevated at day 7 post-infection compared

with the isotype control group (Fig. 3.11C). Second, RB6-C85-treated animals displayed

significant splenomegaly (Fig. 3.13A, 13B). Histopathology revealed marked expansion of the

splenic sinuses and red pulp with extensive extramedullary hematopoiesis, typified by numerous

erythroid islands, megakaryocytes, and leukocyte islands in RB6-C85-treated animals, which was

not observed in infected isotype control mice (Fig. 3.13C).

To examine changes in the inflammatory milieu after RB6-C85 treatment, inflammatory

mediator expression was assessed. Numerous cytokines (IL-1β, G-CSF, and IL-17) and

chemokines (CXCL1, CXCL2, and CCL3) were significantly increased at days 7 and 14 in RB6-

C85-treated animals compared with isotype controls (Fig. 3.14). Similar changes were observed

in the infected knee joint and femur (data not shown). Taken together with the results from 1A8

depletion, these finding demonstrate that MDSCs are critical for limiting the proinflammatory

activity of monocytes and macrophages during *S. aureus* biofilm infection, which sets the stage

for bacterial persistence.

Figure 3.11
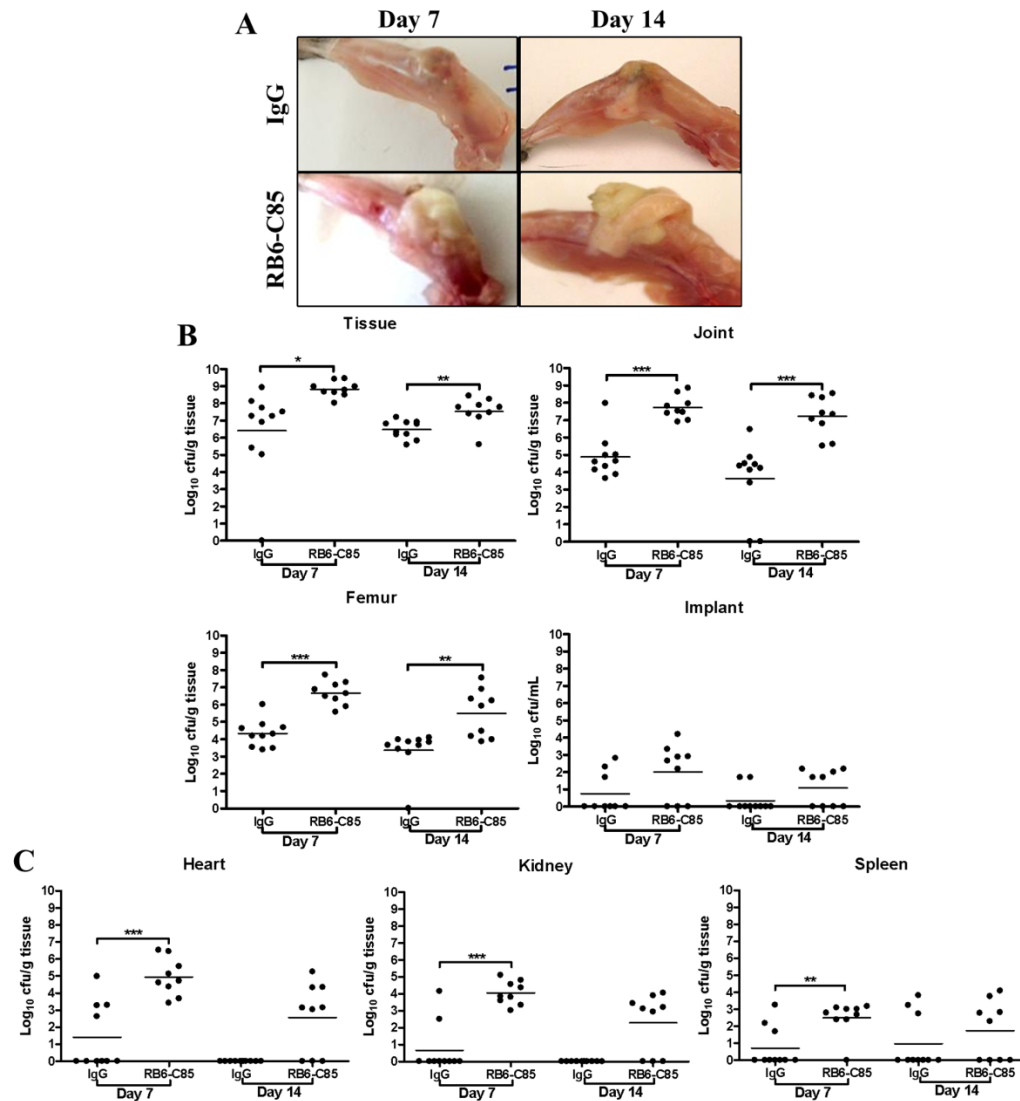
RB6-C85 treatment enhances *S. aureus* biofilm burdens and dissemination. (**A**) Gross appearance of infected tissues from animals receiving RB6-C85 or an isotype-matched IgG revealed a marked caseous exudate in the former. (**B**) Bacterial burdens associated with the knee joint, surrounding soft tissue, femur and orthopedic implant and (**C**) heart, kidney, and spleen of control IgG- or RB6-C85-treated animals at days 7 and 14 postinfection. Results are expressed as CFU per milliliter for orthopedic implants or CFU per gram of tissue to correct for differences in tissue sampling size. Results are representative of 10 mice per group from two independent experiments. Significant differences between IgG and RB6-C85 animals are denoted as *$p < 0.05$, **$p < 0.01$, and ***$p < 0.001$ (unpaired two-tailed Student t test).

Figure 3.12
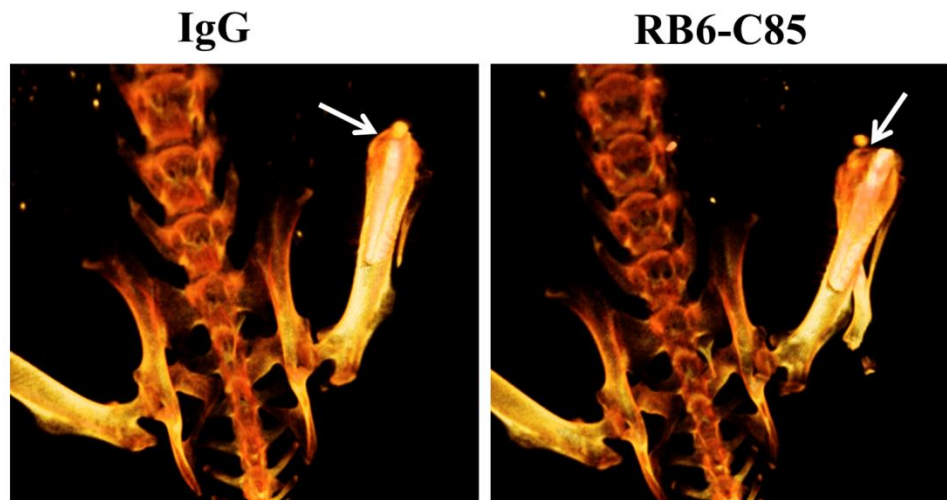
IgG RB6-C85

RB6-C85 administration results in increased osteolysis during *S. aureus* orthopedic biofilm infection. CT images (dorsal view) are presented at day 14 postinfection from mice receiving RB6-C85 or isotype control Ab. Arrows indicate the region of bone loss near the implant tip at the patella. Color intensity is indicative of bone density, where white indicates most dense and dark orange indicates least dense. Images are representative of four individual animals per group.

Figure 3.13
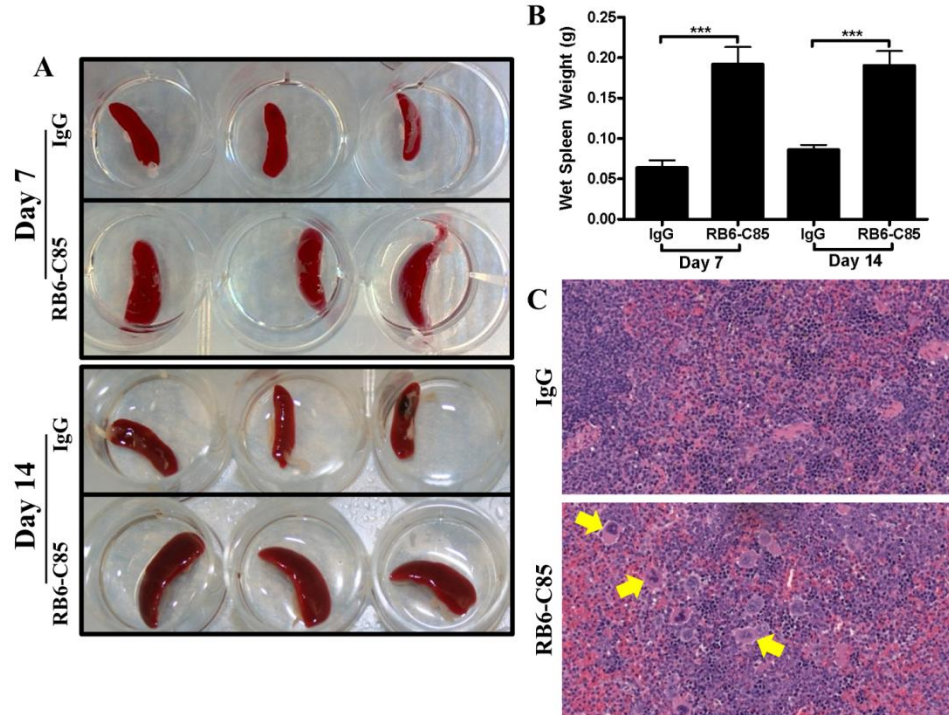
RB6-C85 treatment leads to splenomegaly and extramedullary hematopoiesis during *S. aureus* orthopedic biofilm infection. Gross appearance (**A**) and weight (**B**) of spleens from RB6-C85- or IgG-treated mice at days 7 and 14 after *S. aureus* orthopedic biofilm infection (n = 10/group). (**C**) H&E-stained sections of spleens from IgG- and RB6-C85-treated mice at day 14 postinfection (n = 3/group; original magnification X40; *zoomed images* [original magnification, X60] depict areas delineated by rectangles in the X40 field of view). Arrows indicate presence of megakaryocytes in RB6-C85-treated spleens. Significant differences between IgG and RB6-C85 animals are denoted as ***$p < 0.001$ (unpaired two-tailed Student *t* test).

Figure 3.14
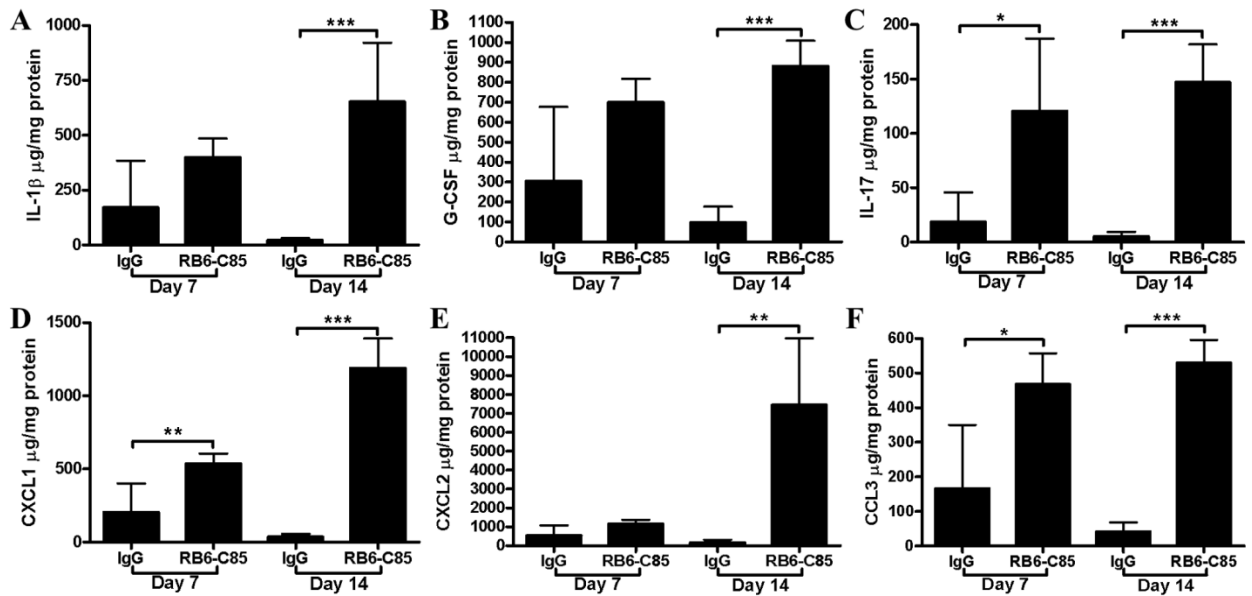
RB6-C85 administration exacerbates inflammatory mediator production during *S. aureus* orthopedic biofilm infection. Tissue homogenates surrounding orthopedic implants were prepared at days 7 and 14 postinfection from RB6-C85- and isotype control-treated mice, whereupon IL-1β (**A**), G-CSF (**B**), IL-17 (**C**), CXCL1 (**D**), CXCL2 (**E**), and CCL3 (**F**) expression was quantitated by Milliplex. Results were normalized to the amount of total protein recovered to correct for alterations in tissue sampling size. Results are representative of five mice per group. *$p < 0.05$, **$p < 0.01$, ***$p < 0.001$, unpaired two-tailed Student *t* test).

Supplemental Figure S3.1
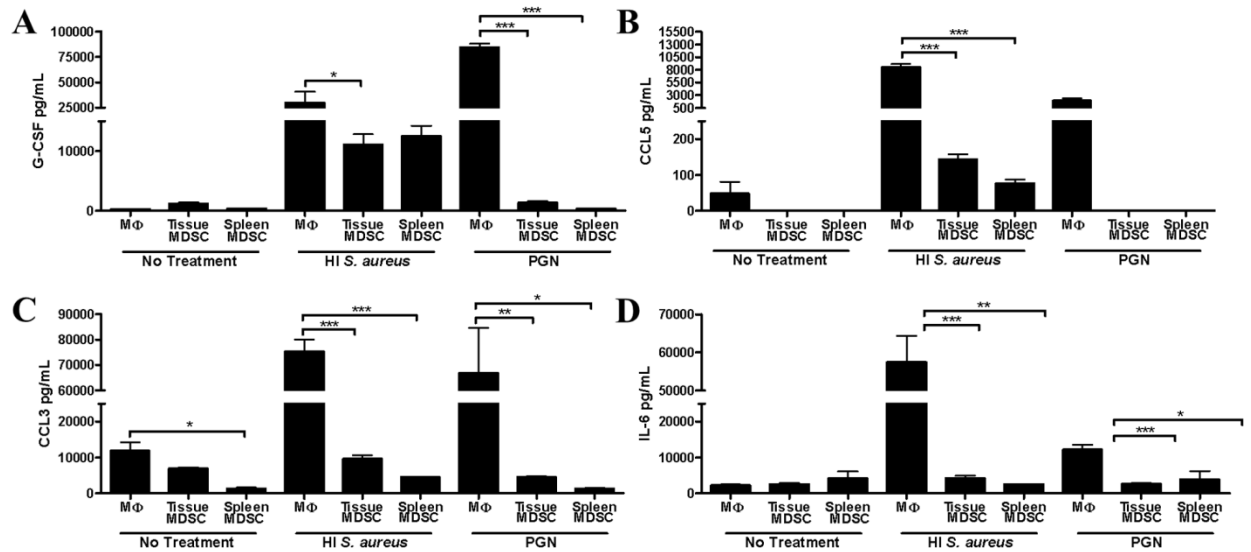
MDSCs exhibit less inherent proinflammatory activity than macrophages. Bone marrow-derived macrophages (MΦ) and FACS-purified Ly6G^{high}Ly6C^{+} MDSCs recovered from the site of *S. aureus* orthopedic biofilm infection (tissue MDSC) or the spleen (spleen MDSC) of infected animals were stimulated with 10^{7} heat-inactivated (HI) *S. aureus* or PGN (10 µg/ml). Supernatants were collected at 24 h, whereupon G-CSF (**A**), CCL5 (**B**), CCL3 (**C**) and IL-6 (**D**) expression was quantitated by Milliplex. Significant differences are denoted by asterisks (*$p <$ 0.05; **$p <$ 0.01; ***$p <$ 0.001; one-way ANOVA with Bonferroni's multiple comparison post-hoc analysis) and are representative of three independent replicates.

Supplemental Figure S3.2
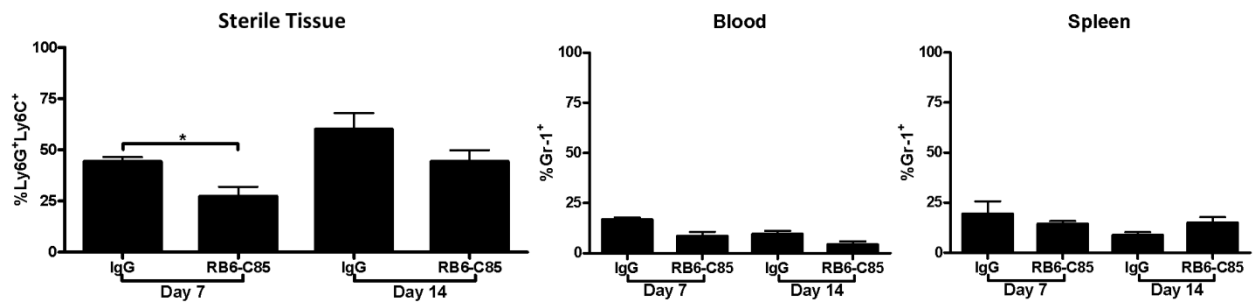
RB6-C85 treatment reduces Ly6G^{high}Ly6C$^+$ MDSC infiltrates in mice receiving sterile orthopedic implants. Implant-associated tissues, blood and spleens from RB6-C85- and isotype control-treated mice were collected at the indicated time points after placement of sterile orthopedic devices and analyzed by flow cytometry. Ly6G^{high}Ly6C$^+$ or Gr-1$^+$ MDSCs are expressed as a percentage of the total CD45$^+$ leukocyte infiltrate. Significant differences are denoted by asterisks (*$p < 0.05$; unpaired two-tailed Student t test) and are representative of two mice per group.

Supplemental Figure S3.3
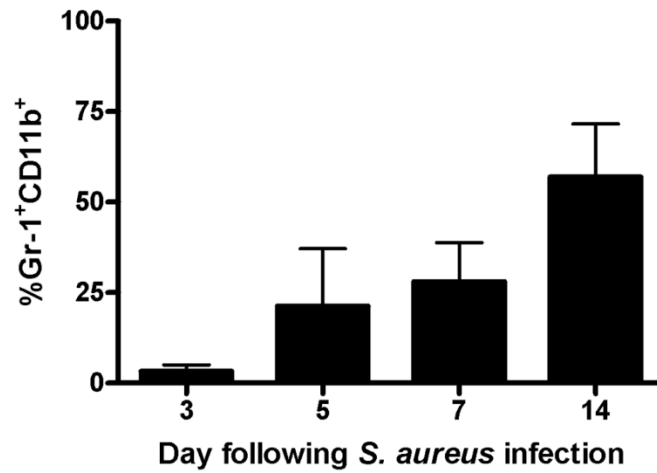
CD11b⁺Gr-1⁺ MDSC infiltrates are observed during _S. aureus_ catheter-associated biofilm infection. Mice (n = 4 per time point) were infected with 10^3 CFU of USA300 LAC::_lux_ in the lumen of surgically implanted catheters to establish biofilm infection. Catheter-associated tissues were collected from mice at the indicated time points, whereupon CD11b$^+$Gr-1$^+$ infiltrates were quantified by flow cytometry. Results are presented as the percentage of the total CD45$^+$ infiltrate.

Supplemental Figure S3.4
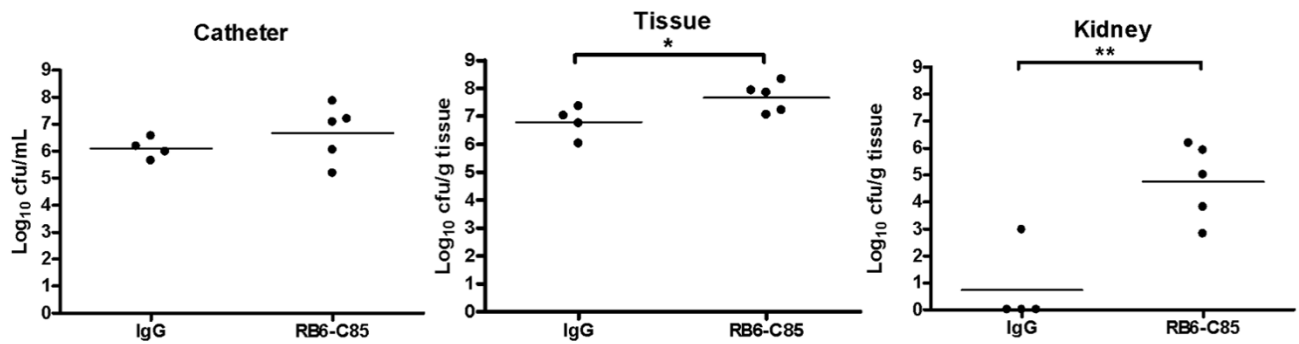
RB6-C85 treatment during *S. aureus* catheter-associated biofilm infection results in increased bacterial burdens and dissemination. Mice (n = 4 IgG and 5 RB6-C85 per time point) were infected with 10^3 CFU of USA300 LAC::*lux* in the lumen of surgically implanted catheters to establish biofilm infection. Animals received i.v. injections of 100 µg RB6-C85 or IgG isotype control Ab at days -1, 2, and 5 following *S. aureus* exposure, whereupon bacterial burdens associated with infected catheters, surrounding tissue, and dissemination to the kidney were quantitated at day 7 post-infection. Significant differences between groups are denoted by asterisks (*$p < 0.05$, **$p < 0.01$; unpaired two-tailed Student *t* test).

Discussion

        An emerging role for MDSCs has been described in several diseases aside from cancer, most recently to include bacterial infections [123, 157-159, 176, 181]. Using a mouse model of *S. aureus* orthopedic biofilm infection, we demonstrate that a population of CD11b$^+$Gr-1$^+$ MDSCs accumulates in the joint tissue and depletion of this population results in improved bacterial clearance by promoting the proinflammatory attributes of infiltrating monocytes and macrophages. These findings suggest that MDSCs are key contributors to the chronicity of *S. aureus* biofilms through their modulation of the host immune response.

        Our previous studies have shown that *S. aureus* biofilms augment Arg-1 expression and polarize macrophages toward an M2 anti-inflammatory state [32]. The present study has expanded the repertoire of immune suppressive effectors to include MDSCs. MDSCs are notable for their robust Arg-1 expression, which depletes extracellular arginine, causing T cell dysfunction at multiple levels, including cell cycle arrest, reduced expression of the CD3ζ chain, and a global reduction in several proteins essential for T cell activity [182-184]. Limited numbers of CD4$^+$ T cells were detected in implant-associated tissues during *S. aureus* biofilm infection (i.e., 2-5%). We expected T cell infiltrates to be enhanced following Gr-1 and Ly6G depletion originating from the loss of MDSC activity; however, this was not the case. One possibility to explain this finding is that the combined action of MDSCs and regulator cytokines serve to limit T cell numbers at the site of biofilm infection, which remains to be determined. Besides actions on T cells, arginine depletion via MDSC Arg-1 activity reduces its availability for iNOS, which thwarts M1 classical macrophage activation, as we have previously shown in *S. aureus* biofilms [32]. By extension, the significant MDSC infiltrate associated with *S. aureus* biofilms *in vivo* is likely an important factor in skewing monocyte/macrophages toward a M2 anti-inflammatory phenotype that promotes bacterial persistence, and our studies confirmed that MDSCs recovered from the site of orthopedic biofilm infection express Arg-1 and IL-10. By further extension, we predicted that depletion of the suppressive MDSC population would allow infiltrating monocytes to act as true effector cells. This was confirmed by the finding that Ly6C$^+$ monocytes recovered from MDSC-depleted animals expressed more proinflammatory genes compared with monocytes recovered

from IgG-treated mice where the MDSC population remained intact. Additionally, MDSC depletion

significantly decreased biofilm burdens, confirming the importance of this population in

orchestrating the anti-inflammatory biofilm milieu to facilitate infection persistence. Besides

MDSCs, regulatory T cells also possess anti-inflammatory attributes similar to MDSCs [185].

However, we did not detect any CD4$^+$CD25$^+$Foxp3$^+$ cells associated with *S. aureus* biofilm

infections (data not shown), whereas another group has reported regulatory T cell involvement in

biofilm clearance [28]. The reasons for these discrepancies are not clear but may arise from

differences in experimental models and/or *S. aureus* strains tested. Based on our analysis, we

propose that MDSCs represent the main immunosuppressive effector cell during *S. aureus*

orthopedic biofilm infection. The signals controlling MDSC recruitment, activation, and

suppressive activity during *S. aureus* biofilm infection remain ill-defined and are ongoing topics of

investigation in our laboratory.

Our RB6-C85 depletion studies revealed significant increases in bacterial dissemination

from the orthopedic infection site. As mentioned previously, RB6-C85 recognizes both Ly6G and

Ly6C epitopes, effectively depleting MDSCs, neutrophils, monocytes, and by extension,

macrophages. Therefore, although MDSC infiltrates were reduced, effector populations were also

targeted, leaving fewer leukocytes either locally or systemically to prevent *S. aureus*

dissemination to peripheral organs. By extension, we propose that the function of each leukocyte

subset differs depending on the local microenvironment; namely, although the inhibitory actions of

MDSCs were negated following RB6-C85 treatment, this coincided with a local reduction in

inflammatory monocytes/macrophages, such that biofilm growth could not be held in check at the

primary infection site (i.e., joint). When biofilm-associated bacteria seeded peripheral sites, the

paucity of systemic neutrophils likely accounted for the failure to effectively clear the infection,

which is essential because neutrophils are a main effector cell against planktonic *S. aureus* [83,

97, 186, 187]. Dissemination was not observed with anti-Ly6G Ab treatment, which was attributed

to the local monocyte/macrophage population that remained intact and exhibited heightened

proinflammatory activity. MDSC infiltrates were also detected in a *S. aureus* catheter-associated

biofilm infection model (Supplemental Fig. S3.3), and RB6-C85 treatment similarly increased

bacterial burdens and dissemination (Supplemental Fig. S3.4), providing independent confirmation that MDSCs are a hallmark of *S. aureus* biofilm infection.

One notable finding in the present study was the extensive extramedullary hematopoiesis observed in the spleens of RB6-C85-treated animals compared with isotype controls. Extramedullary hematopoiesis is frequently seen during chronic inflammatory diseases and cancer [161] and expansion of CD11b$^+$Gr-1$^+$ MDSCs has been reported in tumor and polymicrobial sepsis models [123, 188, 189]. During infection, the requirement for myeloid cells dramatically increases in response to an expanding infectious burden, which creates a need for emergency myelopoiesis and the mobilization of immature myeloid cells from the bone marrow and spleen [161]. The targeted reduction in Gr-1$^+$ cells coincident with increasing biofilm burdens with RB6-C85 treatment likely explains the extensive extramedullary hematopoiesis observed in the spleens of these animals. Another unexpected finding was that Gr-1$^+$ (Ly6G/Ly6C) infiltrates were increased at the site of orthopedic infection following RB6-C85 administration. However, this was likely a compensatory mechanism in response to elevated bacterial burdens both locally and systemically in Gr-1-depleted mice, because these newly recruited Ly6G$^+$Ly6C$^+$ cells were unable to suppress CD4$^+$ T cell proliferation, which agrees with reports of polymicrobial sepsis [123]. Additionally, we also observed enhanced levels of G-CSF, IL-6 and VEGF in the serum of RB6-C85-treated mice, all of which contribute to the expansion of immature myeloid populations [120, 137]. Alternatively, the failure to deplete Ly6G$^+$Ly6C$^+$ infiltrates at later intervals could be explained by the induction of anti-rat IgG Abs that would be expected to impair the efficacy of RB6-C85 treatment (rat anti-mouse Gr-1). However, this appears less likely because RB6-C85 was still capable of significantly reducing inflammatory monocyte and macrophage infiltrates into *S. aureus*-infected joints 2 wk after repeated Ab administration.

Live CT scans revealed significantly more osteolysis in the femurs of RB6-C85-treated animals compared with 1A8 and isotype control mice, which may be attributed to the increased bacterial burdens in the former. The exact mechanisms of osteolysis are still not completely understood, and they differ depending on pathologic conditions [190, 191]. However, several studies suggest that proinflammatory mediators, such as IL-1β, could play a role in the initiation

and progression of osteolysis [192-194], and numerous proinflammatory mediators were significantly elevated in the joint and surrounding soft tissue following RB6-C85 treatment, including IL-1β, that coincided with increased bone destruction. Additionally, *S. aureus* is not only capable of colonizing the bone matrix, but it can also invade osteoblasts, which could contribute to chronicity [195]. Interestingly, a recent study identified phenol-soluble modulins as a key inducer of osteoblast proliferation in and *S. aureus* osteomyelitis model [196]; however, effects on osteoclasts remain to be defined.

Our studies are just beginning to explore the role of MDSCs during *S. aureus* infection. By manipulating these cells with Ab depletion strategies, we demonstrated that their immunosuppressive function prevents monocytes/macrophages from eliminating biofilm-associated bacteria by attenuating their proinflammatory properties. Our findings do not exclude the possibility that the biofilm matrix may also play a role in thwarting immune recognition *in vivo*; however, this remains an area of debate. Although it is clear that intact biofilms do afford some degree of protection against macrophage phagocytosis as previously shown by our laboratory and others [32, 100, 114, 197-199], it is clear that neutrophils are fully capable of invading and phagocytosing biofilm-associated bacteria [61, 100, 112, 200], yet there is no apparent impact on biofilm growth. The fact that staphylococcal biofilms polarize macrophages toward an alternatively activated M2 phenotype does suggest that macrophage surface receptors are triggered to elicit this programming event; however, the identity of these receptors remains unknown. Future studies examining a *S. aureus* biofilm-defective mutant would be valuable for determining whether signals from the biofilm itself are responsible for MDSC recruitment and immunosuppressive activities. Preventing the presumed immunosuppressive action of infiltrating MDSCs may offer a novel therapeutic strategy to thwart these devastating chronic infections.

Chapter 4: Interleukin-12 promotes myeloid-derived suppressor cell (MDSC) recruitment and bacterial persistence during *Staphylococcus aureus* orthopedic implant infection

Published in *Journal of Immunology* 194(8): 3861-72, 2015

Copyright 2015. The American Association of Immunologists, Inc.

Abstract

Staphylococcus aureus is a leading cause of human prosthetic joint infections (PJIs) typified by biofilm formation. We recently identified a critical role for myeloid-derived suppressor cells (MDSCs) in *S. aureus* biofilm persistence. Proinflammatory signals induce MDSC recruitment and activation in tumor models; however, the mechanisms responsible for MDSC homing to sites of biofilm infection are unknown. In this study, we report that several cytokines (IL-12p40, IL-1β, TNF-α, and G-CSF) and chemokines (CXCL2, CCL5) were significantly elevated in a mouse model of *S. aureus* PJI. This coincided with significantly increased MDSC infiltrates concomitant with reduced monocyte, macrophage, and T cell influx compared with uninfected animals. Of the cytokines detected, IL-12 was of particular interest based on its ability to possess either pro- or anti-inflammatory effects mediated through p35-p40 heterdimers, respectively. MDSC recruitment was significantly reduced in both p40 and p35 knockout mice, which resulted in enhanced monocyte and neutrophil influx and bacterial clearance. Adoptive transfer of wild-type MDSCs into infected p40 knockout animals worsened disease outcome, as evidenced by the return of *S. aureus* burdens to level typical of wild-type mice. Tissues obtained from patients undergoing revision surgery for PJI revealed similar patterns of immune cell influx, with increased MDSC-like cells and significantly fewer T cells compared with aseptic revisions. These findings reveal a critical role for IL-12 in shaping the anti-inflammatory biofilm milieu by promoting MDSC recruitment.

<u>Introduction</u>

The number of patients undergoing primary total hip and knee arthroplasties has steadily increased over the past decade, with nearly 800,000 procedures being performed in the United States each year [49]. Prosthetic joint infection (PJI) is a serious complication following arthroplasty, with *S. aureus* being a common inciting pathogen [49]. A recent study using National Inpatient Sample data from 1990-2003 projected the infection incidence following total hip revision to increase from 3,400 in 3005 to 46,000 in 2030, and for total knee replacements from 6,400 in 2003 to 175,500 in 2030 based on the increased volume of prosthetic joint replacement procedures with an aging population [201]. The majority of PJIs are thought to occur during surgery, likely originating from skin commensals. This has led to increased screening for *S. aureus* carriage to ensure that patients undergo decolonization regimens prior to their surgical procedure in an attempt to minimize infection risk [13, 202, 203]. Only a small number of bacteria are required to seed an implanted prosthesis; however, once adherent they can establish a biofilm, affording protection from conventional antimicrobial agents as well as the host immune system [1, 31, 61]. In addition to biofilm formation on prostheses, PJIs are often associated with chronic osteomyelitis, reflecting biofilm growth on a native surface [36, 204]. Due to the difficulty in treating PJIs, patients are often subjected to a staged protocol requiring two surgeries, the first being removal of the infected prosthetic joint and placement of a temporary spacer impregnated with high doses of antibiotics for several weeks, followed by a second surgery for prosthetic joint re-implantation [205-207]. However, patients experiencing a prior PJI are at increased risk for subsequent infections after the placement of a new prosthesis [36, 208]. The significant disease burden associated with PJIs and the increasing prevalence of antibiotic-resistant strains, such as methicillin-resistant and vancomycin intermediate *S. aureus* (MRSA and VISA, respectively), highlights the importance of investigating alternative treatment paradigms. Our approach has been to understand how the host innate immune response is altered during biofilm-associated PJI, with the goal of re-directing this response to facilitate bacterial clearance in combination with conventional antibiotic therapy. This would provide an opportunity for either nonsurgical or one-

stage re-implantation, where removal of the infected prosthesis and reinsertion of the new implant occur simultaneously.

A number of animal models examining *S. aureus* osteomyelitis have shown an elevation of inflammatory cytokines that have been implicated in bone remodeling as well as pathology [209-212]. In contrast, the inflammatory events associated with *S. aureus* PJI remain to be fully elucidated. In particular, the presence of a foreign body may alter the kinetics and/or dynamics of the host immune response to inadvertently facilitate biofilm formation and persistence. Although a recent report described a key role for IL-1β in a mouse model of *S. aureus* post-arthroplasty infection [162], the cellular source of IL-1β and a detailed analysis of infiltrating leukocytes was not assessed. Other investigations using a mouse *S. aureus* tibial implant model have suggested the involvement of Th2 and Treg cells in bacterial clearance [167]; however, an in-depth analysis of innate immune mechanisms was not conducted. A detailed evaluation of the inflammatory events during *S. aureus* PJI is warranted to identify mechanisms whereby the organism is able to subvert host innate immunity to establish chronic disease.

Our recent report documented an important role for myeloid-derived suppressor cells (MDSCs) in *S. aureus* persistence during PJI [60]. In particular, MDSC depletion facilitated biofilm clearance by augmenting the proinflammatory properties of infiltrating monocytes. The objective of the current report was to identify critical cytokines responsible for MDSC action during biofilm formation *in vivo*. One candidate was IL-12p40, which was markedly elevated during *S. aureus* biofilm formation. IL-12p40 pairs with the p35 or p19 polypeptides to form the heterodimeric cytokines IL-12 and IL-23, respectively [213, 214]. However, it is well known that IL-12p40 is produced in excess of the other IL-12 family subunits and can exert negative regulatory effects as a homodimer by competitively binding the IL-12 receptor [215-217]. A recent report demonstrated a role for IL-12p40 in *S. aureus* orthopedic implant infection after treatment with a neutralizing Ab [167]. However, the only readout reported was a reduction in the percentage of mice that remained infected after 21 days; no information pertaining to bacterial burdens, inflammatory infiltrates, or the cytokine's mechanism of action was described. In the current study, we found that both p40 and p35 KO mice displayed significant reductions in MDSC infiltrates during *S.*

aureus PJI, which coincided with significantly increased monocyte and macrophage infiltrates and improved bacterial clearance. A direct role for MDSCs in this process was revealed by the ability of adoptively transferred wild type MDSCs to significantly increase *S. aureus* biofilm burdens in IL-12p40 KO mice, implicating a key role for IL-12 in shaping the local inflammatory milieu to favor MDSC accumulation and biofilm persistence. These effects were not observed in p19 KO mice, demonstrating that IL-23 does not play a role in shaping the biofilm inflammatory milieu. Examination of tissues obtained from patients undergoing revision surgery for PJI revealed increased MDSC-like infiltrates and a paucity of T cells compared with aseptic revisions, along with dramatic increases in a variety of pro-inflammatory mediators. These findings recapitulate what is observed in our mouse model of orthopedic implant infection, demonstrating its utility for deciphering mechanisms of biofilm evasion of host immunity during PJI and therapeutic interventions.

Results

S. aureus orthopedic implant infections are typified by immune skewing and chronicity.

One complication after joint replacement surgery is persistent biofilm-associated PJI, with *S. aureus* being a frequent etiological agent [36, 218, 219]. Here we utilized a mouse model of *S. aureus* post-arthroplasty joint infection that mimics PJI [220, 221]. Prior studies from our laboratory and others have demonstrated ultrastructural evidence of biofilm formation on infected implants in this mouse model by SEM [162, 213](Goriely et al 2008, Bernthal et al 2010). Biofilm formation is typified by bacterial persistence, which was demonstrated in the knee joint, surrounding soft tissue, and femur until day 28 postinfection (Fig. 4.1) with bacterial burdens still evident at 3 mo (data not shown). Fewer bacteria were associated with the implant (10-1000 CFU; data not shown), despite the continued colonization of neighboring sites. This suggests that our model has features of chronic osteomyelitis, which is a common sequelae of PJI [36, 204]. However, the possibility remains that PJI-associated bacteria were dislodged from the implant upon removal from the medullary cavity because of the constricted space. Bacterial growth was never detected in animals receiving aseptic implants in any of the tissues examined (data not shown).

Histological evaluation revealed dramatic inflammation of the soft tissues surrounding infected joints at day 7, which was increased by day 28 (Supplemental Fig. S4.1B and D). Gram stains revealed bacterial localization along the implant-tissue interface in *S. aureus*-infected animals suggestive of biofilm formation (Supplemental Fig. S4.1E). CT analysis revealed substantial bone loss at the distal tip of infected implants near the patella, which was most discernable at later stages of infection (Supplemental Fig. 4.2). In contrast, animals receiving aseptic implants showed no evidence of bone destruction. Collectively, these features demonstrate good fidelity of the mouse model to pathology that occurs during PJIs in humans.

A better understanding of the inflammatory processes that ensue during persistent PJI is needed to develop more effective treatment paradigms. To this end, we first examined the production of inflammatory mediators in the knee joint, surrounding soft tissue, and femur in the mouse model. Several proinflammatory cytokines, including IL-12p40, IL-1β, TNF-α, and G-CSF,

were increased in all tissue regions from *S. aureus*-infected mice throughout the 28 d time course (Fig. 4.2). Likewise, numerous chemokines, such as CXCL2 and CCL5, were also markedly elevated in infected tissues (Fig. 4.2). Aseptic implants elicited transient inflammatory mediator production (Fig. 4.2), which most likely originated from the trauma generated during the surgical procedure. To evaluate whether enhanced chemokine production in *S. aureus*-infected joints translated to increased leukocyte infiltrates, FACS analysis was performed at weekly intervals for 1 mo postinfeciton. Of the total $CD45^+$ leukocyte infiltrate, the predominant cell type detected was $Ly6G^{high}Ly6C^+$, which we have recently identified as functional MDSCs (Fig 4.3A and B) [60]. Contrary to the significant influx of MDSCs into *S. aureus*-infected tissues, monocyte ($Ly6G^-Ly6C^+$), macrophage ($F4/80^+$), and neutrophil ($Ly6G^{low}Ly6C^{low}$) infiltrates were significantly decreased compared with mice receiving aseptic implants (Fig 4.3C, D and F) despite the heightened expression of numerous chemokines that target these specific cell populations (Fig 4.2). In addition to these innate leukocyte populations, $CD3^+$ T cells were significantly decreased in infected tissues, whereas T cell infiltrates were elevated in animals receiving aseptic implants, particularly during the first two weeks post-surgery (Fig 4.3G). Collectively, these results demonstrate that *S. aureus* PJIs actively augment MDSC influx while suppressing the recruitment of numerous leukocyte subsets.

Figure 4.1
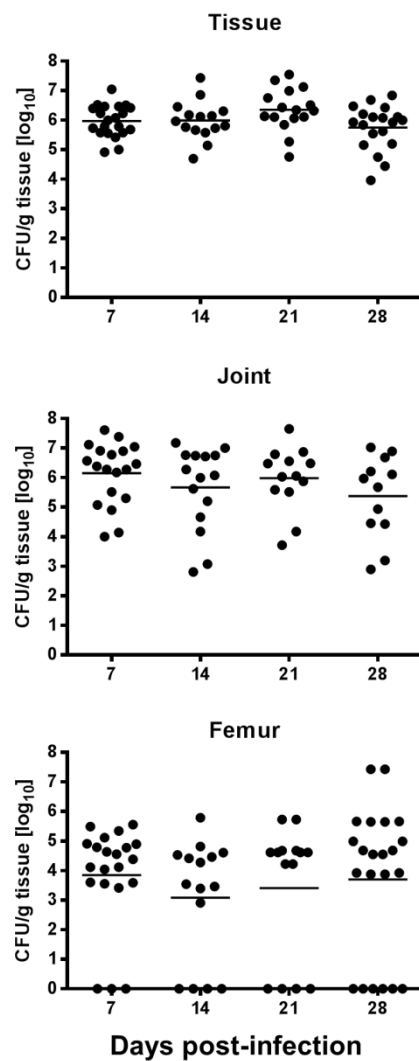
***S. aureus* persistence during orthopedic implant infection.** The femur, knee joint, and surrounding soft tissue associated with *S. aureus*-infected titanium implants were collected at the indicated intervals for quantitation of bacterial burdens. Animals receiving aseptic implants did not display any bacterial growth and are not shown. Results are expressed as CFU per gram of tissue to normalize for differences in sampling size and are presented from individual animals combined from three independent experiments (n = 12-24 mice/group).

Figure 4.2
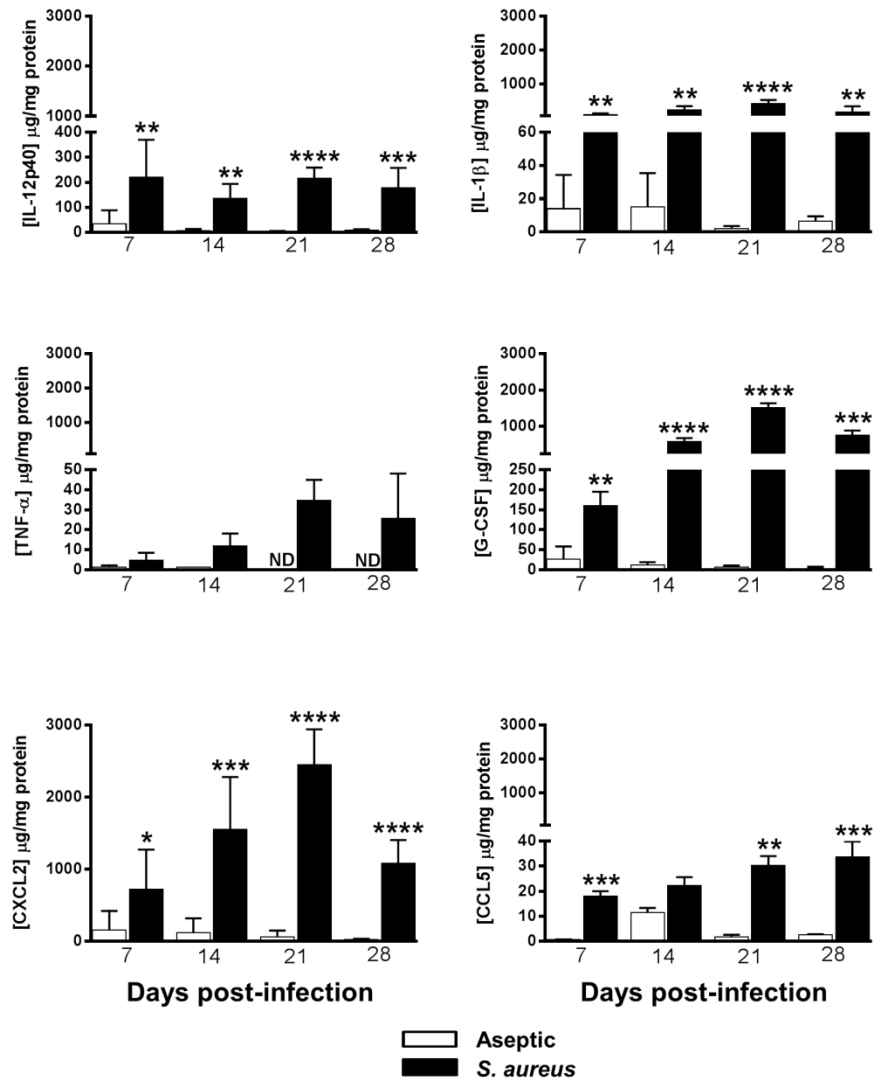
***S. aureus* orthopedic implant infection elicits sustained cytokine and chemokine**

production. Tissues surrounding the knee joint of mice with *S. aureus*-infected (n = 6) or aseptic

(n = 8) implants were collected at the indicated time points, whereupon IL-12p40, IL-1β, TNF-α,

G-CSF, CXCL2, and CCL5 production was measured by multi-analyte bead arrays. Results are

normalized to the amount of total protein to correct for differences in tissue sampling size (*$p <$

0.05; **$p <$ 0.01; ***$p <$ 0.001; ****$p <$ 0.0001; unpaired Student's *t* test). ND, not detected

Figure 4.3
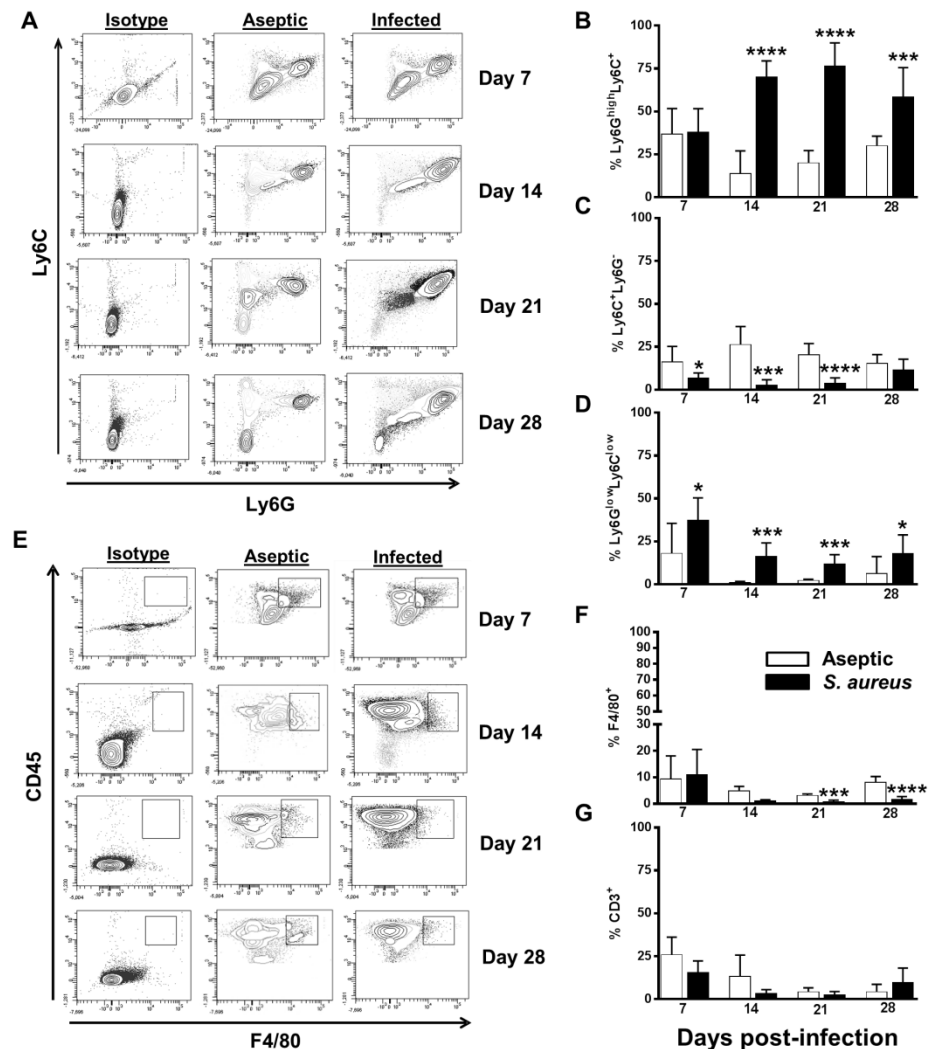
***S. aureus* orthopedic implant infections are typified by a robust MDSC infiltrate.** Soft tissues surrounding the knee joint of mice with *S. aureus*-infected (n = 6-8) or aseptic (n = 8) implants were analyzed by flow cytometry for leukocyte infiltrates at the indicated time days after infection. Results were calculated after gating on the CD45$^+$ population. (**A**) Representative contour plots of Ly6G and Ly6C-stained cells and quantitation of (**B**) Ly6G^{high}Ly6C$^+$ MDSCs; (**C**) Ly6G$^-$Ly6C$^+$ monocytes; and (**D**) Ly6G^{low}Ly6C^{low} neutrophils. (**F**) Representative contour plots of CD45 and F4/80-stained cells and quantification of (**E**) F4/80$^+$ macrophages. (**G**) Quantification of CD3$^+$ T cells. Results are representative of three independent experiments (*$p < 0.05$; ***$p < 0.001$; ****$p < 0.0001$; unpaired Students *t* test).

Tissues from human PJIs display increased MDSC-like and reduced T cell infiltrates with elevated pro-inflammatory mediator expression. To determine whether the patterns of leukocyte infiltration and inflammatory mediator production observed in our mouse model translated to human infection, these parameters were assessed in tissue samples from patients undergoing revision surgeries for PJIs or aseptic loosening as a control (Fig 4.4A). Of the infected tissues analyzed in this study, three were confirmed group B streptococcus and two were *S. epidermidis.* Here we report findings with *S. epidermidis*, since it is most closely related to *S. aureus*, which was utilized throughout our mouse studies. Compared with mice, human MDSC markers are less well-defined, with some reports describing this population as CD33$^+$HLA-DR$^-$ [129, 222]. Similar to our mouse model, a population of MDSC-like cells (CD33$^+$HLA-DR$^-$) was detected in tissues from a patient with confirmed *S. epidermidis* PJI, whereas few of these cells were observed in aseptic samples (Fig 4.4C). In contrast, T cell influx was minimal in infected specimens, whereas T cells were the most abundant infiltrate associated with tissues recovered from aseptic orthopedic revisions (Fig 4.4B). Additional CD45$^+$ leukocyte populations were also detected in infected patient tissues, including CD33$^-$HLA-DR$^+$ (Fig 4.4C) as well as CD66$^+$CD14$^-$ and CD66$^-$CD14$^+$ cells (Fig 4.4D). To better define these leukocyte populations and examine their activation status, subsets were purified from infected patient tissues by FACS, whereupon RNA was immediately isolated to examine gene expression by qRT-PCR. The CD33$^+$HLA-DR$^-$ population recovered from the confirmed *S. epidermidis* infection expressed several genes characteristic of MDSCs, including Arg-1, iNOS, and IDO-1, further strengthening the classification of these cells as MDSC-like (Fig 4.4E) [139, 222]. Interestingly, none of the genes analyzed were detected in CD33$^-$HLA-DR$^-$CD66b$^+$ neutrophil-like cells, whereas CD33$^-$HLA-DR$^+$ monocyte/macrophage infiltrates expressed iNOS, IDO-1, and TNF-α (Fig 4.4E). Analysis of inflammatory mediator expression revealed elevated levels of G-CSF, IL-1β, IL-6, IL-8, and soluble CD40 ligand (sCD40L) in *S. epidermidis*-infected tissues compared to aseptic specimens (Fig. 4.4F). These results confirm that similar leukocyte infiltration patterns are observed between our mouse post-arthroplasty infection model and human PJI tissues; namely, increased MDSC-like cells and a paucity of T cells. In addition, human PJI tissues were typified by elevated

inflammatory mediator expression as was seen in the mouse. These findings demonstrate the utility of the mouse model for deciphering mechanisms of biofilm evasion of host immunity during human PJI and therapeutic interventions.

Figure 4.4

	CD45⁺CD33⁺HLA-DR⁺ MDSC-like	CD45⁺CD33⁻HLA-DR⁺ Monocyte/MΦ	CD45⁺CD33⁻ HLA-DR⁻CD66b⁺ Neutrophil-like
Arg-1*	+	-	-
iNOS	+	+	-
IDO-1	+	+	-
IL-10	-	-	-
PTGS2	-	-	-
MRC1	-	-	-
TNF-α	-	+	-
PRTN3	+	-	-

*Arg-1, arginase-1; iNOS, inducible nitric oxide synthase; IDO-1, indoleamine 2,3-dioxygenase-1; IL-10, interleukin-10; PTGS2, prostaglandin-endoperoxide synthase 2 (COX2); MRC1, mannose receptor C type 1 (CD206); TNF-α, tumor necrosis factor-alpha; PRTN3, proteinase 3
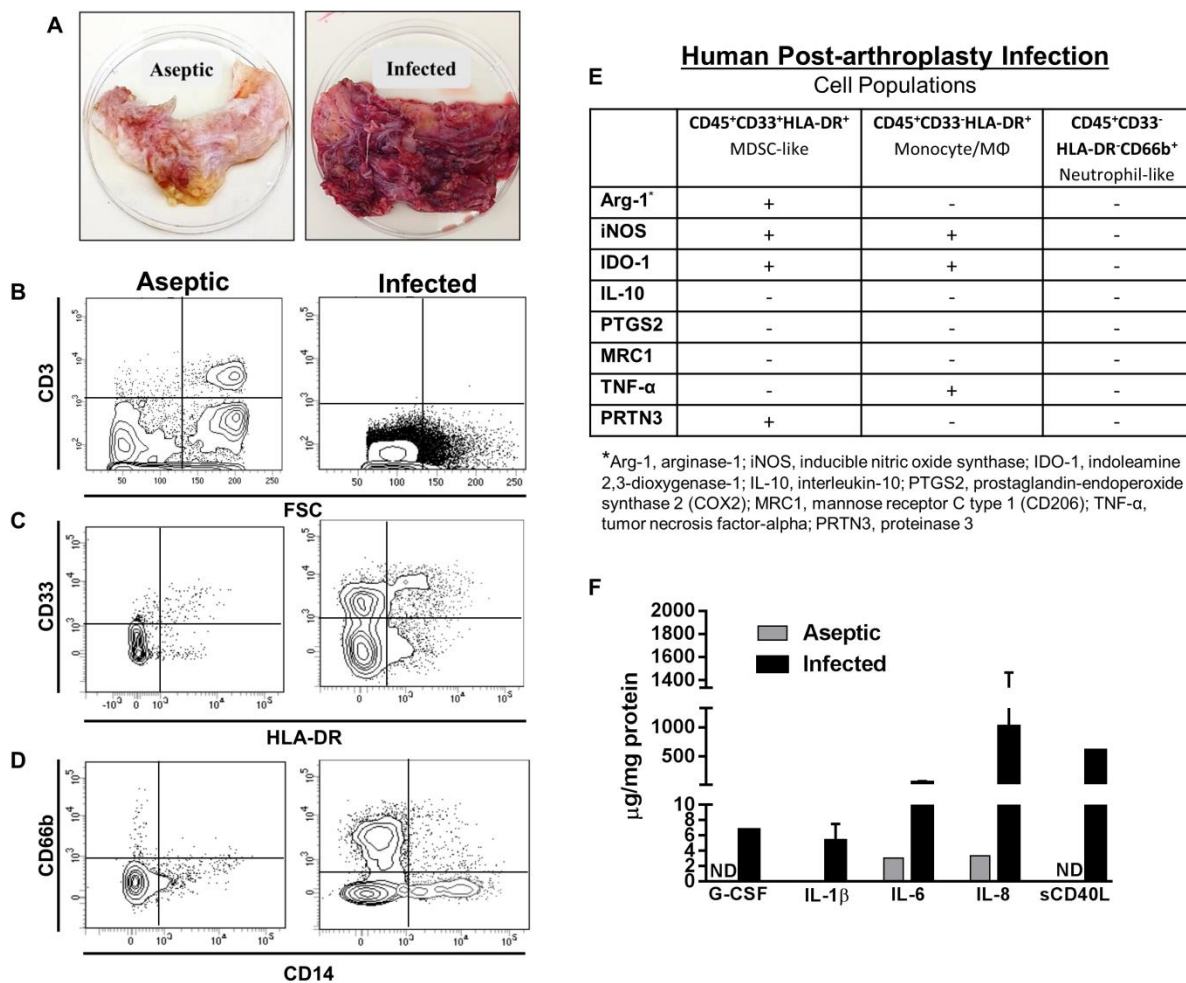
Tissues from human PJIs display increased MDSC-like and reduced T cell infiltrates. (**A**) Tissues surrounding aseptic and *S. epidermidis*-infected knee prostheses were collected for flow cytometric analysis, qRT-PCR, and inflammatory mediator production. Representative contour plots of (**B**) CD3⁺ T cells; (**C**) MDSC-like infiltrates (CD33⁺HLA-DR⁻); (**D**) CD66b⁺ granulocytes and CD14⁺ mononuclear cells gated on the CD45⁺ population. (**E**) qRT-PCR analysis of genes that were detected (**+**) versus absent (**-**) in each sorted cell population and (**F**) quantitation of G-CSF, IL-1β, IL-6, IL-8 and sCD40L expression in tissues shown in (**A**). Results were normalized to the amount of total protein to correct for differences in tissue sampling size. ND, not detected.

IL-12 is critical for MDSC recruitment and attenuating innate immune cell influx during *S. aureus* orthopedic implant infection. The IL-12 family of cytokines possesses pro-inflammatory properties that regulate macrophage and T cell activation [223-225]. In addition, pro-inflammatory cytokines have been reported to recruit and activate MDSCs [121, 226], which are significantly elevated in our *S. aureus* orthopedic implant infection model (Fig 4.3) and inhibit T cell activation [60]. Based on the increases in IL-12p40 expression in human PJI tissues (data not shown) and our mouse model (Fig 4.2) and its ability to exert either pro- or anti-inflammatory activity mediated by p35-p40 heterodimers or p40 homodimers, respectively, we examined the importance of IL-12 family members during early *S. aureus* orthopedic infection using IL-12p40 and p35 KO mice.

Examination of leukocyte recruitment in *S. aureus*-infected IL-12p40 and p35 KO animals revealed significant decreases in Ly6G^{high}Ly6C$^+$ MDSCs (Fig 4.5A and B). To determine whether these residual MDSC infiltrates retained suppressive activity, MDSCs from IL-12p40 and p35 KO mice were purified by FACS at days 7 and 14 after infection and examined for their ability to inhibit polyclonal T cell activation. MDSCs recovered from both IL-12p40 and p35 KO mice were capable of inhibiting T cell proliferation (Fig 4.5C and D, respectively). However, IL-12p40 KO mice do not display any evidence of defects in MDSC development, and analysis of MDSCs from the spleens of WT and IL-12p40 KO mice reveal similar percentages in both naïve animals and following *S. aureus* PJI (data not shown).This finding suggests that IL-12 promotes MDSC recruitment rather than functional activity. Our recent report demonstrated that MDSC depletion during *S. aureus* PJI enhanced monocyte recruitment and intrinsic pro-inflammatory activity (Heim et al 2014). Similarly, the nearly 70-80% reduction in MDSC infiltrates observed in IL-12p40 and p35 KO mice translated into significant increases in Ly6G$^-$Ly6C$^+$ monocyte recruitment (Fig 4.6) and improved bacterial clearance in both IL-12p40 and p35 KO mice compared with WT animals (Fig 4.7). Coincident with reduced bacterial burdens, the production of numerous inflammatory mediators, including IL-1β, TNF-α, G-CSF, and CXCL2 was decreased in IL-12p40 and p35 KO mice (Fig 4.8). Since IL-23p19 also shares the common p40 subunit [227], we examined *S. aureus* infection in p19 KO mice but found no differences in inflammatory indices in comparison with WT animals (data not shown).

To further implicate MDSCs as the key cell type responsible for inhibiting innate immune cell influx and promoting *S. aureus* persistence during PJI, bone marrow-derived MDSCs from WT mice were adoptively transferred into IL-12p40 KO animals one day after infection, whereupon bacterial burdens were assessed 7 and 14 days later (Fig 4.9). MDSCs for these experiments were expanded from bone marrow *in vitro* and confirmed for their ability to inhibit T cell proliferation (Supplemental Fig S4.3). The adoptive transfer of WT MDSCs into IL-12p40 KO animals restored bacterial burdens to those typically observed in WT mice and reduced monocyte and neutrophil infiltrates (Fig. 4.9). These effects are likely the result of MDSC activity and not IL-12 release *per se*, since MDSCs are not a major source of IL-12. This experiment was not performed in p35 KO animals, since all of our prior studies demonstrated a concordance in phenotypes between p40 and p35 KO mice (Figs 4.5-8). Collectively, these findings demonstrate that IL-12 plays a key role in MDSC recruitment during *S. aureus* PJI to actively suppress monocyte and neutrophil influx and promote bacterial persistence.

Figure 4.5
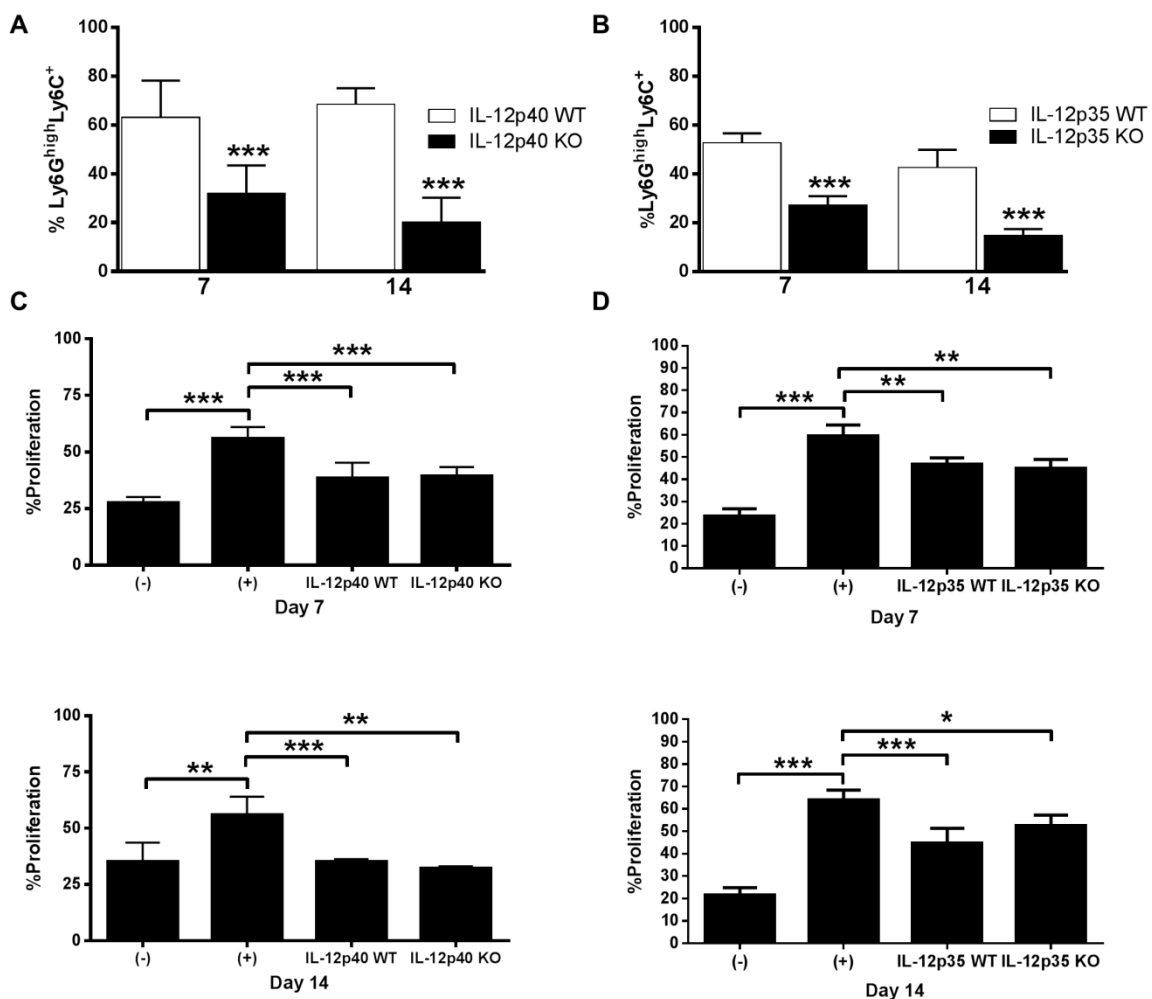
Recruitment of T cell-suppressive MDSCs during *S. aureus* orthopedic infection is regulated by IL-12. LyG^{high}Ly6C$^+$ MDSCs associated with knee joint of *S. aureus*-infected wild-type (WT) and (**A**) IL-12p40 or (**B**) IL-12p35 knockout (KO) mice (n = 8/group) were quantified by flow cytometry at the indicated times after infection. Results were calculated after gating on the CD45$^+$ population and represent the mean ± SEM of three independent experiments. MDSCs were purified from infected knee tissues of WT and (**C**) IL-12p40 or (**D**) IL-12p35 KO mice at days 7 and 14 post-infection for T cell proliferation assays. Results are expressed as the % proliferation with T cells alone (-) and CD3/CD38-stimulated T cells (+) as controls. Results represent two independent experiments. (*$p < 0.05$; **$p < 0.01$; ***$p < 0.001$; unpaired Student's *t* test).

Figure 4.6
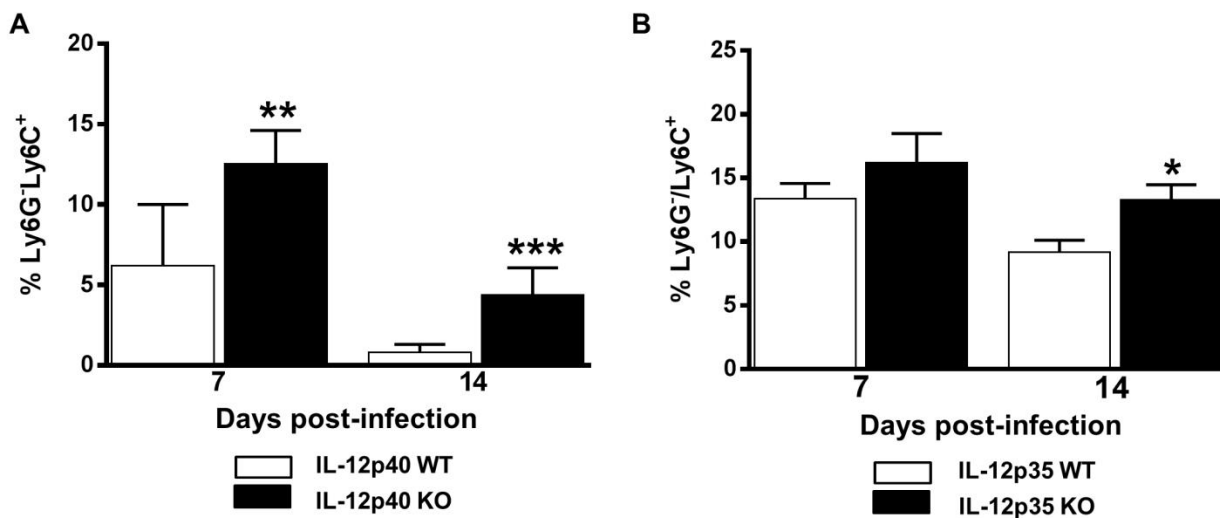
IL-12 deficiency increases monocyte influx during *S. aureus* orthopedic implant infection.

Ly6G⁻Ly6C⁺ monocytes associated with the knee joint of *S. aureus*-infected WT and (**A**) IL-12p40
or (**B**) IL-12p35 KO mice (n = 8/group) were quantified by flow cytometry at the indicated times
after infection. Results were calculated after gating on the CD45⁺ population and are
representative of three independent experiments (*$p < 0.05$; **$p < 0.01$; ***$p < 0.001$; unpaired
Student's *t* test).

Figure 4.7
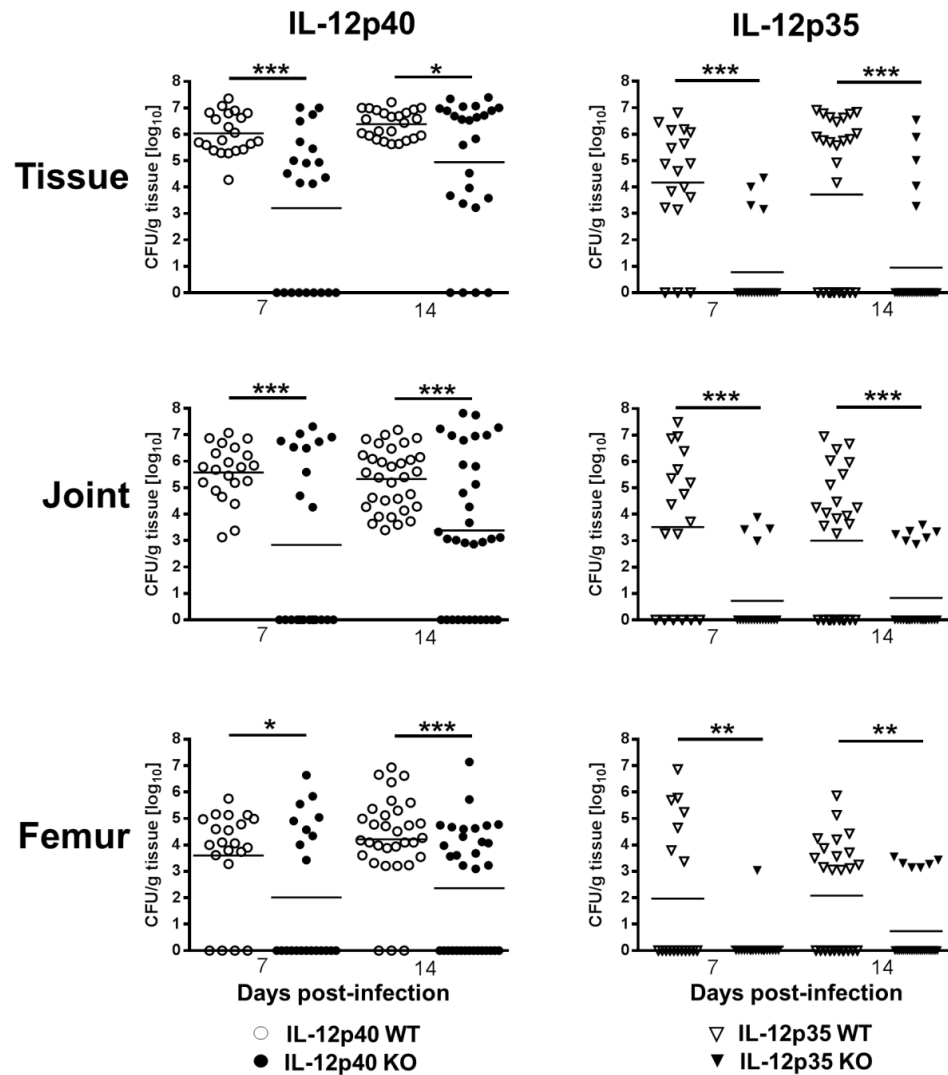
IL-12 is critical for the establishment of *S. aureus* implant-associated infection. A titanium implant was place in the femur of WT and IL-12p40 or IL-12p35 KO mice (n = 8/group) followed by inoculation with 10^3 CFU *S. aureus.* The femur, knee joint, and surrounding soft tissue were collected at the indicated intervals after infection for quantitation of bacterial burdens. Results are expressed as CFU per gram of tissue to normalize for differences in sampling size and are combined from the three independent experiments (*p < 0.05; **p <0.01; ***p < 0.001; Wilcoxon rank sum test).

Figure 4.8
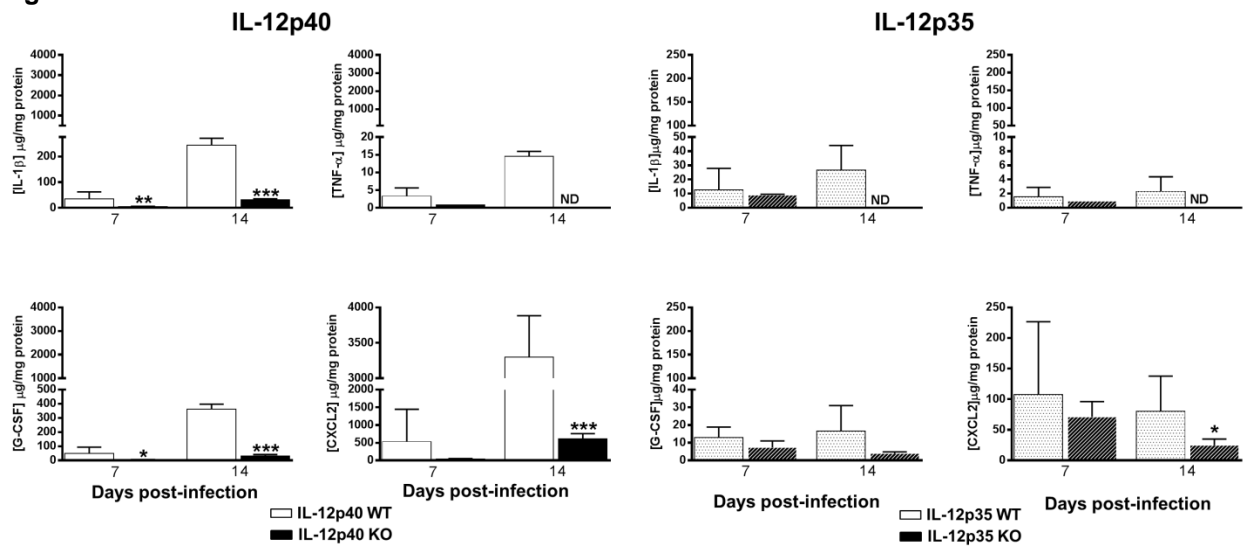
IL-12 regulates inflammatory mediator production during *S. aureu*s orthopedic implant infection. Tissues surrounding the knee joint of *S. aureus*-infected WT (n = 8) and IL-12p40 (n = 8) or IL-12p35 KO (n = 8) mice were collected at days 7 and 14 post-infection, whereupon IL-1β, TNF-α, G-CSF and CXCL2 production was measured using multi-analyte bead arrays. Results are representative of two independent experiments and are normalized to the amount of total protein to correct for differences in tissue sampling size (*$p < 0.05$; **$p < 0.01$; ***$p < 0.001$; unpaired Student's *t* test). ND, not detected.

Figure 4.9
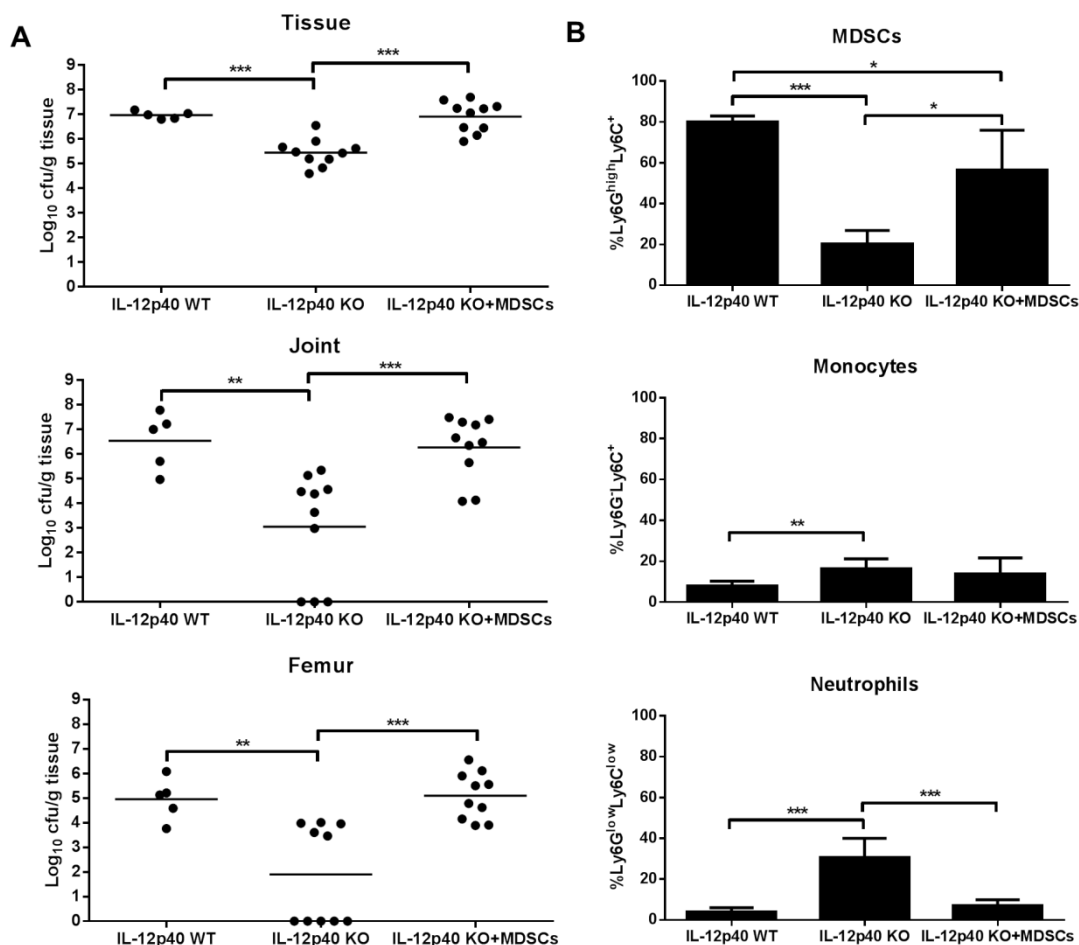
MDSCs are responsible for *S. aureus* persistence and inhibition of immune cell influx during orthopedic implant infection. WT and IL-12p40 KO mice (n = 10/group) were infected with *S. aureus*, whereupon IL-12p40 KO animals received an adoptive transfer of 2.5 x 10^6 purified WT MDSCs s.c. at the implant site one day post-infection, whereas WT and a separate group of IL-12p40 KO animals received s.c. injections of PBS. (Left) The femur, knee joint and surrounding soft tissue were collected at day 7 after infection for quantitation of bacterial burdens. (Right) Quantitation of Ly6G^{high}Ly6C$^+$ MDSCs, Ly6G$^-$Ly6C$^+$ monocytes, and Ly6G^{low}Ly6C^{low} neutrophils. Results were calculated after gating on the CD45$^+$ population and represent two independent experiments (*p < 0.05; **p < 0.01; ***p < 0.001; unpaired Student's *t* test).

Supplemental Figure S4.1

Day 7   **Day 28**
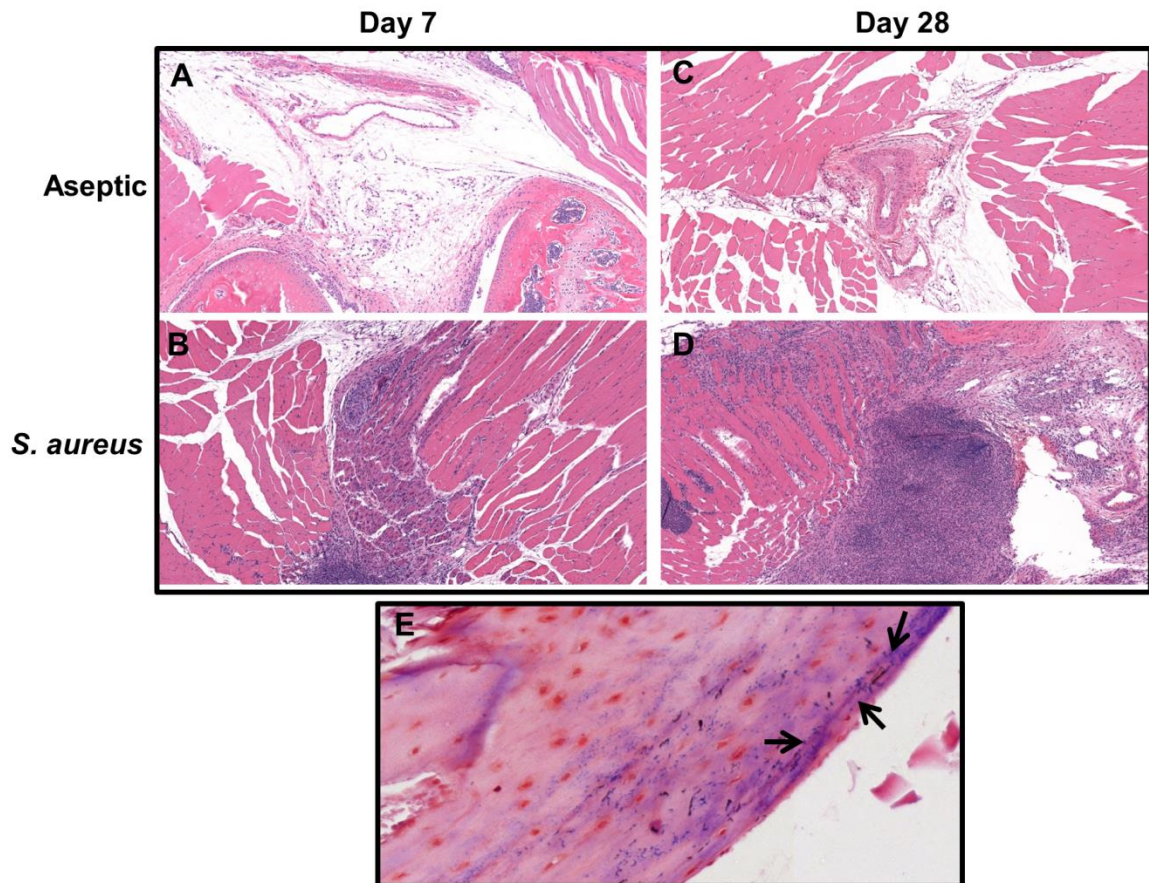
Aseptic

S. aureus

S. aureus **orthopedic implant infections are typified by robust and persistent inflammation.** H&E-stained sections of tissues surrounding the knee joint of animals receiving aseptic (**A** and **C**) or *S. aureus*-infected (**B** and **D**) implants at days 7 (**A** and **B**) and 28 (**C** and **D**) after placement/infection (10x magnification). (**E**) Gram stain of *S. aureus*-infected knee tissue 7 days after infection (40x magnification; arrows indicate *S. aureus* at the implant-tissue interface). Representative images are presented from mice receiving aseptic (n = 2) and *S. aureus*-infected (n = 6) implants.

Supplemental Figure S4.2
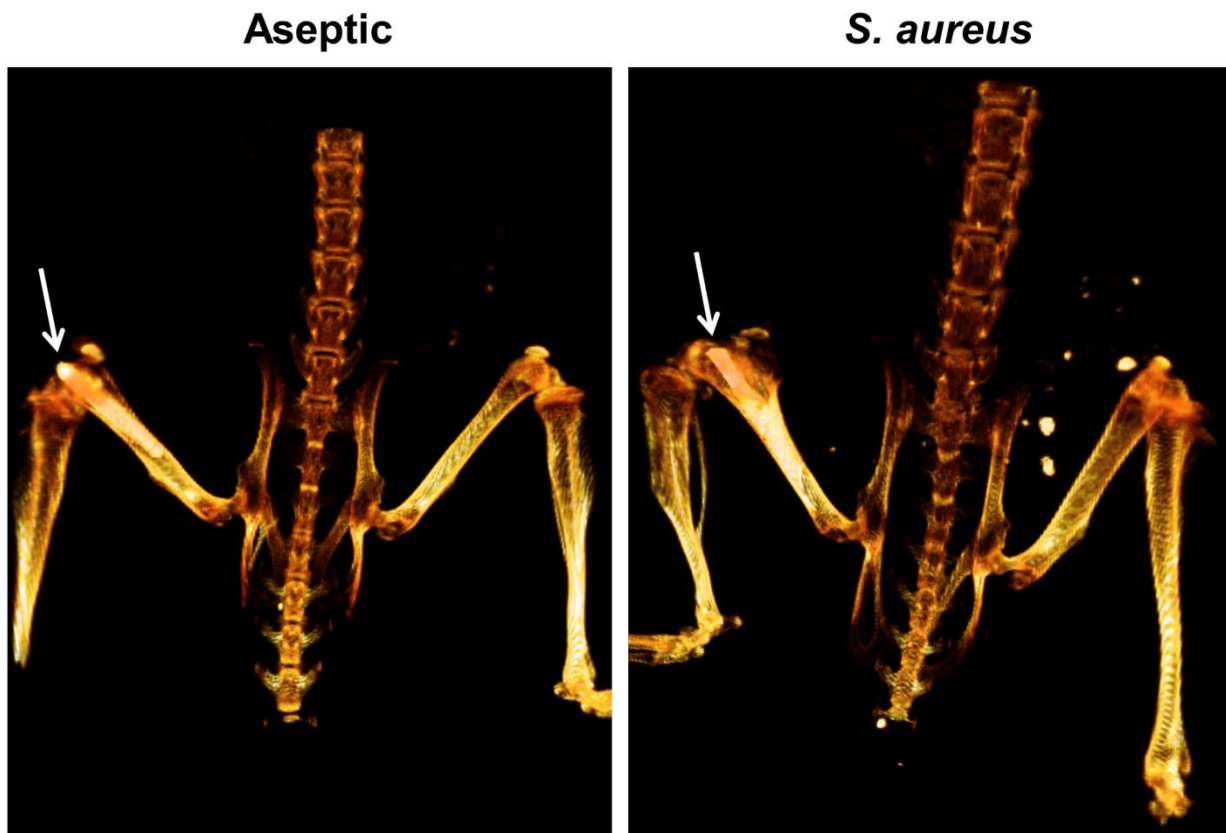
Chronic *S. aureus* orthopedic implant infection results in marked bone loss. Comparison of bone integrity in mice with aseptic or *S. aureus*-infected orthopedic implants 28 days after placement/infection using live CT imaging (ventral view). Color intensity is indicative of bone density, where white = most dense and dark orange = least dense. Arrows indicate the implant protruding into the joint space. Representative images are presented from mice receiving aseptic (n = 2) and *S. aureus*-infected (n = 4) implants.

Supplemental Figure S4.3
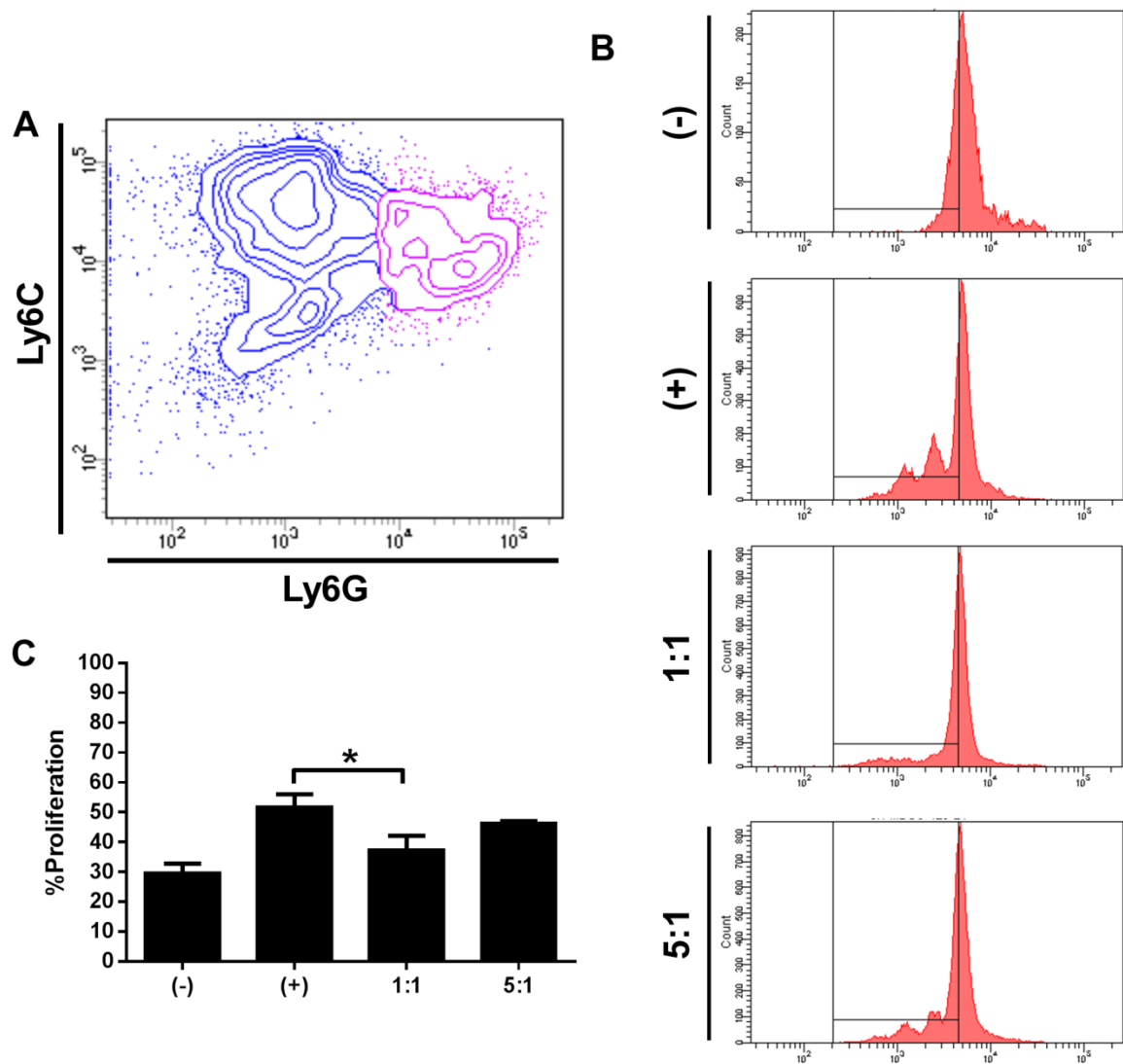
***In vitro* generated MDSCs inhibit polyclonal CD4$^+$ T cell proliferation.** Bone marrow-derived Ly6G$^+$Ly6C$^+$ MDSCs were purified by FACS and cultured with efluor670-labeled CD4$^+$ T cells at either a 1:1 or 5:1 ratio for proliferation assays. (**A**) Representative contour plot depicting Ly6G and Ly6C expression in the expanded population. (**B**) Representative histograms of fluorescence intensity and (**C**) % proliferation compared with T cells alone (-) or CD3/CD28-stimulated T cells (+). Each treatment was performed in triplicate and results represent two independent experiments (*$p < 0.05$; unpaired Student's *t* test).

Discussion

Despite extensive antiseptic precautions, most PJIs are thought to occur by hardware contamination from skin microflora during surgical insertion [36, 228]. As such, PJIs often take several months to years to manifest and most are attributed to *S. aureus* and *S. epidermidis* [27, 229, 230]. The paramount obstacle for effective treatment of PJIs is their recalcitrance to antibiotic therapy coupled with the ability to skew the immune response towards an anti-inflammatory, pro-fibrotic state [31, 61]. Therefore, the current standard-of-care to treat chronic PJIs requires removal of all foreign material, intravenous antibiotics for four to six weeks, and re-implantation of the prosthetic joint. This treatment does carry a high success rate of 80-90%; however, the morbidity and mortality associated with the patient's infection and its treatment is one of the most catastrophic complications in orthopedics [220, 231, 232]. Another important point is that the majority of prosthetic joint replacement surgeries are performed in the elderly, a population known to have waning immunity compared with younger patients [233, 234]. Therefore, with the expanding aging population, the frequency of PJIs is projected to increase. Collectively, these facts highlight the need for a better understanding of the underlying mechanisms involved in immune deviation during PJIs, which facilitate the development of novel therapeutics.

Importantly, our mouse model of PJI utilizes a very low infectious inoculum (i.e. 1,000 bacteria), which represents a realistic level of bacterial exposure that might occur following the inadvertent transfer of organisms during prosthesis insertion in patients. The ability of the mouse model to recapitulate features of human PJI was substantiated by our analysis of tissues collected from patients undergoing revision surgeries for the treatment of PJI. Namely, cells with markers and gene expression profiles indicative of MDSCs (i.e. CD33$^+$HLA-DR$^-$) were evident with few/no T cell infiltrates detected. Both infected human and mouse tissues were typified by heightened inflammatory mediator expression compared with aseptic specimens; however, this was not sufficient to program infiltrating phagocytes for anti-biofilm activity, since infections persisted. We show that this results from MDSC action, which actively inhibits phagocyte microbicidal activity. Of the tissues collected from patients undergoing revision surgeries for PJI in

this study, three were confirmed group B streptococcus and two were *S. epidermidis.* In general, immune profiles were similar among these patient samples, suggesting that common immune responses are elicited during chronic PJI regardless of the inciting pathogen. This is important, since it implies that identifying methods to augment anti-biofilm immunity for the treatment of PJI might be efficacious against numerous bacterial species.

In these studies, IL-12 was critical for organizing the local inflammatory milieu as revealed by the significant reduction in MDSC infiltrates at the site of PJI in both p40 and -35 KO mice. Impaired MDSC recruitment coincided with increased phagocyte influx, including monocytes and neutrophils, which resulted in enhanced biofilm clearance. A direct role for MDSCs in this process was confirmed by the ability of adoptively transferred WT MDSCs to worsen disease outcome in IL-12p40 KO animals, as evidenced by the return of *S. aureus* burdens to levels of WT mice concomitant with significant reductions in monocyte and neutrophil recruitment. Previously, we have reported that IL-12p40 expression is dramatically reduced in MDSCs isolated from PJIs (Heim et al 2014); however, in the current report, we failed to detect IL-12p40 expression in MDSCs recovered from PJIs of WT mice by qRT-PCR (data not shown), indicating that MDSCs are not a major source for IL-12 production. The finding that immune phenotypes were similar in p40 and p35 KO mice and not evident in p19 KO animals suggests that IL-12p70 is important for organizing the immune permissive biofilm response. However, we cannot rule out the potential contribution of inhibitory p40 homodimers, since p40 is secreted in large excess of p40-p35 heterodimers and has recently been shown to bind to other polypeptides distinct from the IL-12 family that may also impact the local biofilm inflammatory milieu. The requirement for IL-12 was unexpected given its prominent role in Th1 polarization, since few T cell infiltrates were detected at the site of infection in both the mouse model and human PJI tissues. Instead, our findings suggest that IL-12 induces MDSC recruitment, as revealed by the 70-80% reduction in MDSC influx into *S. aureus*-infected IL-12p40 and p35 KO properties argues against a role for IL-12 in MDSC activation. Although seemingly counterintuitive based on the suppressive properties of MDSCs, proinflammatory signals have been reported to induce MDSC recruitment and activation in the two-step model proposed by Gabrilovich [121, 226, 235].

Impaired MDSC recruitment and activation in IL-12p35 and p40 KO mice likely accounted for improved bacterial clearance due to the removal of this suppressive population in conjunction with elevated granulocytic and monocytic infiltrates, which was confirmed by our adoptive transfer studies. Similar to our findings, a recent report demonstrated a role for IL-12p40 in *S. aureus* orthopedic implant infection after treatment with a neutralizing Ab [28]; however, the only readout described in this study was a reduction in the percentage of mice that remained infected after 21 days; no information pertaining to bacterial burdens, inflammatory infiltrates, or the effect on other cytokines/chemokines at the infection site was reported. Therefore, our studies provide important mechanistic information regarding the role of IL-12 in the establishment of a local inflammatory microenvironment that is favorable for bacterial persistence. In addition, the proposed mechanism of IL-12 action between this earlier study and our report is strikingly different. Namely, Prabhakara et al. suggested that IL-12p40 promotes Th1/Th17 action to favor infection persistence; however, this is likely not the case in our model, since few T cell infiltrates were observed. Instead, we propose that IL-12 induces MDSC recruitment, leading to the diminished influx of professional phagocytes and impaired bacterial clearance. In addition, a few differences in the models utilized in these studies may account for these distinct findings. For example, Prabhakara et al. inserted implants that were precoated with *S. aureus* [28], whereas our devices were infected after surgical placement and the location of implants was distinct (femur versus tibia).

One question that remains is how does IL-12 promote MDSC recruitment to sites of *S. aureus* PJI? The most plausible explanation is that IL-12 acts indirectly by inducing the expression of a chemokine(s) with actions on MDSCs. Potential candidates include CXCL2 and CCL2 that are elevated at the site of *S. aureus* PJI and MDSCs have been reported to express the associated chemokine receptors CXCR2 and CCR2, respectively [236-240]. Of note, both CXCL2 and CCL2 expression were significantly reduced in *S. aureus*-infected IL-12p40 and p35 KO mice in agreement with the minimal MDSC infiltrates observed in these animals. Alternatively, it is possible that IL-12 plays a non-canonical role in eliciting MDSC recruitment during the course of *S. aureus* post-arthroplasty infection such as augmenting PGE2 expression, which has also

been shown to be a potent MDSC attractant [148, 241-243]. These possibilities remain speculative at the present time and warrant investigation in future studies.

Another intriguing finding in this study was the apparent disconnect between the prolonged elevation of monocyte/macrophage chemokines and cell recruitment in *S. aureus*-infected animals. Specifically, CCL2, CCL3, and CCL5 were chronically elevated during *S. aureus* PJI (Fig. 4.2 and data not shown), yet monocyte/macrophage influx was significantly reduced compared with animals receiving aseptic implants. This could be explained by differential MDSC fates based on the local environment. For example, it is known that MDSCs are recruited to sites of injury where they differentiate into macrophages and neutrophils to protect against potential infection during the wound healing process [150, 161]. However, in the case of tumors or *S. aureus* infection as we recently showed, MDSCs remain arrested in their immature state and exert potent immunosuppressive activity [60, 137]. In the current report, it is challenging to definitively assign this suppressive activity to either MDSC subset, based on the inability to accurately identify each population for downstream analysis. However, our findings to date suggest that G-MDSCs may represent the main effector, based on the propensity of infiltrating MDSCs to express higher levels of the granulocytic marker Ly6G compared with the monocytic marker Ly6C. Our results here suggest that *S. aureus* biofilms play an active role in arresting MDSCs in their suppressive state to foster infection persistence. Indeed, MDSCs can thwart monocyte/macrophage proinflammatory activity [148, 163], which may negatively affect their numbers at the infection site as we observed. Similarly, although neutrophil chemokines were significantly increased throughout the course of infection, little evidence of neutrophil influx (i.e. Ly6G$^+$Ly6C$^-$) was detected. Instead, lesions were dominated by MDSCs, which are responsive to similar chemokines [137].

In conclusion, we have identified that IL-12 is critical for MDSC recruitment to the site of *S. aureus* PJI, where they impair phagocyte influx and biofilm clearance. Analysis of tissues from patients undergoing revision surgeries for PJIs revealed similar immune profiles as our mouse model, reflecting the utility of the mouse system to evaluate the efficacy of anti-biofilm therapeutics. Elucidating the mechanisms whereby bacterial biofilms thwart protective immunity

may lead to the development of novel immune-mediated approaches to facilitate PJI clearance in combination with conventional antibiotics.

<u>Chapter 5: Interleukin-10 production by myeloid-derived suppressor cells (MDSCs)</u>

<u>contributes to bacterial persistence during *S. aureus* orthopedic biofilm infection</u>

Journal of Leukocyte Biology *In Press*

Abstract

Staphylococcus aureus (*S. aureus*) is known to establish biofilms on medical devices. We recently demonstrated that Ly6G^{high}Ly6C^{+} MDSCs are critical for allowing *S. aureus* biofilms to subvert immune-mediated clearance; however, the mechanisms whereby MDSCs promote biofilm persistence remain unknown. IL-10 expression was significantly increased in a mouse model of *S. aureus* orthopedic implant biofilm infection with kinetics that mirrored MDSC recruitment. Since MDSCs produce IL-10, we explored whether it was involved in orchestrating the non-productive immune response that facilitates biofilm formation. Analysis of IL-10-GFP reporter mice revealed that Ly6G^{high}Ly6C^{+} MDSCs were the main source of IL-10 during the first two weeks of biofilm infection, whereas monocytes had negligible IL-10 expression until day 14. MDSC influx into implant-associated tissues was significantly reduced in IL-10 KO mice at day 14 post-infection, concomitant with increased monocyte and macrophage infiltrates that displayed enhanced proinflammatory gene expression. Reduced MDSC recruitment facilitated bacterial clearance as revealed by significant decreases in *S. aureus* burdens in the knee joint, surrounding soft tissue, and femur of IL-10 KO mice. Adoptive transfer of IL-10 WT MDSCs into *S. aureus* infected IL-10 KO mice restored the local biofilm-permissive environment, as evidenced by increased bacterial burdens and inhibition of monocyte proinflammatory activity. These effects were both IL-10-dependent and –independent, as MDSC-derived IL-10 was required for promoting biofilm growth and anti-inflammatory gene expression in monocytes, but was not involved in monocyte recruitment to biofilm-infected tissues. These results demonstrate that IL-10 production by MDSCs contributes to the persistence of *S. aureus* orthopedic biofilm infections.

Introduction

Staphylococcus aureus (*S. aureus*) is a major cause of healthcare- and community-associated infections and due to the increased prevalence of methicillin-resistant *S. aureus* (MRSA) strains, this pathogen has become an even greater therapeutic challenge [4, 16, 244, 245]. The risk of infection increases in the presence of a foreign body, and *S. aureus* is known for its ability to colonize and form biofilms on medical devices, such as indwelling catheters and orthopedic implants [34, 36, 49, 246]. Biofilm-associated bacteria exhibit distinct properties compared to planktonic growth phases of the same species, and it is becoming clear that the composition and kinetics of the host immune response to *S. aureus* biofilms inadvertently facilitates biofilm persistence, whereas planktonic infections, such as abscesses, are often resolved [187, 247]. Our laboratory was the first to identify myeloid-derived suppressor cells (MDSCs) during *S. aureus* biofilm infection, which represents a key immunosuppressive mechanism that supports chronic infection [60].

MDSCs are a heterogeneous population of immature monocytes and granulocytes that are intermediates of normal myeloid development and differentiation [130]. Under typical conditions, MDSCs differentiate at the site of inflammation or injury to generate mature myeloid populations, including neutrophils, macrophages (MΦs) and dendritic cells [130, 135, 137]. However, in pathological situations, such as tumors, chronic inflammation, and bacterial biofilm infection, MDSCs become arrested in an immature state where they negatively regulate inflammatory mechanisms through their suppressive actions [248, 163]. In cancer, MDSC expansion can be induced by various cytokines and growth factors, such as IL-6, G-CSF, GM-CSF, and VEGF; however, it is currently unknown what host or bacterial products promote MDSC propagation during *S. aureus* biofilm infection or their arrest in the immature state. Following MDSC expansion, inflammatory stimuli provide activation signals and induce the acquisition of immunosuppressive properties [121]. Our recent report demonstrated that IL-12 facilitates MDSC accumulation at the site of *S. aureus* biofilm infection, which is likely an indirect effect, since the cytokine is not a chemoattractant [59]. However, IL-12 is not required for MDSC activation during *S. aureus* biofilm infection, as MDSCs from both IL-12p40 and p35 KO mice still inhibited CD4+ T

cell proliferation. Therefore, other inflammatory factors must be involved in inducing the expression Arg-1, IL-10, and other anti-inflammatory mediators expressed by MDSCs that contribute to their immunosuppressive functions during *S. aureus* biofilm infection.

IL-10 is an anti-inflammatory cytokine known for its role in controlling inflammatory responses [249, 250], including inhibiting T cell activation and polarization, and IL-10 secretion by MDSCs has been implicated in programming MΦs toward an anti-inflammatory phenotype [145, 251-254]. Previously, we have shown that IL-10 expression is increased in FACS-purified MDSCs recovered from *S. aureus* biofilms in a mouse orthopedic infection model [60]. Here we sought to identify the role of IL-10 in MDSC-mediated immune suppression during biofilm infection and determine whether its actions contribute to bacterial persistence. The use of IL-10-GFP reporter mice revealed that Ly6GhighLy6C+ MDSCs were the main source of IL-10 during *S. aureus* biofilm infection. To demonstrate the functional importance of IL-10 in shaping the inflammatory milieu typical of biofilm infection, we performed studies in IL-10 knockout (KO) mice. Fewer MDSCs infiltrated implant-associated tissues of IL-10 KO mice at day 14 post-infection concomitant with enhanced monocyte and MΦ infiltrates. The reduction in MDSCs translated into bacterial clearance, as revealed by significant decreases in *S. aureus* burdens in the knee joint, surrounding soft tissue, and femur of IL-10 KO mice, which coincided with increased monocyte proinflammatory gene expression. The adoptive transfer of IL-10 WT MDSCs into IL-10 KO mice during *S. aureus* infection resulted in fewer monocyte infiltrates and attenuated proinflammatory gene expression, which consequently restored bacterial burdens to levels reminiscent of WT animals. In contrast, the adoptive transfer of IL-10 KO MDSCs into IL-10 KO mice did not augment bacterial biofilm growth, indicating that MDSC-derived IL-10 is important for promoting biofilm persistence. Collectively, these data demonstrate that IL-10 production by MDSCs is one mechanism to promote *S. aureus* orthopedic biofilm formation by limiting monocyte/MΦ recruitment and proinflammatory activity.

Results

MDSCs are the main source of IL-10 during S. aureus orthopedic implant biofilm infection.

IL-10 has been shown to inhibit T cell activation and polarize MΦs toward an anti-inflammatory phenotype (Perrin, Taga, Letterio, Sinha). We recently reported that FACS-purified Ly6G^{high}Ly6C^{+} MDSCs recovered from S. aureus biofilm infections had increased IL-10 gene expression compared to Ly6G^{-}Ly6C^{+} monocytes from the same region [60]. However, it remained unclear how much IL-10 was present at the infection site and whether MDSCs or other leukocytes were responsible for its production. In the present study, we used a mouse model of S. aureus orthopedic implant biofilm infection [59, 60, 62] to determine the contribution of MDSC-derived IL-10 in shaping the anti-inflammatory biofilm milieu. We first evaluated the kinetics of IL-10 production associated with sterile and S. aureus-infected implants (Fig 1). IL-10 levels were similar at day 3, the earliest time point examined; however, by day 5, IL-10 expression was significantly increased in biofilm-infected tissues and remained elevated at day 14 (Fig 1).

To determine which cell types were producing IL-10 in infected tissues, IL-10-GFP reporter mice were utilized, since our previous study only compared IL-10 mRNA expression in sorted MDSCs and monocytes and the FACS panels here were designed to also monitor neutrophils, MΦs, and T cells in addition to MDSCs and monocytes. FACS analysis revealed that Ly6G^{high}Ly6C^{+} MDSCs were the main source of IL-10, since nearly 70% were GFP^{+} at day 5 post-infection (Fig 2C). The frequency of IL-10-GFP^{+} MDSCs progressively decreased to approximately 55% and 20% by days 7 and 14 post-infection, respectively (Fig 2C). Previous studies from our laboratory have shown that MDSC infiltrates progressively increase in S. aureus infected tissues from days 3 to 14 and remain relatively stable as the infection persists [59]. Interestingly, GFP levels in the Ly6G^{-}Ly6C^{+} monocyte population were low throughout the first week of S. aureus infection (Fig 2D); however, as the percentage of IL-10-GFP^{+} MDSCs decreased there was a significant increase in IL-10-GFP^{+} monocytes at day 14 post-infection (Fig 2D). These results establish MDSCs as the main source of IL-10 during early S. aureus orthopedic implant biofilm infection.

Figure 5.1
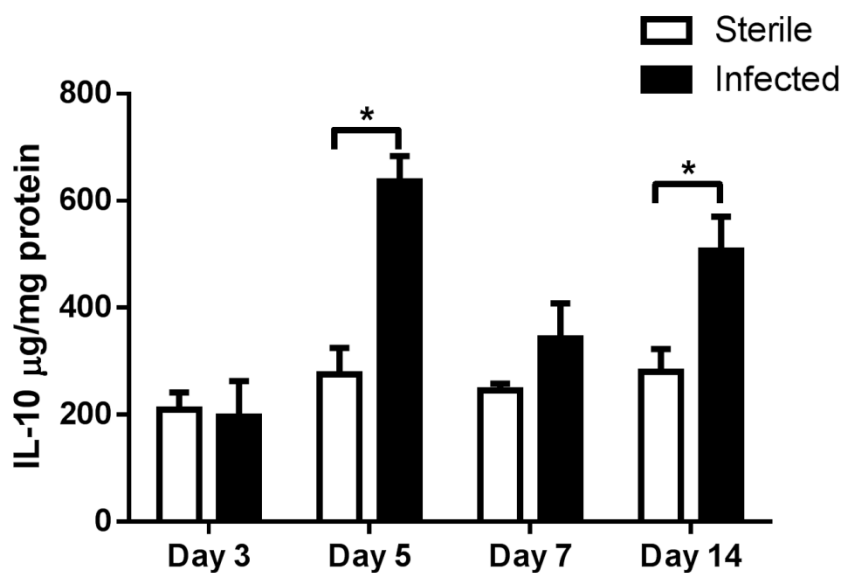
IL-10 production is increased during *S. aureus* orthopedic biofilm infection. Implant-associated tissues from sterile and *S. aureus* infected mice (n = 4-5/group) were collected at the indicated time points, whereupon IL-10 expression was quantitated by ELISA. Results were normalized to the amount of total protein recovered to correct for variances in tissue sampling size and are representative of five mice per group. Statistical differences are denoted by asterisks (*, $p < 0.05$; unpaired two-tailed Students *t*-test).

Figure 5.2
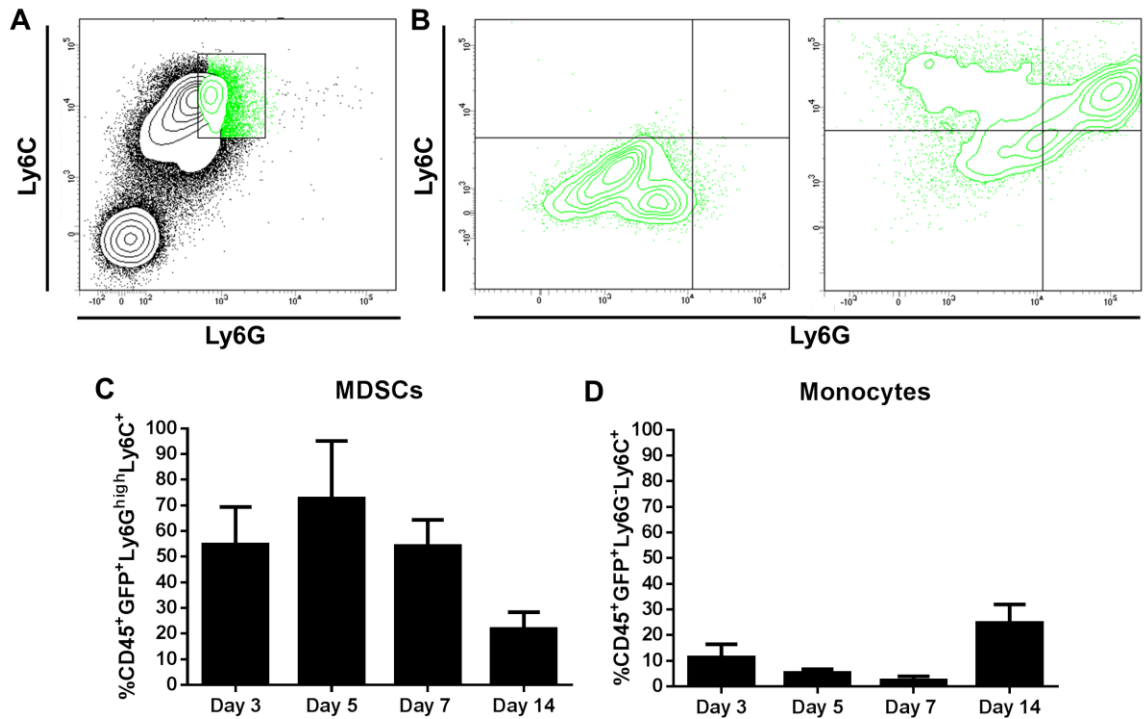
Figure 2. Ly6G^{high}Ly6C⁺ MDSCs are the main source of IL-10 during *S. aureus* orthopedic implant biofilm infection. Implant-associated tissues were collected from IL-10-GFP reporter mice at the indicated intervals following infection and processed for flow cytometry. The CD45$^+$GFP$^+$ leukocyte population from *S. aureus* biofilm infected tissues (**A**) was gated to identify IL-10-GFP expressing Ly6C$^+$ and Ly6G$^+$ cells (**B**). The percentage of CD45$^+$GFP$^+$Ly6G^{high}Ly6C$^+$ MDSCs (**C**) and CD45$^+$GFP$^+$ Ly6G$^-$Ly6C$^+$ monocytes (**D**) is shown. Results are representative of two independent experiments (n = 10 mice/time point). Statistical differences are denoted by asterisks (*, $p < 0.05$; **, $p < 0.01$; unpaired two-tailed Student's *t*-test).

IL-10 is critical for organizing the anti-inflammatory biofilm milieu and maintaining S. aureus orthopedic implant infection. Since MDSCs are the primary cell type responsible for IL-10 production, we next determined the importance of this cytokine to the immunosuppressive function of MDSCs and its role in regulating the anti-inflammatory milieu that allows for biofilm persistence. Examination of leukocyte recruitment in *S. aureus*-infected IL-10 KO animals revealed a significant decrease in Ly6G^{high}Ly6C^{+}MDSCs at day 14 post-infection compared to WT (Fig 3A) concomitant with increased Ly6G^{-}Ly6C^{+} monocytes (Fig 3B) and F4/80^{+} MΦs (Fig 3C). No differences in neutrophil or T cell infiltrates were observed in the absence of IL-10 and both leukocyte populations represented a minor fraction of the CD45^{+} infiltrate (i.e. < 5%; data not shown). Biofilm-associated MDSCs from IL-10 KO mice maintained their ability to inhibit CD4^{+} T cell proliferation (Fig 4), demonstrating that MDSC-mediated T cell suppression during *S. aureus* orthopedic infection is IL-10-independent.

Our recent report demonstrated that MDSC depletion with the Ly6G Ab 1A8 led to significant increases in Ly6C^{+} monocyte infiltrates with heightened pro-inflammatory activity [60]. By extension, we predicted that the reduced MDSC population in IL-10 KO mice at day 14 post-infection would also promote monocyte proinflammatory attributes. This possibility was assessed by monitoring gene expression profiles of FACS-purified IL-10 KO and WT monocytes immediately *ex vivo* by qRT-PCR. Ly6G^{-}Ly6C^{+} cells recovered from IL-10 KO tissues at day 14 post-infection displayed increased expression of iNOS, IL-1β, IL-12p40 and TNF-α and decreased Arg-1 compared with Ly6G^{-}Ly6C^{+} monocytes from WT tissues (Fig 5). Since MDSCs are a main source of IL-10 at day 14 post-infection when monocyte proinflammatory attributes were heightened, this finding suggests that both the presence of MDSCs as well as their expression of IL-10 polarizes infiltrating monocytes towards an anti-inflammatory phenotype during *S. aureus* biofilm formation.

The ability of IL-10 to promote biofilm persistence was confirmed by significant reductions in *S. aureus* burdens in the tissue, knee joint, and femur of IL-10 KO animals by days 7 to 14 post-infection depending on the site (Fig 6). In addition, IL-10 KO mice displayed altered cytokine/chemokine expression patterns during *S. aureus* biofilm infection. For example, G-CSF

levels in IL-10 KO animals were significantly decreased at day 14 (Fig 7A). G-CSF has been

implicated in initiating granulocytic MDSC accumulation [255] and the decrease in G-CSF in IL-10

KO tissues at day 14 was concomitant with reduced MDSC infiltrates (Fig 3A), indicating that G-

CSF may play a critical role in the expansion and accumulation of this population. In addition, IL-

1β and CCL3 levels were significantly decreased at day 14 post-infection (Fig 7C and F),

whereas IL-1α and CCL2 levels were significantly increased in IL-10 KO tissues at day 3 (Fig 7B

and E). Interestingly, IL-9 levels were significantly increased in IL-10 KO mice at day 14 post-

infection (Fig 7D) even though there is a paucity of T cell infiltrates in this model as determined by

CD3^{+}CD4^{+} or CD3^{+}CD8^{+} staining (data not shown) [32, 59, 60].

Figure 5.3
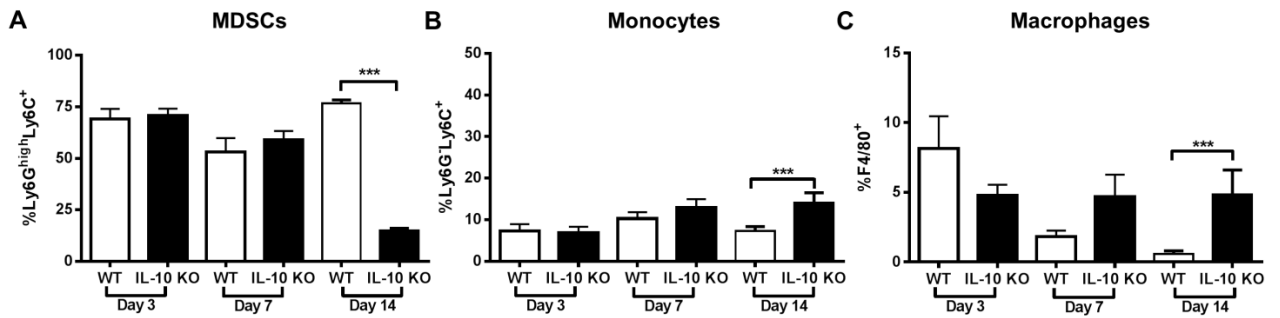
IL-10 loss augments monocyte/macrophage recruitment during *S. aureus* orthopedic biofilm infection. Implant-associated tissues from IL-10 KO and WT mice (n = 10/group) were collected at the indicated time points after infection and analyzed by flow cytometry. (**A**) Quantitation of Ly6G^{high}Ly6C$^+$ MDSCs, (**B**) Ly6G$^-$Ly6C$^+$ monocytes, and (**C**) F4/80$^+$ macrophages from the total CD45$^+$ leukocyte infiltrate. Results are presented from two independent experiments where significant differences between WT and IL-10 KO animals are denoted with asterisks (***, $p < 0.001$; unpaired two-tailed Student's *t*-test).

Figure 5.4
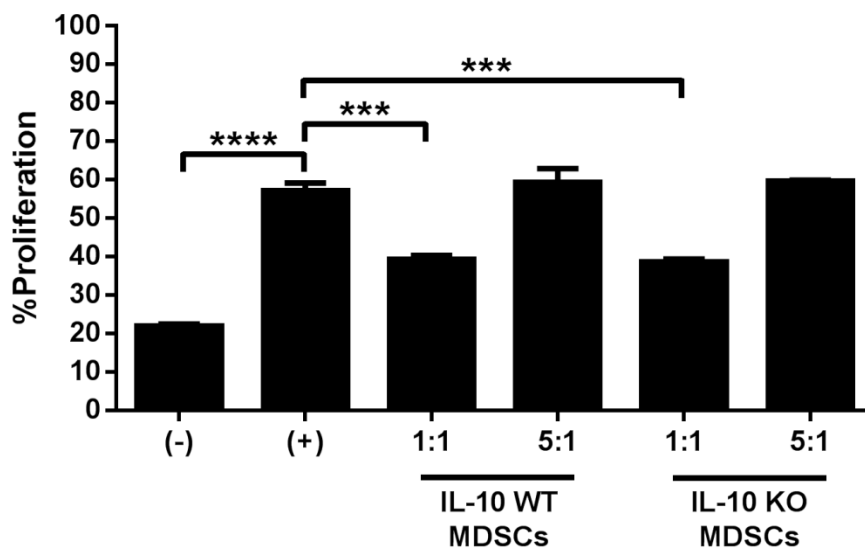
S. aureus* biofilm-associated MDSCs inhibit T cell activation in and IL-10-independent manner.** MDSCs were purified by FACS from infected WT and IL-10 KO mice at day 14 post-infection for T cell proliferation assays at a 1:1 or 5:1 ratio (T cell:MDSC). Results are expressed as the % proliferation with T cells alone (-) and CD3/CD28-stimulated T cells (+) as controls. Results represent two independent experiments with significant differences denoted by asterisks (, $p < 0.001$; ****, $p < 0.0001$; unpaired Student's t–test).

Figure 5.5
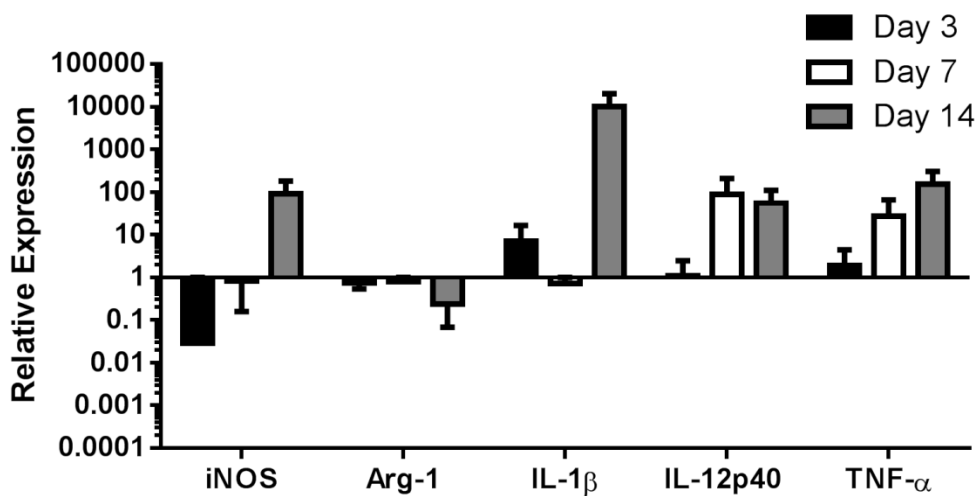
Loss of IL-10 augments proinflammatory gene expression in Ly6C$^+$ monocytes during *S. aureus* biofilm infection. Ly6G$^-$Ly6C$^+$ monocytes were purified from tissues surrounding the infected joints of IL-10 WT and KO mice (n = 10/group) at days 3, 7 and 14 post-infection by FACS, whereupon RNA was immediately isolated for qRT-PCR analysis. Gene expression levels in IL-10 KO monocytes were calculated after normalizing signals against GAPDH and are presented as the fold-change relative to WT monocytes.

Figure 5.6
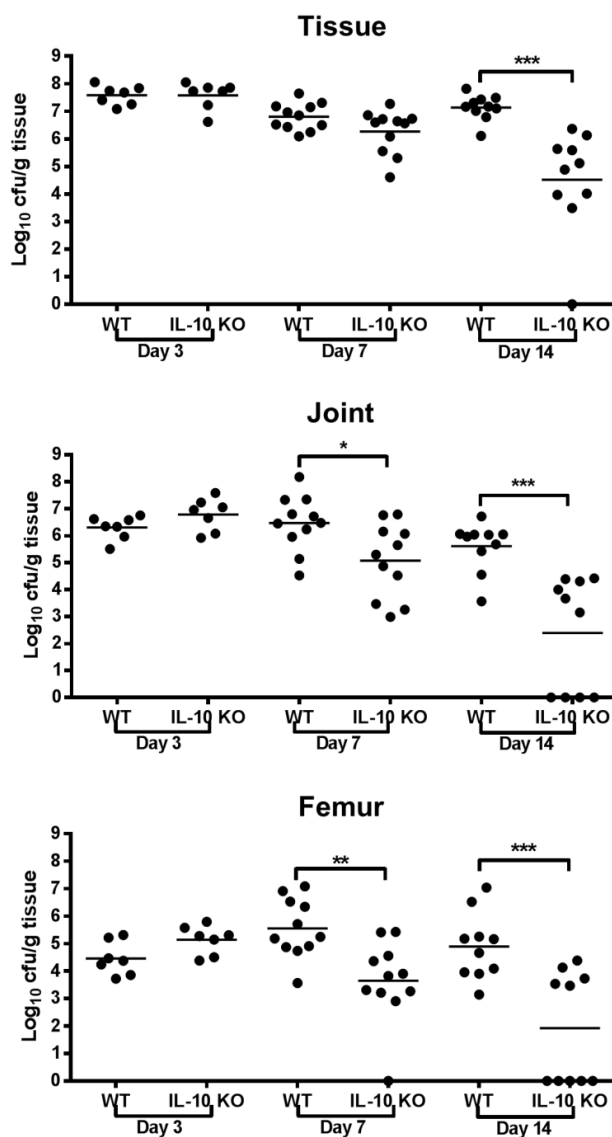
IL-10 is critical for *S. aureus* persistence during orthopedic biofilm infection. Bacterial

burdens associated with the implant-associated tissue, femur, and knee joint of WT and IL-10 KO

mice (n = 10/group) were determined at days 3.7 and 14 post-infection. Results are expressed as

the number of CFU per gram tissue to correct for alteration in tissue sampling sizes. Significant

differences in bacterial burdens between WT and IL-10 KO mice are denoted by asterisks (*, $p <$

0.05; **, $p < 0.01$; ***, $p < 0.001$; unpaired two-tailed Student's *t*-test) and are from two

independent experiments.

Figure 5.7
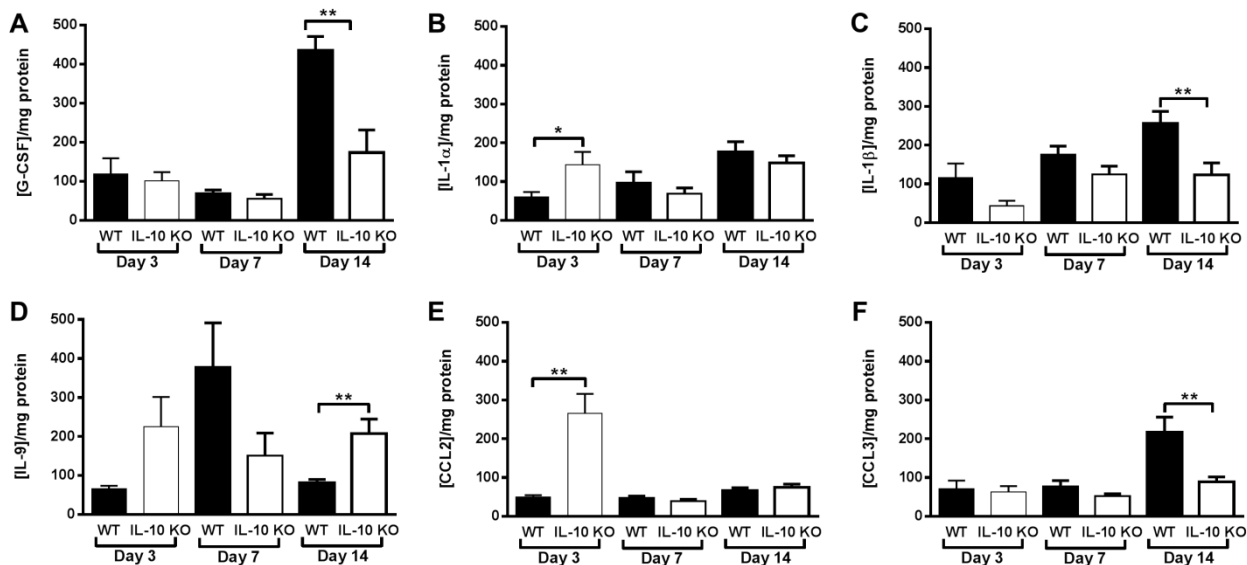
IL-10 KO mice have altered cytokine and chemokine expression patterns. Tissues surrounding the knee joint of WT or IL-10 KO mice (n = 10/group) with *S. aureus*-infected implants were collected at the indicated time points, whereupon (**A**) G-CSF, (**B**) IL-1α, (**C**) IL-1β, (**D**) IL-9, (**E**) CCL2, and (**F**) CCL3 production was measured by multi-analyte bead arrays. Results are normalized to the amount of total protein to correct for differences in tissue sampling size and are representative of two independent experiments. Significant differences are denoted by asterisks (*, $p < 0.05$; **, $p < 0.01$; unpaired two-tailed Student's *t*-test).

MDSCs influence bacterial burdens and monocyte infiltrates during S. aureus orthopedic implant biofilm infection via both IL-10-dependent and –independent mechanisms. To directly assess the contribution of MDSC-derived IL-10 in inhibiting innate immune cell function and promoting *S. aureus* persistence during orthopedic implant biofilm infection, bone marrow-derived MDSCs from either WT or IL-10 KO mice were adoptively transferred into IL-10 KO animals 7 days after infection, whereupon bacterial burdens were assessed at day 14. This timing strategy was selected since most differences in IL-10 KO mice were observed at day 14. *In vitro*-derived MDSCs have been previously used in our laboratory and were confirmed to inhibit T cell proliferation [59]. The adoptive transfer of WT MDSCs into WT mice failed to significantly alter bacterial burdens or immune cell infiltrates at the site of *S. aureus* biofilm infection (data not shown), which eliminated this approach as a control. This is likely because MDSCs already represent approximately 50% of the total CD45$^+$ population at day 7 [59], and the adoptive transfer of additional MDSCs does not exacerbate *S. aureus* infection. Instead, the reduced numbers of MDSCs in IL-10 KO mice at day 14 post-infection allowed us to detect the impact of adoptively transferred MDSCs in these animals. Therefore, WT MDSCs represented the control cell population, whereas IL-10 KO MDSCs were the experimental group, with both populations being transferred to IL-10 KO mice to monitor effects on bacterial burdens and leukocyte infiltrates. Indeed, the utility of WT MDSCs as a control was demonstrated by the finding that bacterial burdens were restored to levels typically observed in WT mice following the adoptive transfer of WT MDSCs into IL-10 KO animals (Fig 8A), which coincided with an increase in Ly6G^{high}Ly6C$^+$ MDSCs (Fig 8B) and reduced Ly6G$^-$Ly6C$^+$ monocytes compared to IL-10 KO mice that did not receive MDSCs (Fig 8C).

To determine whether IL-10 produced by MDSCs is solely responsible for promoting biofilm growth and inhibiting monocyte recruitment, we also performed adoptive transfers of IL-10 KO MDSCs into *S. aureus* infected tissues of IL-10 KO mice at day 7 post-infection. The results demonstrated the complex involvement of both IL-10-dependent and –independent mechanisms. With regard to the former, MDSC-derived IL-10 was required for promoting bacterial biofilm growth in the tissue, joint, and femur, since the transfer of IL-10 KO MDSCs had no impact on

these measures compared to IL-10 KO animals that did not receive MDSCs (Fig 8A). However, the effect of MDSCs on monocyte recruitment was found to be IL-10-independent, since the adoptive transfer of both WT and IL-10 KO MDSCs into IL-10 KO mice resulted in similar changes in monocyte infiltrates (Fig 8C).

Monocytes recovered from infected tissues of IL-10 KO animals have increased pro-inflammatory gene expression (Fig 5), which is likely not only due to the absence of IL-10 but also decreased MDSCs. To further validate these findings, gene expression profiles of FACS-purified Ly6G$^-$Ly6C$^+$ monocytes following adoptive transfer were performed. The adoptive transfer of WT MDSCs into IL-10 KO mice decreased monocyte proinflammatory gene expression, with reductions in iNOS, IL-1β, IL-12p40, and TNF-α, demonstrating a direct effect of MDSCs on monocyte activation state (Fig 9).

Figure 5.8
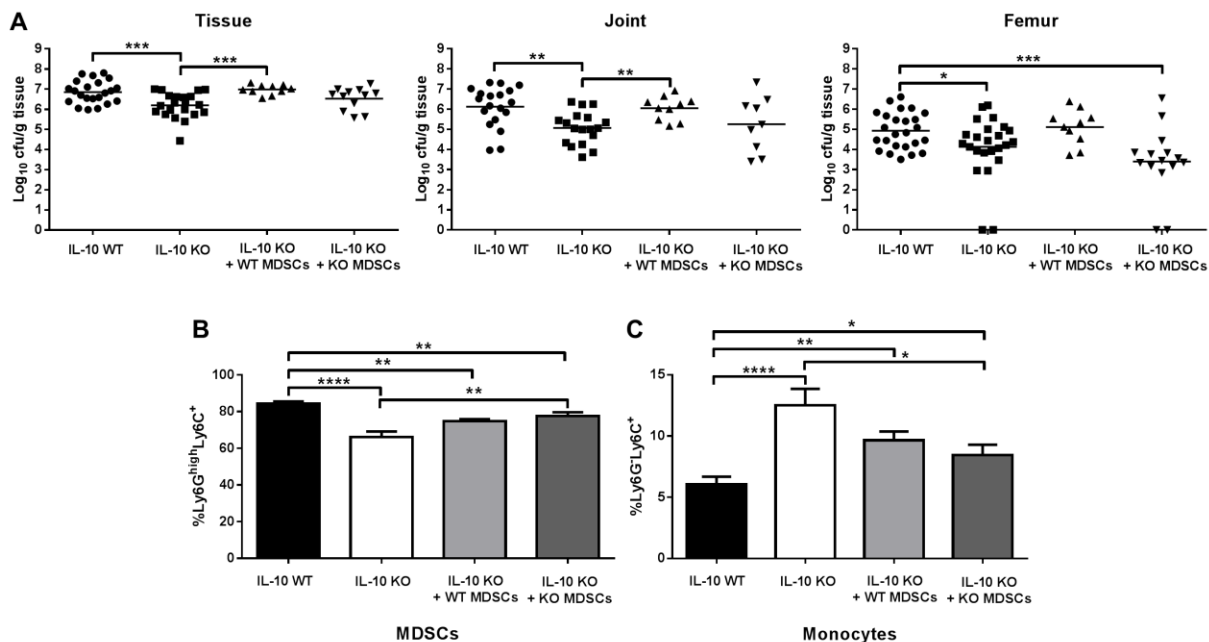
MDSCs influence bacterial burdens and monocyte infiltrates during *S. aureus* orthopedic implant biofilm infection via both IL-10-dependent and –independent mechanisms. *S. aureus* orthopedic implant infection was established in IL-10 KO and WT mice, whereupon IL-10 KO animals received an adoptive transfer of 2.5×10^6 purified IL-10 WT or IL-10 KO MDSCs s.c. at the implant site at day 7 post-infection, whereas WT and a separate group of IL-10 KO animals received s.c. injections of PBS (n = 10/group). (**A**) Implant-associated tissue, knee joint, and femur were collected at day 7 following MDSC transfer (day 14 after infection) for quantitation of bacterial burdens. (**B**) Quantitation of Ly6G^{high}Ly6C$^+$ MDSCs and (**C**) Ly6G$^-$Ly6C$^+$ monocytes at day 7 following MDSC adoptive transfer (day 14 post-infection). Results were calculated after gating on the CD45$^+$ population and represent two independent experiments. Significant differences are denoted by asterisks (*, $p < 0.05$; **, $p < 0.01$; ***, $p < 0.001$; ****, $p < 0.0001$; unpaired two-tailed Student's *t*-test).

Figure 5.9
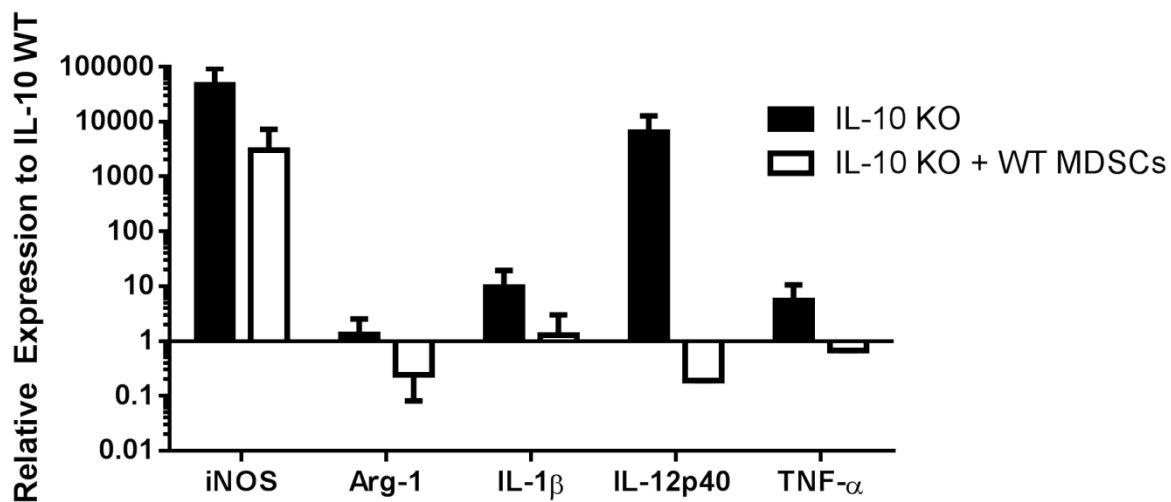
Monocyte proinflammatory gene expression is reduced following adoptive transfer of WT MDSCs. Ly6G⁻Ly6C⁺ monocytes were purified from infected tissues of WT and IL-10 KO mice ± MDSC adoptive transfer at day 14 post-infection by FACS (n = 10/group), whereupon RNA was immediately isolated for qRT-PCR analysis. Gene expression levels in monocytes from IL-10 KO animals or IL-10 KO mice receiving WT MDSCs were calculated after normalizing signals against GAPDH and are presented as the fold-change relative to monocytes recovered from IL-10 WT animals.

Figure 5.10
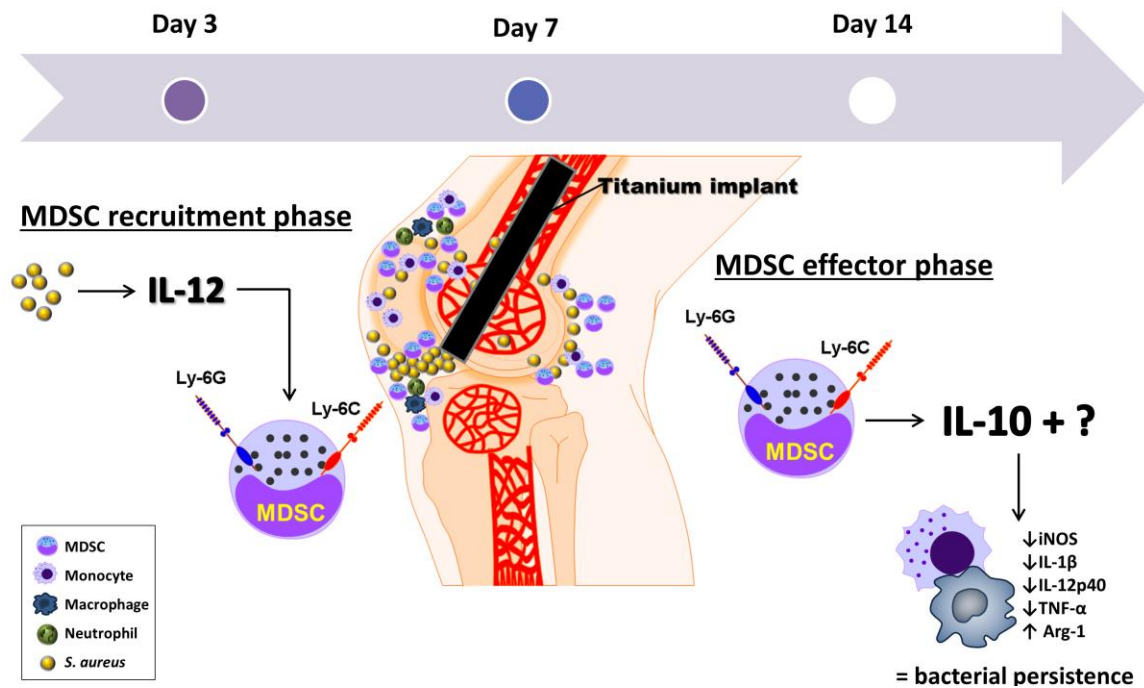
Temporal relationship between IL-10 and IL-12 actions during S. aureus orthopedic implant biofilm infection. IL-12 plays a key role in MDSC recruitment during biofilm infection via a chemoattractant that remains to be identified. IL-10 is produced by infiltrating MDSCs at the site of S. aureus biofilm infection, whereupon it plays a critical role in polarizing monocytes towards an anti-inflammatory phenotype, thereby promoting bacterial persistence. Loss of either IL-12 or IL-10 during the early MDSC recruitment or effector phases, respectively, promotes biofilm clearance, implicating key roles for each cytokine at distinct stages of infection.

DISCUSSION

MDSCs are emerging as a critical player in the anti-inflammatory response to *S. aureus* and promote chronic infection [59, 60, 149, 257]. Biofilm infections are known to skew the host innate immune response towards an anti-inflammatory phenotype [32, 100, 167]. In this setting, IL-10 could facilitate the establishment of persistent infection and allow organisms to subvert traditional mechanisms of bacterial clearance. Although IL-10 production has been implicated as an immunosuppressive mechanism by MDSCs [145, 258], to date there are no reports examining whether MDSC function is dependent on IL-10 during biofilm infection. This study is the first to demonstrate that MDSCs express significant amounts of IL-10 in response to biofilm-associated bacteria, which limits monocyte proinflammatory gene expression and directly contributes to *S. aureus* biofilm persistence during later stages of infection. Of note, the consequences of IL-10 action are likely context-dependent, since several studies have reported a beneficial role for IL-10 during *S. aureus* sepsis by controlling damaging inflammation and minimizing pathology [209, 250, 251, 259-262]. In contrast, our study suggests a deleterious role for IL-10 in preventing the genesis of an effective microbicidal response to facilitate biofilm clearance.

In terms of kinetics, IL-10 levels in *S. aureus* biofilm tissues were not significantly increased compared to animals receiving sterile orthopedic implants until day 5. This delay in IL-10 elevation implies that the biofilm is directing cytokine production and our results indicate that MDSCs are responsible for IL-10 synthesis. Here we demonstrate that nearly 70% of the MDSCs recruited to the site of *S. aureus* biofilm infection at day 5 expressed IL-10, whereas monocytes represented a minor fraction in comparison. Our recent publication reported a progressive increase in the percentages of Ly6G^{high}Ly6C$^+$ MDSCs until day 21 post-infection that was significantly more pronounced compared to mice receiving sterile implants [59]. It is important to note that in addition to the percentages of MDSC infiltrates, their activation status is also influenced by biofilm infection. Indeed, we previously reported that only MDSCs recovered from *S. aureus* biofilm infected animals, but not those receiving sterile implants, were capable of attenuating T cell proliferation, reflecting the inhibitory nature of MDSCs specifically recruited to the biofilm infection site. Therefore, MDSC levels are only one aspect of the equation, with their

inhibitory capacity and gene expression profiles representing other important attributes, both of which were studied in the current report. MDSC-derived IL-10 began to decline by day 7 post-infection, which coincided with the decrease in total IL-10 measured in infected tissues by ELISA. However, tissue IL-10 levels exhibited a bi-phasic increase at day 14, which may reflect cytokine production by both MDSCs and monocytes, the latter which exhibited a late rise in IL-10 expression. It is currently unclear what causes MDSC-derived IL-10 to decrease after day 5 post-infection while the percentage of MDSCs remains constant (data not shown). Although we currently have no evidence of regulatory T cells at the site of *S. aureus* biofilm infection as determined by CD4 and FoxP3 staining (data not shown), IL-10 production by MDSCs has been shown to induce Tregs that can produce IL-10 [258], which could perpetuate the anti-inflammatory circuit. It remains possible that the number of Tregs associated with *S. aureus* biofilms in our orthopedic model remain below the limit of detection by FACS. Alternatively, synovial cells could contribute to sustained IL-10 levels during *S. aureus* biofilm infection when IL-10 producing MDSCs have begun to decline (i.e. day 14 post-infection). It has been shown that cultured fibroblast-like synoviocytes constitutively express IL-10 along with functional IL-10 receptors and could modulate cellular responses in the joint. However, these and other tissue resident populations would need to be analyzed during *S. aureus* biofilm infection to determine if they contribute to IL-10 production and potentially assist in bacterial persistence.

A direct role for MDSC-derived IL-10 in setting the stage for *S. aureus* biofilm persistence at later time points was supported by our observations in IL-10 KO mice. In general, in the absence of IL-10, infiltrating monocytes acquired a proinflammatory gene expression profile that translated into improved biofilm clearance at days 7 and 14 post-infection. These changes coincided with significant decreases in MDSC infiltrates and the adoptive transfer of MDSCs from WT but not IL-10 KO mice were capable of reversing these changes. In terms of mechanism, *S. aureus* could be co-opting MDSCs to promote their immunosuppressive activity during acute infection, which occurs via an IL-10-independent manner. When IL-10 expression peaks in MDSCs (i.e. day 5) we begin to see a reduction in biofilm burdens in IL-10 KO mice at day 7 and an inability to effectively skew monocytes toward an anti-inflammatory phenotype, which

altogether demonstrate that MDSC-derived IL-10 is critical for the chronicity of *S. aureus* biofilm infection.

Currently, the signals responsible for eliciting IL-10 production by MDSCs during biofilm infection have yet to be identified. It is known that IL-10 can be induced by Toll-like receptor (TLR) stimulation [263-265], that MDSCs express TLRs [163, 266], and TLR ligands can induce MDSC accumulation in tumor-bearing and septic mice [123, 124, 267]. However, this possibility appears less plausible in the context of biofilm infection, since we and others have reported that *S. aureus* biofilms circumvent recognition by TLR2 [187, 32, 62], although MDSCs were not examined in these studies. Regardless of the inciting signal that triggers IL-10 production, the cytokine can then signal through the IL-10R to activate signal transducer and activator of transcription 3 (STAT3), a critical factor for driving MDSC development as well as polarizing monocytes/MΦs toward an anti-inflammatory phenotype [125, 268-270]. In addition, STAT3 activation can augment IL-10 production [271]. The role of IL-10 in inducing STAT3 activation during *S. aureus* biofilm infection and its subsequent contribution to the anti-inflammatory biofilm milieu are current topics of investigation in our laboratory.

G-CSF preferentially signals through STAT3, where it induces MDSC expansion and accelerates the proliferation and release of granulocytic precursors in tumor-bearing mice in addition to its well-known ability to direct neutrophilic granulocyte differentiation [255, 272]. We have previously reported that G-CSF is significantly increased in *S. aureus*-infected tissues during the time when MDSCs represent the main cellular infiltrate in implant-associated tissue [59]. Interestingly, in the current study, G-CSF levels were reduced in IL-10 KO mice at day 14 post-infection, concomitant with reduced MDSC infiltrates. By extension, it is possible that G-CSF contributes to MDSC expansion and accumulation during *S. aureus* biofilm infection and that IL-10 loss may limit STAT3 activation and subsequent G-CSF production. However, this possibility remains speculative.

Both IL-10 and STAT3 are known to inhibit IL-12 production, and MDSCs are traditionally thought to secrete IL-10 to down-regulate IL-12 release from monocytes/MΦs. This relationship appears to be operative during *S. aureus* biofilm infection; however, unlike planktonic infections,

MDSCs persist and maintain the biofilm milieu in an anti-inflammatory state. For example, our recent report showed that IL-12 was increased in *S. aureus* infected tissues over a one month period and IL-12p40 and p35 KO animals had significantly fewer MDSC infiltrates concomitant with reduced bacterial burdens as early as day 7 post-infection [59]. In the current study, because IL-10 is not elevated in infected tissues until day 5 and MDSC infiltrates are not significantly reduced in IL-10 KO animals until day 14, this indicates that IL-10 operates downstream of MDSC recruitment and IL-12 action (Fig 10). Indeed, IL-12p40 gene expression was increased in monocytes from IL-10 KO mice beginning at day 7 post-infection, revealing a negative effect of MDSC-derived IL-10 on monocyte IL-12 expression. This was also directly demonstrated by the ability of adoptively transferred WT MDSCs to inhibit IL-12 in monocytes from IL-10 KO animals. Despite these cell type-specific changes, IL-12p40 levels in tissue homogenates of both IL-10 KO and WT animals were similar at days 3, 7 and 14 post-infection (data not shown) and since MDSC recruitment was unaffected during the first week of *S. aureus* orthopedic biofilm infection, this suggests the delayed action of an alternative chemoattractant that is IL-12-independent. Taken together, it appears that IL-12 produced during early *S. aureus* biofilm infection is key for MDSC recruitment, which is likely an indirect effect mediated by chemoattractants that remain to be defined, whereupon MDSCs produce IL-10 that dampens the proinflammatory immune response of monocytes/macrophages and contributes to biofilm persistence (Fig 10). These studies assessing the role of IL-10 in regulating innate immune responses have focused on monocytes, as they represent the most numerous population after MDSCs in our *S. aureus* orthopedic biofilm infection model. It remains possible that MDSCs could be influencing neutrophil responses; however, neutrophils represent a very minor infiltrate and no significant differences were observed between IL-10 KO and WT animals. Therefore, we did not explore the possible effects of MDSCs and IL-10 on neutrophil function.

Recently, we and others have shown that the adoptive transfer of MDSCs significantly exacerbates *S. aureus* infection [59, 149]; however, the mediators released by MDSCs that are responsible for this effect remain to be defined. Here we show that IL-10 is one factor, since the adoptive transfer of MDSCs from IL-10 KO mice did not exacerbate biofilm growth, whereas WT

MDSCs significantly increased biofilm burdens in the joint, surrounding soft tissue, and femur. However, it is apparent that IL-10 is not the only immunosuppressive mechanism of MDSCs during *S. aureus* biofilm infection, since IL-10 KO MDSCs still impacted monocyte recruitment during biofilm infection, reflecting an IL-10-independent mechanism of action. Originally, IL-10 was defined by its ability to inhibit Th1 activation and cytokine production; however, it is now recognized that the biological effects of IL-10 are also directed at monocytes/MΦs [273]. Indeed, we found that MDSC inhibition of CD4$^+$ T cell proliferation was IL-10-independent, in agreement with another recent report [149], again indicating the existence of additional inhibitory effector mechanisms for MDSCs. A potential candidate is Arg-1, which we have previously shown is elevated in MDSCs recovered from the site of *S. aureus* orthopedic biofilm infection in both our mouse model and in tissue specimens from humans with prosthetic joint infections [32, 59, 60]. A role for Arg-1 in the anti-inflammatory response to *S. aureus* biofilms is a topic of ongoing investigation in our laboratory.

Inflammatory mediator analysis in infected IL-10 KO mice revealed some interesting disparities, particularly with respect to the timing of when differences were apparent. For example, both IL-1α and CCL2 were significantly increased in IL-10 KO animals at day 3 post-infection but not at later time points. In contrast, more differences were evident at day 14, which coincided with the significant decrease in biofilm burdens in IL-10 KO mice, namely reductions in G-CSF, IL-1β, and CCL3. However, not all mediators were reduced, since IL-9 production was significantly elevated in IL-10 KO animals at this later interval. The fact that IL-9 was detected is intriguing, since this cytokine is only produced by select T cell subsets; however, minimal T cell infiltrates (CD3$^+$CD4$^+$ or CD3$^+$CD8$^+$) were observed in either IL-10 KO or WT mice in this and our prior reports, making it difficult to predict the source of IL-9 production. Another interesting finding is that IL-9 has been reported to promote Treg expansion, yet we have not been able to detect CD4$^+$FoxP3$^+$ cells in any of our *S. aureus* biofilm infection models (data not shown) [32, 59, 60]. However, IL-9 is known to stimulate mast cell expansion from the bone marrow [274-276] and mast cells have been shown to release several cytokines and nitric oxide into the knee joint during osteoarthritis [277] and drive tissue metaplasia and heterotrophic ossification in patients

following total knee arthroplasty [278]. It is possible that the absence of IL-10 at later time points allows the proinflammatory activities of IL-9 to be heightened, although the presence of mast cells and their role during *S. aureus* orthopedic biofilm infection have not yet been examined.

The role of MDSCs during *S. aureus* biofilm infection and the mechanisms involved in their expansion, accumulation, and effector functions are only beginning to be explored. By manipulating the ability of these cells to exert their immunosuppressive pressure, we have demonstrated that they directly attenuate monocyte proinflammatory properties. However, there are still many areas of MDSC-biofilm interaction that remain to be examined. For instance, we know that IL-12 is involved in MDSC recruitment to biofilm infections, but it is unclear whether biofilm-derived products directly contribute to MDSC accumulation by interfering with myeloid precursor differentiation. In addition, whether MDSCs can recognize *S. aureus* PAMPs through TLRs or other PRRs to activate genes essential for their effector functions could contribute to our understanding of their role during infection. Our findings to date do not exclude the possibility that *S. aureus* biofilms cooperate with MDSCs to directly inhibit monocyte/MΦ effector functions and studies are ongoing in our laboratory to address these interactions. However, preventing the immunosuppressive action of infiltrating MDSCs may offer a novel therapeutic strategy to treat chronic biofilm infections.

Chapter 6: Targeting macrophage activation for the prevention and treatment of

***Staphylococcus aureus* biofilm infections**

Published in *Journal of Immunology* 190:2159-2168, 2013

Copyright 2013. The American Association of Immunologists, Inc.

Abstract

Biofilm infections often lead to significant morbidity due to their chronicity and recalcitrance to antibiotics. We have demonstrated that methicillin-resistant *Staphylococcus aureus* (MRSA) biofilms can evade macrophage (MΦ) antibacterial effector mechanisms by skewing MΦ toward an alternatively activated M2 phenotype. To overcome this immune evasion, we have used two complimentary approaches. In the first, a proinflammatory milieu was elicited by local administration of classically activated M1 MΦs and in the second by treatment with the C5a receptor (CD88) agonist EP67, which invokes MΦ proinflammatory activity. Early administration of M1-activated MΦ or EP67 significantly attenuated biofilm formation in a mouse model of MRSA catheter-associated infection. Several proinflammatory mediators were significantly elevated in biofilm-infected tissues from MΦ- and EP67-treated animals, revealing effective reprogramming of the biofilm environment to a proinflammatory milieu. A requirement for MΦ proinflammatory activity was demonstrated by the fact that transfer of MyD88-deficient MΦ had minimal impact on biofilm growth. Likewise, neutrophil administration had no effect on biofilm formation. Treatment of established biofilm infections with M1-activated MΦ also significantly reduced catheter-associated biofilm burdens compared with antibiotic treatment. Collectively, these results demonstrate that targeting MΦ proinflammatory activity can overcome the local immune inhibitory environment created during biofilm infections and represents a novel therapeutic strategy.

Introduction

       Biofilms are heterogeneous bacterial communities that can form on both natural body surfaces as well as foreign devices, such as indwelling catheters and orthopedic implants [27, 33]. The presence of a foreign body increases the likelihood of infection and drastically lowers the threshold for device colonization [279]. Methicillin-resistant *Staphylococcus aureus* (MRSA) is a common etiologic agent of biofilms and often causes chronic and recurrent infections when associated with indwelling medical devices [1, 246]. The current therapeutic option for managing device-associated biofilm infections is a staged-replacement of the hardware, either as a single step exchange, whereby the entire implant is replaced in a single procedure, or, more commonly, as a two-stage exchange [49]. In the latter case, patients receive extended antibiotic regimens in addition to surgical management, which generally consists of device removal and replacement with an antibiotic-impregnated temporary spacer, followed by insertion of a new prosthesis after a 2 to 8 week period. This long and debilitating process is associated with significant morbidity and economic impact for patients. Further complicating available treatment strategies is that antibiotics alone are generally ineffective for biofilm eradication [36, 280], which is thought to result from altered metabolism during biofilm growth [281, 282]. The difficulties of biofilm treatment are further underscored in the context of more permanent implants such as artificial hips and knees, procedures that are particularly common in the elderly, who grow increasingly less immune responsive over time [283].

       Based on these challenges, an urgent need exists for developing novel paradigms to prevent and/or facilitate biofilm eradication without the need for radical surgical interventions. One promising approach involves the exploitation of natural host immune mechanisms for therapeutic benefit. Targeting the host response rather than the pathogen itself offers certain advantages by largely avoiding selective pressures for the evolution of microbial resistance. Indeed, stimulating adaptive immunity through vaccination has remained resilient to microbial resistance over decades of clinical use, although not all pathogens have been amenable to vaccination strategies, most notable *Staphylococcus aureus* (*S. aureus*) [284, 285]. Furthermore, the fact that innate immune defenses are geared to rapidly recognize an infinite pathogen repertoire, suggests

that their modulation will afford broad-spectrum protection against a range of microbial pathogens, including *S. aureus*, and enable prophylactic use in high-risk groups or provide early treatment options prior to the identification of the causative infectious agent(s).

      Earlier views regarding the host immune response to biofilm infections suggested that biofilms evaded immune recognition altogether [197, 286]. Recent reports by our group and others have proposed an alternative possibility, namely that biofilms can skew the immune response to favor anti-inflammatory and pro-fibrotic pathways, which contribute to biofilm persistence [32, 162]. Specifically, although macrophages (MΦs) are a prominent infiltrate in *S. aureus* biofilm infections, their penetration into the biofilm itself is impeded by a robust fibrotic response surrounding the infection. In addition, biofilm-associated MΦ are polarized towards an alternatively activated M2 phenotype that possess anti-inflammatory and pro-fibrotic properties that limit bacterial clearance [32]. By extension, the programming of MΦs towards a microbicidal M1 response is diverted, which led us to examine whether the exogenous administration of M1-activated MΦs directly into sites of biofilm infection would overcome the local immune inhibitory environment and fibrotic barrier associated with biofilms. As a complementary approach to augment MΦ proinflammatory activity, we administered the MΦ activating peptide EP67, to facilitate bacterial clearance by inducing a proinflammatory milieu. EP67 (Tyr-Ser-Phe-Lys-Asp-Met-Pro-(N-methylLeu)-D-Ala-Arg, or YSFKDMP(MeL)aR) is a response-selective agonist of the human C5a receptor (C5aR/CD88) that preferentially elicits proinflammatory mediator production from CD88^{+} MΦ without any effects on CD88^{+} neutrophils [287, 288]. Here we demonstrate that targeting MΦ activity with EP67 or the introduction of exogenous M1-activated MΦ inhibits *S. aureus* biofilm formation and provides a novel therapeutic treatment for these persistent infections. This therapeutic approach is not afforded by neutrophils, which agrees with our findings that neutrophils are not a prominent infiltrate in this model of *S. aureus* biofilm infection [31]. Collectively, these finding suggest that immune cell-based therapy using M1-acitvated MΦ may overcome the current confounds associated with biofilm treatment and control.

Results

Activated MΦs exhibit *S. aureus* biofilm bactericidal activity *in vitro*. We have previously demonstrated that MRSA biofilms are capable of attenuating traditional proinflammatory responses explaining, in part, why these infections persist in an immunocompetent host [32]. To determine whether MΦs that were preprogrammed towards a proinflammatory M1 phenotype were capable of overcoming the immune inhibitory aspects of biofilms, MΦs were stimulated with IFN-γ or TNF-α and *S. aureus*-derived peptidoglycan (PGN) for 6 h prior to their addition to *S. aureus*-GFP biofilms or planktonic cultures. Several attributes characteristic of M1-activated MΦs were detected using this treatment paradigm, including significant increases in CD86 and reactive oxygen species production (Supplemental Fig. S6.1). All MΦ populations were capable of phagocytosing planktonic bacteria regardless of their activation state (Fig. 6.1A, left column, "Planktonic"), whereas only M1-acitvated MΦs stimulated with either IFN-γ or TNF-α + PGN were capable of phagocytosing biofilm-associated organisms (Fig. 6.1A, right column, "Biofilm"), which resulted in significant reductions in bacterial burdens following a 24 h co-culture period (Fig. 6.1B). In contrast, non-activated MΦs displayed no indication of intracellular bacteria when incubated with biofilms, confirming our earlier report [32], but were still able to decrease biofilm bacterial burdens (Fig. 6.1B). The ability of non-activated MΦs to reduce biofilm burdens without any evidence of phagocytic activity, suggests that antimicrobial mediator(s) are secreted upon contact with either organisms dispersed from the biofilm and/or bacterial components shed during biofilm growth. The ability of M1-activated MΦs to reduce biofilm burdens required MyD88-dependent signals, since MyD88 KO MΦs treated with IFN-γ and PGN had no impact on biofilm growth (Fig. 6.1B).

To compare the efficacy of MΦ versus neutrophils in regulating MRSA biofilm growth, neutrophils were isolated from murine bone marrow and co-cultured with biofilms. Unlike MΦs, neutrophils were not activated prior to biofilm addition, wince this would lead to rapid degranulation and reduced cell viability. Interestingly, neutrophils were able to phagocytose MRSA biofilms, yet this did not translate into reduced bacterial numbers (Supplemental Fig. S6.2), revealing disconnect between the two processes. This may result from additional virulence

determinants released by *S. aureus* during biofilm growth, since the organism is known to produce numerous factors that interfere with neutrophil function [200, 289, 290]. Alternatively, *S. aureus* can survive inside neutrophils, which could explain why phagocytosis was observed without concomitant reductions in bacterial burdens [291]. On a comparative basis, biofilm formation did afford some protection against phagocytic uptake compared to planktonic growth conditions, since both MΦs and neutrophils actively phagocytosed planktonic *S. aureus* but were less capable of internalizing biofilm-associated bacteria (Fig. 6.1A and Supplemental Fig. S6.2).

Figure 6.1
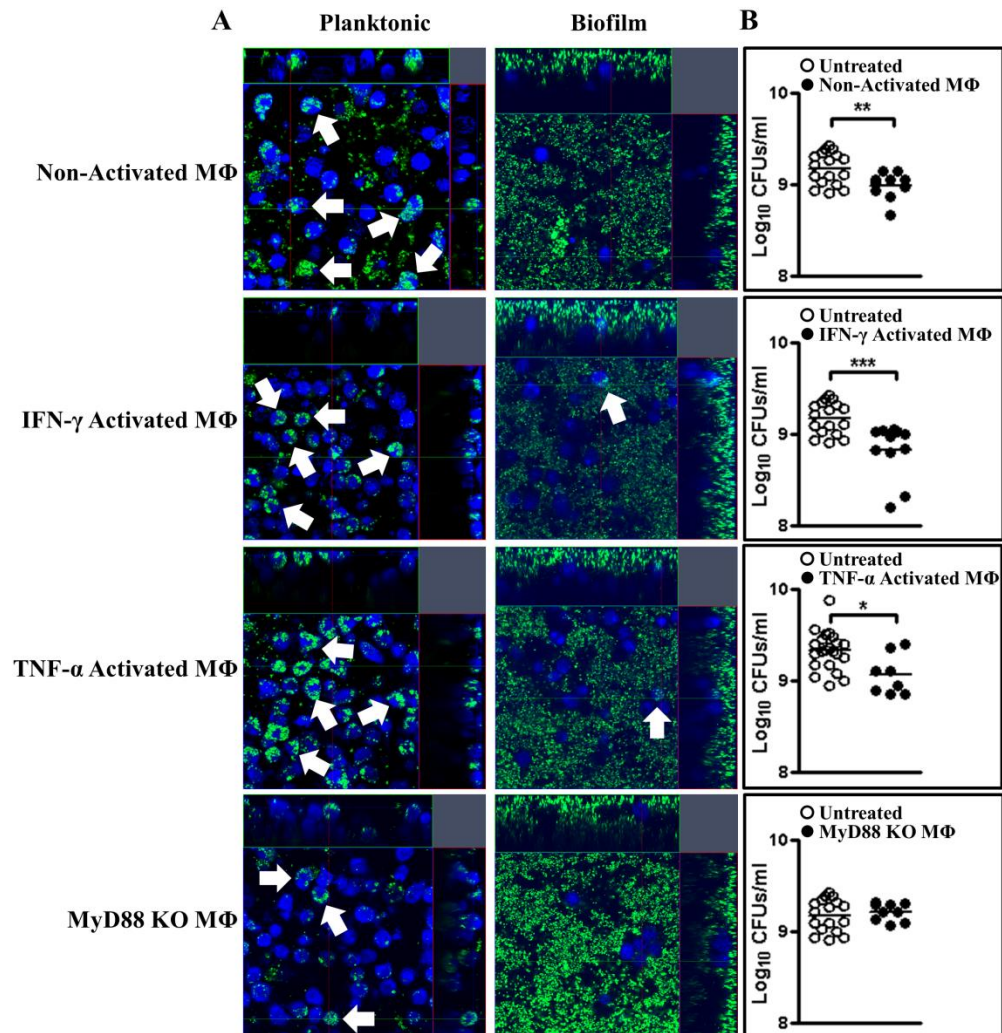
M1 macrophage polarization enhances phagocytosis and killing of *S. aureus* biofilms. (**A**) Non-activated macrophages (MΦs) and M1-activated MΦs (10 ng/ml IFN-γ or 100 ng/ml TNF-α + 10 µg/ml PGN) from C57BL/6 mice, as well as MyD88 knockout (KO) MΦs were labeled with CellTracker Blue (blue) and co-cultured with *S. aureus*-GFP (green) during biofilm or planktonic growth for 2 h and imaged to observe their phagocytic ability. (**B**) After 24 h, biofilms were sonicated to quantitate bacterial burdens to evaluate the ability of the various MΦ populations to attenuate biofilm growth. Biofilms without MΦs were used as untreated controls. White arrows indicated phagocytic cells and significant difference are denoted by asterisks (**$p < 0.01$; ***$p < 0.001$). Results are representative of at least three independent experiments.

M1-activated MΦs limit MRSA biofilm formation *in vivo*. Based on our *in vitro* studies

demonstrating the ability of M1-polarized MΦs to phagocytose biofilm-associated *S. aureus* and

reduce bacterial burdens, we next examined whether this could translate *in vivo*. These

experiments utilized a mouse model of MRSA catheter-associated biofilm infection that we have

previously shown limits MΦ invasion into biofilms and skews these cells toward an alternatively

activated M2 phenotype [32]. We first employed an approach where M1-activated MΦs were

administered beginning at 12 h following MRSA infection, with repeat injections occurring at 24

and 48 h after bacterial exposure. The introduction of M1-activated MΦs directly into the biofilm

infection site significantly reduced bacterial burdens on both infected catheters and in surrounding

tissues at day 3 post-infection (Fig. 6.2A and 2B). More importantly this early intervention with

M1-activated MΦs led to long-term effectiveness against biofilm formation, since catheters

showed minimal evidence of biofilm growth at day 14 without any additional MΦ treatment and

although some bacteria were observed in the surrounding tissues, this was significantly reduced

compared to vehicle treatment (Fig. 6.3A and 3B). Interestingly, the introduction of non-activated

MΦs also reduced biofilm burdens, although significant differences were only observed at day 14

post-infection (Figs. 6.2 and 6.3). To better illustrate the superior efficacy of M1-activated

compared to non-activated MΦs, a dose-response experiment was performed where animals

were treated with increasing numbers (10^4, 10^5, or 10^6) of either non-activated or M1-activated

MΦs. Results from this experiment indicated that 10^5 or 10^6 M1-activated MΦs were capable of

significantly reducing biofilm burdens compared to vehicle controls, whereas non-activated MΦs

were not statistically effective at any dose (Fig. 6.4). Similar to the *in vitro* studies, MyD88-

dependent mechanisms were critical, since MΦs from MyD88 KO mice did not demonstrate any

efficacy in controlling biofilm burdens on either infected catheters or surrounding tissues *in vivo*

(Fig. 6.5). In addition, neutrophils had no impact on biofilm formation, even when the number of

cells was increased to 10^7 per injection (Fig. 6.2, and data not shown), which confirmed our *in*

vitro findings and the fact that neutrophils are not a significant infiltrate in the MRSA catheter-

associated biofilm model utilized here (Supplemental Fig. S6.3).

Previous work from our laboratory demonstrated that MRSA biofilms attenuated the expression of numerous proinflammatory mediators compared to a sterile foreign body [32]. The introduction of M1-activated, but not non-activated MΦs significantly increased CXCL9, CCL5, and IFN-γ expression within biofilm-infected tissues (Fig. 6.6) revealing the successful re-direction towards a proinflammatory milieu. CXCL9 is an IFN-γ-induced T cell chemoattractant, whereas CCL5 recruits a broader array of leukocytes, including T cells, eosinophils, and basophils, although the influx of these target populations was not further examined in these studies following M1 MΦ treatment. The proinflammatory activity of M1-activated MΦs is likely a key mechanism responsible for limiting biofilm growth. Interestingly, no significant changes in IL-10 were detected following M1 MΦ transfer (Fig. 6.6D), which suggests that the broader balance of pro- versus anti-inflammatory factors may be a better predictor of inflammatory outcome compared to individual mediators.

Figure 6.2
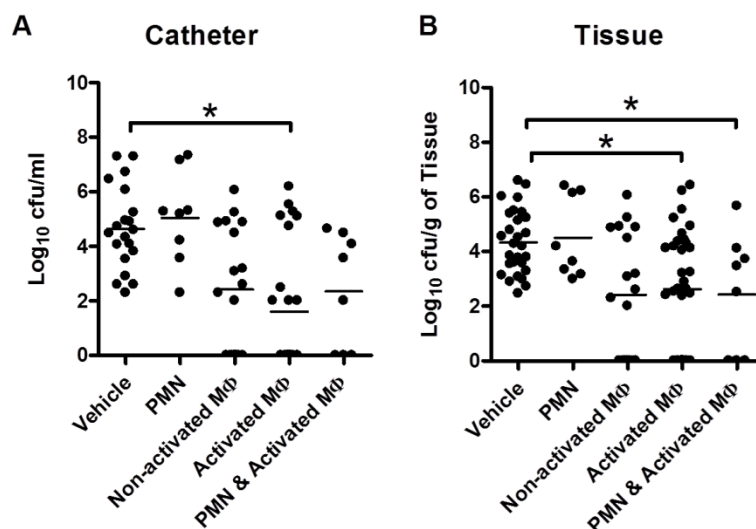
Activated macrophages, but not neutrophils, impair MRSA biofilm formation *in vivo.*

C57BL/6 mice were infected with 10^3 colony forming units (cfu) of USA300 LAC in the lumen of

surgically implanted catheters to establish biofilm infection. Animals were treated with vehicle, 10^6

neutrophils (PMN), 10^6 non-activated macrophages (MΦs), or 10^6 M1-activated MΦs at 12, 24,

and 48 h post-infection, whereupon catheters (**A**) and surrounding tissues (**B**) were collected at

72 h to quantitate bacterial burdens. Results are expressed as the number of cfu per ml for

catheters or cfu per mg tissue, to correct for differences in tissue sampling size. Significant

differences are denoted by asterisks (*$p < 0.05$). Results are presented from individual animals

combined from at least two independent experiments.

Figure 6.3

A Catheter **B** Tissue
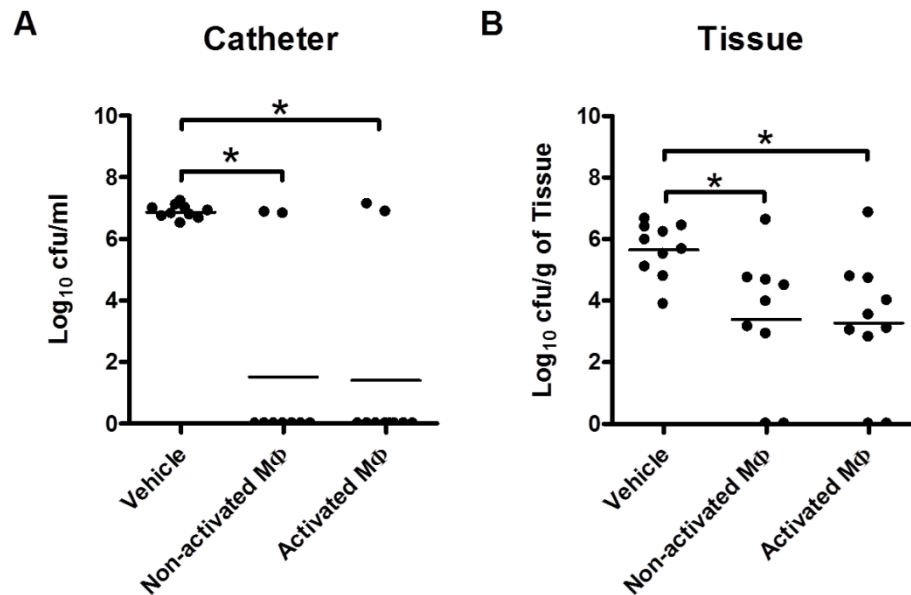
Activated macrophages provide long-lasting defense from MRSA biofilm infections *in vivo*. C57BL/6 mice were infected with 10^3 colony forming units (cfu) of USA300 LAC in the lumen of surgically implanted catheters to establish biofilm infection. Animals were treated with vehicle, 10^6 non-activated or 10^6 M1-activated macrophages (MΦs) at 12, 24, and 48 h post-infection, whereupon catheters (**A**) and surrounding tissues (**B**) were recovered at day 14 to quantitate bacterial burdens. Results are expressed as the number of cfu per ml for catheters or cfu per mg tissue, to correct for differences in tissue sampling size. Significant differences in bacterial burdens between vehicle and MΦ-treated mice are denoted by asterisks (*$p < 0.05$).

Figure 6.4
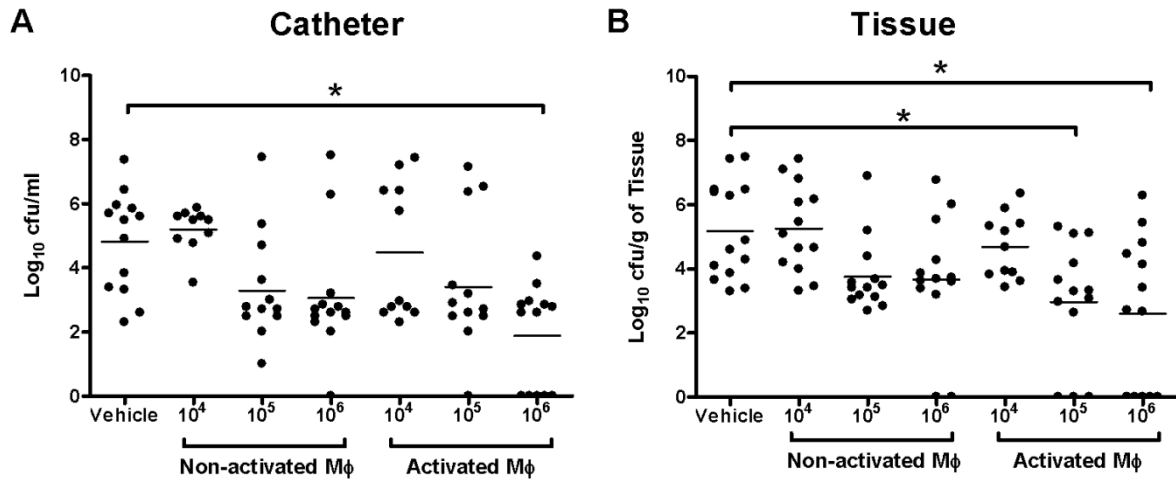
M1-polarized macrophages display superior efficacy at impairing MRSA biofilm formation.

C57BL/6 mice were infected with 10^3 colony forming units (cfu) of USA300 LAC in the lumen of

surgically implanted catheters to establish biofilm infection. Animals were treated with either

vehicle or increasing numbers of non-activated or M1-activated macrophages (MΦs) at 12, 24,

and 48 h post-infection, whereupon catheters (**A**) and surrounding tissues (**B**) were recovered at

day 3 to quantitate bacterial burdens. Results are expressed as the number of cfu per ml for

catheters of cfu per mg tissue, to correct for differences in tissue sampling size. Significant

differences in bacterial burdens between vehicle and MΦ-treated mice are denoted by asterisks

(*$p < 0.05$).

Figure 6.5
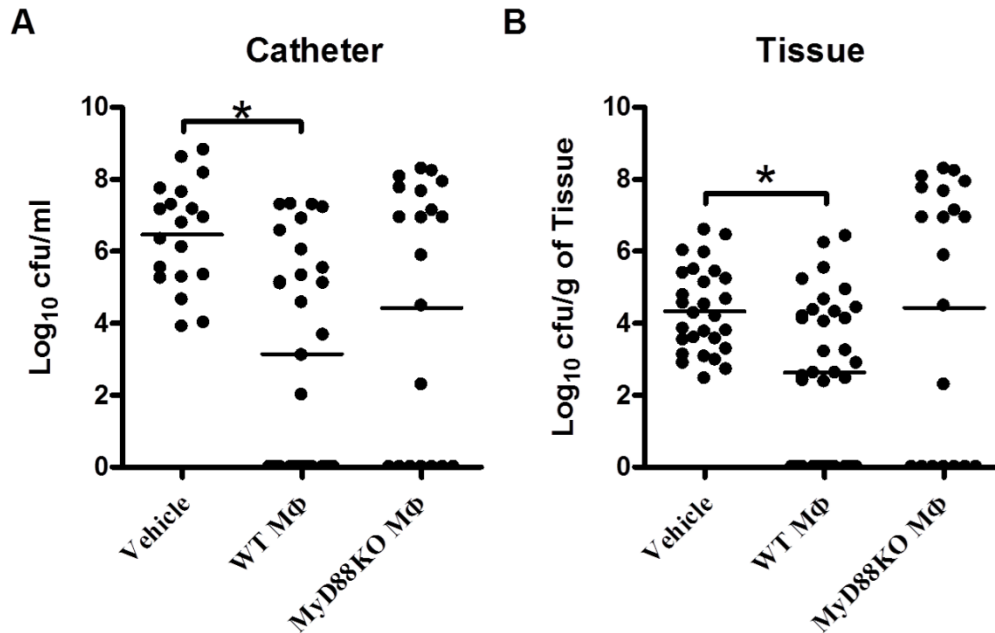
The ability of M1-polarized macrophages to impair MRSA biofilm development is mediated by MyD88-dependent signals. C57BL/6 mice were infected with 10^3 colony forming units (cfu) of USA300 LAC in the lumen of surgically implanted catheters to establish biofilm infection. Animals were treated with vehicle or 10^6 M1-activated macrophages (MΦs) derived from wild type (WT) or MyD88 knockout (KO) mice at 12, 24, and 48 h post-infection, whereupon catheters (**A**) and surrounding tissues (**B**) were recovered at day 3 to quantitate bacterial burdens. Results are expressed as the number of cfu per ml for catheters or cfu per mg tissue, to correct for differences in tissue sampling size. Results are presented from individual animals combined from at least two independent experiments. Significant differences are denoted by asterisks (*$p <$ 0.05).

Figure 6.6

Early Treatment
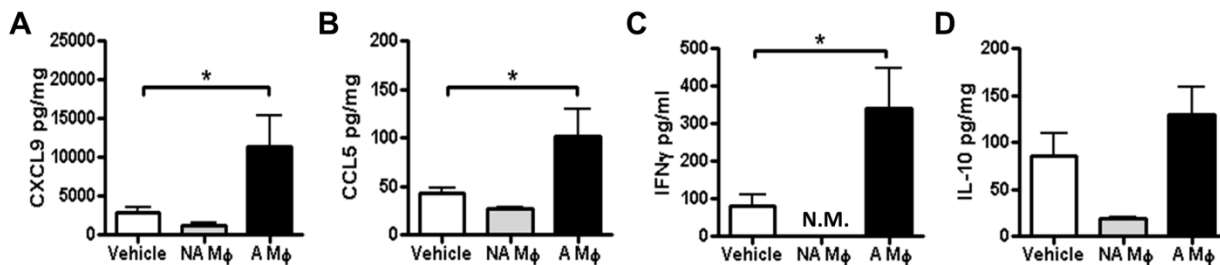
Established Biofilm Treatment
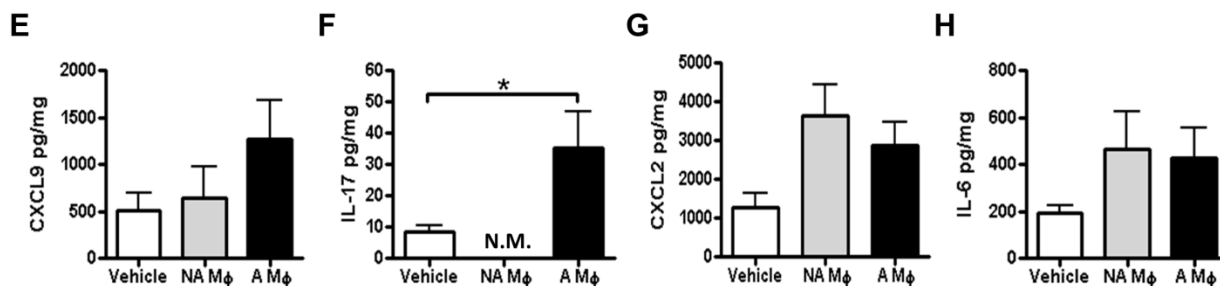
M1-activated macrophage therapy augments the local proinflammatory milieu during MRSA biofilm infection. Tissues surrounding *S. aureus* biofilms of vehicle, non-activated macrophage (NA MΦ), and M1-activated MΦ (A MΦ) treated mice were collected at day 3 (early treatment) or day 10 (established biofilm treatment) post-infection and homogenized to quantitate CXCL9 (**A** and **E**), CCL5, (**B**), IFN-γ (**C**), IL-10 (**D**), IL-17 (**F**), CXCL2 (**G**) and IL-6 (**H**) expression by Milliplex analysis. Results were normalized to the amount of total protein recovered to correct for differences in tissue sampling size. Significant differences are denoted by asterisks (*$p < 0.05$) and are representative of 5-8 mice/group (N.D. = not detected).

Introduction of M1-activated MΦs for the treatment of established MRSA biofilm infections.
Based on the efficacy of our M1 MΦ early treatment paradigm, we next examined whether this
would extend to attenuate bacterial growth in established MRSA biofilm infections. We employed
a similar strategy to the early treatment regimen for MΦ administration except that M1 MΦs were
initially given at day 7 following *S. aureus* infection, a point where robust biofilm has formed [32],
with a repeat injection occurring at day 9. Similar to the early treatment paradigm, the introduction
of M1-activated MΦs directly into the biofilm infection site led to significant reductions in bacterial
burdens on infected catheters at day 10 post-infection, although no effect was seen in
surrounding tissues (Fig. 6.7A and B, respectively). In contrast to M1 MΦ delivery, antibiotic
treatment had no effect on biofilm formation (Fig. 6.7). As expected, Iba-1 immunofluorescence
was significantly increased following the administration of both non-activated and M1-activated
MΦs compared to the endogenous MΦ population in vehicle-treated mice (Fig. 6.8H).
Importantly, arginase-1 expression surrounding biofilms was significantly decreased only
following M1 MΦ treatment, whereas non-activated MΦs had no effect (Fig. 6.8G). In addition,
the introduction of M1-activated MΦs into established biofilms augmented CXCL9, CXCL2, IL-7
and IL-6 expression (Fig. 6.6E-H), although only IL-17 reached statistical significance.
Collectively, these results demonstrate the successful re-direction towards a proinflammatory
milieu following M1 MΦ transfer.

To investigate the longevity of M1-activated MΦs after introduction into biofilm infection
sites, MΦs were labeled with near-infrared Quantum Dots (Qtracker® 800) and injected either at
the time of infection or on day 7, representing early and established treatment paradigms,
respectively. Animals were subjected to IVIS imaging immediately following MΦ transfer and
every 24 h thereafter. Qdot-labeled M1 MΦs were still visible at 4 days post-injection (Fig. 6.9),
which likely accounts for their ability to significantly limit MRSA biofilm formation. Although it is
well established that Qdots are retained in intact cells, it remains possible that they could be
internalized by neighboring phagocytic cells if donor macrophages are dying *in situ*.

Figure 6.7

A
Catheter

B
Tissue
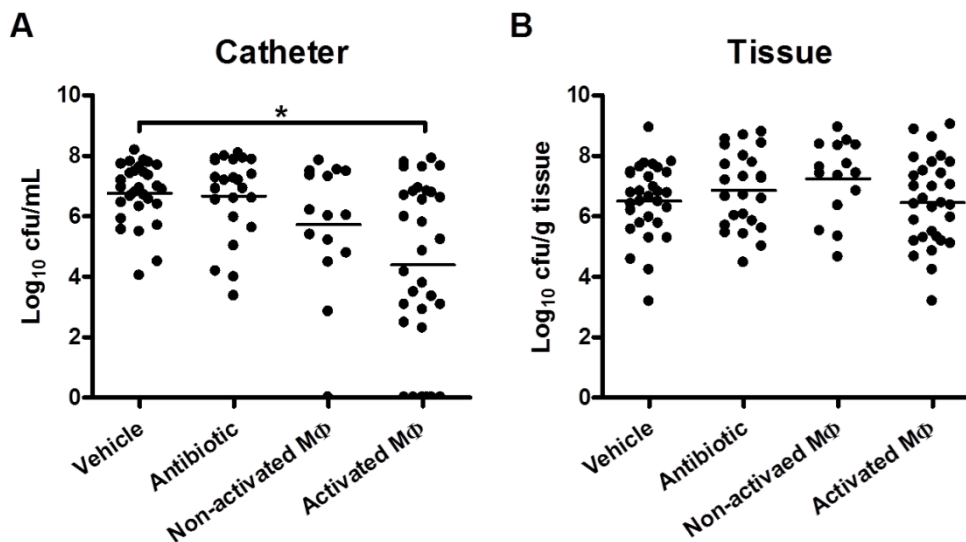
M1-activated macrophages attenuate established MRSA biofilm infection. C57BL/6 mice were infected with 10^3 colony forming units (cfu) of USA300 LAC in the lumen of surgically implanted catheters to establish infection. On days 7 and 9 post-infection, animals received injections of vehicle, antibiotic (rifampicin + daptomycin), 10^6 non-activated macrophages (MΦs), or 10^6 M1-activated MΦs, whereupon catheters (**A**) and surrounding tissues (**B**) were recovered at day 10 to quantitate bacterial burdens. Significant differences between groups are denoted by asterisks (*$p < 0.05$) and represent animals from two independent experiments.

Figure 6.8
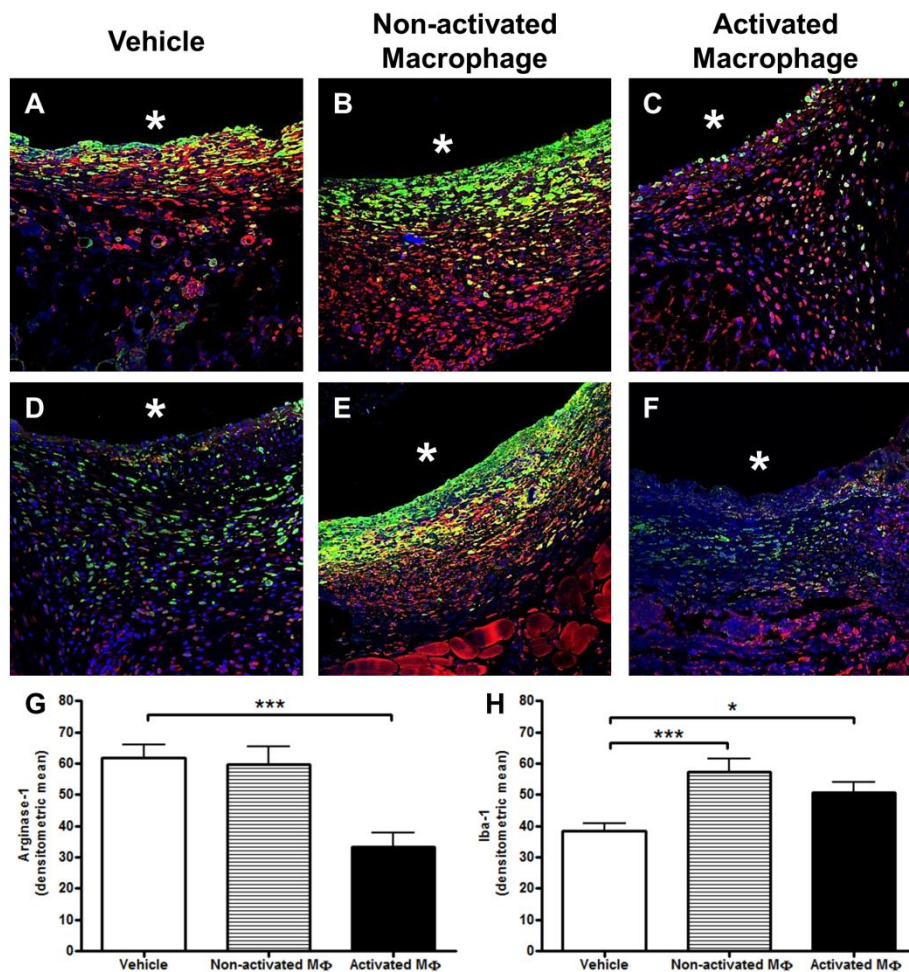
Administration of M1-activated macrophages attenuates arginase-1 expression in established biofilms. Mice received injections of vehicle (**A** & **D**), 10^6 non-activated macrophages (**B** & **E**) or 10^6 M1-activated macrophages (**C** & **F**) beginning at days 7 and 9 post-infection, whereupon tissues surrounding infected catheters were collected at day 10 and subjected to immunofluorescence staining with Iba-1 to identify MΦs (red), arginase-1 (green), and nuclear staining with DAPI (blue). Asterisks represent the original location of the catheter, which is non-adherent to glass slides. (**G** & **H**). Quantitation of arginase-1 and Iba-1 immunofluorescence staining associated with *S. aureus* biofilms of vehicle-, non-activated- or M1 MΦ-treated animals. Significant differences are indicated with asterisks (*$p < 0.05$; **$p < 0.01$; ***$p < 0.001$) and are representative of two independent experiments with 8 mice per group.

Figure 6.9
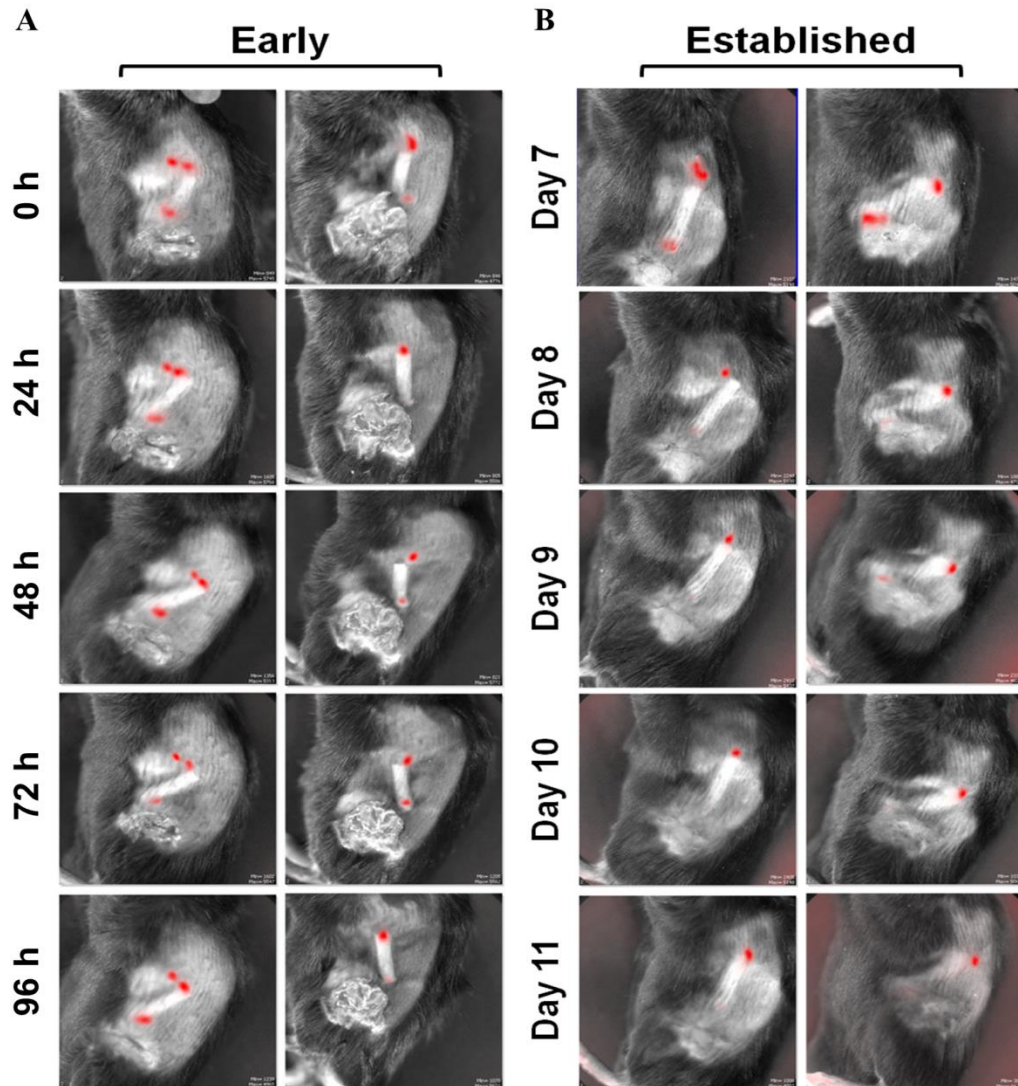
M1-activated macrophages remain localized at the site of biofilm infection and maintain a M1 phenotype. Mice received one dose of 10^7 Quantum Dot-labeled M1-activated macrophages (MΦs; red) either at the time of *S. aureus* challenge (**A**) or at day 7 following infection (**B**), representing early and established therapies, respectively. The same cohort of animals was subjected to daily IVIS imaging to visualize MΦ persistence. Results are representative of 10 individual animals per group.

EP67 attenuates MRSA biofilm formation *in vivo* and stimulates local proinflammatory responses. As a complimentary approach to the introduction of exogenous M1-activated MΦs, we next examined whether the CD88 agonist EP67 would re-program the endogenous MΦ infiltrates associated with MRSA biofilms *in vivo* from an anti-inflammatory M2 to a proinflammatory M1 phenotype to facilitate bacterial clearance. Animals were initially treated with EP67 at the time of infection with additional injections occurring at 24 and 48 h. Bacterial burdens associated with biofilm-infected catheters as well as surrounding tissues were significantly decreased following EP67 treatment compared to animals receiving an inactive scrambled sequence of EP67 (sEP67) or vehicle control (Fig. 6.10). Importantly, early EP67 treatment was key to restricting MRSA biofilm establishment, since minimal bacterial growth was detected at day 14 following infection, even though the last dosing interval of EP67 occurred at 48 h (Fig. 6.10C and 10D).

To determine whether EP67 could skew the biofilm environment to a proinflammatory state, we evaluated cytokine and chemokine expression in biofilm-infected tissues. Several inflammatory mediators predominantly expressed by activated MΦs, such as IL-12p40 and RANTES, were significantly increased in EP67- compared to vehicle-treated animals (Fig. 6.11A and 11B). To further investigate mechanisms of EP67 action during biofilm infections, we compared the degree of MΦ influx into tissues surrounding MRSA biofilms using two complementary approaches. Immunofluorescence staining revealed that MΦ accumulation into EP67-treated biofilms was significantly increased at day 3 post-infection compared to vehicle (Fig. 6.12A). Importantly, while only a few MΦs were recruited to the biofilm surface in vehicle treated mice, EP67 administration dramatically increased the numbers of MΦs that migrated into the biofilm (Fig. 6.12B). The ability of EP67 to augment MΦ infiltrates in MRSA biofilms was confirmed by FACS (Fig. 6.12C). Collectively, these findings demonstrate that EP67 induces a proinflammatory milieu by augmenting MΦ recruitment and cytokine/chemokine production, which effectively counteracts the anti-inflammatory environment elicited by MRSA biofilms. We also investigated whether EP67 treatment could impact established biofilms; however, the peptide did

not exert any beneficial effects in this setting, suggesting its optimal use as a prophylactic modality under the conditions used in this study.

Collectively, our results have identified a previously unappreciated role for signals provided by M1-activated MΦs in biofilm containments and bacterial clearance. By extension, it is not unexpected that MRSA biofilms have the capacity to thwart this response by skewing MΦs away from a pro-inflammatory M1 to an anti-inflammatory M2 phenotype, which ensures biofilm persistence in an immunocompetent host.

Figure 6.10
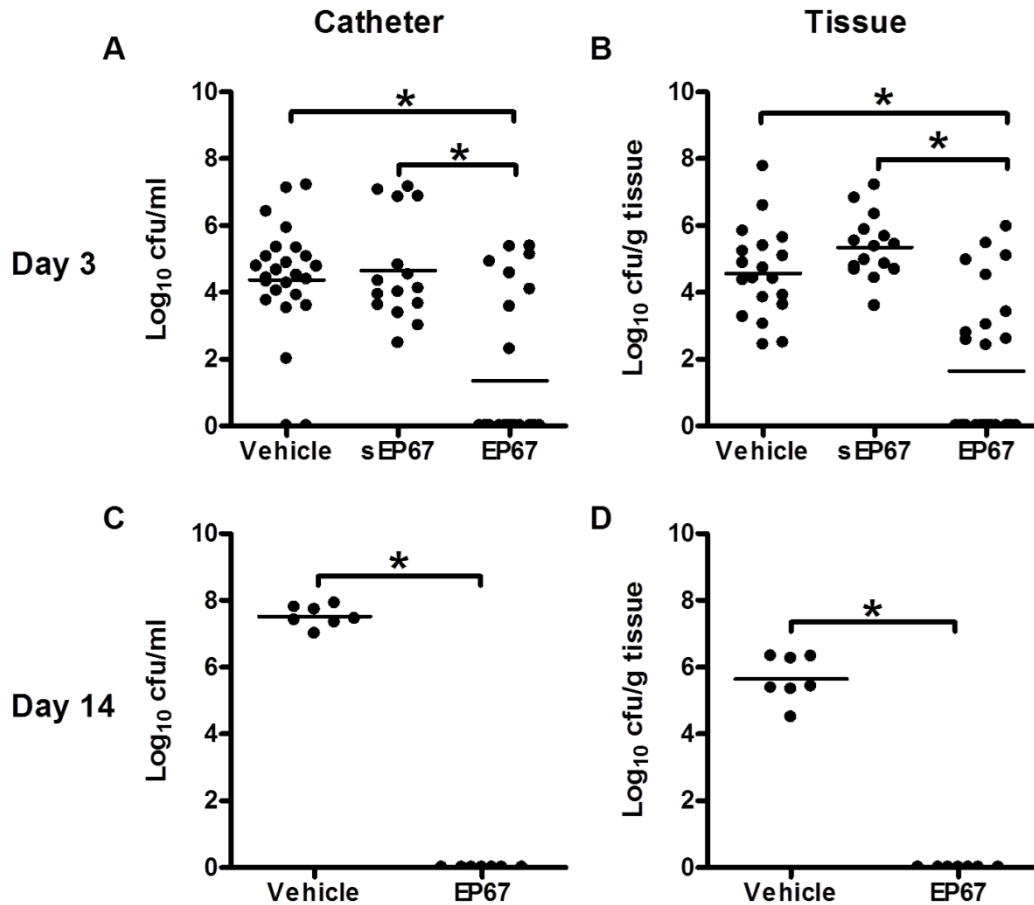
The macrophage activating peptide EP67 attenuates _S. aureus_ biofilm growth _in vivo._ Mice were infected with 10^3 cfu of USA300 LAC in the lumen of surgically implanted catheters to establish biofilms. Animals were treated with vehicle, EP67, or a biologically inactive scrambled derivative peptide (sEP67), beginning at the time of infection and again at 24 and 48 h, whereupon catheters (**A** & **C**) and surrounding tissues (**B** & **D**) were recovered to quantitate bacterial burdens at days 3 or 14 after infection. Data are expressed as the number of cfu per ml for catheters or cfu per mg host tissue for normalization. Results are presented from individual animals from at least two independent experiments. Significant differences are denoted by asterisks (*$p < 0.05$).

Figure 6.11
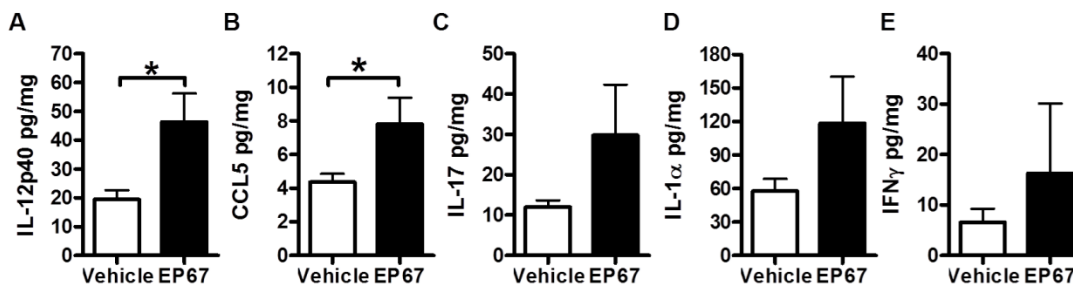
EP67 augments proinflammatory mediator expression in biofilm infected tissues. Mice were infected with 10^3 cfu of USA300 LAC in the lumen of surgically implanted catheters to establish biofilms. Animals were treated with vehicle or EP67 beginning at the time of infection and again at 24 and 48 h, whereupon tissues were collected at day 3 to quantitate the effects of EP67 treatment on IL-12p40 (**A**), CCL5, (**B**), IL-17 (**C**), IL-1α (**D**) and IFN-γ (**E**) expression by MIlliplex analysis. Results were normalized to the amount of total protein recovered to correct for differences in tissue sampling size. Results are presented from individual animals combined from two independent experiments (n = 14 per group). Significant differences between EP67- vs. vehicle-treated tissues are denoted by asterisks (*$p < 0.05$).

Figure 6.12
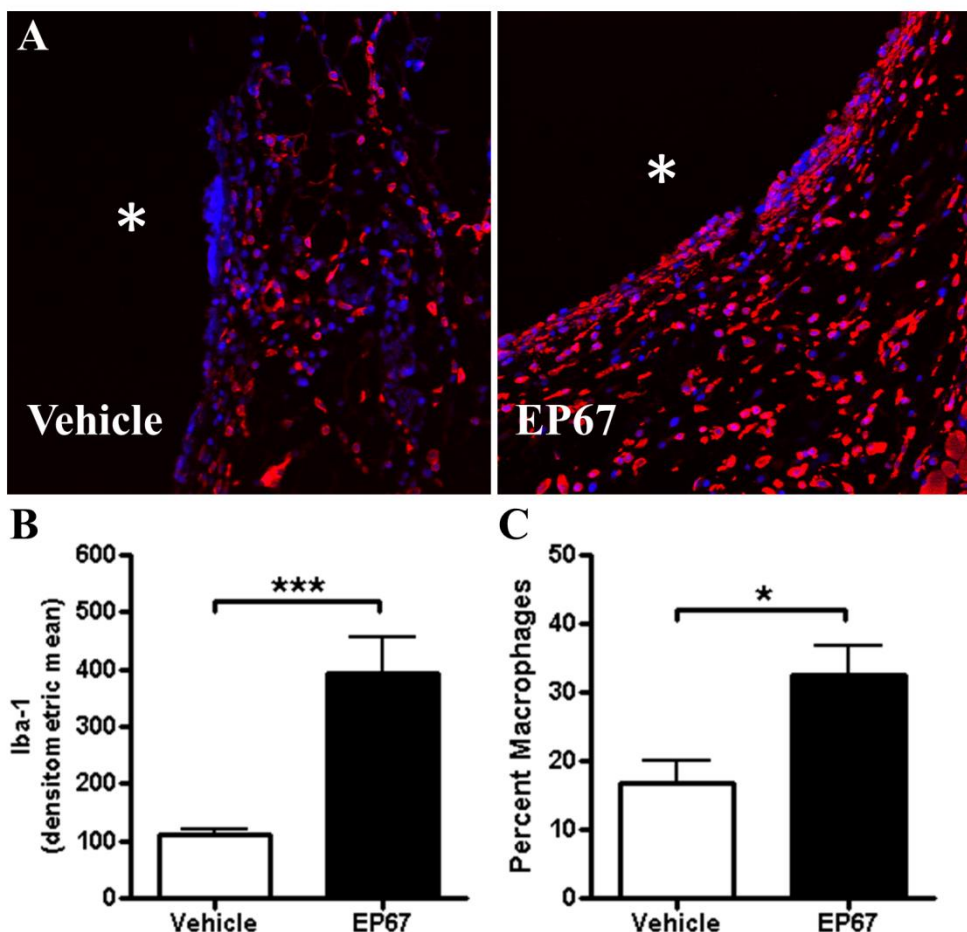
EP67 augments macrophage infiltration into MRSA biofilms. (**A** & **B**) Mice were infected with

10^3 cfu of USA300 LAC in the lumen of surgically implanted catheters to establish biofilms.

Animals were treated with vehicle or EP67 beginning at the time of infection and again at 24 and

48 h, whereupon tissues surrounding infected catheters were collected at day 3 and subjected to

immunofluorescence staining with Iba-1 to identify macrophages (MΦs; red) and nuclear staining

with DAPI (blue). Asterisks represent the original location of the catheter, which is non-adherent

to glass slides. (**C**) Macrophage (F4/80$^+$) infiltrates in tissues surrounding infected catheters from

vehicle- or EP67-treated animals were quantitated by FACS. Results are expressed as the

percentage of cells after correction for isotype control staining and are representative of three

independent experiments with 8 mice per group (*$p < 0.05$; ***$p < 0.001$).

Supplemental Figure S6.1
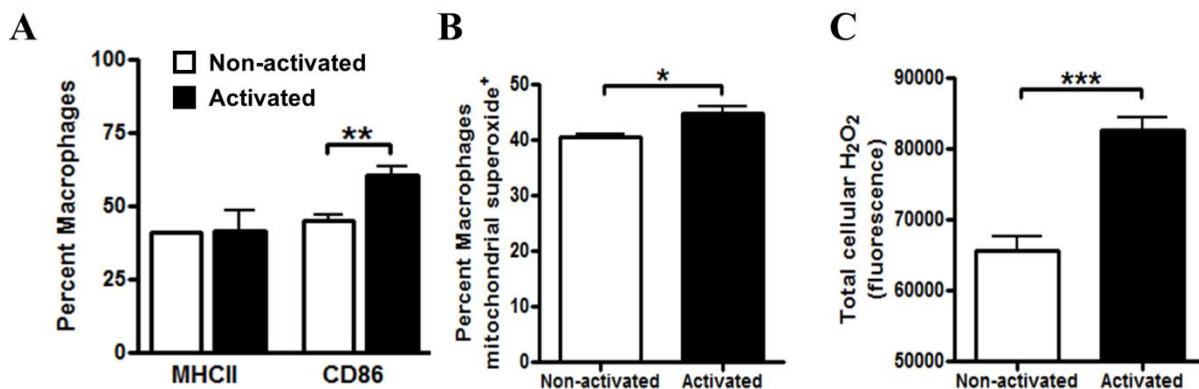
M1 macrophage polarization enhances co-stimulatory molecule and reactive oxygen species (ROS) production. Bone marrow-derived macrophages (MΦs) from C57BL/6 mice were stimulated with 10 ng/ml IFN- γ + 10 µg/ml PGN for 6 h to induce M1-activation or medium alone (non-activated MΦs). Expression of the cell surface markers MHC Class II and CD86 was assessed by FACS analysis (**A**). MΦs were also incubated with MitoSOX (**B)** or CM-H$_2$DCFDA (**C**) to measure mitochondrial superoxide (mROS) and determine total cellular H$_2$O$_2$, respectively. Significant differences are denoted by asterisks (*$p < 0.05$; **$p < 0.01$; ***$p < 0.001$).

Supplemental Figure S6.2
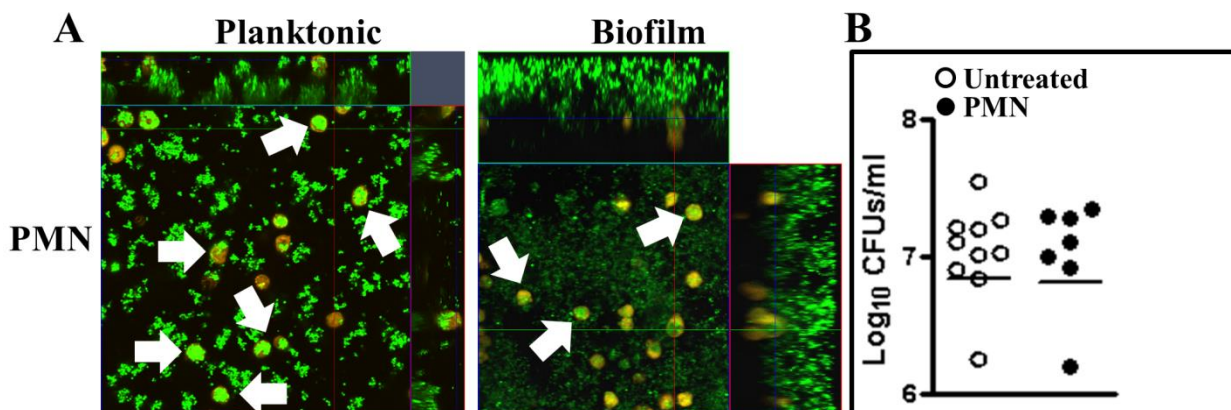
Neutrophils are capable of phagocytosing _S. aureus_ biofilms but do not reduce bacterial burdens. (**A**) Neutrophils (PMN) were isolated from the bone marrow of C57BL/6 mice, labeled with CellTracker Orange (orange-yellow), and co-cultured with _S. aureus_-GFP (green) during biofilm or planktonic growth for 2 h and imaged to observe their phagocytic ability. (**B**) After 24 h, biofilms were sonicated to quantitate bacterial burdens to evaluate the ability of PMNs to attenuate biofilm growth. Biofilms without PMNs were used as untreated controls. White arrows indicate phagocytic cells.

Supplemental Figure S6.3
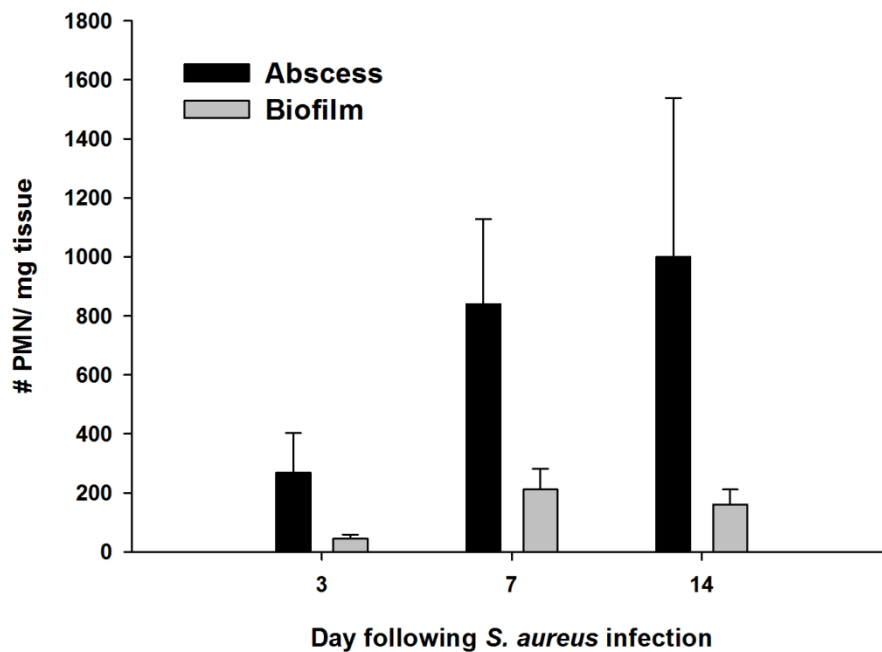
Neutrophil infiltrates into catheter-associated biofilms are minimal compared to abscesses. C57BL/6 mice were infected with $5x10^5$ CFU USA300 LAC either in the lumen of surgically implanted catheters or s.c. in the absence of any indwelling device to establish biofilm and abscess infections, respectively. Animals were sacrificed at days 3, 7, or 14 following *S. aureus* exposure, whereupon tissues surrounding infected catheters or s.c. injection sites were collected to quantitate neutrophil infiltrates by FACS. Results are expressed as the percent of Ly6G+ neutrophils after correction for isotype control staining and represent the mean ± SEM of three independent experiments.

Discussion

S. aureus is a frequent etiological agent of biofilm infections on indwelling devices and orthopedic implants [36, 292] and recent reports by our group and others have demonstrated that biofilms can skew the immune response to favor anti-inflammatory and pro-fibrotic pathways, which likely contribute to biofilm persistence [32, 162]. To overcome this immune deviation and provide a novel treatment strategy for biofilm infections, we augmented antimicrobial activity through the local administration of classically-activated M1 MΦs or treatment with the CD88 agonist EP67, which invokes MΦ proinflammatory responses. Early administration of M1-activated MΦs or EP67 limited biofilm formation, and treatment of established biofilm infections with M1-activated MΦ also significantly reduced catheter-associated biofilm burdens. Based on this evidence, we have identified a novel therapeutic strategy to limit *S. aureus* catheter-associated biofilm infections by targeting MΦ activation, which may extend to other artificial implants.

The greatest therapeutic benefit of both MΦ targeting strategies in this study was achieved with early interventions to boost proinflammatory activity against biofilm infections. By extension, targeting MΦ proinflammatory activity may prove useful when administered to patients undergoing orthopedic surgery or other device-related implants to prevent nosocomial infections, particularly for individuals who are at high-risk for developing infectious complications. Although our M1-activated MΦ therapy did not completely eliminate established biofilms on infected devices, this strategy may prove beneficial in combination with antibiotics for patients who are unable or unwilling to undergo additional surgeries to manage the infection and maintain the implanted device. The significance of this approach is even more pronounced against the backdrop of the rapidly increasing elderly population, which becomes progressively less immune responsive and represents the primary recipients of hip and knee replacements. To achieve enhanced efficacy against established biofilms we are currently refining our M1-acitvated MΦ delivery; nonetheless, these results clearly demonstrate proof-of-principle that induction of a proinflammatory milieu during MRSA biofilm infection is beneficial for bacterial clearance.

The therapeutic potential of activated MΦs is supported by our results demonstrating that early treatment with proinflammatory M1-activated MΦs significantly limited *S. aureus* biofilm growth *in vivo* and provided long-term protection from biofilm colonization. Likewise, activated MΦs were also effective at reducing *S. aureus* burdens in established biofilms. The cytokine/chemokine milieu elicited following M1-activated MΦ transfer reflects products derived from both T cells (i.e. IFN-γ and IL-17) and MΦs (i.e. CXCL9, CCL5, and IL-1), suggesting the coordinate activity of both cell types. This complex profile was only significant in the early intervention paradigm with M1-activated MΦs and the functional impact of these mediators on biofilm burdens remains to be determined. When querying the inflammatory milieu associated with established biofilms following M1 MΦ injection, only IL-17 was significantly increased. Although the other mediators examined did not show statistically significant increases, the trends towards elevated production may translate into increased efficacy when considering their combined action. This may explain why bacterial burdens were decreased on the catheter itself but not in the surrounding tissue because heightened inflammatory mediator levels may be required to impact the latter. It was not feasible to measure all of the microbicidal effectors associated with biofilm infections; therefore, it is likely that alternative factors not examined here could be significantly elevated after M1 MΦ treatment to account for the decreased bacterial burdens observed on infected catheters. It was unexpected that M1-activated MΦ transfer had no effect on tissue burdens in established biofilms. One explanation to account for this finding is that the number of MΦs injected was not sufficient to effectively manage bacterial burdens within the infected tissue. It is clear that M1-activated MΦs limit biofilm growth on the catheter itself; however, it remains to be determined whether this results from direct killing of the biofilm and/or enhanced dispersal of organisms from the biofilm into the surrounding tissue. In the latter case, this would lead to increased tissue-associated bacteria, which would likely overwhelm the microbicidal capacity of M1-activated MΦs injected at the infection site. In future studies, it would be interesting to determine whether M1-activated MΦs display synergy with antibiotics to facilitate biofilm clearance, since the former facilitates the dispersal of organisms from the biofilm, which, in

turn, would restore their metabolic activity and potential susceptibility to antibiotics. However, this is beyond the scope of the current report.

One interesting finding from this study was that non-activated MΦs demonstrated a trend towards reduced biofilm burdens *in vivo*, although most of these differences did not reach statistical significance. This suggests that MΦ activation signals are present at sites of biofilm infection; however, additional stimuli are required to achieve maximal MΦ microbicidal action. One such signal could be direct MΦ contact with the biofilm, which is impeded by the host-derived fibrotic matrix deposited around the infected device. Another possibility is that the degree of endogenous MΦ recruitment is insufficient to prevent biofilm establishment and therefore, the injection of a large number of MΦs at the site of infection is sufficient to limit biofilm growth, regardless of their activation state. Nonetheless, the superior action of M1-activated compared to non-activated MΦs at thwarting *S. aureus* biofilm formation was demonstrated by the ability of the former to significantly reduce bacterial burdens *in vivo*.

The use of EP67 may overcome the principal issues of biofilm immune dysfunction, as EP67 appears to provide the correct activation signals to CD88^{+} MΦs (and perhaps other APCs) [293], to engage a robust microbicidal response in the developing biofilm and surrounding tissues. Indeed, EP67 has been shown to enhance the immune status of aged mice by re-establishing an immunologically productive Th1/Th2 balance [294], indicating that this peptide may be a valuable therapeutic option in the aged population where multiple surgeries to manage infected devices is not desirable. However, unlike M1-activated MΦ transfer, EP67 treatment did not impact established biofilms, suggesting that additional therapeutic obstacles are present. One such hurdle is the fibrotic capsule that typically surrounds biofilm infections [295-297]. Although it is presumed that biofilm encapsulation by the host represents a protective response to contain the infection, this process may inadvertently provide survival advantages to the bacteria [298, 299]. The signals responsible for eliciting this fibrotic response are currently under investigation; nonetheless in the current study the injection of MΦs immediately adjacent to the biofilm bypasses this fibrotic barrier and enables MΦ activation to occur.

Neutrophils represent a first line of defense against bacterial infections and possess a potent arsenal of bactericidal compounds, including defensins, cathelicidins, and lysozyme [300, 301]. In terms of their bactericidal activity, neutrophils are most notable for their ability to produce large amounts of reactive oxygen intermediates catalyzed by NADPH oxidase. In addition, neutrophils also degranulate and generate neutrophil extracellular traps (NETs), a meshwork of DNA and enzymes that lead to the extracellular killing of *S. aureus* and other bacteria [302]. Despite these microbicidal mechanisms, neutrophil transfer did not attenuate *S. aureus* biofilm growth even when higher numbers of cells were injected. One possibility to explain this finding is that neutrophils rapidly degranulated following *in vivo* transfer and did not survive long enough to provide a measurable effect on biofilm growth. Nevertheless, it is important to acknowledge that neutrophils may contribute to biofilm clearance at other sites of infection, which remains to be determined. The reasons responsible for differential neutrophil recruitment in various biofilm models may be influenced by the degree of tissue vascularization and/or extent of biofilm development. Another factor to consider is the type of device. For example, bacteria colonizing the lumen of a hollow catheter are initially shielded from immune recognition by the catheter wall, which may afford additional protection. In the case of a solid device, bacteria are immediately exposed to host tissues, in theory enabling an immediate proinflammatory response. We are currently investigating these possibilities utilizing other *in vivo* models of staphylococcal biofilm infection.

Collectively, these studies have identified a previously unappreciated role for M1-activated MΦs in biofilm containment and bacterial clearance. By extension, it is not unexpected that *S. aureus* biofilms have the capacity to thwart this response by skewing MΦs away from a pro-inflammatory M1 to an anti-inflammatory M2 phenotype, which ensures biofilm persistence in an immunocompetent host. The implementation of our "M1-activated MΦ Transfer" therapy would allow MΦs to be "on board" to neutralize potential device contamination from normal skin flora during surgical insertion. While conventional antibiotics are ineffective for treating biofilms, they are commonly used to control bacteria that escape the biofilm matrix to prevent their colonization of other tissue sites. Such use of antibiotics imposes mutational pressures on the bacteria and

portends the possibilities of developing antibiotic resistance. MΦ-based immune cell therapy is not only efficacious at controlling biofilm infections, but has the added advantage of doing so by utilizing the host's endogenous innate immune cells, thus eliminating mutational pressures imposed directly on the bacteria and decreasing the likelihood of the emergence of antibiotic resistant strains.

Chapter 7: Discussion

Key Findings and Conclusions:

The innate immune system is the first line of defense against invading pathogens. Macrophages are a critical component of this response, as they exhibit potent antibacterial properties and link innate and adaptive immunity with the capability to present antigen to T cells. However, bacteria like *S. aureus* have developed sophisticated ways to evade traditional immune mechanisms of clearance by developing biofilms on native tissues and indwelling medical devices. A key component of this subversion is the induction of MDSCs. MDSCs use a variety of mechanisms to alter macrophage phenotypes, suppress T cell responses, and dramatically alter the biofilm milieu, all of which play a role in the chronicity of biofilm infection [59, 60].

Our laboratory has found that when *S. aureus* is seeded at a low inoculum (i.e. 10^3 CFU) onto either titanium implants or into subcutaneous catheters, bacteria is able to adhere and accumulate, forming a biofilm with the ability to persist for several months [59, 60]. There is a divergence between these two models though in the degree of the inflammatory response that occurs following infection. Catheter-associated *S. aureus* biofilms attenuate proinflammatory mediator expression compared to sterile catheter implantation [32], whereas we have now shown that *S. aureus* orthopedic implant infection elicits sustained cytokine and chemokine production [59](Heim et al 2015). In large part this can be attributed to the site of the implanted device. The subcutaneous catheter is implanted into the flank where more mature tissue-resident populations, such as macrophages, elicit initial responses [32]. Furthermore, it is known that *S. aureus* biofilms elicit exaggerated macrophage infiltrates compared to abscesses and soon after encountering biofilms macrophages acquire anti-inflammatory characteristics and readily die [32]. However, the orthopedic implant infection is being established in close proximity to the bone marrow, which is rich in progenitor cells that can elicit a rapid inflammatory response following bacterial assault. This is not without consequence though, as we have shown that these immature cells become stuck in their differentiation and develop immunosuppressive properties allowing the biofilm to establish itself on the device and persist for long periods of time [59, 60]. Indeed, MDSCs rather than neutrophils or monocyte/macrophage populations are the primary immune infiltrate to the site of orthopedic implant-associated infection. In addition, only a very small percentage of CD3^{+}

T cells are observed in infected tissue [59, 60]. Although MDSCs also accumulate during subcutaneous catheter biofilm infection, their numbers are greater in the orthopedic model and therefore we chose to use it for the majority of our studies characterizing the mechanisms of MDSC immunosuppression.

To determine the clinical significance of this model, and determine whether similar patterns of leukocyte infiltration and inflammatory mediator production occur in mice and humans, these parameters were assessed in tissue samples from patients undergoing revision surgeries for PJIs or aseptic loosening as a control. MDSCs in humans can be identified as CD33^{+}HLA-DR^{-}, and a population with this MDSC-like phenotype was detected in tissues from a patient with a confirmed *S. epidermidis* PJI, whereas few of these cells were observed in aseptic samples [59]. The CD33^{+}HLA-DR^{-} population recovered from the *S. epidermidis*-infected tissue expressed genes characteristic of MDSCs, including Arg-1, iNOS, and IDO-1. Although we did not recover enough CD33^{+}HLA-DR^{-} cells from these tissues to confirm their suppressive ability *in vitro*; they do exhibit MDSC-like characteristics. In addition, T cell influx was minimal in infected tissues, while T cells represented the most abundant infiltrate associated with aseptic orthopedic revisions [59]. Ultimately these results demonstrate the utility of our mouse model for understanding mechanisms involved in evasion of host immunity during PJI and potentially identify therapeutic targets. To this point we have not seen major discrepancies between immune profiles of tissues infected with different pathogens, although this is something we are paying close attention to in an effort to determine whether staphylococcal species are unique in the responses they elicit or if this is a consistent response.

In comparing the number of Gr-1^{+}CD11b^{+}MDSC infiltrates in sterile and *S. aureus*-infected tissues and found sterile tissues contained cells resembling MDSCs even though numbers were significantly increased in the presence of an infection [60]. This was an important finding, because although MDSCs isolated from sterile implants were unable to inhibit T cell proliferation, it suggested that an immature myeloid population is recruited to sites of injury with the capability to differentiate into effector populations if needed. However, *S. aureus*-derived

products could elicit proinflammatory mediator production which then causes these immature cells to acquire immunosuppressive function and remain arrested in an immature state.

Early studies were performed using the Gr-1 Ab, as it is a common marker for mouse MDSCs. However, Gr-1 recognizes both the Ly6G and Ly6C epitopes and therefore cannot discern between subsets of MDSCs. Staining for Ly6G and Ly6C revealed three distinct populations, namely Ly6G^{high}Ly6C$^+$, Ly6G^{low}Ly6C^{low}, and Ly6G$^-$Ly6C$^+$, of which only the Ly6G^{high}Ly6C$^+$ cells significantly inhibited CD4$^+$ T cell proliferation [60]. In addition, FACS-purified Ly6G^{high}Ly6C$^+$ infiltrates expressed genes characteristics of MDSCs, and cytospins revealed the Ly6G^{high}Ly6C$^+$ population of suppressive cells had immature granulocyte morphology, characterized by numerous ringed nuclei. Together, these results are highly suggestive of these cells as G-MDSCs. The Ly6G$^-$Ly6C$^+$ population displayed monocyte-like morphology, and the Ly6G^{low}Ly6C^{low} cells had some characteristics of neutrophils, including multi-lobed nuclei [60]. Both G- and M-MDSC subsets are found in a variety of pathologic conditions, and are thought to arise due to differences in the cytokine milieu during differentiation. In our laboratory's mouse model of *S. aureus* PJI large amounts of G-CSF are produced relative to sterile implants, while very low levels of GM-CSF are detected [59], which could account for the favored G-MDSC response in this setting. A recent study comparing the phenotype of MDSCs in sepsis patients found that G-MDSCs are favored in patients with gram-positive sepsis, while M-MDSCs are expanded during infection gram-negative bacteria [303]. Currently, it is unclear whether this observation is true for PJI, but would correlate with our observations thus far.

There is currently no direct way to deplete only MDSCs *in vivo*, due in large part to the surface markers shared with other myeloid populations. In our model, the immunosuppressive MDSCs express the highest levels of Ly6G, whereas the monocyte population was Ly6G$^-$. Therefore, we attempted to assess the functional role of MDSCs by using the anti-Ly6G Ab 1A8. Ly6G$^+$ cells were depleted during the entire course of *S. aureus* biofilm infection, which led to increased monocyte recruitment at days 7 and 14 post-infection, potentially as a compensation mechanism due to depletion. Interestingly, monocytes isolated from infected tissues of Ly6G depleted mice had increased expression of iNOS, IL-1β, IL-12p40 and IL-6 compared to

monocytes from IgG-treated mice (Heim et al 2014). This increased proinflammatory profile was concomitant with significantly reduced bacterial burdens in the tissue and knee joint of Ly6G-treated mice. For the first time, we were able to show that MDSCs are negatively regulating innate immune responses to *S. aureus* biofilm infection, which includes the active inhibition of monocyte proinflammatory responses that contribute to bacterial clearance. These conclusions were confirmed when mice were treated with the Gr-1 Ab, which targets and depletes MDSCs, neutrophils and monocyte macrophage populations. With this strategy, higher bacterial burdens were observed in implant-associated tissues in the absence of MDSCs and monocyte/macrophage effector populations [60].

Interestingly, during Gr-1 Ab treatment, we observed an increase in Gr-1$^+$ (Ly6G/Ly6C) infiltrates [60]. This was likely, a compensatory mechanism in response to increased bacterial burdens at the implant site and systemically, as bacteria disseminated to the heart, kidney and spleen. In addition, there was extensive extramedullary hematopoiesis occurring in the spleens of mice treated with Gr-1 Ab, which could contribute to the compensatory increase in Gr-1$^+$ cells during infection. Extramedullary hematopoiesis is a phenomenon that is common during chronic inflammatory diseases and cancer. During infection the requirement for myeloid cells dramatically increases and creates a need for emergency myelopoiesis and subsequent mobilization of immature cells from the bone marrow and spleen. Once again, this data suggests that the accumulation of MDSCs is a direct result of signals derived from the establishing *S. aureus* biofilm infection.

During the initial characterization of immune infiltrates to *S. aureus* orthopedic biofilm infection, we observed FACS-purified MDSCs had increased expression of IL-10 relative to monocytes [60]. In addition, IL-10 expression was increased in implant-associated tissues of *S. aureus* infected mice. IL-10 is an anti-inflammatory cytokine important in regulating immune responses and has been shown to be secreted by MDSCs to polarize macrophages toward an anti-inflammatory phenotype and induce Treg accumulation. IL-10-GFP reporter mice enabled us to demonstrate that Ly6G^{high}Ly6C$^+$ MDSCs are indeed a major source of IL-10 during infection, and the loss of IL-10 enhances monocyte/macrophage recruitment to implant-associated tissues.

Although during *S. aureus* biofilm infection MDSCs do not suppress T cell proliferation via IL-10, which agrees with another recent report using a different model of *S. aureus* infection [149], production of IL-10 does influence the phenotype and effector functions of monocyte/macrophage populations. We observed increased proinflammatory gene expression in Ly6G⁻Ly6C⁺ monocytes in IL-10 KO mice, which paralleled significantly reduced bacterial burdens by day 14 post-infection. Adoptive transfer experiments revealed that the effects of MDSCs on bacterial burdens and leukocyte influx into *S. aureus* biofilm infections are only partially dependent on IL-10. It was not surprising that the effects of MDSCs were not mediated solely through IL-10. There are a number of other factors implicated in MDSC immunosuppressive function, including Arg-1 expression which is currently an area of investigation in our laboratory.

In addition to the function of MDSCs, we were also interested in understanding how host- or bacteria-derived factors influence the recruitment and activation of MDSCs that ultimately permit biofilm establishment and promote chronicity. The accumulation and subsequent activation of MDSCs is thought to occur in a two-step manner. The first process of MDSC expansion being induced by various cytokines and growth factors produced by tumors, cells responding to infectious agents, or chronic stimulation, and the second signal provided by proinflammatory molecules. In our model of *S. aureus* orthopedic biofilm infection, we observed significantly fewer MDSC infiltrates in IL-12p40 and p35 KO tissues compared to WT [59]. However, FACS-purified MDSCs from KO mice retained their ability to suppress CD4⁺ T cell proliferation *in vitro*, indicating that in this model IL-12 is not a proinflammatory signal associated with MDSC activation. Rather, IL-12 appears to regulate MDSC recruitment, and the absence of MDSCs in IL-12-deficient mice results in increased monocyte influx and significantly reduced bacterial burdens in implant-associated tissues. Adoptive transfer of WT MDSCs into IL-12p40 KO animals worsened disease outcome and confirmed a direct role for MDSCs in the inhibition of biofilm clearance and suppression of monocyte/macrophage responses [59]. Importantly, these studies demonstrate that IL-12p70 is important for this organization of the biofilm permissive response. Similar phenotypes were observed in both p40 and p35 KO mice but not in p19 KO animals.

Although our findings do not exactly follow the two-step model for MDSC expansion and activation as proposed by Gabrilovich et al [121], IL-12 appears to play a key role in the recruitment of MDSCs into biofilm infection via a chemoattractant that remains to be identified. It is possible that the induction of a proinflammatory cytokine like IL-12 induces COX-2 production of PGE2 and subsequent generation of MDSCs. Once recruited, MDSCs are activated and produce significant amounts of IL-10 by day 5 post-infection, which plays a critical role in polarizing monocytes/macrophages toward an anti-inflammatory phenotype. It could be argued that IL-10 does not play a critical role because differences were only observed at two weeks post-infection. However, IL-10 could be modulating inflammation in a manner that was not examined in these studies. Ultimately, the loss of either IL-12 or IL-10 during the early MDSC recruitment (days 3-7) or effector phases (days 7-14), respectively, promotes biofilm clearance and implicates a role for each cytokine at distinct stages of infection. Collectively, these findings point to the complexity in the MDSC response to *S. aureus* biofilms, and the identification of other mechanisms contributing to this response is ongoing in our laboratory.

As our understanding of MDSCs and their immunosuppressive mechanisms during *S. aureus* biofilm infection develop, we hope to be able to identify potential therapeutic targets to treat these devastating and chronic infections. Of particular interest, is the manipulation of the innate immune response to promote clearance. Although complex, this approach would bypass the need to identify elusive *S. aureus* epitopes to induce a memory response and eliminate the evolution of more antibiotic resistant strains of bacteria. Previously, the Kielian laboratory demonstrated that upon co-culture with *S. aureus* biofilms *in vitro* macrophages acquired an anti-inflammatory phenotype characterized by increased Arg-1 expression and were readily killed before any clearance could take place [32]. These results were also confirmed *in vivo* using the mouse model of subcutaneous catheter biofilm infection. More recent experiments have shown that M1-activated macrophages stimulated with IFN-γ plus PGN were capable of phagocytizing biofilm-associated organisms resulting in significant reductions in bacterial burdens following 24 h of co-culture [100]. To assess the ability of M1-activated macrophages to attenuate biofilm formation *in vivo*, animals were treated with 10^6 neutrophils, nonactivated macrophages, or M1-

activated macrophages at 12, 24 and 48 h post-infection. The introduction of M1-activated macrophages at the site of biofilm infection significantly reduced bacterial burdens on catheters and in surrounding tissues at day 3 post-infection and perhaps more importantly, led to long-term effectiveness against biofilm formation, as catheters showed minimal evidence of biofilm growth at day 14 without any additional macrophage treatment [100]. This ability of M1-polarized macrophages to impair biofilm development is mediated by MyD88-dependent signals, further emphasizing that the production of proinflammatory cytokines is critical for bacterial clearance at early stages of infection. Addition of neutrophils had no impact on biofilm formation. These experiments indicate that the introduction of *S. aureus* near an implanted device rapidly alters the environment to promote a biofilm-permissive setting, which includes the skewing of macrophage phenotypes that prevent bacterial clearance.

Based on the efficacy of this early treatment paradigm, where animals received treatment at 12, 24 and 48 h post-infection, we wanted to determine whether the introduction of M1-activated macrophages could attenuate growth of established biofilm infections. Macrophages were administered on days 7 and 9 post-infection; however, significant reductions in bacterial burdens were only observed on infected catheters at day 10 post-infection, no effect was seen in surrounding tissues. The addition of M1 macrophages was associated with reductions in Arg-1^{+} macrophages surrounding biofilms and augmented inflammatory cytokine and chemokine expression [100]. This suggests that the transfer of M1-macrophages is able to begin transforming the environment toward one that would promote bacterial clearance, but the biofilm is still a formidable force. We thought that perhaps this limited ability to clear bacteria could be due to exhausted cells following administration into the already established biofilm. However, labeling M1-activated macrophages with Quantum Dots showed that these cells remain localized at the site of biofilm infection 96 h and 4 days after being injected at the time of infection or day 7, respectively [100]. It is likely that the prolonged signal was due to quantum dots within macrophages, as they are relatively stable. However, it is possible that some of the continued signal is due to residual dots in the extracellular milieu following macrophage death.

Collectively, these studies demonstrate that *S. aureus* biofilm infections skew the local milieu to promote immunosuppression which favors bacterial persistence. This is achieved through the induction of MDSCs, which rapidly accumulate at the infection site following inoculation and skew the activation of monocyte/macrophage infiltrates toward an anti-inflammatory phenotype that renders them unable to clear bacteria. Additionally, there is a paucity of T cell infiltrates associated with these biofilm infections, which could be a direct result of MDSC suppressive activity and have severe implications on the success of vaccines currently in development. We have found that manipulation of MDSCs by limiting their recruitment to the site of infection, or alternatively their function once accumulated, does allow for some degree of proinflammatory immune responses and clearance of biofilm-associated bacteria. Although the host immune system-biofilm interaction is multi-faceted and complex, these results demonstrate that targeting the host immune response to biofilm could lead us toward novel therapeutic interventions to treat these chronic infections.

References

1. Otto, M., *Staphylococcal biofilms.* Curr Top Microbiol Immunol, 2008. **322**: p. 207-28.
2. Rasigade, J.P. and F. Vandenesch, *Staphylococcus aureus: a pathogen with still unresolved issues.* Infect Genet Evol, 2014. **21**: p. 510-4.
3. Foster, T.J., *Immune evasion by staphylococci.* Nat Rev Microbiol, 2005. **3**(12): p. 948-58.
4. Boucher, H., L.G. Miller, and R.R. Razonable, *Serious infections caused by methicillin-resistant Staphylococcus aureus.* Clin Infect Dis, 2010. **51 Suppl 2**: p. S183-97.
5. Zecconi, A. and F. Scali, *Staphylococcus aureus virulence factors in evasion from innate immune defenses in human and animal diseases.* Immunol Lett, 2013. **150**(1-2): p. 12-22.
6. Stryjewski, M.E. and G.R. Corey, *Methicillin-resistant Staphylococcus aureus: an evolving pathogen.* Clin Infect Dis, 2014. **58 Suppl 1**: p. S10-9.
7. Shorr, A.F., *Epidemiology of staphylococcal resistance.* Clin Infect Dis, 2007. **45 Suppl 3**: p. S171-6.
8. Drago, L., et al., *In vitro evaluation of antibiotics' combinations for empirical therapy of suspected methicillin resistant Staphylococcus aureus severe respiratory infections.* BMC Infect Dis, 2007. **7**: p. 111.
9. Kennedy, A.D., et al., *Epidemic community-associated methicillin-resistant Staphylococcus aureus: recent clonal expansion and diversification.* Proc Natl Acad Sci U S A, 2008. **105**(4): p. 1327-32.
10. Naimi, T.S., et al., *Comparison of community- and health care-associated methicillin-resistant Staphylococcus aureus infection.* JAMA, 2003. **290**(22): p. 2976-84.
11. Akins, R.L. and M.J. Rybak, *In vitro activities of daptomycin, arbekacin, vancomycin, and gentamicin alone and/or in combination against glycopeptide intermediate-resistant Staphylococcus aureus in an infection model.* Antimicrob Agents Chemother, 2000. **44**(7): p. 1925-9.
12. Gardete, S. and A. Tomasz, *Mechanisms of vancomycin resistance in Staphylococcus aureus.* J Clin Invest, 2014. **124**(7): p. 2836-40.
13. Goyal, N., et al., *Methicillin-resistant Staphylococcus aureus (MRSA): colonisation and pre-operative screening.* Bone Joint J, 2013. **95-B**(1): p. 4-9.
14. Hartman, B. and A. Tomasz, *Altered penicillin-binding proteins in methicillin-resistant strains of Staphylococcus aureus.* Antimicrob Agents Chemother, 1981. **19**(5): p. 726-35.
15. Laarman, A.J., et al., *Staphylococcus aureus metalloprotease aureolysin cleaves complement C3 to mediate immune evasion.* J Immunol, 2011. **186**(11): p. 6445-53.
16. Parry, M.C. and C.P. Duncan, *The challenge of methicillin resistant staphylococcal infection after total hip replacement: overlooked or overstated?* Bone Joint J, 2014. **96-B**(11 Supple A): p. 60-5.
17. Klevens, R.M., et al., *Invasive methicillin-resistant Staphylococcus aureus infections in the United States.* JAMA, 2007. **298**(15): p. 1763-71.
18. Sifri, C.D., et al., *Fatal brain abscess due to community-associated methicillin-resistant Staphylococcus aureus strain USA300.* Clin Infect Dis, 2007. **45**(9): p. e113-7.
19. Iyer, S. and D.H. Jones, *Community-acquired methicillin-resistant Staphylococcus aureus skin infection: a retrospective analysis of clinical presentation and treatment of a local outbreak.* J Am Acad Dermatol, 2004. **50**(6): p. 854-8.
20. Rosario-Rosado, R.V., A.A. Rene, and B. Jones, *Descriptive analysis of patients with community-onset and hospital-onset methicillin-resistant Staphylococcus aureus infections.* Infect Control Hosp Epidemiol, 2004. **25**(2): p. 171-3.

21.   Tenover, F.C., et al., *Characterization of a strain of community-associated methicillin-resistant Staphylococcus aureus widely disseminated in the United States.* J Clin Microbiol, 2006. **44**(1): p. 108-18.

22.   Nimmo, G.R., *USA300 abroad: global spread of a virulent strain of community-associated methicillin-resistant Staphylococcus aureus.* Clin Microbiol Infect, 2012. **18**(8): p. 725-34.

23.   Diep, B.A. and M. Otto, *The role of virulence determinants in community-associated MRSA pathogenesis.* Trends Microbiol, 2008. **16**(8): p. 361-9.

24.   Chambers, H.F. and F.R. Deleo, *Waves of resistance: Staphylococcus aureus in the antibiotic era.* Nat Rev Microbiol, 2009. **7**(9): p. 629-41.

25.   Rooijakkers, S.H., K.P. van Kessel, and J.A. van Strijp, *Staphylococcal innate immune evasion.* Trends Microbiol, 2005. **13**(12): p. 596-601.

26.   Fey, P.D., et al., *A genetic resource for rapid and comprehensive phenotype screening of nonessential Staphylococcus aureus genes.* MBio, 2013. **4**(1): p. e00537-12.

27.   Fitzpatrick, F., H. Humphreys, and J.P. O'Gara, *The genetics of staphylococcal biofilm formation--will a greater understanding of pathogenesis lead to better management of device-related infection?* Clin Microbiol Infect, 2005. **11**(12): p. 967-73.

28.   Prabhakara, R., et al., *Murine immune response to a chronic Staphylococcus aureus biofilm infection.* Infect Immun, 2011. **79**(4): p. 1789-96.

29.   Watkins, R.R., M.Z. David, and R.A. Salata, *Current concepts on the virulence mechanisms of meticillin-resistant Staphylococcus aureus.* J Med Microbiol, 2012. **61**(Pt 9): p. 1179-93.

30.   Lister, J.L. and A.R. Horswill, *Staphylococcus aureus biofilms: recent developments in biofilm dispersal.* Front Cell Infect Microbiol, 2014. **4**: p. 178.

31.   Hanke, M.L. and T. Kielian, *Deciphering mechanisms of staphylococcal biofilm evasion of host immunity.* Front Cell Infect Microbiol, 2012. **2**: p. 62.

32.   Thurlow, L.R., et al., *Staphylococcus aureus biofilms prevent macrophage phagocytosis and attenuate inflammation in vivo.* J Immunol, 2011. **186**(11): p. 6585-96.

33.   Donlan, R.M. and J.W. Costerton, *Biofilms: survival mechanisms of clinically relevant microorganisms.* Clin Microbiol Rev, 2002. **15**(2): p. 167-93.

34.   Otto, M., *Understanding the epidemic of community-associated MRSA and finding a cure: are we asking the right questions?* Expert Rev Anti Infect Ther, 2009. **7**(2): p. 141-3.

35.   McCarthy, H., et al., *Methicillin resistance and the biofilm phenotype in Staphylococcus aureus.* Front Cell Infect Microbiol, 2015. **5**: p. 1.

36.   Zimmerli, W., A. Trampuz, and P.E. Ochsner, *Prosthetic-joint infections.* N Engl J Med, 2004. **351**(16): p. 1645-54.

37.   Periasamy, S., et al., *How Staphylococcus aureus biofilms develop their characteristic structure.* Proc Natl Acad Sci U S A, 2012. **109**(4): p. 1281-6.

38.   Otto, M., *Staphylococcal infections: mechanisms of biofilm maturation and detachment as critical determinants of pathogenicity.* Annu Rev Med, 2013. **64**: p. 175-88.

39.   Rohde, H., et al., *Polysaccharide intercellular adhesin or protein factors in biofilm accumulation of Staphylococcus epidermidis and Staphylococcus aureus isolated from prosthetic hip and knee joint infections.* Biomaterials, 2007. **28**(9): p. 1711-20.

40.   Heilmann, C., et al., *Molecular basis of intercellular adhesion in the biofilm-forming Staphylococcus epidermidis.* Mol Microbiol, 1996. **20**(5): p. 1083-91.

41.   Mack, D., et al., *Association of biofilm production of coagulase-negative staphylococci with expression of a specific polysaccharide intercellular adhesin.* J Infect Dis, 1996. **174**(4): p. 881-4.

42. Rupp, M.E., et al., *Characterization of Staphylococcus epidermidis polysaccharide intercellular adhesin/hemagglutinin in the pathogenesis of intravascular catheter-associated infection in a rat model.* Infect Immun, 1999. **67**(5): p. 2656-9.

43. Rupp, M.E., et al., *Characterization of the importance of polysaccharide intercellular adhesin/hemagglutinin of Staphylococcus epidermidis in the pathogenesis of biomaterial-based infection in a mouse foreign body infection model.* Infect Immun, 1999. **67**(5): p. 2627-32.

44. Kogan, G., et al., *Biofilms of clinical strains of Staphylococcus that do not contain polysaccharide intercellular adhesin.* FEMS Microbiol Lett, 2006. **255**(1): p. 11-6.

45. Schaeffer, C.R., et al., *Accumulation-associated protein enhances Staphylococcus epidermidis biofilm formation under dynamic conditions and is required for infection in a rat catheter model.* Infect Immun, 2015. **83**(1): p. 214-26.

46. Gross, M., et al., *Key role of teichoic acid net charge in Staphylococcus aureus colonization of artificial surfaces.* Infect Immun, 2001. **69**(5): p. 3423-6.

47. Whitchurch, C.B., et al., *Extracellular DNA required for bacterial biofilm formation.* Science, 2002. **295**(5559): p. 1487.

48. Yarwood, J.M. and P.M. Schlievert, *Quorum sensing in Staphylococcus infections.* J Clin Invest, 2003. **112**(11): p. 1620-5.

49. Del Pozo, J.L. and R. Patel, *Clinical practice. Infection associated with prosthetic joints.* N Engl J Med, 2009. **361**(8): p. 787-94.

50. Davies, D.M., et al., *Effect of adjunctive range-of-motion therapy after primary total knee arthroplasty on the use of health services after hospital discharge.* Can J Surg, 2003. **46**(1): p. 30-6.

51. Weber, D.J. and W.A. Rutala, *Central line-associated bloodstream infections: prevention and management.* Infect Dis Clin North Am, 2011. **25**(1): p. 77-102.

52. Corvec, S., et al., *Epidemiology and new developments in the diagnosis of prosthetic joint infection.* Int J Artif Organs, 2012. **35**(10): p. 923-34.

53. Yousif, A., M.A. Jamal, and I. Raad, *Biofilm-based central line-associated bloodstream infections.* Adv Exp Med Biol, 2015. **830**: p. 157-79.

54. Gutierrez-Murgas, Y. and J.N. Snowden, *Ventricular shunt infections: immunopathogenesis and clinical management.* J Neuroimmunol, 2014. **276**(1-2): p. 1-8.

55. Snowden, J.N., et al., *Staphylococcus aureus sarA regulates inflammation and colonization during central nervous system biofilm formation.* PLoS One, 2013. **8**(12): p. e84089.

56. Snowden, J.N., et al., *Biofilm-infected intracerebroventricular shunts elicit inflammation within the central nervous system.* Infect Immun, 2012. **80**(9): p. 3206-14.

57. Dimick, J.B., et al., *Increased resource use associated with catheter-related bloodstream infection in the surgical intensive care unit.* Arch Surg, 2001. **136**(2): p. 229-34.

58. Lorenz, U., et al., *Functional antibodies targeting IsaA of Staphylococcus aureus augment host immune response and open new perspectives for antibacterial therapy.* Antimicrob Agents Chemother, 2011. **55**(1): p. 165-73.

59. Heim, C.E., et al., *IL-12 Promotes Myeloid-Derived Suppressor Cell Recruitment and Bacterial Persistence during Staphylococcus aureus Orthopedic Implant Infection.* J Immunol, 2015. **194**(8): p. 3861-72.

60. Heim, C.E., et al., *Myeloid-derived suppressor cells contribute to Staphylococcus aureus orthopedic biofilm infection.* J Immunol, 2014. **192**(8): p. 3778-92.

61. Scherr, T.D., et al., *Hiding in Plain Sight: Interplay between Staphylococcal Biofilms and Host Immunity.* Front Immunol, 2014. **5**: p. 37.

62.   Bernthal, N.M., et al., *Protective role of IL-1beta against post-arthroplasty Staphylococcus aureus infection.* J Orthop Res, 2011. **29**(10): p. 1621-6.

63.   Ribeiro, M., F.J. Monteiro, and M.P. Ferraz, *Infection of orthopedic implants with emphasis on bacterial adhesion process and techniques used in studying bacterial-material interactions.* Biomatter, 2012. **2**(4): p. 176-94.

64.   Kawai, T. and S. Akira, *Toll-like receptors and their crosstalk with other innate receptors in infection and immunity.* Immunity, 2011. **34**(5): p. 637-50.

65.   Kopp, E. and R. Medzhitov, *Recognition of microbial infection by Toll-like receptors.* Curr Opin Immunol, 2003. **15**(4): p. 396-401.

66.   Kielian, T., *Toll-like receptors in central nervous system glial inflammation and homeostasis.* J Neurosci Res, 2006. **83**(5): p. 711-30.

67.   Konat, G.W., T. Kielian, and I. Marriott, *The role of Toll-like receptors in CNS response to microbial challenge.* J Neurochem, 2006. **99**(1): p. 1-12.

68.   Esen, N. and T. Kielian, *Toll-like receptors in brain abscess.* Curr Top Microbiol Immunol, 2009. **336**: p. 41-61.

69.   Kielian, T., *Overview of toll-like receptors in the CNS.* Curr Top Microbiol Immunol, 2009. **336**: p. 1-14.

70.   Fournier, B. and D.J. Philpott, *Recognition of Staphylococcus aureus by the innate immune system.* Clin Microbiol Rev, 2005. **18**(3): p. 521-40.

71.   Yoshimura, A., et al., *Cutting edge: recognition of Gram-positive bacterial cell wall components by the innate immune system occurs via Toll-like receptor 2.* J Immunol, 1999. **163**(1): p. 1-5.

72.   Takeuchi, O., K. Hoshino, and S. Akira, *Cutting edge: TLR2-deficient and MyD88-deficient mice are highly susceptible to Staphylococcus aureus infection.* J Immunol, 2000. **165**(10): p. 5392-6.

73.   Mullaly, S.C. and P. Kubes, *The role of TLR2 in vivo following challenge with Staphylococcus aureus and prototypic ligands.* J Immunol, 2006. **177**(11): p. 8154-63.

74.   Stevens, D.L., *Treatments for skin and soft-tissue and surgical site infections due to MDR Gram-positive bacteria.* J Infect, 2009. **59 Suppl 1**: p. S32-9.

75.   Strunk, T., et al., *TLR2 mediates recognition of live Staphylococcus epidermidis and clearance of bacteremia.* PLoS One, 2010. **5**(4): p. e10111.

76.   Flemming, H.C. and J. Wingender, *The biofilm matrix.* Nat Rev Microbiol, 2010. **8**(9): p. 623-33.

77.   Bardoel, B.W., et al., *Evasion of Toll-like receptor 2 activation by staphylococcal superantigen-like protein 3.* J Mol Med (Berl), 2012. **90**(10): p. 1109-20.

78.   Vilaysane, A. and D.A. Muruve, *The innate immune response to DNA.* Semin Immunol, 2009. **21**(4): p. 208-14.

79.   Hornung, V. and E. Latz, *Intracellular DNA recognition.* Nat Rev Immunol, 2010. **10**(2): p. 123-30.

80.   Girardin, S.E., et al., *Nod2 is a general sensor of peptidoglycan through muramyl dipeptide (MDP) detection.* J Biol Chem, 2003. **278**(11): p. 8869-72.

81.   Volz, T., et al., *Natural Staphylococcus aureus-derived peptidoglycan fragments activate NOD2 and act as potent costimulators of the innate immune system exclusively in the presence of TLR signals.* FASEB J, 2010. **24**(10): p. 4089-102.

82.   Sethi, S. and T. Chakraborty, *Role of TLR- / NLR-signaling and the associated cytokines involved in recruitment of neutrophils in murine models of Staphylococcus aureus infection.* Virulence, 2011. **2**(4): p. 316-28.

83. Rigby, K.M. and F.R. DeLeo, *Neutrophils in innate host defense against Staphylococcus aureus infections.* Semin Immunopathol, 2012. **34**(2): p. 237-59.

84. Greenlee-Wacker, M.C., et al., *Phagocytosis of Staphylococcus aureus by human neutrophils prevents macrophage efferocytosis and induces programmed necrosis.* J Immunol, 2014. **192**(10): p. 4709-17.

85. Standiford, T.J., et al., *Lipoteichoic acid induces secretion of interleukin-8 from human blood monocytes: a cellular and molecular analysis.* Infect Immun, 1994. **62**(1): p. 119-25.

86. Krakauer, T., *Interleukin-8 production by human monocytic cells in response to staphylococcal exotoxins is direct and independent of interleukin-1 and tumor necrosis factor-alpha.* J Infect Dis, 1998. **178**(2): p. 573-7.

87. Schmeling, D.J., et al., *Chemotaxigenesis by cell surface components of Staphylococcus aureus.* Infect Immun, 1979. **26**(1): p. 57-63.

88. Cassatella, M.A., *The production of cytokines by polymorphonuclear neutrophils.* Immunol Today, 1995. **16**(1): p. 21-6.

89. Witko-Sarsat, V., et al., *Neutrophils: molecules, functions and pathophysiological aspects.* Lab Invest, 2000. **80**(5): p. 617-53.

90. Faurschou, M. and N. Borregaard, *Neutrophil granules and secretory vesicles in inflammation.* Microbes Infect, 2003. **5**(14): p. 1317-27.

91. Gamberale, R., et al., *Modulation of human neutrophil apoptosis by immune complexes.* J Immunol, 1998. **161**(7): p. 3666-74.

92. Wilke, G.A. and J. Bubeck Wardenburg, *Role of a disintegrin and metalloprotease 10 in Staphylococcus aureus alpha-hemolysin-mediated cellular injury.* Proc Natl Acad Sci U S A, 2010. **107**(30): p. 13473-8.

93. Nizet, V., *Understanding how leading bacterial pathogens subvert innate immunity to reveal novel therapeutic targets.* J Allergy Clin Immunol, 2007. **120**(1): p. 13-22.

94. Haggar, A., et al., *The extracellular adherence protein from Staphylococcus aureus inhibits neutrophil binding to endothelial cells.* Infect Immun, 2004. **72**(10): p. 6164-7.

95. Kobayashi, S.D., et al., *Rapid neutrophil destruction following phagocytosis of Staphylococcus aureus.* J Innate Immun, 2010. **2**(6): p. 560-75.

96. Graham, D.B., et al., *Neutrophil-mediated oxidative burst and host defense are controlled by a Vav-PLCgamma2 signaling axis in mice.* J Clin Invest, 2007. **117**(11): p. 3445-52.

97. Voyich, J.M., et al., *Insights into mechanisms used by Staphylococcus aureus to avoid destruction by human neutrophils.* J Immunol, 2005. **175**(6): p. 3907-19.

98. Leid, J.G., et al., *Human leukocytes adhere to, penetrate, and respond to Staphylococcus aureus biofilms.* Infect Immun, 2002. **70**(11): p. 6339-45.

99. Gunther, F., et al., *Host defence against Staphylococcus aureus biofilms infection: phagocytosis of biofilms by polymorphonuclear neutrophils (PMN).* Mol Immunol, 2009. **46**(8-9): p. 1805-13.

100. Hanke, M.L., et al., *Targeting macrophage activation for the prevention and treatment of Staphylococcus aureus biofilm infections.* J Immunol, 2013. **190**(5): p. 2159-68.

101. Labonte, A.C., A.C. Tosello-Trampont, and Y.S. Hahn, *The role of macrophage polarization in infectious and inflammatory diseases.* Mol Cells, 2014. **37**(4): p. 275-85.

102. Jantsch, J., et al., *Macrophages in homeostatic immune function.* Front Physiol, 2014. **5**: p. 146.

103. Duque, C., et al., *Different responses of human mononuclear phagocyte populations to Mycobacterium tuberculosis.* Tuberculosis (Edinb), 2014. **94**(2): p. 111-22.

104. Silva, M.F., et al., *Phenotypic and functional characterization of pulmonary macrophages subpopulations after intratracheal injection of Paracoccidioides brasiliensis cell wall components.* Immunobiology, 2011. **216**(7): p. 821-31.

105. Silva, M.T., *Neutrophils and macrophages work in concert as inducers and effectors of adaptive immunity against extracellular and intracellular microbial pathogens.* J Leukoc Biol, 2010. **87**(5): p. 805-13.

106. Serbina, N.V., et al., *Monocyte-mediated defense against microbial pathogens.* Annu Rev Immunol, 2008. **26**: p. 421-52.

107. Gonzalez-Mejia, M.E. and A.I. Doseff, *Regulation of monocytes and macrophages cell fate.* Front Biosci (Landmark Ed), 2009. **14**: p. 2413-31.

108. Verreck, F.A., et al., *Human IL-23-producing type 1 macrophages promote but IL-10-producing type 2 macrophages subvert immunity to (myco)bacteria.* Proc Natl Acad Sci U S A, 2004. **101**(13): p. 4560-5.

109. Benoit, M., B. Desnues, and J.L. Mege, *Macrophage polarization in bacterial infections.* J Immunol, 2008. **181**(6): p. 3733-9.

110. Shaughnessy, L.M. and J.A. Swanson, *The role of the activated macrophage in clearing Listeria monocytogenes infection.* Front Biosci, 2007. **12**: p. 2683-92.

111. Arango Duque, G. and A. Descoteaux, *Macrophage cytokines: involvement in immunity and infectious diseases.* Front Immunol, 2014. **5**: p. 491.

112. Guenther, F., et al., *Phagocytosis of staphylococci biofilms by polymorphonuclear neutrophils: S. aureus and S. epidermidis differ with regard to their susceptibility towards the host defense.* Int J Artif Organs, 2009. **32**(9): p. 565-73.

113. Hamza, T. and B. Li, *Differential responses of osteoblasts and macrophages upon Staphylococcus aureus infection.* BMC Microbiol, 2014. **14**: p. 207.

114. Schommer, N.N., et al., *Staphylococcus epidermidis uses distinct mechanisms of biofilm formation to interfere with phagocytosis and activation of mouse macrophage-like cells 774A.1.* Infect Immun, 2011. **79**(6): p. 2267-76.

115. Curran, J.N., D.C. Winter, and D. Bouchier-Hayes, *Biological fate and clinical implications of arginine metabolism in tissue healing.* Wound Repair Regen, 2006. **14**(4): p. 376-86.

116. Wynn, T.A., *Cellular and molecular mechanisms of fibrosis.* J Pathol, 2008. **214**(2): p. 199-210.

117. Hanke, M.L., A. Angle, and T. Kielian, *MyD88-dependent signaling influences fibrosis and alternative macrophage activation during Staphylococcus aureus biofilm infection.* PLoS One, 2012. **7**(8): p. e42476.

118. Cheatle, J., et al., *Compartmentalization of immune responses during Staphylococcus aureus cranial bone flap infection.* Am J Pathol, 2013. **183**(2): p. 450-8.

119. Haile, L.A., T.F. Greten, and F. Korangy, *Immune suppression: the hallmark of myeloid derived suppressor cells.* Immunol Invest, 2012. **41**(6-7): p. 581-94.

120. Serafini, P., I. Borrello, and V. Bronte, *Myeloid suppressor cells in cancer: recruitment, phenotype, properties, and mechanisms of immune suppression.* Semin Cancer Biol, 2006. **16**(1): p. 53-65.

121. Condamine, T. and D.I. Gabrilovich, *Molecular mechanisms regulating myeloid-derived suppressor cell differentiation and function.* Trends Immunol, 2011. **32**(1): p. 19-25.

122. Zhang, C., et al., *Accumulation of myeloid-derived suppressor cells in the lungs during Pneumocystis pneumonia.* Infect Immun, 2012. **80**(10): p. 3634-41.

123. Delano, M.J., et al., *MyD88-dependent expansion of an immature GR-1(+)CD11b(+) population induces T cell suppression and Th2 polarization in sepsis.* J Exp Med, 2007. **204**(6): p. 1463-74.

124. Nagaraj, S. and D.I. Gabrilovich, *Regulation of suppressive function of myeloid-derived suppressor cells by CD4+ T cells.* Semin Cancer Biol, 2012. **22**(4): p. 282-8.

125. Gabrilovich, D.I., et al., *The terminology issue for myeloid-derived suppressor cells.* Cancer Res, 2007. **67**(1): p. 425; author reply 426.

126. Ribechini, E., et al., *Subsets, expansion and activation of myeloid-derived suppressor cells.* Med Microbiol Immunol, 2010. **199**(3): p. 273-81.

127. Gabrilovich, D.I., *Molecular mechanisms and therapeutic reversal of immune suppression in cancer.* Curr Cancer Drug Targets, 2007. **7**(1): p. 1.

128. Lappat, E.J. and M. Cawein, *A Study of the Leukemoid Response to Transplantable a-280 Tumor in Mice.* Cancer Res, 1964. **24**: p. 302-11.

129. Talmadge, J.E. and D.I. Gabrilovich, *History of myeloid-derived suppressor cells.* Nat Rev Cancer, 2013. **13**(10): p. 739-52.

130. Dai, J., et al., *Myeloid-derived suppressor cells: paradoxical roles in infection and immunity.* J Innate Immun, 2015. **7**(2): p. 116-26.

131. Lai, D., C. Qin, and Q. Shu, *Myeloid-derived suppressor cells in sepsis.* Biomed Res Int, 2014. **2014**: p. 598654.

132. Kusmartsev, S.A., Y. Li, and S.H. Chen, *Gr-1+ myeloid cells derived from tumor-bearing mice inhibit primary T cell activation induced through CD3/CD28 costimulation.* J Immunol, 2000. **165**(2): p. 779-85.

133. Gabrilovich, D., et al., *Vascular endothelial growth factor inhibits the development of dendritic cells and dramatically affects the differentiation of multiple hematopoietic lineages in vivo.* Blood, 1998. **92**(11): p. 4150-66.

134. Watson, G.A., Y.X. Fu, and D.M. Lopez, *Splenic macrophages from tumor-bearing mice co-expressing MAC-1 and MAC-2 antigens exert immunoregulatory functions via two distinct mechanisms.* J Leukoc Biol, 1991. **49**(2): p. 126-38.

135. Sica, A. and V. Bronte, *Altered macrophage differentiation and immune dysfunction in tumor development.* J Clin Invest, 2007. **117**(5): p. 1155-66.

136. Peranzoni, E., et al., *Myeloid-derived suppressor cell heterogeneity and subset definition.* Curr Opin Immunol, 2010. **22**(2): p. 238-44.

137. Gabrilovich, D.I. and S. Nagaraj, *Myeloid-derived suppressor cells as regulators of the immune system.* Nat Rev Immunol, 2009. **9**(3): p. 162-74.

138. Pak, A.S., et al., *Mechanisms of immune suppression in patients with head and neck cancer: presence of CD34(+) cells which suppress immune functions within cancers that secrete granulocyte-macrophage colony-stimulating factor.* Clin Cancer Res, 1995. **1**(1): p. 95-103.

139. Talmadge, J.E., et al., *Immunologic attributes of cytokine mobilized peripheral blood stem cells and recovery following transplantation.* Bone Marrow Transplant, 1996. **17**(1): p. 101-9.

140. Lathers, D.M., et al., *Phase IB study of 25-hydroxyvitamin D(3) treatment to diminish suppressor cells in head and neck cancer patients.* Hum Immunol, 2001. **62**(11): p. 1282-93.

141. Bronte, V. and P. Zanovello, *Regulation of immune responses by L-arginine metabolism.* Nat Rev Immunol, 2005. **5**(8): p. 641-54.

142. Bronte, V., et al., *L-arginine metabolism in myeloid cells controls T-lymphocyte functions.* Trends Immunol, 2003. **24**(6): p. 302-6.

143. Corzo, C.A., et al., *Mechanism regulating reactive oxygen species in tumor-induced myeloid-derived suppressor cells.* J Immunol, 2009. **182**(9): p. 5693-701.

144. Terabe, M., et al., *Transforming growth factor-beta production and myeloid cells are an effector mechanism through which CD1d-restricted T cells block cytotoxic T lymphocyte-mediated tumor immunosurveillance: abrogation prevents tumor recurrence.* J Exp Med, 2003. **198**(11): p. 1741-52.

145. Sinha, P., et al., *Myeloid-derived suppressor cells express the death receptor Fas and apoptose in response to T cell-expressed FasL.* Blood, 2011. **117**(20): p. 5381-90.

146. Nagaraj, S. and D.I. Gabrilovich, *Myeloid-derived suppressor cells.* Adv Exp Med Biol, 2007. **601**: p. 213-23.

147. Hoechst, B., et al., *Plasticity of human Th17 cells and iTregs is orchestrated by different subsets of myeloid cells.* Blood, 2011. **117**(24): p. 6532-41.

148. Sinha, P., et al., *Cross-talk between myeloid-derived suppressor cells and macrophages subverts tumor immunity toward a type 2 response.* J Immunol, 2007. **179**(2): p. 977-83.

149. Tebartz, C., et al., *A major role for myeloid-derived suppressor cells and a minor role for regulatory T cells in immunosuppression during Staphylococcus aureus infection.* J Immunol, 2015. **194**(3): p. 1100-11.

150. Brudecki, L., et al., *Myeloid-derived suppressor cells evolve during sepsis and can enhance or attenuate the systemic inflammatory response.* Infect Immun, 2012. **80**(6): p. 2026-34.

151. Kuhn, R., et al., *Interleukin-10-deficient mice develop chronic enterocolitis.* Cell, 1993. **75**(2): p. 263-74.

152. Fremond, C.M., et al., *Fatal Mycobacterium tuberculosis infection despite adaptive immune response in the absence of MyD88.* J Clin Invest, 2004. **114**(12): p. 1790-9.

153. Kawai, T., et al., *Unresponsiveness of MyD88-deficient mice to endotoxin.* Immunity, 1999. **11**(1): p. 115-22.

154. Adachi, O., et al., *Targeted disruption of the MyD88 gene results in loss of IL-1- and IL-18-mediated function.* Immunity, 1998. **9**(1): p. 143-50.

155. Ochoa, A.C., et al., *Arginase, prostaglandins, and myeloid-derived suppressor cells in renal cell carcinoma.* Clin Cancer Res, 2007. **13**(2 Pt 2): p. 721s-726s.

156. Sander, L.E., et al., *Hepatic acute-phase proteins control innate immune responses during infection by promoting myeloid-derived suppressor cell function.* J Exp Med, 2010. **207**(7): p. 1453-64.

157. Obregon-Henao, A., et al., *Gr1(int)CD11b+ myeloid-derived suppressor cells in Mycobacterium tuberculosis infection.* PLoS One, 2013. **8**(11): p. e80669.

158. Poe, S.L., et al., *STAT1-regulated lung MDSC-like cells produce IL-10 and efferocytose apoptotic neutrophils with relevance in resolution of bacterial pneumonia.* Mucosal Immunol, 2013. **6**(1): p. 189-99.

159. Rieber, N., et al., *Neutrophilic myeloid-derived suppressor cells in cord blood modulate innate and adaptive immune responses.* Clin Exp Immunol, 2013. **174**(1): p. 45-52.

160. Wenzel, R.P., *Health care-associated infections: major issues in the early years of the 21st century.* Clin Infect Dis, 2007. **45 Suppl 1**: p. S85-8.

161. Cuenca, A.G., et al., *A paradoxical role for myeloid-derived suppressor cells in sepsis and trauma.* Mol Med, 2011. **17**(3-4): p. 281-92.

162. Bernthal, N.M., et al., *A mouse model of post-arthroplasty Staphylococcus aureus joint infection to evaluate in vivo the efficacy of antimicrobial implant coatings.* PLoS One, 2010. **5**(9): p. e12580.

163. Ostrand-Rosenberg, S. and P. Sinha, *Myeloid-derived suppressor cells: linking inflammation and cancer.* J Immunol, 2009. **182**(8): p. 4499-506.

164. Haverkamp, J.M., et al., *In vivo suppressive function of myeloid-derived suppressor cells is limited to the inflammatory site.* Eur J Immunol, 2011. **41**(3): p. 749-59.

165. Maenhout, S.K., et al., *Enhanced suppressive capacity of tumor-infiltrating myeloid-derived suppressor cells compared with their peripheral counterparts.* Int J Cancer, 2014. **134**(5): p. 1077-90.

166. Lee, P.Y., et al., *Ly6 family proteins in neutrophil biology.* J Leukoc Biol, 2013. **94**(4): p. 585-94.

167. Prabhakara, R., et al., *Suppression of the inflammatory immune response prevents the development of chronic biofilm infection due to methicillin-resistant Staphylococcus aureus.* Infect Immun, 2011. **79**(12): p. 5010-8.

168. Niska, J.A., et al., *Monitoring bacterial burden, inflammation and bone damage longitudinally using optical and muCT imaging in an orthopaedic implant infection in mice.* PLoS One, 2012. **7**(10): p. e47397.

169. Archer, N.K., J.M. Harro, and M.E. Shirtliff, *Clearance of Staphylococcus aureus nasal carriage is T cell dependent and mediated through interleukin-17A expression and neutrophil influx.* Infect Immun, 2013. **81**(6): p. 2070-5.

170. Pillay, J., et al., *Immune suppression by neutrophils and granulocytic myeloid-derived suppressor cells: similarities and differences.* Cell Mol Life Sci, 2013. **70**(20): p. 3813-27.

171. Saiwai, H., et al., *Ly6C+ Ly6G- Myeloid-derived suppressor cells play a critical role in the resolution of acute inflammation and the subsequent tissue repair process after spinal cord injury.* J Neurochem, 2013. **125**(1): p. 74-88.

172. Rodriguez, P.C., et al., *Arginase I in myeloid suppressor cells is induced by COX-2 in lung carcinoma.* J Exp Med, 2005. **202**(7): p. 931-9.

173. Xiang, X., et al., *Induction of myeloid-derived suppressor cells by tumor exosomes.* Int J Cancer, 2009. **124**(11): p. 2621-33.

174. Eruslanov, E., et al., *Pivotal Advance: Tumor-mediated induction of myeloid-derived suppressor cells and M2-polarized macrophages by altering intracellular PGE(2) catabolism in myeloid cells.* J Leukoc Biol, 2010. **88**(5): p. 839-48.

175. Wojtasiak, M., et al., *Depletion of Gr-1+, but not Ly6G+, immune cells exacerbates virus replication and disease in an intranasal model of herpes simplex virus type 1 infection.* J Gen Virol, 2010. **91**(Pt 9): p. 2158-66.

176. Carr, K.D., et al., *Specific depletion reveals a novel role for neutrophil-mediated protection in the liver during Listeria monocytogenes infection.* Eur J Immunol, 2011. **41**(9): p. 2666-76.

177. Ribes, S., et al., *Resistance of the brain to Escherichia coli K1 infection depends on MyD88 signaling and the contribution of neutrophils and monocytes.* Infect Immun, 2013. **81**(5): p. 1810-9.

178. Serbina, N.V. and E.G. Pamer, *Monocyte emigration from bone marrow during bacterial infection requires signals mediated by chemokine receptor CCR2.* Nat Immunol, 2006. **7**(3): p. 311-7.

179. Gordon, S. and P.R. Taylor, *Monocyte and macrophage heterogeneity.* Nat Rev Immunol, 2005. **5**(12): p. 953-64.

180. Austyn, J.M. and S. Gordon, *F4/80, a monoclonal antibody directed specifically against the mouse macrophage.* Eur J Immunol, 1981. **11**(10): p. 805-15.

181. Chandra, D., et al., *Myeloid-derived suppressor cells have a central role in attenuated Listeria monocytogenes-based immunotherapy against metastatic breast cancer in young and old mice.* Br J Cancer, 2013. **108**(11): p. 2281-90.

182. Zhu, X., et al., *The central role of arginine catabolism in T-cell dysfunction and increased susceptibility to infection after physical injury.* Ann Surg, 2014. **259**(1): p. 171-8.

183. Rodriguez, P.C., D.G. Quiceno, and A.C. Ochoa, *L-arginine availability regulates T-lymphocyte cell-cycle progression.* Blood, 2007. **109**(4): p. 1568-73.

184. Rodriguez, P.C., et al., *L-arginine consumption by macrophages modulates the expression of CD3 zeta chain in T lymphocytes.* J Immunol, 2003. **171**(3): p. 1232-9.

185. Josefowicz, S.Z., L.F. Lu, and A.Y. Rudensky, *Regulatory T cells: mechanisms of differentiation and function.* Annu Rev Immunol, 2012. **30**: p. 531-64.

186. Palazzolo-Ballance, A.M., et al., *Neutrophil microbicides induce a pathogen survival response in community-associated methicillin-resistant Staphylococcus aureus.* J Immunol, 2008. **180**(1): p. 500-9.

187. Cho, J.S., et al., *Neutrophil-derived IL-1beta is sufficient for abscess formation in immunity against Staphylococcus aureus in mice.* PLoS Pathog, 2012. **8**(11): p. e1003047.

188. Gabrilovich, D.I., et al., *Mechanism of immune dysfunction in cancer mediated by immature Gr-1+ myeloid cells.* J Immunol, 2001. **166**(9): p. 5398-406.

189. Kusmartsev, S. and D.I. Gabrilovich, *Inhibition of myeloid cell differentiation in cancer: the role of reactive oxygen species.* J Leukoc Biol, 2003. **74**(2): p. 186-96.

190. Ollivere, B., et al., *Current concepts in osteolysis.* J Bone Joint Surg Br, 2012. **94**(1): p. 10-5.

191. Abu-Amer, Y., *Inflammation, cancer, and bone loss.* Curr Opin Pharmacol, 2009. **9**(4): p. 427-33.

192. Purdue, P.E., et al., *The cellular and molecular biology of periprosthetic osteolysis.* Clin Orthop Relat Res, 2007. **454**: p. 251-61.

193. Burton, L., et al., *Orthopedic wear debris mediated inflammatory osteolysis is mediated in part by NALP3 inflammasome activation.* J Orthop Res, 2013. **31**(1): p. 73-80.

194. Epstein, N.J., et al., *Interleukin-1 modulates periprosthetic tissue formation in an intramedullary model of particle-induced inflammation.* J Orthop Res, 2005. **23**(3): p. 501-10.

195. Shi, S. and X. Zhang, *Interaction of Staphylococcus aureus with osteoblasts (Review).* Exp Ther Med, 2012. **3**(3): p. 367-370.

196. Cassat, J.E., et al., *A secreted bacterial protease tailors the Staphylococcus aureus virulence repertoire to modulate bone remodeling during osteomyelitis.* Cell Host Microbe, 2013. **13**(6): p. 759-72.

197. Kristian, S.A., et al., *Biofilm formation induces C3a release and protects Staphylococcus epidermidis from IgG and complement deposition and from neutrophil-dependent killing.* J Infect Dis, 2008. **197**(7): p. 1028-35.

198. Cerca, F., et al., *Staphylococcus epidermidis biofilms with higher proportions of dormant bacteria induce a lower activation of murine macrophages.* J Med Microbiol, 2011. **60**(Pt 12): p. 1717-24.

199. Spiliopoulou, A.I., et al., *Bacterial adhesion, intracellular survival and cytokine induction upon stimulation of mononuclear cells with planktonic or biofilm phase Staphylococcus epidermidis.* FEMS Microbiol Lett, 2012. **330**(1): p. 56-65.

200. Graves, S.F., S.D. Kobayashi, and F.R. DeLeo, *Community-associated methicillin-resistant Staphylococcus aureus immune evasion and virulence.* J Mol Med (Berl), 2010. **88**(2): p. 109-14.

201. Kurtz, S.M., et al., *Infection burden for hip and knee arthroplasty in the United States.* J Arthroplasty, 2008. **23**(7): p. 984-91.

202. Rao, N., et al., *A preoperative decolonization protocol for staphylococcus aureus prevents orthopaedic infections.* Clin Orthop Relat Res, 2008. **466**(6): p. 1343-8.

203. Kim, D.H., et al., *Institutional prescreening for detection and eradication of methicillin-resistant Staphylococcus aureus in patients undergoing elective orthopaedic surgery.* J Bone Joint Surg Am, 2010. **92**(9): p. 1820-6.

204. Lew, D.P. and F.A. Waldvogel, *Osteomyelitis.* Lancet, 2004. **364**(9431): p. 369-79.

205. Fitzgerald, R.H., Jr., *Experimental osteomyelitis: description of a canine model and the role of depot administration of antibiotics in the prevention and treatment of sepsis.* J Bone Joint Surg Am, 1983. **65**(3): p. 371-80.

206. Salgado, C.D., et al., *Higher risk of failure of methicillin-resistant Staphylococcus aureus prosthetic joint infections.* Clin Orthop Relat Res, 2007. **461**: p. 48-53.

207. Walls, R.J., et al., *Surgical site infection with methicillin-resistant Staphylococcus aureus after primary total hip replacement.* J Bone Joint Surg Br, 2008. **90**(3): p. 292-8.

208. Schwarzkopf, R., et al., *Treatment Failure Among Infected Periprosthetic Patients at a Highly Specialized Revision TKA Referral Practice.* Open Orthop J, 2013. **7**: p. 264-71.

209. Garcia-Alvarez, F., et al., *Effect of age on cytokine response in an experimental model of osteomyelitis.* Biogerontology, 2009. **10**(5): p. 649-58.

210. Yoshii, T., et al., *Local levels of interleukin-1beta, -4, -6 and tumor necrosis factor alpha in an experimental model of murine osteomyelitis due to staphylococcus aureus.* Cytokine, 2002. **19**(2): p. 59-65.

211. Claro, T., et al., *Staphylococcus aureus protein A binding to osteoblast tumour necrosis factor receptor 1 results in activation of nuclear factor kappa B and release of interleukin-6 in bone infection.* Microbiology, 2013. **159**(Pt 1): p. 147-54.

212. Horst, S.A., et al., *A novel mouse model of Staphylococcus aureus chronic osteomyelitis that closely mimics the human infection: an integrated view of disease pathogenesis.* Am J Pathol, 2012. **181**(4): p. 1206-14.

213. Goriely, S. and M. Goldman, *Interleukin-12 family members and the balance between rejection and tolerance.* Curr Opin Organ Transplant, 2008. **13**(1): p. 4-9.

214. Trinchieri, G., S. Pflanz, and R.A. Kastelein, *The IL-12 family of heterodimeric cytokines: new players in the regulation of T cell responses.* Immunity, 2003. **19**(5): p. 641-4.

215. Cooper, A.M. and S.A. Khader, *IL-12p40: an inherently agonistic cytokine.* Trends Immunol, 2007. **28**(1): p. 33-8.

216. Gillessen, S., et al., *Mouse interleukin-12 (IL-12) p40 homodimer: a potent IL-12 antagonist.* Eur J Immunol, 1995. **25**(1): p. 200-6.

217. Wang, X., et al., *Characterization of mouse interleukin-12 p40 homodimer binding to the interleukin-12 receptor subunits.* Eur J Immunol, 1999. **29**(6): p. 2007-13.

218. Kilgus, D.J., D.J. Howe, and A. Strang, *Results of periprosthetic hip and knee infections caused by resistant bacteria.* Clin Orthop Relat Res, 2002(404): p. 116-24.

219. Volin, S.J., S.H. Hinrichs, and K.L. Garvin, *Two-stage reimplantation of total joint infections: a comparison of resistant and non-resistant organisms.* Clin Orthop Relat Res, 2004(427): p. 94-100.

220. Diwanji, S.R., et al., *Two-stage reconstruction of infected hip joints.* J Arthroplasty, 2008. **23**(5): p. 656-61.

221. Sherman, S.L., et al., *Custom total femur spacer and second-stage total femur arthroplasty as a novel approach to infection and periprosthetic fracture.* J Arthroplasty, 2008. **23**(5): p. 781-6.

222. Greten, T.F., M.P. Manns, and F. Korangy, *Myeloid derived suppressor cells in human diseases.* Int Immunopharmacol, 2011. **11**(7): p. 802-7.

223. Gately, M.K., et al., *The interleukin-12/interleukin-12-receptor system: role in normal and pathologic immune responses.* Annu Rev Immunol, 1998. **16**: p. 495-521.

224. O'Garra, A., et al., *The role of macrophage- and dendritic cell-derived IL12 in Th1 phenotype development.* Res Immunol, 1995. **146**(7-8): p. 466-72.

225. Hsieh, C.S., et al., *Development of TH1 CD4+ T cells through IL-12 produced by Listeria-induced macrophages.* Science, 1993. **260**(5107): p. 547-9.

226. Gabrilovich, D.I., S. Ostrand-Rosenberg, and V. Bronte, *Coordinated regulation of myeloid cells by tumours.* Nat Rev Immunol, 2012. **12**(4): p. 253-68.

227. Vignali, D.A. and V.K. Kuchroo, *IL-12 family cytokines: immunological playmakers.* Nat Immunol, 2012. **13**(8): p. 722-8.

228. Pulido, L., et al., *Periprosthetic joint infection: the incidence, timing, and predisposing factors.* Clin Orthop Relat Res, 2008. **466**(7): p. 1710-5.

229. Kurtz, S., et al., *Projections of primary and revision hip and knee arthroplasty in the United States from 2005 to 2030.* J Bone Joint Surg Am, 2007. **89**(4): p. 780-5.

230. Teterycz, D., et al., *Outcome of orthopedic implant infections due to different staphylococci.* Int J Infect Dis, 2010. **14**(10): p. e913-8.

231. Cui, Q., et al., *Antibiotic-impregnated cement spacers for the treatment of infection associated with total hip or knee arthroplasty.* J Bone Joint Surg Am, 2007. **89**(4): p. 871-82.

232. Chiu, F.Y. and C.F. Lin, *Antibiotic-impregnated cement in revision total knee arthroplasty. A prospective cohort study of one hundred and eighty-three knees.* J Bone Joint Surg Am, 2009. **91**(3): p. 628-33.

233. Shaw, A.C., D.R. Goldstein, and R.R. Montgomery, *Age-dependent dysregulation of innate immunity.* Nat Rev Immunol, 2013. **13**(12): p. 875-87.

234. Montecino-Rodriguez, E., B. Berent-Maoz, and K. Dorshkind, *Causes, consequences, and reversal of immune system aging.* J Clin Invest, 2013. **123**(3): p. 958-65.

235. Solito, S., et al., *Highlights on molecular mechanisms of MDSC-mediated immune suppression: paving the way for new working hypotheses.* Immunol Invest, 2012. **41**(6-7): p. 722-37.

236. Katoh, H., et al., *CXCR2-expressing myeloid-derived suppressor cells are essential to promote colitis-associated tumorigenesis.* Cancer Cell, 2013. **24**(5): p. 631-44.

237. Highfill, S.L., et al., *Disruption of CXCR2-mediated MDSC tumor trafficking enhances anti-PD1 efficacy.* Sci Transl Med, 2014. **6**(237): p. 237ra67.

238. Norris, B.A., et al., *Chronic but not acute virus infection induces sustained expansion of myeloid suppressor cell numbers that inhibit viral-specific T cell immunity.* Immunity, 2013. **38**(2): p. 309-21.

239. Lesokhin, A.M., et al., *Monocytic CCR2(+) myeloid-derived suppressor cells promote immune escape by limiting activated CD8 T-cell infiltration into the tumor microenvironment.* Cancer Res, 2012. **72**(4): p. 876-86.

240. Huang, B., et al., *CCL2/CCR2 pathway mediates recruitment of myeloid suppressor cells to cancers.* Cancer Lett, 2007. **252**(1): p. 86-92.

241. Mao, Y., et al., *Melanoma-educated CD14+ cells acquire a myeloid-derived suppressor cell phenotype through COX-2-dependent mechanisms.* Cancer Res, 2013. **73**(13): p. 3877-87.

242. Obermajer, N., et al., *PGE(2)-driven induction and maintenance of cancer-associated myeloid-derived suppressor cells.* Immunol Invest, 2012. **41**(6-7): p. 635-57.

243. Fujita, M., et al., *COX-2 blockade suppresses gliomagenesis by inhibiting myeloid-derived suppressor cells.* Cancer Res, 2011. **71**(7): p. 2664-74.

244. Grundmann, H. and B. Hellriegel, *Mathematical modelling: a tool for hospital infection control.* Lancet Infect Dis, 2006. **6**(1): p. 39-45.
245. Shorr, A.F., *Epidemiology and economic impact of meticillin-resistant Staphylococcus aureus: review and analysis of the literature.* Pharmacoeconomics, 2007. **25**(9): p. 751-68.
246. Fitzsimmons, K., A.I. Bamber, and H.B. Smalley, *Infective endocarditis: changing aetiology of disease.* Br J Biomed Sci, 2010. **67**(1): p. 35-41.
247. Feuerstein, R., et al., *MyD88 in macrophages is critical for abscess resolution in staphylococcal skin infection.* J Immunol, 2015. **194**(6): p. 2735-45.
248. Youn, J.I., et al., *Characterization of the nature of granulocytic myeloid-derived suppressor cells in tumor-bearing mice.* J Leukoc Biol, 2012. **91**(1): p. 167-81.
249. Murray, P.J., *The primary mechanism of the IL-10-regulated antiinflammatory response is to selectively inhibit transcription.* Proc Natl Acad Sci U S A, 2005. **102**(24): p. 8686-91.
250. Couper, K.N., D.G. Blount, and E.M. Riley, *IL-10: the master regulator of immunity to infection.* J Immunol, 2008. **180**(9): p. 5771-7.
251. Bunt, S.K., et al., *Inflammation enhances myeloid-derived suppressor cell cross-talk by signaling through Toll-like receptor 4.* J Leukoc Biol, 2009. **85**(6): p. 996-1004.
252. Perrin, G.Q., H.M. Johnson, and P.S. Subramaniam, *Mechanism of interleukin-10 inhibition of T-helper cell activation by superantigen at the level of the cell cycle.* Blood, 1999. **93**(1): p. 208-16.
253. Taga, K., H. Mostowski, and G. Tosato, *Human interleukin-10 can directly inhibit T-cell growth.* Blood, 1993. **81**(11): p. 2964-71.
254. Letterio, J.J. and A.B. Roberts, *Regulation of immune responses by TGF-beta.* Annu Rev Immunol, 1998. **16**: p. 137-61.
255. Waight, J.D., et al., *Tumor-derived G-CSF facilitates neoplastic growth through a granulocytic myeloid-derived suppressor cell-dependent mechanism.* PLoS One, 2011. **6**(11): p. e27690.
256. Sawanobori, Y., et al., *Chemokine-mediated rapid turnover of myeloid-derived suppressor cells in tumor-bearing mice.* Blood, 2008. **111**(12): p. 5457-66.
257. Skabytska, Y., et al., *Cutaneous innate immune sensing of Toll-like receptor 2-6 ligands suppresses T cell immunity by inducing myeloid-derived suppressor cells.* Immunity, 2014. **41**(5): p. 762-75.
258. Fujimura, T., Y. Kambayashi, and S. Aiba, *Crosstalk between regulatory T cells (Tregs) and myeloid derived suppressor cells (MDSCs) during melanoma growth.* Oncoimmunology, 2012. **1**(8): p. 1433-1434.
259. Corsetti, P.P., et al., *Lack of endogenous IL-10 enhances production of proinflammatory cytokines and leads to Brucella abortus clearance in mice.* PLoS One, 2013. **8**(9): p. e74729.
260. Wang, J., G. Roderiquez, and M.A. Norcross, *Control of adaptive immune responses by Staphylococcus aureus through IL-10, PD-L1, and TLR2.* Sci Rep, 2012. **2**: p. 606.
261. Sasaki, H., et al., *IL-10, but not IL-4, suppresses infection-stimulated bone resorption in vivo.* J Immunol, 2000. **165**(7): p. 3626-30.
262. Gjertsson, I., et al., *Formylated peptides are important virulence factors in Staphylococcus aureus arthritis in mice.* J Infect Dis, 2012. **205**(2): p. 305-11.
263. Redford, P.S., P.J. Murray, and A. O'Garra, *The role of IL-10 in immune regulation during M. tuberculosis infection.* Mucosal Immunol, 2011. **4**(3): p. 261-70.

264. Frodermann, V., et al., *A modulatory interleukin-10 response to staphylococcal peptidoglycan prevents Th1/Th17 adaptive immunity to Staphylococcus aureus.* J Infect Dis, 2011. **204**(2): p. 253-62.

265. Peres, A.G. and J. Madrenas, *The broad landscape of immune interactions with Staphylococcus aureus: from commensalism to lethal infections.* Burns, 2013. **39**(3): p. 380-8.

266. Ray, A., K. Chakraborty, and P. Ray, *Immunosuppressive MDSCs induced by TLR signaling during infection and role in resolution of inflammation.* Front Cell Infect Microbiol, 2013. **3**: p. 52.

267. Maruyama, A., et al., *Pam2 lipopeptides systemically increase myeloid-derived suppressor cells through TLR2 signaling.* Biochem Biophys Res Commun, 2015. **457**(3): p. 445-50.

268. Bromberg, J., *Stat proteins and oncogenesis.* J Clin Invest, 2002. **109**(9): p. 1139-42.

269. Nefedova, Y., et al., *Regulation of dendritic cell differentiation and antitumor immune response in cancer by pharmacologic-selective inhibition of the janus-activated kinase 2/signal transducers and activators of transcription 3 pathway.* Cancer Res, 2005. **65**(20): p. 9525-35.

270. Nefedova, Y., et al., *Hyperactivation of STAT3 is involved in abnormal differentiation of dendritic cells in cancer.* J Immunol, 2004. **172**(1): p. 464-74.

271. Yu, H., M. Kortylewski, and D. Pardoll, *Crosstalk between cancer and immune cells: role of STAT3 in the tumour microenvironment.* Nat Rev Immunol, 2007. **7**(1): p. 41-51.

272. Chakraborty, A. and D.J. Tweardy, *Stat3 and G-CSF-induced myeloid differentiation.* Leuk Lymphoma, 1998. **30**(5-6): p. 433-42.

273. Hedrich, C.M. and J.H. Bream, *Cell type-specific regulation of IL-10 expression in inflammation and disease.* Immunol Res, 2010. **47**(1-3): p. 185-206.

274. Townsend, J.M., et al., *IL-9-deficient mice establish fundamental roles for IL-9 in pulmonary mastocytosis and goblet cell hyperplasia but not T cell development.* Immunity, 2000. **13**(4): p. 573-83.

275. Matsuzawa, S., et al., *IL-9 enhances the growth of human mast cell progenitors under stimulation with stem cell factor.* J Immunol, 2003. **170**(7): p. 3461-7.

276. Goswami, R. and M.H. Kaplan, *A brief history of IL-9.* J Immunol, 2011. **186**(6): p. 3283-8.

277. Renoux, M., et al., *Release of mast cell mediators and nitrites into knee joint fluid in osteoarthritis--comparison with articular chondrocalcinosis and rheumatoid arthritis.* Osteoarthritis Cartilage, 1996. **4**(3): p. 175-9.

278. Freeman, T.A., et al., *Mast cells and hypoxia drive tissue metaplasia and heterotopic ossification in idiopathic arthrofibrosis after total knee arthroplasty.* Fibrogenesis Tissue Repair, 2010. **3**: p. 17.

279. Fong, T., et al., *Problem gambling knowledge and perceived community impact among Asian-Pacific Islanders and non Asian-Pacific Islanders.* J Immigr Minor Health, 2010. **12**(2): p. 173-8.

280. Sia, I.G., E.F. Berbari, and A.W. Karchmer, *Prosthetic joint infections.* Infect Dis Clin North Am, 2005. **19**(4): p. 885-914.

281. Anderl, J.N., et al., *Role of nutrient limitation and stationary-phase existence in Klebsiella pneumoniae biofilm resistance to ampicillin and ciprofloxacin.* Antimicrob Agents Chemother, 2003. **47**(4): p. 1251-6.

282. Ceri, H., et al., *The Calgary Biofilm Device: new technology for rapid determination of antibiotic susceptibilities of bacterial biofilms.* J Clin Microbiol, 1999. **37**(6): p. 1771-6.

283. Agarwal, S. and P.J. Busse, *Innate and adaptive immunosenescence.* Ann Allergy Asthma Immunol, 2010. **104**(3): p. 183-90; quiz 190-2, 210.

284. Scherer, A. and A. McLean, *Mathematical models of vaccination.* Br Med Bull, 2002. **62**: p. 187-99.

285. Proctor, R.A., *Challenges for a universal Staphylococcus aureus vaccine.* Clin Infect Dis, 2012. **54**(8): p. 1179-86.

286. Otto, M., *Bacterial evasion of antimicrobial peptides by biofilm formation.* Curr Top Microbiol Immunol, 2006. **306**: p. 251-8.

287. Taylor, S.M., et al., *Development of response-selective agonists of human C5a anaphylatoxin: conformational, biological, and therapeutic considerations.* Curr Med Chem, 2001. **8**(6): p. 675-84.

288. Morgan, E.L., et al., *Enhancement of in vivo and in vitro immune functions by a conformationally biased, response-selective agonist of human C5a: implications for a novel adjuvant in vaccine design.* Vaccine, 2009. **28**(2): p. 463-9.

289. Urban, C.F., S. Lourido, and A. Zychlinsky, *How do microbes evade neutrophil killing?* Cell Microbiol, 2006. **8**(11): p. 1687-96.

290. Foster, T.J., *Colonization and infection of the human host by staphylococci: adhesion, survival and immune evasion.* Vet Dermatol, 2009. **20**(5-6): p. 456-70.

291. Gresham, H.D., et al., *Survival of Staphylococcus aureus inside neutrophils contributes to infection.* J Immunol, 2000. **164**(7): p. 3713-22.

292. Gristina, A.G., *Biomaterial-centered infection: microbial adhesion versus tissue integration.* Science, 1987. **237**(4822): p. 1588-95.

293. Short, A.J., et al., *Response-selective C5a agonists: differential effects on neutropenia and hypotension in the rat.* Br J Pharmacol, 1999. **128**(3): p. 511-4.

294. Morgan, E.L., et al., *A novel adjuvant for vaccine development in the aged.* Vaccine, 2010. **28**(52): p. 8275-9.

295. Buret, A., et al., *An in vivo model to study the pathobiology of infectious biofilms on biomaterial surfaces.* J Biomed Mater Res, 1991. **25**(7): p. 865-74.

296. Duch, J.M. and J. Yee, *Successful use of recombinant tissue plasminogen activator in a patient with relapsing peritonitis.* Am J Kidney Dis, 2001. **37**(1): p. 149-153.

297. Pickering, S.J., et al., *Urokinase: a treatment for relapsing peritonitis due to coagulase-negative staphylococci.* Nephrol Dial Transplant, 1989. **4**(1): p. 62-5.

298. Xu, K.D., G.A. McFeters, and P.S. Stewart, *Biofilm resistance to antimicrobial agents.* Microbiology, 2000. **146 (Pt 3)**: p. 547-9.

299. Singh, R., et al., *Penetration of antibiotics through Staphylococcus aureus and Staphylococcus epidermidis biofilms.* J Antimicrob Chemother, 2010. **65**(9): p. 1955-8.

300. Nathan, C., *Neutrophils and immunity: challenges and opportunities.* Nat Rev Immunol, 2006. **6**(3): p. 173-82.

301. Nauseef, W.M., *How human neutrophils kill and degrade microbes: an integrated view.* Immunol Rev, 2007. **219**: p. 88-102.

302. Brinkmann, V., et al., *Neutrophil extracellular traps kill bacteria.* Science, 2004. **303**(5663): p. 1532-5.

303. Janols, H., et al., *A high frequency of MDSCs in sepsis patients, with the granulocytic subtype dominating in gram-positive cases.* J Leukoc Biol, 2014. **96**(5): p. 685-93.